Spring 2018

Strengthening of reinforced masonry walls subjected to out-of-plane pseudo-static cyclic load using advanced composite

Zuhair Al-Jaberi

Department: Civil, Architectural and Environmental Engineering

STRENGTHENING OF REINFORCED MASONRY WALLS SUBJECTED TO OUT-OF-PLANE PSEUDO-STATIC CYCLIC LOAD USING ADVANCED COMPOSITE

by

ZUHAIR AL-JABERI

A DISSERTATION

Presented to the Faculty of the Graduate School of the

MISSOURI UNIVERSITY OF SCIENCE AND TECHNOLOGY

In Partial Fulfillment of the Requirements for the Degree

DOCTOR OF PHILOSOPHY

IN

CIVIL ENGINEERING

2018

Approved by:
John J. Myers; Advisor
Mohamed A. ElGawady
Lesley H. Sneed
Guirong Yan
K. Chandrashekhara

PUBLICATION DISSERTATION OPTION

This dissertation consists of the following six articles, formatted in the style used by Missouri University of Science and Technology:

Paper I: Pages 20-59 “Out-Of-Plane Flexural Behavior of Reinforced Masonry Walls Strengthened with NSM FRP." This manuscript was accepted in the *ACI Structural Journal*.

Paper II: Pages 60-87 “Evaluation of FRP and FRCM composites for the strengthening of reinforced masonry walls." This manuscript was accepted in *Journal of ACI Special Publication*.

Paper III: Pages 88-130 “Pseudo-Static Cyclic Loading Comparison of Reinforced Masonry Walls Strengthened with FRCM or NSM FRP." This manuscript was published in *Journal of Construction and Building Material.*

Paper IV: Pages 131-171 “Experimental and Analytical Approach for Prediction Out-of-Plane Capacity of Reinforced Masonry Walls Strengthened with EB-FRP." This manuscript was submitted for publication in the *Journal of ASCE Composites for Construction.*

Paper V: Pages 172-214 “The Durability Performance of the Advanced Composite Bonded to Masonry Walls after Exposure to Environmental Conditioning Cycles." This manuscript is intended for submission to *Journal of Composites Part B: Engineering.*

Paper VI: Pages 215-248 “Bond between Advanced Composite and Concrete Masonry Unit at Different Temperatures for NSM and EB Techniques." This manuscript was submitted for publication in the *Journal of Composite Structures.*

ABSTRACT

A number of researchers have conducted experimental tests on unreinforced masonry walls (URM) strengthened with advanced composite materials. Consequently, the strengthening design guidelines are limited in their scope to URM. This research aimed to investigate the behavior of reinforced masonry walls strengthened with advanced composite and subjected to out-of-plane pseudo-static cyclic load. Experimental and analytical studies were conducted to evaluate the performance of different techniques such as near surface mounted (NSM) and externally bonded (EB) fiber reinforced polymer (FRP) with epoxy resin, in addition to NSM with cementitious adhesive and fiber reinforced cementitious material (FRCM). The experimental part included three phases. In the first phase, a series of 42 reinforced masonry walls were tested to study the effectiveness of advanced composites in enhancing out-of-plane flexural capacity. The effect of long-term environmental exposure on strengthening systems was investigated in the second phase of study by testing 10 reinforced masonry walls. The third phase focused on bond behavior between the advanced composite and the concrete masonry unit at different temperatures; 56 specimens were used for this purpose. The results indicated that the non-arching strengthened reinforced masonry wall's behavior was significantly dependent on the type of fiber and fiber reinforcement ratio. The specimens strengthened with glass under combined environmental cycles exhibited an insignificant change in terms of ultimate strength as compared to laboratory conditioned specimens. The theoretical part included the investigation of bond reduction factors, seismic performance, and the nonlinear analysis of strengthened reinforced masonry wall using moment-curvature analysis. As a result of this study, the proposed model for predicting debonding strain and the moment-curvature relation presented an excellent prediction compared to the experimental results.

ACKNOWLEDGMENTS

Words are not enough to express my gratitude to have such an outstanding professor and excellent advisor like Dr. John J. Myers. I would like to express my appreciation to him for his guidance, encouragement, support, and assistance throughout this project. Special thanks to my advisory committee members, Dr. Mohamed A. ElGawady (for his valuable comments in my papers), Dr. Lesley H. Sneed, Dr. Guirong Yan, and Dr. K. Chandrashekhara, for their time and input during review of this document.

I would like to thank my mother for her love, prayers, and continuous support. Also, I would like to express my sincere gratitude to my lovely wife, Rana Mahdi, without her support and help; this research would not be possible. Also, I owe much to my lovely children who were so patient since I was in my office or lab most of the weekends and holidays. Special thanks to my family members and friends who were a great support.

My great thanks to my wonderful research group members, Hayder Alghazali, Zena AlJazaeri, Eli Hernandez, and to my colleagues. I could not have survived the duration of this study without my close friend Ahmed Gheni; I want to express my gratitude and deepest appreciation to him. My sincere appreciation to Jason Cox, Brian Swift, Gary Abbott, John Bullock, and Greg Leckrone for their technical assistance.

Last but not least, I would like to acknowledge the support of Midwest Block & Brick in Jefferson City, Missouri; Ruredil S.p.A., San Donato Milanese, Italy; Hughes Brothers in Seward, Nebraska; and HCED (The Higher Committee for Education Development in Iraq) for their support and help to provide the materials for this research.

TABLE OF CONTENTS

Page

LIST OF ILLUSTRATIONS

PAPER IV

PAPER V

LIST OF TABLES

SECTION

1. INTRODUCTION

1.1. BACKGROUND

Masonry refers to a construction system where clay, concrete masonry units, or natural stones are bonded together to form a load-bearing structure or a component in a structure. Masonry elements are used in flexural applications such as retaining walls, roof and floor beams, and lintels, or in load-bearing walls primarily resisting compression loads. Masonry walls are an important structural element that plays a significant role in lateral load resistance systems to resist wind and earthquake loads (ACI 440.7R-10, 2010). Reinforced masonry walls are a typical type of wall system. Although the reinforcement of masonry buildings against earthquake damage was known as early as 1755, it only came of age in the United States in the late 1930s (Tobriner, 1984). Thus, unreinforced masonry (URM) buildings are widely recognized as the most dangerous type of construction for resistance to earthquakes. Adding steel reinforcement is very important for masonry buildings in coastal areas and earth-retaining walls that are subjected to out-of-plane loading to increase flexural capacity and provide ductility.

The strengthening or retrofitting of existing concrete masonry structures to resist higher design loads, correct strength loss due to deterioration, and correct design or construction deficiencies has been accomplished through traditional means. Many traditional techniques for strengthening are available, such as externally bonded steel plates, steel or concrete jackets, and external post-tensioning (ACI 440.2R-08, 2008). These traditional strengthening techniques can be labor intensive, add considerable mass, and cause significant impact on the occupant, all resulting in very high costs (Hamilton

and Dolan, 2001). Due to recent change in the seismic code and some other causes, all historical structures need to be retrofitted (Grillo, 2003). Fiber reinforced polymers (FRPs) have been used as an alternative to traditional material in strengthening systems. The main advantage of the FRP strengthening systems is the high strength-to-weight ratio alongside its corrosion resistance. Using FRP systems has reduced labor cost and impact on occupants due to easy installation. FRP with epoxy has some drawbacks: poor behavior of the resin at temperatures above the glass transition temperature, emission of toxic fumes, and moisture impermeability (Hashemi and Al-Mahaidi, 2008). Using a cementitious material as an alternative adhesive agent is very appealing and eliminates these drawbacks.

1.2. OBJECTIVES AND SCOPE OF WORK

The overall aim of this research was to investigate and gather knowledge on strengthening reinforced masonry walls with near surface mounted (NSM) and externally bonded (EB) fiber reinforced polymer (FRP), also using fiber reinforced cementitious material (FRCM) system. This will be done by reviewing and interpreting the experimental test results and failure mechanisms to understand the contribution of different strengthening systems on improving the flexural strength, stiffness, energy absorption, energy dissipation and ductility of masonry walls. The suitability of using cement-based material as a bonding agent instead of epoxy in strengthening of existing (RMW) for NSM technique was also investigated by considering NSM with cement adhesive. The other objective was to develop an analytical model based on (ACI 440.2R-08, 2008) to compute the flexural capacity of retrofitted masonry walls and compare it with the experimental database results, in addition to predict the full behavior using

moment–curvature analysis. Finally, the effect of environmental conditions and the effect of different temperature subjected simultaneously with tensile load on strengthening systems were investigated in this study. The dissertation objectives were achieved through the following tasks: (1) review of applicable literature about out-of-plane behavior of strengthened masonry walls; (2) experimentally characterize the mechanical properties for all materials used within the composite system and retrofitted structure; (3) investigate the Out-of-Plane pseudo-static cyclic behavior of the strengthened RMW; (4) investigate the durability performance of the advanced composite bonded to masonry walls after exposure to environmental conditioning cycles; (5) investigate the seismic characterization for strengthened walls; (6) investigate the bond between advanced composite and concrete masonry unit at different temperatures for NSM and EB techniques; (7) summarize findings and develop conclusions and recommendations.

1.3. DISSERTATION LAYOUT

This dissertation is organized to include three sections and two appendices according to the stages followed for the development this project. The first section gives an introduction and the significant of the strengthening of reinforced masonry walls. The section presents also the objective and the scope of work, in addition to review of the previous literature, including previous study and design guides on FRP strengthened unreinforced concrete masonry structures.

The second section presents a six journal papers discussing the behavior of out-of-plane reinforced masonry walls strengthened with advanced composite and subjected to pseudo-static cyclic load. In addition to discuss the durability performance and bond

behavior between advanced composites and concrete masonry unit at different temperatures.

The third section summarizes the conclusions of this dissertation and proposes future research.

2. LITERATURE REVIEW

The purpose of this section is to conduct a comprehensive literature review of previous research on flexural strengthening of unreinforced masonry walls, with particular attention to the impact of many parameters on flexural capacity and displacement ductility of these walls.

The reinforcement of masonry buildings against lateral loads was known as early as 1755, and it is started being applied in the United States in the late 1930s. These reinforced masonry buildings has not been built in California since 1935. Many URM and RM buildings that have been built in the past do not meet today's current code requirements. An effective technique was needed to strengthen masonry structures against overloading conditions and improve the load carrying capacity. FRP composites can be used as an effective technique due to many advantages such as, lightweight and available in multiple forms, many of which could easily be manipulated to match variable structural shapes and geometries. Testing reinforced and unreinforced masonry walls in the in-plane direction to evaluate the walls' behavior under lateral loads has been conducted by many research programs. Significant works has also evaluated the out-of-plane performance of unreinforced masonry wall systems. This includes research on small scale masonry walls and prediction the out-of-plane capacity considering arching action. Walls with low slenderness ratios, typically less than 12, and built between rigid supports can develop arching action when subjected to out-of-plane loads. This action induces in-plane compressive forces which act to restrain the outward movement and does not require strengthening (Nanni and Tumialan, 2003). Three hinges formed due to

this action, the locations of hinges are at midspan and at each of the rigid supports (Tumialan et al., 2001) as shown in (Figure 2.1).

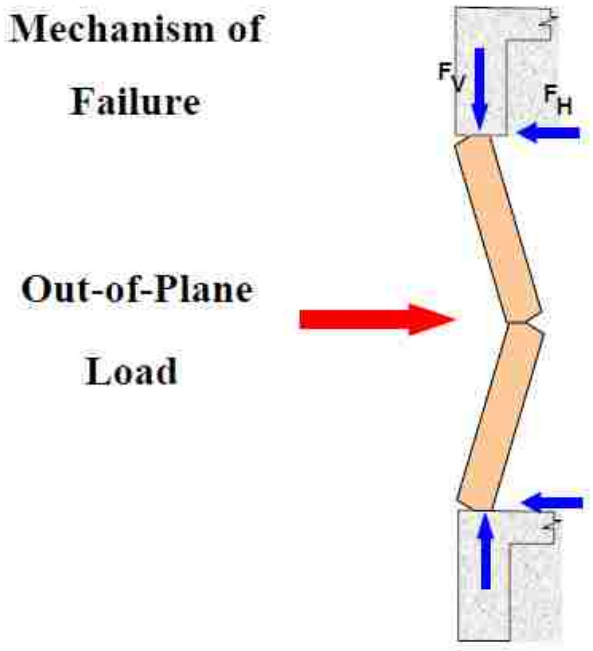

Figure 2.1. Arching Action Mechanism (Tumialan et al., 2001)

This study is an attempt to extend the design of structures that consider in (ACI 440.7R-10, 2010) (Guide for the Design and Construction of Externally Bonded Fiber-Reinforced Polymer Systems for Strengthening Unreinforced Masonry Structures) from unreinforced masonry to reinforced masonry walls without considering arching action.

2.1. STRENGTHENING MASONRY WALLS USING NSM-FRP

Many techniques are available to strengthen and retrofit reinforced masonry structures as alternative to the traditional strengthening techniques. Near-surface mounted (NSM) fiber-reinforced polymer (FRP) reinforcement is one of the promising strengthening techniques for reinforced concrete and masonry structures (De Lorenzis

and Teng, 2007). Research on this topic started since the past few decades but has by now attracted worldwide attention since their application does not require any surface preparation work and requires minimal installation time compared to FRP laminates (Tumialan et al., 2002). FRP reinforcement is very effective for strengthening of slender masonry walls or walls with slenderness (h/t or l/t) less than 10 provided simply-supported boundary conditions.

A number of researchers have conducted masonry tests on unreinforced masonry walls (URM) strengthened with FRP. As a result of this work, a number of masonry design guidelines, such as the ACI Committee 440.7R-10 (ACI 440.7R-10, 2010) were developed. Tumialan et al. (2002) presented three applications of FRP bars to strengthen URM walls. The first application strengthens masonry walls with NSM FRP as a flexural reinforcement to resist out-of-plane loads. The second application was an investigation of structural repointing; in this system, the FRP is placed in a masonry bed joint and act as a shear reinforcement to help the wall resist in-plane loads. In the third application, masonry walls exhibiting deficient anchorage to the base beam or frame are retrofitted by placing NSM FRP bars in the heal region of the wall. In the last 20 years, many studies and field applications on FRP bars as an NSM strengthening technique have been reported (Willis et al., 2009, Stone et al., 2002, Petersen et al., 2009, Griffith et al., 2013, Willis et al., 2010, De Lorenzis et al., 2000a, De Lorenzis et al., 2000b). The FRP bars were used as anchors to increase the flexural capacity of walls subjected to in-plane and out-of-plane loads. Out-of-plane strengthening of URM walls using NSM-FRP Was conducted by (Dizhur et al., 2014). The results of the experimental tests of this study confirmed that the NSM CFRP vertically oriented, significantly increased both the post-

cracked ductility and flexural capacity up to 6.2 times the control capacity. Based on cyclic loading, high stiffness degradation was observed at low drift ratios, while gradual degradation of stiffness was evident over the higher ranges of applied drift. De Lorenzis et al. (2000a) focused on the bond behavior of NSM rods that were embedded in concrete masonry units (CMU). Flexural tests revealed an increase in the flexural capacity of URM walls as the specimens strengthened with one and two GFRP rods failed at 7 and 15.7 times the load of the control specimen, respectively. Research by (Willis et al., 2010) has investigated the effect of horizontally oriented FRP on out-of-plane capacity. The results of this study showed that NSM strips are very effective to increase the flexural capacity but they are more susceptible to displacement induced debonding due to their orientation. However, this problem may be eliminated by developing a suitable anchorage system. Tumialan et al. (2000) conducted field experiments on URM walls strengthened with both FRP sheets (GFRP, AFRP, and CFRP) and GFRP rods as an NSM. Various parameters were evaluated including the type of composite system used, strip width applied, and the FRP installation methods chosen. It was observed that the walls, on which the FRP had been applied to the tile surface, after the plaster was removed, exhibited a better performance than did their counterparts which had been strengthened, but the plaster had not been removed. The use of NSM rods is attractive because the removal of plaster is not required.

2.2. STRENGTHENING MASONRY WALLS USING EB-FRP

Many existing masonry structures around the world have been constructed to resist gravity and wind loads. Most of these structures were built with unreinforced masonry (URM) walls and perform poorly when subjected to out-of-plane load as shown

in (Figure. 2.2). Using steel reinforcement in grouted cells of masonry walls led to improve the out-of-plane flexural capacity. The structure may need to be strengthened due to the change of the building function, construction or design defects, or to repair damage or deterioration.

Figure 2.2. Failure of unreinforced wall due to out-of-plane seismic forces [Nisqually Earthquake, 28 February 2001].

For these reasons, masonry walls that have insufficient out-of- plane strength to resist the lateral loads are in need of an upgrading capacity. EB-FRP is one of the effective strengthening techniques have been suggested to improve out-of-plane capacity of existing masonry walls. The following researchers (Al-Jaberi et al., 2016, Galati et al., 2006, Velazquez-Dimas et al., 2000, Valluzzi et al., 2014, Churilov and Dumova-Jovanoska, 2012) confirmed that the EB-FRP composite increases the out-of-plane capacity of URM or RM walls. Full scale test focused on evaluating the out0of-plane behavior of URM walls strengthened with EB-FRP was conducted by (Mosallam, 2007). The effect of applying a cross-ply laminate on the ultimate capacity and failure mode has been investigated. The results confirmed the effectiveness of two types of FRP (E-

glass/epoxy and carbon/epoxy FRP composite) in upgrading the flexural performance of URM walls. The coupling effect of in-plane and out-of- plane strengthening was proven to have positive effects on both flexural capacity and the ductility of the retrofitted wall specimen. The mode of failure for strengthened specimens was due to a combination of compression failure of the masonry unit followed by a cohesive failure of FRP epoxy. The debonding failure is the major issue of concern due to the lack of good preparation of the substrate surface in contact with FRP composite system. Ehsani and Saadatmanesh (1996) studied the behavior of unreinforced masonry walls strengthened with FRP composite. The results of this study showed the effectiveness of EB-FRP for increasing flexure, shear strength, and ductility, for tested specimens. The mode of failure was governed by the amount of fiber reinforcement ratio. Tension failure occurred for specimens strengthened with low fiber reinforcement ratio, while a debonding failure happened for specimen strengthened with high fiber reinforcement ratio. The effect of configuration of externally bonded fibers strengthened URM walls was evaluated by (Hamoush et al., 2002). The conclusions resulted from this investigation confirm that the ultimate flexural capacity is not achievable unless the shear premature failure at the support is controlled. The configuration of continuous web overlay on the entire wall area presented a slightly higher strength than walls strengthened with unidirectional strips configuration applied in two directions. The effect of surface preparation was investigated for application of EB-FRP sheet and laminate in strengthening concrete structures (Mostofinejad and Mahmoudabadi, 2010). The results indicated that the effect of surface preparation prior to installing FRP sheets increased ultimate failure strength by 5-15% as compared to specimens strengthened without surface preparation. Simply

supported URM walls strengthened with unidirectional E-glass fabric and subjected to out-of-plane load were tested (Hamilton and Dolan, 2001). In this study, the application of GFRP composite was proven equivalent to #5 reinforcing bar spaced at 610 mm (24 in.). The identified modes of failure were GFRP rupture and a combination of GFRP rupture and delamination. The influence of surface treatment was presented considering two types of treatment as a surface preparation (Toutanji and Ortiz, 2001). The results showed that surface preparation using water jet provides a better bonding strength comparing with specimen treated with sand blasting. URM wall strengthened by GFRP and subjected to cyclic loading was studied by (Kuzik et al., 2003). This study showed that the general behavior of the walls was very predictable. The strength and deformation characteristics of the strengthened wall were evaluated by presenting a simple model of the wall behavior. They concluded that increasing and decreasing the amount of bonded GFRP sheet reinforcement increased and decreased both the wall stiffness and the ultimate strength, respectively. Using an FRP composite dramatically increased the flexural capacity by more than twenty times that of unreinforced masonry wall.

The vast majority of previous studies have focused on the behavior of unreinforced masonry walls. The first experimental database of reinforced masonry walls strengthened with EB-FRP was created (Shen, 2014). Three parameters were investigated in this study: type of FRP, FRP width, and number of FRP layers. It was proven that flexural capacity and post-crack stiffness of strengthened walls were related to the fiber reinforcement ratio. Also, the specimen strengthened with one GFRP layer failed by premature rupture of fiber, while the specimens strengthened with double layer of GFRP failed by IC debonding.

2.3. STRENGTHENING MASONRY WALLS USING CEMENT ADHESIVE SYSTEMS

Extensive studies of masonry structures in the past two decades have been focused on strengthening masonry structures with emphasis on FRP and epoxy adhesive as a strengthening technique (Velazquez-Dimas et al., 2000, Valluzzi et al., 2001, Tumialan et al., 2003, Tan and Patoary, 2004, Hamilton and Dolan, 2001, Carney and Myers, 2003, Al-Jaberi et al., 2016). Although epoxy adhesive was approved as an effective bonding agent in many structural applications for strengthening, it may not be an optimal choice for other applications due to some limitations. These include hazardous poor behavior of epoxy at and above the glass transition temperature (T_g), incompatibility with the masonry surface, inability to be applied on damp surface, emission of toxic fumes, moisture impermeability, and flammability (Hashemi and Al-Mahaidi, 2008, Al-Jabari et al., 2015, Al-Abdwais and Al-Mahaidi, 2016). When an FRP system is subjected to high temperature, the guidelines for the design of FRP-strengthened structures state that the contribution of FRP is neglected unless a fire protection system or insulation is used (Soudki and Alkhrdaji, 2005). In order to overcome these drawbacks of FRP and an epoxy system, NSM with cementitious material adhesive, or FRCM, has emerged as an alternative technique. Cementitious material is less expensive and preferable as a bonding agent due to its compatibility with masonry substrate and has sufficient bonding properties (Turco et al., 2006). A few studies have considered cementitious material as an adhesive material. One of the disadvantages of using cement paste adhesive in NSM is the low viscosity which causes flow it away from the groove and affects the applicability of this material. Hashemi and Al-Mahaidi (2010) improved a new cement-based adhesive by adding polymer to increase the viscosity of adhesive agent, significant ductile

behavior was observed for specimens strengthened with NSM and modified cement-based adhesive. The comparison study for flexural behavior of URM walls strengthened using NSM FRP with epoxy and cementitious material was conducted (Turco et al., 2006, Galati et al., 2006). Similar flexural capacity was achieved by using both materials, but the specimens with cementitious material had gradual stiffness degradation and debonding failure. As a recommendation of these studies, improved performance for this system was observed when the size of the groove was approximately 2.25 times the diameter of FRP bar. Also, the maximum fiber debonding strain for specimen with cement-based adhesive was recommended as 0.55 times the ultimate fiber strain for circular FRP bars.

FRCM, also known as textile-reinforced mortar (TRM) or textile-reinforced concrete (TRC), is an alternative strengthening technique and complementary to FRP systems. FRCM systems consist of fibers (carry tensile stresses) embedded in cementitious matrix (to transfer the load to the fibers). Open fabric meshes is the typical fiber in this system and the closed fiber fabrics are not suitable to ensure fully penetrate of cementitious matrix and impregnate the fiber filaments. An FRCM system has almost the same advantages of an FRP system, such as high strength to weight ratio, corrosion resistance and ease of installation, but also overcomes some FRP drawbacks, especially the elevated temperature/T_g issue and application on damp surfaces. Previous studies have investigated strengthening URM walls using an FRCM system focusing on ultimate strength. Strengthening of URM concrete or clay brick walls with FRCM system under uniformly distributed lateral load subjected by air bag was conducted (Babaeidarabad and Nanni, 2015), and an enhancement in flexural capacity ranging from 2.7 to 7.8 compared

to control specimen was reported. The potential modes of failure for these strengthened specimens were identified, including flexure and shear failure, depending on fiber reinforcement ratio. Clay brick walls strengthened with carbon-FRCM and subjected to out-of-plane cyclic loading was tested (Papanicolaou et al., 2008). The effectiveness of FRCM overlays was evaluated in comparison to that provided by FRP in the form of overlays or near-surface mounted (NSM) reinforcement. It was concluded that FRCM overlays provide substantial increase in strength and ductility and comprise an extremely promising solution for the structural upgrading of masonry structures under out-of-plane loading. Compared with FRCM, NSM strips offer lower strength, but higher ductility due to a more controlled debonding.

2.4. DURABILITY AND BOND BEHAVIOR OF STRENGTHENING SYSTEMS

There is a lack of long-term data on the performance of strengthened masonry walls under combined environmental exposure. The evaluation of the long-term performance of a strengthened structure requires the assessment of the durability of both the strengthening components and the involved materials under combined environmental action to simulate the natural weathering conditions. The assessment of long-term durability required evaluation for flexural and bond behavior of the masonry strengthened with advanced composite material. In terms of durability, the existing researches on strengthening using FRP were focuses on the effect of environmental degradations factors individually on concrete structural elements. The temperature action is one of these environmental factors. Silva et al. (Silva et al., 2014) investigated the behavior of concrete specimens strengthened with NSM-CFRP strips under thermal cycles. These specimens were submitted to thermal cycles and tested up to failure using four point

bending and pullout direct test for slab and cubic specimens respectively. The results indicate that the slabs capacity and damage mechanism were not affected by thermal cycle's range of -15°C to 60°C. Nevertheless, the bond strength increased with the number of thermal cycles. The effect of elevated service temperature on EB FRP and concrete surface was reported (Leone et al., 2009). Relevant influence of the temperature on bond strength and mode of failure was proven as results of this study. At 80 ^{o}C (176 ^{o}F), the bond strength of FRP sheet, GFRP sheet, and CFRP laminate was reduced by 54%, 72%, and 25%, respectively. Changing the temperature from 50 to 80 ^{o}C (122-176 ^{o}F) resulted in changing the mode of failure from cohesion to adhesion failure. Bond failure at interface occurred at temperature higher than T_g due to loss the bonding strength of adhesive material at interface.

Effects of elevated temperature on NSM-FRP strengthening systems were conducted (Burke et al., 2013). Under sustained service loads, the strengthened system was capable of withstanding over 40 min at 100 °C but less than 10 min at 200 °C. NSM technique fails at elevated temperature by debonding at the adhesive-concrete interface. A significant losses in bond resistance at elevated temperature, since the experimental tests occurred at temperatures exceeding the glass transition temperature (T_g) of the epoxy adhesive. Using a cementitious material as an alternative adhesive agent in the NSM technique or in FRCM system is very attractive especially at high temperature applications. Cementitious material was able to support sustained load for more than four hours when the temperature was 100 °C (212 °F) and approximately one hour at 200 °C (392 °F) (Burke et al., 2013). The mode of failure was by debonding at the FRP-cementitious interface. The performance of NSM and cementitious material was

evaluated by Burke (Burke, 2008). For high temperature exposure 100 °C (212 °F), cementitious adhesive presented excellent behavior, allowing the strengthening system to remain structurally effective for more than five hours under sustained load. The effect of high temperature ranging from 20 to 120 ^{o}C (68 to 248 ^{o}F) on mechanical behavior of FRCM system was conducted by Donnini et al. (Donnini et al., 2017). The tensile strength of FRCM reinforced with carbon was reduced by 11% when subjected to the elevated temperature up to 120 ^{o}C (248 ^{o}F) which is insignificant in terms of resistance applied load and bond to the substrate.

Cold environments and freeze-thaw cycling of NSM FRP is the second factor that was investigated individually. Flexural performance of NSM carbon/vinylester FRP tape strengthened concrete slabs at low temperatures was investigated (Burke et al., 2008). The effects of adhesive type (cementitious or epoxy) and groove width are discussed at both room (21°C) and low (-26°C) temperature. The results show no discernable negative impacts on the performance of any of the strengthened members using epoxy or cementitious grout adhesives at low temperature. The experimental results for the flexural and bond performance of NSM FRP to evaluate the freeze-thaw durability were presented (Mitchell, 2010). No negative impacts on the performance of NSM with grout adhesive material after exposure to freeze-thaw cycles. Minor changes in ultimate capacity of NSM with epoxy system after exposure to freeze-thaw cycles. The Pull-out test of NSM with epoxy adhesive experienced a 27% average drop in ultimate load after 150 freeze-thaw cycles. Soliman et al. (2010) conducted a small scale pull-out test to study the bond performance of NSM FRP under 200 freeze/thaw cycles. The main mode of failure for exposed specimens with cement adhesive was splitting of adhesive material with a failure

load about 40-56% of that of their counterparts with epoxy adhesive. Al-Mahmoud et al. (2014) investigated the effect of environmental exposure (freeze-thaw cycles and salt water immersion) on NSM CFRP rod strengthened specimens and embedded in cementitious material. The specimens were exposed to up to 300 freeze–thaw cycles; no change in bond strength for NSM FRP rod resulted after this exposure. The effects of freezing and thawing conditions on EB FRP was reported by (Cromwell et al., 2011). This factor can degrade FRP material and the bond at fiber/matrix interfaces due to micro-cracking that results from expanded the frozen absorbed moisture led to more brittle FRP behavior.

Moisture has been observed to be another important deteriorating agent for specimens strengthened with advanced composites. Pull-off tests were used to evaluate the effect of moisture on FRP-masonry bond(Ghiassi et al., 2012). Constant relative humidity (RH) of 100% at 23°C (73.4°F) was applied on strengthened specimens for eight weeks. The degradation was investigated on the conditioned specimens for two periods (four and eight weeks) of exposure to evaluate the bond performance. The results indicate 15% and 23% reductions in bond strength for conditioned specimens after four and eight weeks of exposure, respectively. Based on this result, moisture exposure can reduce the bond strength of the FRP-masonry elements significantly within a two month period of exposure. The bond failure mode was affected by exposure to accelerated wet/dry cycling. The failure after this exposure occurred at the adhesive-substrate interface. In contrast, for the specimens not exposed to wet/dry cycling, bond failure always occurred in a very thin mortar layer of the concrete(Dai et al., 2010). In terms of bond, pull-out test was used to characterize the bond behavior of the NSM FRP to

masonry unit (Masia et al., 2015). This test was conducted to evaluate the temperatures at which the FRP bond becomes ineffective and also to investigate whether the bond deterioration due to elevated temperatures is reversible or not. It was found that under sustained load, relative movement between FRP bar and the masonry unit was initiated at temperatures close to the T_g of epoxy adhesive. For specimens under heating and cooling process prior to loading, the original bond strength was restored after cooling and the specimen failed with the same mode as the control specimens. The mode of failure was affected by temperature (Palmieri et al., 2011). The failure was characterized by debonding with splitting of the resin, but as a result of increasing the temperature, FRP bar was pulled out due to loss of bond at the FRP/resin interface and the mechanical properties of resin changed. The bond-slip behavior of NSM FRP bars under low and high temperature was investigated by (Alvarez et al., 2007, Soliman et al., 2010, Fernandes et al., 2018, Novidis et al., 2007). The results of specimens reinforced with GFRP subjected to 40 and 60 ^{o}C (104 and 140 ^{o}F) and also specimens reinforced with glass fiber reinforced polymer (GFRP) and carbon fiber reinforced polymer (CFRP) subjected to 200 freeze/thaw cycles were presented. Based on the experimental results, a reduction in bond strength by 26% occurred for specimens subjected to 60 ^{o}C (140 ^{o}F), and there is no significant deterioration in the bond after 200 freeze/thaw cycles. The mode of failure for specimens' strengthened using epoxy adhesive was concrete tension with or without splitting of adhesive material, while there was splitting at the concrete adhesive interface when using cementitious material. The results of an experimental test to investigate the effect of elevated service temperature on EB FRP bonding were reported (Leone et al., 2009, Burke et al., 2013). At 80 ^{o}C (176 ^{o}F), the bond strength was

reduced by 54%, 72%, and 25% for CFRP sheet, GFRP sheet, and CFRP laminate, respectively. With increasing temperature from 50 to 80 ^{o}C (122-176 ^{o}F), the mode of failure changed from cohesion to adhesion failure. If the temperature was higher than T_g, the bonding strength of adhesive material decreased less than that of concrete and led to bond failure at the interface. The EB system loss the bond strength at 60 ^{o}C (140 ^{o}F), which is close to the epoxy T_g due to phase change and markedly different material properties(Cromwell et al., 2011).

The mechanical behavior of FRCM system at high temperature was evaluated by (Donnini et al., 2017). This evaluation includes bond testing for specimens strengthened with dry carbon fabrics and subjected to temperature ranging from 20 to 120 ^{o}C (68 to 248 ^{o}F). Although the result of FRCM reinforced with carbon has experienced a reduction by 11% in tensile strength when subjected to the elevated temperature up to 120 ^{o}C (248 ^{o}F), the FRCM system still maintains adequate resistance and bond to the substrate. The FRCM and FRP bond performance at ambient and high temperature was examined by (Bisby et al., 2011). The results showed that the FRCM system exhibited superior performance at elevated temperature up to 80 °C (176 ^{o}F). The capacity of specimens strengthened with FRCM experienced reductions of only 6% at 50 °C (122 ^{o}F) and 28% at 80 °C (176 ^{o}F), while the capacity of specimens strengthened with FRP reduced by 52% at 50 °C (122 ^{o}F) and 74% at 80 °C (176 ^{o}F). Developed research on strengthening using advanced composite has focused on the short-term durability performance of strengthened structural elements and has rarely considered the full structure's lifetime. In addition, durability research has been mostly dedicated to examining environmental degradation factors individually rather than all together.

PAPER

I. OUT-OF-PLANE FLEXURAL BEHAVIOR OF REINFORCED MASONRY WALLS STRENGTHENED WITH NSM FRP

Zuhair Al-Jaberi, John J. Myers F.ACI, Mohamed A. ElGawady

ABSTRACT

Eighteen reinforced masonry walls were built as a part of this study. These reinforced walls were strengthened with carbon fiber-reinforced polymer FRP (bars and strips) and glass FRP (bars) using a near surface mounted technique (NSM); different mild steel reinforcement ratios (ρ) were used. These simply supported walls were tested under an out-of-plane cyclic load that was applied along two line loads. Various parameters were investigated, including those related to FRP (type and amount), bond pattern (stack and running), mortar pattern (face shell bedding and fully bedding), embedding material (epoxy and cementitious paste), amount of internal steel reinforcement, existence of compression FRP bars, and groove size. The ultimate load, deflection at ultimate load, and mode of failure were investigated in this study. The test results indicated a significant increase in stiffness and flexural capacity of out-of-plane reinforced walls strengthened with FRP compared to the unstrengthened reinforced walls. Different modes of failure occurred in the strengthened reinforced walls, including a flexure- shear failure through the concrete block, as well as a debonding of FRP reinforcement from the masonry substrate. Furthermore, a simple analytical model for computing the moment capacity of strengthened reinforced masonry walls is proposed and compared with the experimental results.

1. INTRODUCTION

Masonry walls are commonly used throughout the world because they are inexpensive, easily constructed and use readily available materials. Many unreinforced masonry structures are damaged when subjected to either natural or man-made lateral load, calling into question the safety of unreinforced masonry for specific applications (Al-Jaberi et al., 2015). System ductility must be addressed in regions with high seismic activity. The brittle nature of unreinforced masonry due to low tensile strengthresults in masonry structures sensitive to lateral loads. In the early 1900's reinforcing steel was introduced into masonry construction to provide increased resistance to lateral dynamic forces (Hochwalt & Amrhein, 2012).

There is a large number of existing buildings around the world and in North America, especially in the State of California, that have been constructed with reinforced masonry since 1930. These old reinforced masonry walls do not meet the current seismic standards so, following each new earthquake, the reinforcement strategies evolve (Gilstrap & Dolan, 1998). These structures may need to be strengthened for different reasons, among which, changes in use, construction or design defect, or service stage changing which include, ageing of structures or deterioration due to exposure to aggressive environmental conditions. For these reasons, masonry walls that have an insufficient out-of- plane strength to resist lateral loads are in need of upgrade.

An effective technique was needed to strengthen reinforced masonry structures against overloading conditions and improve the load carrying capacity. Many techniques are available to strengthen and retrofit reinforced masonry structures. Externally bonded steel plate, post tension, grout and epoxy injections, and surface treatment are common

examples for traditional strengthening techniques. These methods of strengthening need a skilled labor, add a considerable mass to the structure, and cause a significant impact on the occupant.

FRP composites can be used as a near surface mounted technique (NSM) system. FRP reinforcement is lightweight and available in multiple forms, many of which could easily be manipulated to match variable structural shapes and geometries (R-06, 2006). The use of NSM FRP bars is attractive, since their application does not require any surface preparation work and requires minimal installation time compared to FRP laminates (Tumialan et al.,2002). FRP reinforcement is very effective for strengthening of slender masonry walls or walls with slenderness (h/t or l/t) less than 10 provided simply-supported boundary conditions. Walls with low slenderness ratios, typically less than 12, and built between rigid supports can develop arching action when subject to out-of-plane loads. This action induces in-plane compressive forces which act to restrain the outward movement and does not require strengthening (Nanni & Tumialan, 2003).

A number of researchers have conducted masonry tests on unreinforced masonry walls (URM) strengthened with FRP. A number of masonry design guidelines, such as the ACI Committee 440.7R-10, were developed as a result of this work. Tumialan et al. (2002) presented three applications of FRP bars to strengthen URM walls. The first application strengthens masonry walls with NSM FRP as a flexural reinforcement to resist out-of-plane loads. The second application was an investigation of structural repointing; in this system, the FRP is placed in a masonry bed joint and act as a shear reinforcement to help the wall resist in-plane loads. In the third application, masonry walls exhibiting deficient anchorage to the base beam or frame are retrofitted by placing

NSM FRP bars in the heal region of the wall. In the last 20 years, many studies and field applications on FRP bars as an NSM strengthening technique have been reported (De Lorenzis et al., 2000a; De Lorenzis et al., 2000b; Griffithet al., 2013; Petersen et al., 2009; Stoneet al., 2002; Willis et al., 2009a; Willis et al., 2010). The FRP bars were used as anchors to increase the flexural capacity of walls subjected to in-plane and out-of-plane loads. De Lorenzis and Nanni, (2000) focused on the bond behavior of NSM rods that were embedded in concrete masonry units (CMU). Flexural tests revealed an increase in the flexural capacity of URM walls as the specimens strengthened with one and two GFRP rods failed at 7 and 15.7 times the load of the control specimen, respectively. Tumialan et al., (2000) conducted field experiments on URM walls strengthened with both FRP sheets (GFRP, AFRP, and CFRP) and GFRP rods as an NSM. Various parameters were evaluated including the type of composite system used, strip width applied, and the FRP installation methods chosen. It was observed that the walls, on which the FRP had been applied to the tile surface, after the plaster was removed, exhibited a better performance than did their counterparts which had been strengthened, but the plaster had not been removed. The use of near-surface-mounted rods is attractive because the removal of plaster is not required.

A previous investigation has demonstrated the feasibility and effectiveness of using FRP for increasing out-of-plane capacity of unreinforced masonry walls. This study is an attempt to extend the design of structures that consider in ACI 440.7R-10 (Guide for the Design and Construction of Externally Bonded Fiber-Reinforced Polymer Systems for Strengthening Unreinforced Masonry Structures) from unreinforced masonry to reinforced masonry walls. In this study, eighteen reinforced masonry walls were

constructed to evaluate the effect of different parameters. They were strengthened with different types of FRP namely, carbon FRP (bars and strips) and glass FRP (bars) as an (NSM). These walls were subjected to an out-of-plane cyclic load along two line loads. This experimental study present the effects of different parameters, these parameters and the reasons for choosing these parameters are: type and amount of FRP (there are many types of fibers used in structural application; the most common types are glass and fiber, this study considered these types to gain benefits of each one.), bond and mortar pattern (for masonry walls, there are two construction styles, stack and running in addition to two mortar bond pattern, fully and faceshell pattern), type of embedding material (using a cementitious material as an alternative adhesive agent is very attractive especially in the regions subjected to high temperature), amount of internal steel reinforcement (Increasing the amount of fiber reinforcement may result in changing the mode of failure from debonding to shear failure) and groove size (this factor affect the amount of adhesive agent used in this technique and bond between the FRP bar and the substrate).

2. RESEARCH SIGNIFICANCE

Much of the previous research on the strengthening of masonry walls has focused on the behavior of strengthened unreinforced masonry walls. This investigation evaluates the behavior of reinforced masonry walls strengthened with FRP composites and provides a database of experimental results. This study and the development of the database was undertaken to be used to validate a proposed design model in a revised version of the ACI 440.7R guideline for non-arching reinforced masonry walls with NSM out-of-plane strengthening. In addition, the bond reduction factor and ductility of these wall systems are investigated.

3. EXPERIMENTAL PROGRAM

This study was done using FRP NSM composites as a strengthening system. The system consisted of the installation of FRP reinforcing bars in slots that had been grooved into the masonry tension surface, as presented in Fig.1. Both E-glass and carbon fiber were used.

3.1. TEST MATRIX

This study was conducted to investigate the effectiveness of strengthening reinforced masonry walls with several variables, as shown in Table 1. Eighteen reinforced masonry walls were constructed for this experimental program using fully grouted concrete blocks and type S mortar using standard masonry blocks152.5 mm (6 in.). The nominal dimensions of these walls were 1220 by 600 by 152.5 mm (48 by 24 by 6 in.) as shown in Fig.2. Different reinforcement amounts of 2#4, 2#3, and 1#5 mild reinforcing bars were used to reinforce the specimens that constructed either in running bond or stack bond. The walls were grouted four days after construction to ensure stability during the vibration process. The specimens were air cured in the laboratory ambiance at an average temperature of 21o C (70o F). They were strengthened with Aslan 500 CFRP tape size 3 - 4.5x16 mm (0.17x0.63-in.), Aslan 200 CFRP bar size 3 – 10 mm (3/8-in.) diameter and Aslan 100 GFRP bar size 3 - 10 mm (3/8-in.) diameter. Testing was performed after a minimum of 28 day curing period.

3.2. SPECIMEN DESIGNATION

The specimen ID consisted of three parts. The first part consisted of three characters representing FRP information (type, shape and size). The first character

identified the FRP type: namely, “C” for carbon FRP and “G” for glass FRP. The second character referenced the bars cross section: an ‘‘S’’ represented a FRP strip and a ‘‘B’’ represented a circular bar. The third character referred to the size of FRP bar or strip. The second part of the ID consisted of two numbers (number and size of rebar respectively) identified the internal steel reinforcement. The third part of the ID identified the type of paste material, the number of strengthening bars, the wall bond pattern, and the mortar pattern. The first character represented the type of paste material used: “E” for epoxy paste and “C” for cementitious paste. The second character referred to the number of bars. The third character represented the wall bond pattern applied: “R” for running and “S” for stack. The fourth character was added in case of mortar pattern face shell bedding (F), the groove size greater than 2.5d (W), and Number of FRP compression reinforcement bars. As an example, the code (GB3-2#4-E1R2) referred to a reinforced masonry wall having flexural reinforcement of 2#4 strengthened with one GFRP bar (GB) embedded in a normal groove by means of epoxy material (E1) for a running wall pattern (R) and two compression FRP bars.

3.3. MATERIAL CHARACTERIZATION

A series of tests were performed to determine each material’s mechanical properties. Compressive strength for masonry prisms constructed with two masonry concrete units and cured with the same lab condition of the walls was conducted. Also, the 28 day average compressive strength of the grout, cementitious material, and type S mortar was evaluated. Experimental tensile test on three specimens of mild steel was conducted. The results of all these tests based on ASTM standards associated with each test are summarized in Table 2. The manufacturing average tensile strength, ultimate

strain, and modulus of elasticity (MOE) of CFRP (bars and strips) and GFRP bars according to ASTM D7205-11, D3039-13, are presented in Table 3.

3.4. TEST SETUP

The reinforced masonry specimens used in this study were tested under four-point bending with simply supported boundaries. The test setup, wall cross section and NSM groove dimension specification are shown in Fig. 3. An MTS double-acting hydraulic jack with a push-pull on two opposite sides capacity of 965 MPa (140 kips) was used to apply a vertical load on the wall panel. This load was transferred to the masonry specimen by means of continuous steel plates and bars along the full width of the external face of the reinforced walls to provide two equal line loads. The distance between these two lines was 100 mm (4-in.) (from mid-span of wall panel). The load was applied in cycles of loading and unloading, as a displacement control, at a rate of 1.25 mm/min (0.05-in./min) through an MTS computer control station up to the load peak value as shown in Fig. 4. Data acquisition was carried out through a computer system as displacement and corresponding loads. Deflections at the mid and third spans were measured using three Linear Variable Displacement Transducers (LVDTs) at each side. In addition, strain gauges were placed on the steel and FRP bars to record their strains during loading.

4. TEST RESULTS AND DISCUSSION

4.1. BEHAVIOR OF STRENGTHENED WALLS AND CRACKS PATTERN

Reinforced concrete masonry walls generally behave in a flexural ductile mode comparing with URM as a result of their steel reinforcement. Load-deflection curves

under cyclic loading are plotted for all the eighteen test specimens, but due to lack of space, curves for only six specimens (to cover different parameters such as, type and amount of FRP, steel reinforcement ratio, masonry bond pattern and existence of compression FRP bars) are presented here for example in Fig.5. In order to study the effect of FRP composite on cracking load, stiffness and steel yielding load, the behavior of strengthened walls can be divided into approximately three segments. The first segment of the envelope varies linearly with a small deflection up to the first mortar crack. This segment represents the pre-crack segment. Insignificant effect of FRP bars on stiffness of this segment and only a little effect on cracking load were observed. The second segment is pre-yielding segment, its ends with yielding of the steel reinforcement in strengthened wall. This segment is recognized through the change of the slope. In general, the stiffness and the steel yielding load of strengthened walls were found be higher compared to the control specimen. The third segment of the load-deflection envelope is post-yielding segment. It begins with the yielding of steel and ends with either shear failure or debonding of FRP system. The load and deflection increased in a rate more than second stage due to high strength of FRP (responsible about increased capacity) and steel yielding (responsible about increased deflection). For the pre-crack phase, the load-deflection behavior for all strengthened and unstrengthened walls was similar. This behavior indicates that, the contribution of NSM FRP reinforcements was insignificant to increasing the stiffness in the elastic range. For post cracks phases, however, the flexural stiffness and strength of the strengthened reinforced walls were significantly improved compared with the unstrengthened reinforced wall and nonlinear behavior was observed up to failure.

The following section describes the cracks generated and crack development stages. The first flexural tensile crack was initiated at the block mortar in the maximum moment region (between two line loads) as a hair line crack. These cracks were developed at the mortar masonry unit interface and progressed upward into the grout. The deflection increased dramatically beyond these cracks in case of the unstrengthened walls. Further flexural tensile cracks developed during loading, beyond the cracking load / moment (M_{cr}). The FRP reinforcement that was encapsulated with an epoxy material caused cracks to propagate in the masonry units. The masonry cracks were oriented at 45^{o}. These cracks extended along the groove sides as the load increased. They developed in the CMU as a result of the epoxy's high tensile strength (when compared to the block unit's tensile strength). The factor that affects the crack pattern is the embedding material (epoxy vs. cementitious material). The cementitious material itself, however, cracked during loading. As a result, the embedding material deteriorated gradually and the failure, in general, is debonding. The cracks also moved vertically toward the compression face in a straight line, as illustrated in Fig. 6. Flexural shear cracks outside the constant moment region or spalled off the compression side of bed joint mortar at maximum moment section were generated in the later stages of loading.

The observations of the crack propagation have yielded insight about the relation between the crack patterns and the modes of failure for specimens strengthened using different embedding materials. The sudden failure of specimens strengthened with FRP and epoxy as adhesive material occurred due to cracks generated in the masonry unit along the groove side. Also, the gradual failure of specimens strengthened with FRP and cementitious material occurred due to cracks in the adhesive material itself.

4.2. LOAD-TENSILE STRAIN BEHAVIOR OF FRP BARS

The load-tensile strain behavior of the NSM FRP reinforcing bars and strips is linear up to cracking of the concrete block. At the onset of cracking, a significant increase in the measured tensile strain was observed for all tested walls measured by the strain gage attached to the NSM FRP reinforcing bars or strips. Based on steel bar strain gage, the steel bars yielded before failure of FRP bar or strip. At failure, the minimum measured tensile strain in the NSM FRP reinforcing bars prior to debonding was 1.08 %, which is 60 % of the rupture strain of the FRP reinforcing bar for NSM with epoxy as a paste material. The minimum debonding tensile strain for NSM with cementitious as a paste material was 1.3 % which is 72.5 % of the rupture strain of FRP bar. It's evident that the debonding strains for NSM FRP for unreinforced masonry walls according to ACI 440.7R is underestimated which is 35 % of rupture strain for circular bar with epoxy. Galati et al. 2006 present debonding strain 55% of rupture strain for circular bar with cementitious adhesive material. Griffith et al. (Griffith et al., 2013) found that $\varepsilon_{mesureed}/\varepsilon_{max}$ approximately 0.58 % for specimens strengthened using NSM FRP and subjected to out of plane load.

4.3. MODES OF FAILURE

This investigation present different modes of failure occurred during the test. One of the modes was flexure- shear through the concrete block, and the other mode was debonding of FRP reinforcement from the masonry substrate. The control specimen failed by yielding of the tension reinforcement, followed by concrete crushing (i.e., flexure failure) as shown in Fig.7a. The majority of the FRP bars still had masonry attached to the bars after failure in case of epoxy adhesive layer. That illustrates the

debonding failure surface is in the masonry material and not in adhesive layer or at the FRP- adhesive interface. On the other hand, the debonding failure surface in case of cementitious paste was at adhesive layer itself and the failure of this wall was intermediate crack IC debonding due to localized splitting of the embedding material as shown in Fig.7b. IC debonding describes the mechanism where the FRP bars deboned from the masonry starting at a flexural crack and then propagating away from the peak bending moment region where the first crack occurs towards the 'unloaded' end of the FRP bar (Konthesingha et al. , 2009; Willis et al. 2009b). Flexural-shear failure was observed in case of large amounts of FRP reinforcement. Flexural-shear failure starts with vertical crack at the bed joint of maximum moment region then the crack propagate with 45o orientation to the point of concentrated load as shown in Fig.7c.

4.4. BOND REDUCTION COEFFICIENT

The effective strain in FRP reinforcement should be limited to the strain level at which debonding may occur. The formulation for the effective strain level in the EB-FRP for concrete structures at ultimate ε_{fe} was expressed in the ACI 440.2R-08 as follows:

$$\varepsilon_{fd} = 0.41\sqrt{\frac{\grave{f_c}}{nE_f * t_f}} \leq 0.9\varepsilon_{fu} \qquad (1)$$

Bond reduction factor is defined as the ratio between the debonding strain ε_{fd} and ultimate rupture strain of FRP reinforcement ε_{fu}. For NSM system, the bond reduction factor ranged from 0.6 to 0.9. This factor depend on member dimension, steel and FRP reinforcement ratio, and surface roughness (Parretti & Nanni, 2004). ACI 440.7R- has

recommended this factor as 0.45 for EB-FRP and 0.35 for NSM-FRP in the current revised draft version. Moreover, (Barros etal., 2007) indicate that the bond reduction factor or (debonding dependent factor) $\frac{\varepsilon_{fd}}{\varepsilon_{fu}}$ for flexural members strengthened with NSM was decreased with an increase the equivalent reinforcement ratio $\rho_{l,eq}$, that can be obtained from the following equation:

$$\rho_{l,eq} = A_s/(b\,d_s) + (A_f E_f/E_s)/(bd_f) \quad (2)$$

The analysis found in the available experimental results of RC beams and slabs strengthened with NSM technique that the relation of the $\frac{\varepsilon_{fd}}{\varepsilon_{fu}}$ and $\rho_{l,eq}$ is contrary relationship and this relation has been represented by (Barros & Kotynia, 2008) as the following equation:

$$\frac{\varepsilon_{fd}}{\varepsilon_{fu}} = 0.9342 - 29.965\,\rho_{l,eq} \quad (3)$$

In this study, the same variable (equivalent reinforcement ratio) was considered to propose the bond reduction coefficient for masonry walls strengthened with NSM and subjected to out of plane loading. It can be observed that there is a contrary relationship between $\frac{\varepsilon_{fd}}{\varepsilon_{fu}}$ and $\rho_{l,eq}$, this relationship was expressed as follow in Eq. 4 and its consistence with the previous study that done for RC beams and slabs as shown in Fig. 8.

$$\frac{\varepsilon_{fd}}{\varepsilon_{fu}} = 1.17 - 60.3\,\rho_{leq} \leq 0.9 \quad (4)$$

The value of ε_{fd} obtained from Eq. 4 may be used in the design scheme of next version of ACI 440.7R guide as an upper limit of FRP strain instead of current constant value of 0.35 ε_{fu}.

4.4. DUCTILITY

Ductility of a structural element can be defined as its ability to sustain inelastic deformation without loss in load carrying capacity, prior to collapse. It's one of the important characteristics that give an indication of the presence of sufficient warning before catastrophic failure. There are many different ductility indices namely deflection, curvature or rotation were calculated as the ratio of the ultimate deformation to that at the first yielding of steel reinforcement. The ductility of strengthened wall is defined as the ratio of ultimate deflection at mid span to the mid span deflection at yielding of the longitudinal steel reinforcement $\mu = \frac{\Delta_u}{\Delta_y}$ (Priestley et al., 1996). In case of continuous load deflection curve with a descending branch, the deflection considered at the level of capacity 20% below the peak load (Priestley et al., 1996).

Ductility ratios were obtained by dividing the ductility indices by corresponding ductility index of virgin masonry wall. The relation between deflection ductility ratios and fiber axial stiffness (E_fA_f) for various specimens are presented in Fig. 9. It can be noted that as the axial stiffness increases, the ductilities of strengthened masonry wall decrease. The ductility of stack wall and running wall with cementitious bonding agents is about 41, 15% higher than the same running wall with epoxy bonding agent respectively.

4.5. DISCUSSION OF TEST RESULTS

The fiber reinforcement ratio must be normalized before any comparison due to different stiffness of each fiber type. In order to reflect the combination of amount of fiber and stiffness, the adjusted stiffness was introduced as a multiplication of reinforcement ratio by modulus of elasticity of the fiber for each specimen. The resulting number is normalized with respect to lowest value of adjusted stiffness as shown in Table 3. Based on literature, the flexural capacity of URM walls strengthened with FRP increased by an average 15 times the flexural capacity of the control specimen, while the maximum increase in flexural capacity of strengthened RM walls from this study was 2.36 times the control capacity due to existing steel reinforcement. It should be noted that the strengthening wall using one GFRP bar or two GFRP bars (normalized stiffness = 1 or 2) resulted in a 50 or 105 % increase in the ultimate load in comparison with that of the unstrengthened control reinforced wall respectively. In the case of strengthened wall with one or two carbon strip (normalized stiffness = 1.25 or 2.5) the percentage of increasing is 76% or 236 % respectively. The percentage of increase in flexural capacity for specimens strengthened with one or two carbon bar(s) [normalized stiffness = 2.68 or 5.37] is 115%, Comparing the results of testing specimen based on normalized stiffness show that, the doubling amount of fiber will result only 88% increasing in ultimate capacity. From Fig. 10, it can be concluded that the relationship between the amount of fiber in terms of axial stiffness and ultimate capacity is not one to one and there is an optimum amount of fiber that maintains the effectivity of strengthening technique. The optimum amount of fiber is represented by fiber reinforcement index and it is defined by

the axial stiffness ratio between fiber and masonry. When the fiber reinforcement index is greater than 0.45 %, a shear failure controls the mode of failure.

In order to make comparisons between tests performed for different specimens tested, load-deflection envelope (backbone) curves are plotted as shown in Fig. 11. The unstrengthened reinforced walls (control specimens) were failed in typical ductile behavior. This mode of failure is due to yielding of steel bars followed by crushing of concrete in maximum moment region. The corresponding deflection for these specimens was very large, also no shear cracks observer during the test. For strengthened specimens, the moment capacity and stiffness of the reinforced walls strengthened with FRP increased (as compared to the control specimen). Interestingly, the wall's capacity dropped to approximately a load level equivalent to the measured yielding load and the deflection kept on increasing and the capacity dropped until failure occurred. This is due to block unit cracking and damage accumulating after strengthening system failure occurred.

The general behavior of strengthened walls showed that the fiber reinforcement doesn't contribute greatly on the stiffness in pre-cracked phase as shown in Fig. 11. The stiffness of the strengthened walls increased significantly in comparison to the control wall in pre-yield phase due to the contribution from FRP reinforcement. The stiffness of specimens strengthened with CFRP and GFRP increased by 65% and 25 % respectively. This difference is determined by comparing the slope of the second segment (preyielding stage) of load - deflection curve for specimens as shown in Fig. 11a.

The FRP composite that was added as an NSM significantly increased the stiffness and out-of-plane load carrying capacity for strengthened specimens. In order to

evaluate the influence of fiber reinforcement ratio, all other variables were selected to be constant. From Fig 11b, the capacity increased by 76% comparing with the control wall in case of strengthening using one carbon strip. It was noticed that, doubling the fiber reinforcement ratio for carbon strip led to an increase of 136% in flexural strength, also the mode of failure changed from debonding to a shear-type failure. In case of flexural–shear cracks, the FRP bars debonds from masonry substrate due to out-of-plane differential displacement of the adjacent wall segments which happened as a result of shear force transmitted along crack side in the shear plane (Hamoushet al., 2002; Tumialan et al., 2003).

The masonry bond pattern effect is illustrated in Fig. 11c (effect of bond pattern). In terms of displacement ductility, The behavior of walls with stack bond pattern was more desirable than the behavior of the walls with running bond pattern. This behavior improved when the head joint was reinforced with an FRP bar. Therefore, the flexural strength and ductility can be improved significantly by adding a joint reinforcement to the stack bond walls. The specimen's width was 1.5 CMU. Therefore, the stack specimen after debonding behaved as two beams: a small (half CMU) beam and a large (full CMU) beam.

The effect of the mortar pattern is depicted in Fig. 11d (effect of mortar pattern). Mortar is typically placed on the face shell (in a face shell bedding pattern) or on the face and web shells (in a fully bedding pattern). In this study, the mortar pattern has no effect in term of flexural capacity and displacement ductility. The reason behind that is part of mortar expanded to the web shell after the CMU was laid. Also, the ratio of the web shell area to the net cross - section area for this specimen was kept small (approximately

=18%) to demonstrate this factor impact. Finally, the specimens were fully grouted with part of the grout extending to webs of the CMU. As a recommendation for studying this effect in the next series of studies, non-grouted or partially grouted specimens with a width dimension greater than 1.5 CMU are required. Both the GB3-2#4-C2R and GB3-2#4-C2RF specimens failed gradually as the cementitious material that was used as an embedding material cracked gradually during loading which is resulted in gradual drop of capacity comparing with sudden jump of the capcity of specimen strengthened with GFRP and epoxy as an adhesive agent.

The GB3-2#4-E2R and GB3-2#4-E2RW specimens shown in Fig.11e (effect of groove size) exhibited a similar mode of failure. There is no effect for increasing groove size from 2 to 3 times bar diameter since the splitting of the epoxy cover in the groove not occurred in case of regular groove size. Increasing groove size (its mean increase the thickness of epoxy) will reduce the shear stresses at masonry–epoxy interface and could lead to increase debonding load. (De Lorenzis & Nanni, 2002) reported that increasing the groove size and the cover thickness leads to higher bond strength when failure is controlled by splitting of the epoxy cover.

The effect of replacing epoxy with cementitious material was investigated. These results are illustrated in Fig.11f (effect of embedding material). An improved behavior was observed for the strengthening system using cementitious material instead of epoxy and this system is capable of achieving results competitive to the system with epoxy. Two observations were recorded for GB3-2#4-C2R and GB3-2#4-E2R specimens. The first observation was related to the mode of failure. Specimen GB3-2#4-C2R failed gradually as a result of the cementitious material comparing with sudden failure due to

existing of epoxy. The second observation was related to the moment capacity after the post-peak behavior occurred. The moment capacity of specimen GB3-2#4-C2R, after post – peak, was approximately the same as the control specimen's moment capacity. In contrast, the moment capacity of specimen GB3-2#4-E2R dropped rapidly under the capacity of the control specimen as a result of CMU damage after debonding of FRP bars. The specimen strengthened with FRP bonded with cementitious was failed by debonding of the bond material from the groove (the debonding failure surface in adhesive layer itself). The specimen strengthened with epoxy was failed by pullout of the FRP bar and concrete peeling off the block faceshell.

The change of reinforcement ratio affected the stiffness but had little effect on the ultimate strength since the stiffness depended on steel and FRP as shown in Fig.11g (effect of steel reinforcement ratio). FRP bars compensated for the change of reinforcement ratio due to the change in the mode of failure, so the FRP bars played the main role in the ultimate capacity of the reinforced masonry wall. The strengthening system will not improve the behavior of wall reinforced with one central steel bars 1#5 comparing with walls reinforced with 2 #3 or 2#4 bars. The uneven distribution of steel reinforcement and change in stiffness between the two segments of walls led to create a stress concentration in the concrete block, often initiating cracks that cause the sudden and brittle failure.

The compression fiber reinforcement has insignificant impact on the stiffness of the preyielding stage. The flexural capacity of specimens reinforced with two bars and epoxy material was increased by 11% comparing with strengthened wall without compression fiber reinforcement as illustrated in Fig.11h (effect of compression

reinforcement). Also the compression fiber reinforcement did not rupture or deboned from the compression face at any time during the load testing. At failure, the maximum measured compressive strain in the NSM FRP reinforcing bars prior to debonding was 0.2% which is 11% of the rupture strain of the FRP reinforcing bar. The fiber reinforcement acting in compression didn't affect the behavior of the wall other than, possibly, increasing the shear resistance of the specimen (Albert et al., 2001).

5. ANALYTICAL APPROACH

The analytical model of the moment capacity specified in Guide for the Design and Construction of Externally Bonded FRP Systems for Strengthening Concrete Structures (ACI 440.2R-08) was adopted. Based on this guideline, four assumptions were assumed in order to estimate the flexural capacity of reinforced masonry wall strengthened with FRP bars. (1) The distribution of strain is linear along the depth of the wall (compatibility of strain). (2) Masonry concrete block crushing is assumed to occur if the compressive strain reaches its maximum usable strain ($\varepsilon_{mu} = 0.0025$). Rupture of FRP bar is assumed to occur if the strain in the FRP bar reaches its design rupture strain ($\varepsilon_f = \varepsilon_{fu}$) before the block reaches its maximum usable strain. (3) The tensile strength of block and the tensile contribution of the epoxy were neglected. (4) Internal forces must be balanced with external forces to satisfy the equilibrium condition. FRP debonding or delamination can occur if the force in FRP bar cannot be sustained by the substrate.

5.1. STRESS-STRAIN RELATIONSHIP

The maximum usable strain ε_{mu} according to MSJC-13 was considered to be 0.0035 mm/mm (in./in.) for clay and 0.0025 mm/mm (in./in.) for concrete masonry. The

stress block parameters, β_1 and γ , associated with a parabolic distribution are assumed to be equal to 0.8 for simplicity (Tumialan et al., 2003).

5.2. DISTRIBUTION OF STRAIN WITHIN CROSS SECTION

In analyzing the flexure behavior of reinforced masonry wall, it's assumed that the concrete block will crack at the ultimate tensile strain. For cracked section, the entire tension load would be carried by two components: FRP and steel bars. It's assumed that plane section before loading remains plane after loading; that mean linear strain within the section. The relationship between the neutral axis depth and the strain for all components are given by:

$$\varepsilon_s = \varepsilon_{mu} \frac{d_s - c}{c} \tag{5}$$

$$\varepsilon_{fe} = \varepsilon_{mu} \frac{d_f - c}{c} \leq \varepsilon_{fd} \tag{6}$$

Where d_s and d_f are the effective depth of the tensile steel and FRP reinforcement respectively, ε_s and ε_{fe} are the tensile strain for steel and effective strain in the FRP reinforcement respectively, c is depth to the neutral axis. If the left side term governed this equation, then concrete masonry crushing would be the failure mode, otherwise FRP debonding would be the failure mode.

5.3. EQUILIBRIUM EQUATIONS AND ULTIMATE MOMENT CAPACITY

The forces induced due to bending as shown in Fig.12, these forces are derived in the following expressions:

$$C = \gamma\, f_m^- * \beta * c * b \quad (7)$$

$$T_s = A_s f_s \quad (8)$$

$$T_f = A_f f_{fu} \quad (9)$$

Where, C is concrete compression force at the centroid of the effective area of concrete, T_s and T_f are tension force at the centroid of steel and FRP reinforcement. A_s and A_f are the cross sectional areas of the longitudinal steel reinforcement and FRP, and b is width of a compression zone. In order to arrive at the ultimate strength, the trial and error procedure has been used. This procedure starts with assuming depth to the neutral axis then calculating the strain level in each material using the Eq. 5 and 6. If the fiber strain greater or equal to the ultimate fiber strain, concrete crushing controls flexural failure of the section. If the fibers strain less than the ultimate fiber strain, FRP failure controls flexural failure of the section.

The effective stress in FRP can be found from Eq. 10.

$$f_{fe} = E_f * \varepsilon_{fe} \quad (10)$$

The stress in the steel is determined from stress strain curve according to the Eq. 11.

$$f_s = E_s * \varepsilon_s \leq f_y \quad (11)$$

From the equilibrium equation, check the assumed depth of neutral axis c.

$$T_s + T_f = C \quad (12)$$

$$A_s f_s + A_f f_{fe} = 0.8\, f_m^- * 0.8 * c * b \quad (13)$$

$$c = \frac{A_s f_s + A_f f_{fe}}{0.64\, f_m^- * b} \quad (14)$$

The nominal flexural strength (M_n)of the section strengthened with NSM FRP is computed from the Eq. 15 or the value calculated from theoretical shear capacity when the fiber reinforcement index greater than 0.45%.

$$M_n = A_s f_s \left(d_s - \frac{\beta c}{2}\right) + A_f f_{fe} \left(d_f - \frac{\beta c}{2}\right) \quad (15)$$

5.4. VALIDITY OF ANALYTICAL APPROACH

To evaluate the applicability of the presented analytical approach, the theoretical ultimate capacity of reinforced walls has been calculated and compared with experimental results. The geometry, material properties, and strengthening details have been presented previously in Tables 1 and 2. Table 3 present the analytical and experimental results. The ratio M^{exp}/M^{the} for the walls failed in shear was determined based on bending moment associated with shear capacity. In general, the proposed approach predicts the wall strengths with reasonably good accuracy.

6. CONCLUSIONS

An experimental investigation was conducted to evaluate the performance and effectiveness of using NSM-FRP technique for strengthening reinforced masonry walls. Eighteen walls were constructed and tested as part of the experimental program. A design

approach was developed using the moment capacity method specified in ACI 440.2R-08. According to this research, the following conclusions can be drawn:

1- The strengthened reinforced masonry wall's (a non-arching wall) behavior was significantly dependent on the type of FRP used. A wall strengthened with GFRP had higher displacement ductility than the same wall strengthened with CFRP due to high stiffness of CFRP. The non-arching wall's capacity was increased when NSM was used to strengthen reinforced masonry walls. This capacity increase was between 150% for the specimen strengthened with one GFRP bar and 236% for the specimen strengthened with two carbon strips compared to the control wall. This increased capacity not necessarily in a proportional with increasing of FRP amount especially when mode of failure changed from debonding to shear failure.

2- Two basic types of failure modes were identified from the test results. The first was related to FRP debonding. The second was related to the concrete block unit (described herein as a shear-type failure). Shear failure was observed when the amount of FRP was large. The gradual failure of the specimens strengthened with a cementitious bonding material was observed comparing with a more sudden failure for specimen strengthened using an epoxy material.

3- In terms of ductility, the behavior of the specimen was improved significantly by adding a joint reinforcement to the walls in a stack bond pattern.

4- The compression fiber reinforcement has insignificant impact on the stiffness of the pre-yielding stage but flexural capacity of specimens reinforced with two bars and epoxy material was increased by 11% comparing with strengthened wall without compression fiber reinforcement. Also the maximum measured compressive strain in

the NSM FRP reinforcing bars was 0.2% which is 11 % of the rupture strain of the FRP reinforcing bar.

5- The change of reinforcement ratio affected the stiffness but had little effect on the ultimate strength since the stiffness depended on the steel and FRP. The behavior of the wall with 1#5 steel bar was brittle due to stress concentration that initiate cracks and led to sudden failure.

6- The suggested design approach may be used effectively for computing the flexural capacity of reinforced masonry walls strengthened with NSM-FRP.

ACKNOWLEDGEMENTS

The authors wish to acknowledge the support of Midwest Block & Brick in Jefferson City, Missouri and Hughes Brothers in Seward, Nebraska and HCED (The Higher Committee for Education Development in Iraq). The authors also wish to thank the technical support staff in not only the Department of Civil and Environmental Engineering but also the Center for Infrastructure Engineering Studies (CIES) at Missouri University of Science and Technology for their efforts in this research study. Any opinions, findings, conclusions, and recommendations presented in this paper are those of the authors and do not necessarily reflect the views of the sponsor or supporting agencies.

TABLES AND FIGURES

LIST OF TABLES:

LIST OF FIGURES:

Table 1- Wall specimen description

Wall	Specimen Designations	FRP Type	Steel bars	Embedment material	FRP bars	Wall bond pattern	Mortar pattern	Groove dimension (mm*mm)
1	Control- 2#4-R	-	2#4	-	-	running	fully bedding	-
2	Control-2#4-S	-	2#4	-	-	Stack	fully bedding	-
3	Control- 2#3-R	-	2#3	-	-	running	fully bedding	-
4	CS3-2#4-E1R	carbon strip	2#4	Epoxy	1	running	fully bedding	17.8*25.5
5	CS3-2#4-E2R	carbon strip	2#4	Epoxy	2	running	fully bedding	17.8*25.5
6	CB3-2#4-E1R	carbon bar	2#4	Epoxy	1	running	fully bedding	19*19
7	CB3-2#4-E2R	carbon bar	2#4	Epoxy	2	running	fully bedding	19*19
8	GB3-2#4-E1R	glass bar	2#4	Epoxy	1	running	fully bedding	19*19
9	GB3-2#4-E2R	glass bar	2#4	Epoxy	2	running	fully bedding	19*19
10	GB3-2#4-E2Rw	glass bar	2#4	Epoxy	2	running	fully bedding	31.75*25.5
11	GB3-2#4-C2R	glass bar	2#4	cementitious	2	running	fully bedding	19*19
12	GB3-2#4-E2S	glass bar	2#4	Epoxy	2	stack	fully bedding	19*19
13	GB3-2#4-E2SF	glass bar	2#4	Epoxy	2	stack	face shell bedding	19*19
14	GB3-2#4-C2RF	glass bar	2#4	cementitious	2	running	face shell bedding	19*19
15	GB3-2#3-E1R	glass bar	2#3	Epoxy	1	running	fully bedding	19*19
16	GB3-1#5-E1R	glass bar	1#5	Epoxy	1	running	fully bedding	19*19
17	GB3-1#5-E2R	glass bar	1#5	Epoxy	2	running	fully bedding	19*19
18	GB3-2#4-E1R2	glass bar	2#4	Epoxy	1	running	fully bedding	19*19

Conversion: 1-in. = 25.4 mm

Table 2- Mechanical Properties of masonry wall components and steel bars

Material	Properties	values (MPa)	Method
Concrete block	Prism compressive strength	21	ASTM C1314-
Type S mortar	Compressive strength	17.5	ASTM C109-13
Grout	Compressive strength	35	ASTM C109-13
Cementitious-based material	Compressive strength	59.1	ASTM C109-13
Steel bar	Yield strength	471	ASTM A370-13
	Modulus of Elasticity	20300	

Conversion: 1 psi = 6.89 kPa

Table 3- Mechanical properties of FRP bars

Type of FRP	Dimension (mm)	Average maximum tensile strength (MPa)	Average maximum strain % (mm/mm)	Average modulus of elasticity (GPa)
Aslan 500 CFRP tape	4.5x16	1965	1.5	124
Aslan 200 CFRP bar	10	2172	1.75	124
Aslan 100 GFRP bar	10	827	1.79	46

Conversion: 1-in. = 25.4 mm; 1 psi = 6.89 kPa

Table 4- Comparison between experimental and analytical results

$No.$	$Specimen$	$Adjusted\ stiffness\ \rho_f E$	$Normalized\ stiffness\ \frac{\rho_f E_f}{\rho_f E_f)_{min}}$	$Moment\ M^{exp}\ kN.m$	$Moment\ M^{the}\ kN.m$	$\frac{M^{exp}}{M^{the}}$	$Shear\ V^{exp}\ kN$	$Shear\ V^{the}\ kN$	$Mode\ of\ failure$
1	Control R2#4	-	-	9.55	8.42	1.13	21	54	flexure
2	Control S2#4	-	-	8.66	8.42	1.03	19	54	flexure
3	Control R2#3	-	-	6.35	4.8	1.32	14	54	flexure
4	CS3-2#4-E1R	7.31	1.25	16.83	21.46	0.78	36.82	54	debonding
5	CS3-2#4-E2R	14.63	2.5	22.67	24.63	0.92	49.6	54	shear failure
6	CB3-2#4-E1R	15.71	2.68	20.54	24.63	0.833	45	54	shear failure
7	CB3-2#4-E2R	31.43	5.37	20.43	24.63	0.83	44.7	54	shear failure

Table 4- Comparison between experimental and analytical results (cont.)

8	GB3-2#4-E1R	5.85	1.0	14.35	15.14	0.94	31.4	54	debonding
9	GB3-2#4-E2R	11.7	2.0	19.52	24.63	0.79	42.7	54	shear failure
10	GB3-2#4-E2Rw	11.7	2.0	18.81	24.63	0.76	41.14	54	shear failure
11	GB3-2#4-C2R	11.7	2.0	14.93	19.32	0.77	32.67	54	debonding
12	GB3-2#4-E2S	11.7	2.0	18.30	19.32	0.94	40	54	debonding
13	GB3-2#4-E2SF	11.7	2.0	17.51	19.32	0.9	38.35	54	debonding
14	GB3-2#4-C2RF	11.7	2.0	15.36	19.32	0.79	33.58	54	debonding
15	GB3-2#3-E1R	5.85	1.0	14.35	12.76	1.12	31.38	54	debonding
16	GB3-1#5-E1R	5.85	1.0	9.35	14.35	0.65	20.46	54	debonding
17	GB3-1#5-E2R	11.7	2.0	14.28	18.75	0.76	31.25	54	debonding
18	GB3-2#4-E1R2	5.85	1.0	15.76	19.32	0.81	34.47	54	debonding

Conversion: 1 kip = 4.45 kN; 1 kip-ft = 1.356 kN-m

(a) (b)

Figure 1. Experimental program: (a) Construct walls and (b) Installation of FRP strip in grooves

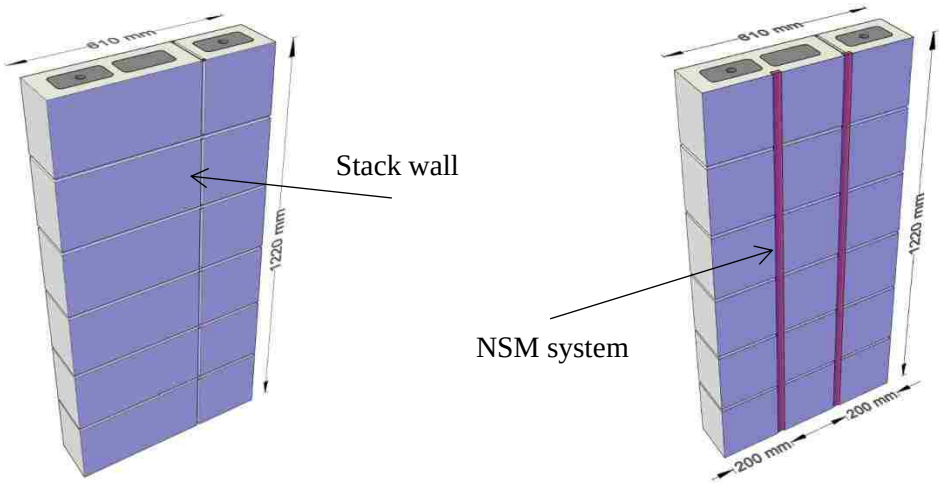

(a) (b)

Figure 2. Test specimens: (a) stack pattern, (b) strengthened wall

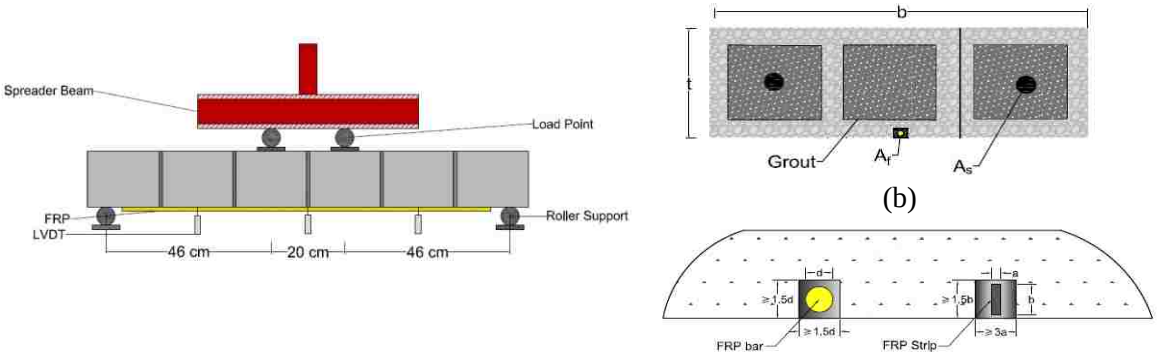

(a) (b) (c)

Figure 3. Specimen details: (a) four point load setup, (b) wall cross-section, (c) NSM groove dimension

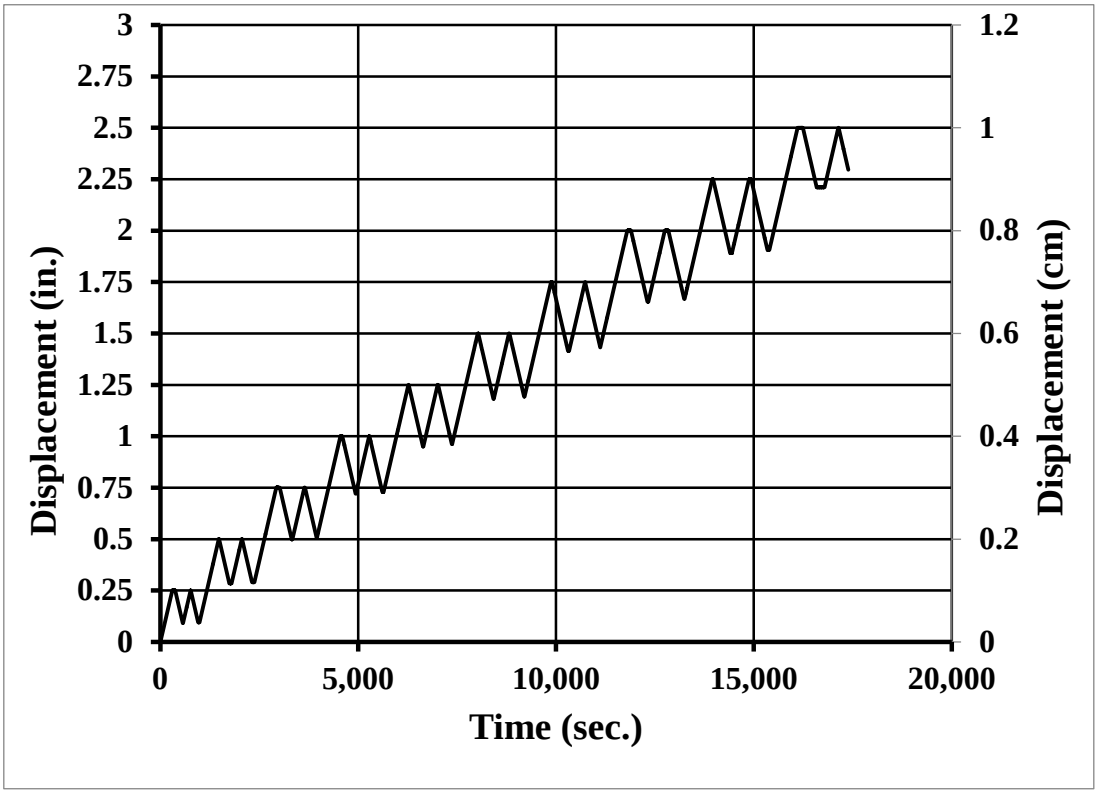

Figure 4. Cyclic loading protocol

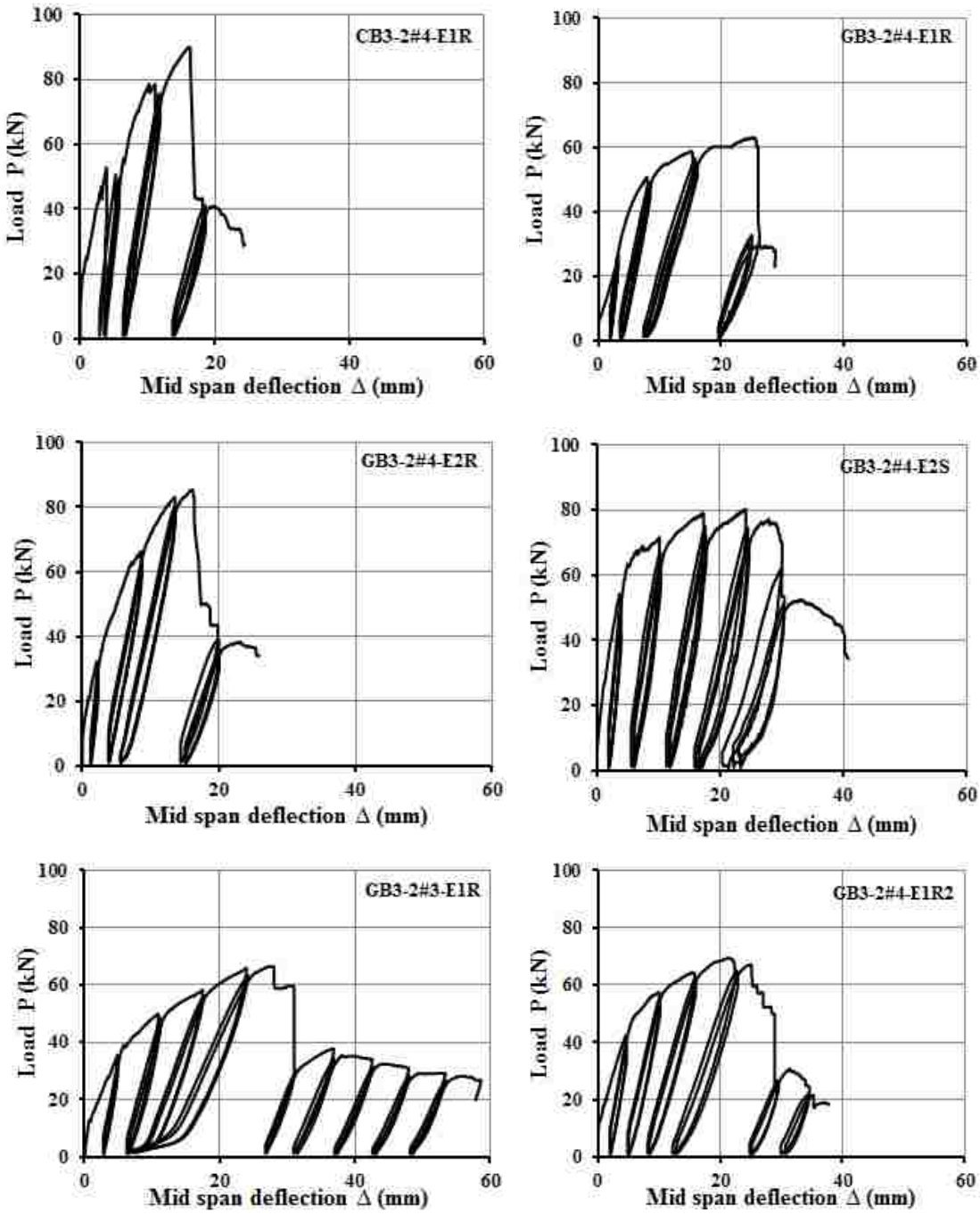

Figure 5. Cyclic-load deflection curve for strengthened walls

(a) (b) (c) (d)

Figure 6. Crack development during load testing (a) block mortar crack, (b) masonry unit cracks, (c) flexural cracks , (d) flexure shear cracks

(a) (b) (c)

Figure 7. Observed modes of failure: (a) flexural failure, (b) debonding of FRP bar, (c) flexural-shear failure

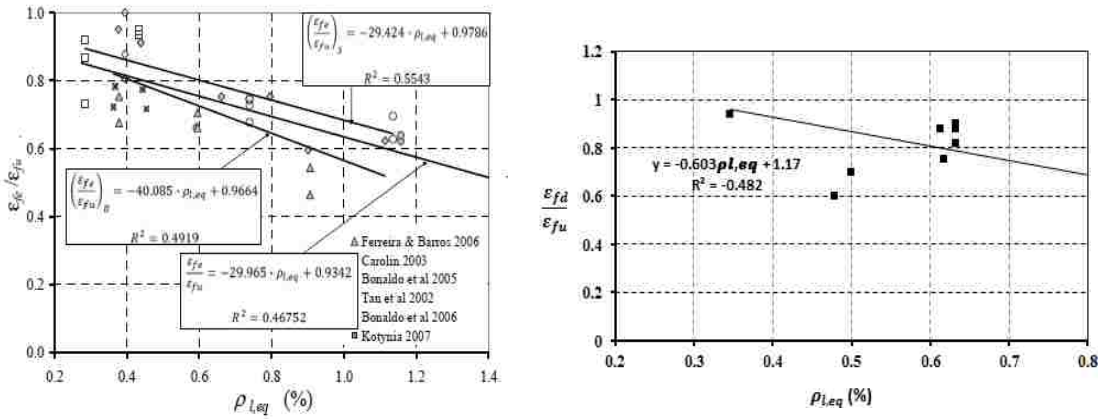

(a) (b)

Figure 8. Debonding dependent factor vs. equivalent reinforcement ratio:(a) RC beams and slabs (Barros & Kotynia, 2008) (b) reinforced masonry walls

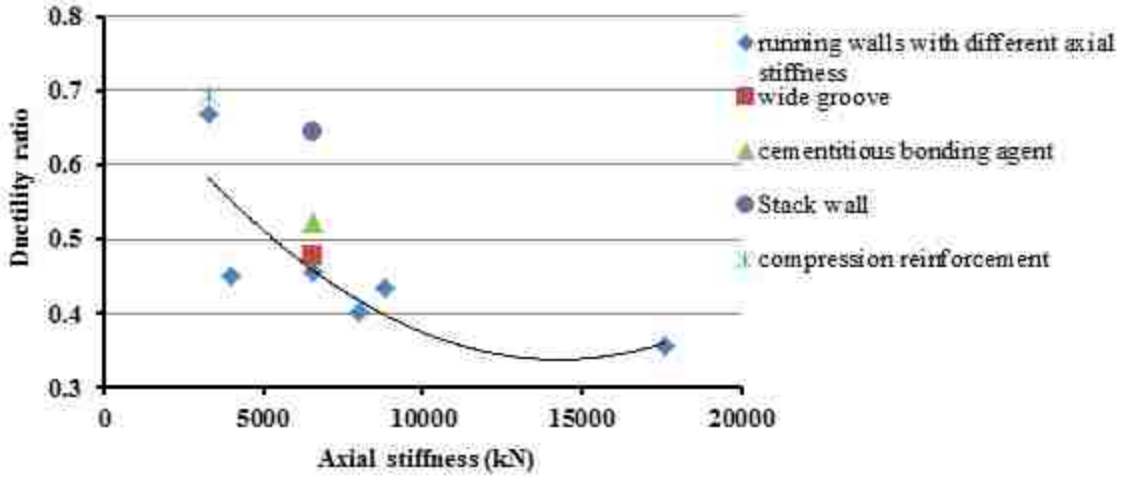

Figure 9. Ductility vs. axial stiffness of strengthened walls

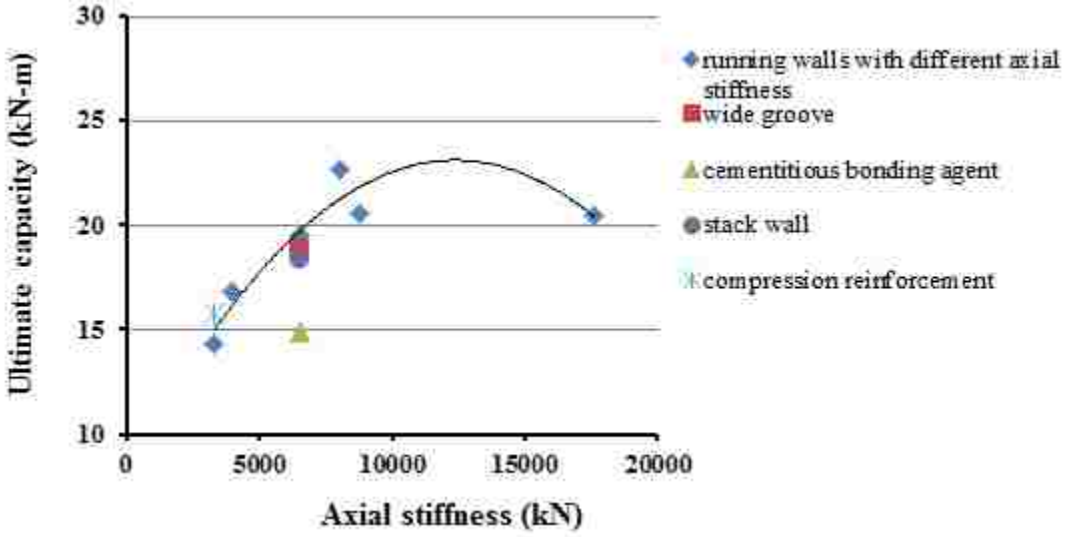

Figure 10. Ultimate capacity vs. axial stiffness of strengthened walls

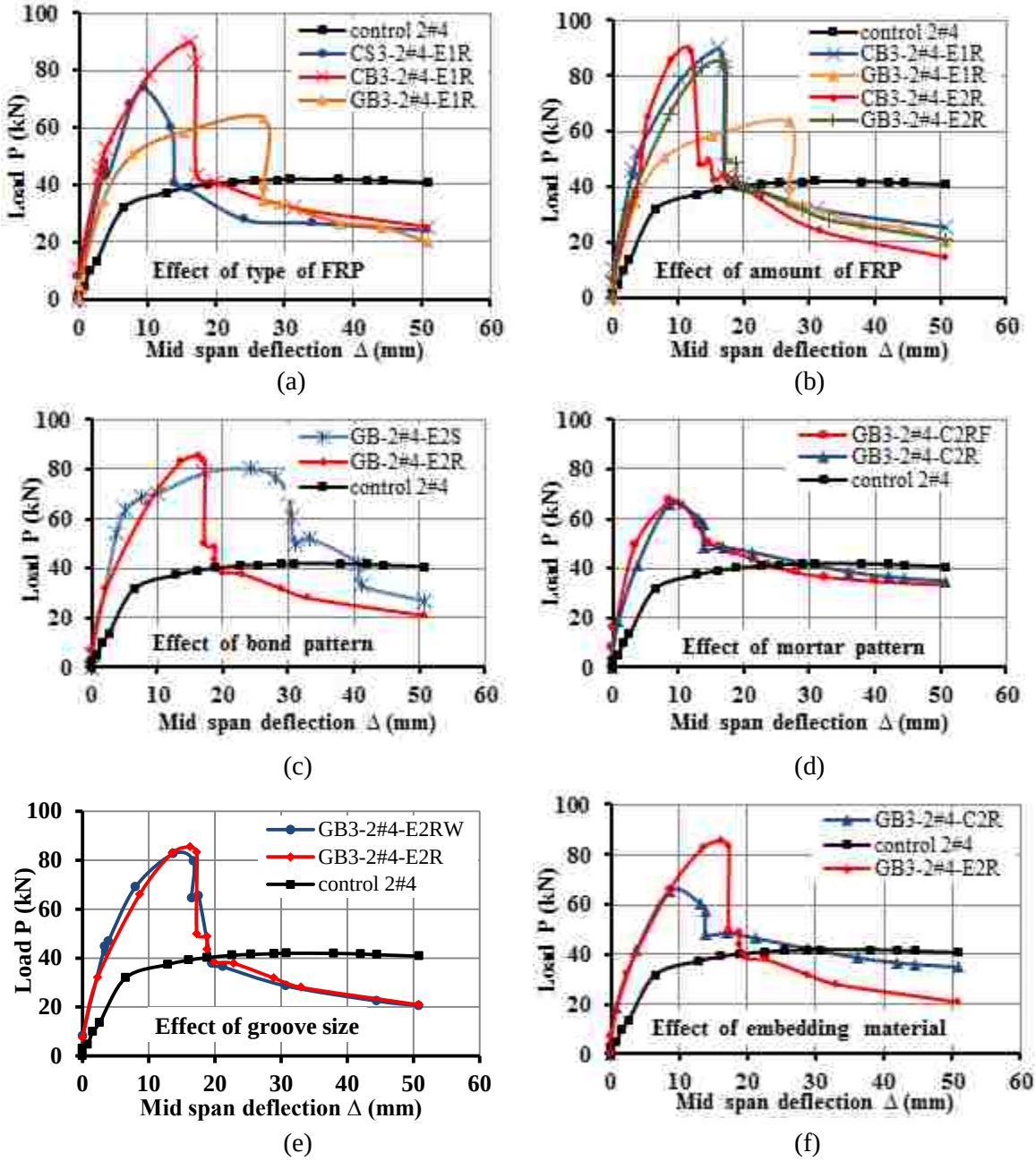

Figure 11. Load verses deflection curves for test specimens

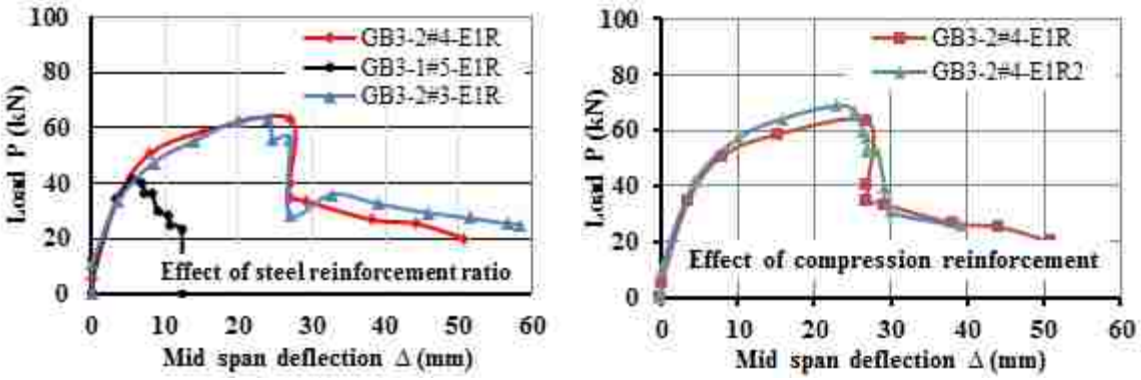

(g) (h)

Figure 11. Load verses deflection curves for test specimens (cont.)

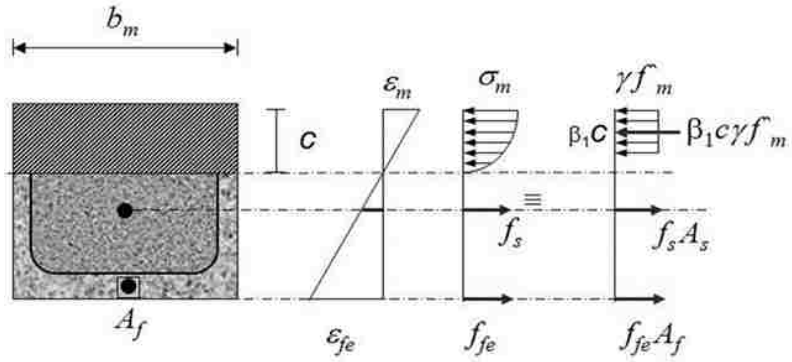

Figure 12. Flexure analysis of reinforced masonry walls strengthened with NSM

APPENDIX

The following symbols are used in the paper:

A_f = cross sectional area of the longitudinal FRP reinforcement, in.^{2} (mm^2)

A_s = cross sectional area of the longitudinal steel reinforcement, in.^{2} (mm^2)

C = compression force at the centroid of the effective area of concrete, lb. (kN)

E_f = design or guaranteed modulus of elasticity of FRP defined as mean modulus of sample of test specimens, psi (MPa)

E_s = modulus of elasticity of steel, psi (MPa)

M_n = nominal moment capacity, lb-in. (N-mm)

M^{exp} = experimental moment capacity, lb-in. (N-mm)

M^{the} = theoretical moment capacity, lb-in. (N-mm)

T_f = tensile force at the centroid of FRP, lb. (kN)

T_s = tensile force at the centroid of steel, lb. (kN)

a = depth of equivalent rectangular compression block, in. (mm)

b = width of the beam, in. (mm)

c = distance from the extreme compression fiber to the neutral axis, in. (mm)

c_b = distance from the extreme compression fiber to neutral axis at balanced strain condition, in. (mm)

d_s = dist. to the c.g.s. of the steel in the tension zone, in. (mm)

d_f = dist. to the c.g.s. of the FRP in the tension zone, in. (mm)

ε_f = tensile strain in the FRP, in./in. (mm/mm)

ε_{fe} = effective tensile strain in the FRP, in./in. (mm/mm)

ε_s = tensile strain in the steel, in./in. (mm/mm)

ε_{mu} = maximum usable strain in the masonry, in./in. (mm/mm)

$\hat{f}_c$ = compressive strength of the concrete, psi (MPa)

f_s = allowable stress in the steel reinforcement, psi (MPa)

f_{fe} = bar stress that can be developed for embedment length l_e, psi (MPa)

f_{fu} = design tensile strength of FRP, considering reductions for service environments, psi (MPa)

f_m'' = compressive strength of the masonry, psi (MPa)

n = number of plies of FRP reinforcement

γ = multiplier of f'_m to determine the intensity of an equivalent rectangular stress distribution for masonry

β = ratio of distance from neutral axis to extreme tension fiber to distance from neural axis to center of tensile reinforcement

μ = displacement ductility, in./in. (mm/mm)

Δ_u = ultimate deflection at mid span, in. (mm)

Δ_y = mid span deflection at yielding of the longitudinal steel reinforcement, in. (mm)

REFERENCES

ACI 440.7R-10 (2010), "Guide for the Design and Construction of Externally Bonded FRP Systems for Strengthening Masonry Structures", Reported by ACI Committee 440.

ACI 440.2R-08 (2008), "Guide for the Design and Construction of Externally Bonded FRP Systems for Strengthening Concrete Structures", Reported by ACI Committee 440.

Al-Jaberi, Z., Myers, J. J., & ElGawady, M. (2015). Influence of Near-Surface Mounted (NSM) FRP on the Out-of-Plane Behavior of Reinforced Masonry Walls. Paper presented at the 12th North American Masonry Conference.

Albert, M. L., Elwi, A. E., & Cheng, J. R. (2001). Strengthening of unreinforced masonry walls using FRPs. Journal of Composites for Construction, 5(2), 76-84.

Barros, J. A., Dias, S. J., & Lima, J. L. (2007). Efficacy of CFRP-based techniques for the flexural and shear strengthening of concrete beams. Cement and Concrete Composites, 29(3), 203-217.

Barros, J. A., & Kotynia, R. (2008). Possibilities and challenges of NSM for the flexural strengthening of RC structures.

De Lorenzis, L., & Nanni, A. (2002). Bond between near-surface mounted fiber-reinforced polymer rods and concrete in structural strengthening. ACI structural Journal, 99(2), 123-132.

De Lorenzis, L., Nanni, A., & La Tegola, A. (2000a). Bond of Near Surface Mounted FRP Rods in Concrete Masonry Units. Paper presented at the Proceedings of the Seventh Annual International Conference on Composites Engineering (ICCE/7), Denver, Colorado, July.

De Lorenzis, L., Tinazzi, D., & Nanni, A. (2000b). Near surface mounted FRP rods for masonry strengthening: bond and flexural testing. Paper presented at the Proceedings of the international conference on composite engineering.

Galati, N., Tumialan, G., & Nanni, A. (2006). Strengthening with FRP bars of URM walls subject to out-of-plane loads. Construction and Building Materials, 20(1), 101-110.

Gilstrap, J. M., & Dolan, C. W. (1998). Out-of-plane bending of FRP-reinforced masonry walls. Composites Science and Technology, 58(8), 1277-1284.

Griffith, M. C., Kashyap, J., & Ali, M. M. (2013). Flexural displacement response of NSM FRP retrofitted masonry walls. Construction and Building Materials, 49, 1032-1040.

Hamoush, S., McGinley, M., Mlakar, P., & Terro, M. J. (2002). Out-of-plane behavior of surface-reinforced masonry walls. Construction and Building Materials, 16(6), 341-351.

Hochwalt, J., & Amrhein, J. (2012). Reinforced Masonry Engineering Handbook: Masonry Institute of America and International Code Council, Torrance, CA, USA.

Konthesingha, K., Masia, M., Petersen, R., & Page, A. (2009). Bond behaviour of NSM FRP strips to modern clay brick masonry prisms under cyclic loading| NOVA. The University of Newcastle's Digital Repository.

Nanni, A., & Tumialan, J. G. (2003). Fiber-reinforced composites for the strengthening of masonry structures. Structural engineering international, 13(4), 271-278.

Parretti, R., & Nanni, A. (2004). Strengthening of RC members using near-surface mounted FRP composites: Design overview. Advances in Structural Engineering, 7(6), 469-483.

Petersen, R. B., Masia, M. J., & Seracino, R. (2009). Bond behavior of near-surface mounted FRP strips bonded to modern clay brick masonry prisms: influence of strip orientation and compression perpendicular to the strip. Journal of Composites for Construction.

Priestley, M. N., Seible, F., & Calvi, G. M. (1996). Seismic design and retrofit of bridges: John Wiley & Sons.

R-06, A. (2006). Guide for the Design and Construction of Concrete Reinforced with FRP Bars (ACI 440.1 R-06). American Concrete Institute, Detroit, Michigan.

Stone, D., Tumialan, G., Nanni, A., & Parretti, R. (2002). Near-surface mounted FRP reinforcement: application of an emerging technology. Concrete, 36(5).

Tumialan, G., Tinazzi, D., Myers, J., & Nanni, A. (2000). Field evaluation of unreinforced masonry walls strengthened with FRP composites subjected to out-of-plane loading. Paper presented at the 2000 Structures Congress, American Society of Civil Engineers, Philadelphia, Pennsylvania.

Tumialan, J. G., Galati, N., Namboorimadathil, S. M., & Nanni, A. (2002). Strengthening of masonry with FRP bars. Paper presented at the 3rd. Int. Conf. on Composites in Infrastructure (ICCI 2002).

Tumialan, J. G., Galati, N., & Nanni, A. (2003). FRP strengthening of UMR walls subject to out-of-plane loads. ACI Structures Journal, 100(3), 312-329.

Willis, C., Kashyap, J., & Griffith, M. (2009a). Flexural behaviour of NSM CFRP retrofitted masonry wallettes under static and cyclic loading. Paper presented at the International Symposium on FRP Reinforcement for Concrete Structures (9th: 2009: Sydney, Australia).

Willis, C., Seracino, R., & Griffith, M. (2010). Out-of-plane strength of brick masonry retrofitted with horizontal NSM CFRP strips. Engineering Structures, 32(2), 547-555.

Willis, C., Yang, Q., Seracino, R., & Griffith, M. (2009b). Bond behaviour of FRP-to-clay brick masonry joints. Engineering Structures, 31(11), 2580-2587.

II. EVALUATION OF FRP AND FRCM COMPOSITES FOR THE STRENGTHENING OF REINFORCED MASONRY WALLS

Zuhair Al-Jaberi, John J. Myers and Mohamed A. ElGawady

ABSTRACT

There are large numbers of existing buildings around the world and in North America especially in California have been constructed with reinforced masonry since 1930s. These old reinforced masonry walls have not been improved to meet the current standards. Current ACI 440.7R reported as Guide for Design & Construction of externally bonded FRP System for Strengthening Unreinforced Masonry Structures. This document does not address strengthening of existing reinforced masonry structures (i.e. with steel reinforcement). The principle objective of this study was to determine and discuss the failure mechanism as well as to investigate the flexural behavior of reinforced masonry walls strengthened with externally bonded system and subjected to out-of-plane cyclic loading. This will be evaluated by comparing the flexural capacity and ability to sustain large deflection of specimens strengthened with different strengthening systems. In addition, the effect of specific parameters on the flexural response of reinforced masonry wall was investigated including: type and amount of fiber and masonry bond pattern. This study aimed to develop a database of experimental test results to validate the design model presented in next version of ACI 440.7R document. The performance of twelve strengthened masonry specimens was investigated. The strengthening systems that used in this study are fiber reinforced cementitious matrix (FRCM) and fiber reinforced polymer (FRP) technique. Two reinforced walls constructed in running and stack bond pattern were reinforced with 2 No. 4 steel bars and investigated as control specimens. The

other specimens were strengthened using different types and amount of fibers. These simply supported walls were tested in four-point bending with an effective span of 1.12 m (44-in.) between the supports under an out-of-plane cyclic load at a rate 1.27 mm/min (0.05-in./min). The test results indicated that the flexural behavior of reinforced masonry walls strengthened externally by FRP may be controlled by either FRP rupture or debonding (intermediate crack or plate end debonding failure). The flexural behavior of reinforced masonry walls strengthened externally by FRCM may be controlled by either fiber slippage or debonding.

1. INTRODUCTION

Most of the strengthening design guides are limited to unreinforced masonry (URM) structures due to the lack of experimental studies related to reinforced masonry (RM) structures. There are large numbers of existing reinforced masonry structures around the world in need for strengthening. The effectiveness of fiber reinforced polymer (FRP) systems for the repair and strengthening of masonry structures have been proven for upgrading capacity (Al-Jabari, Myers, & ElGawady, 2015; Al-Jaberi, Myers, & ElGawady, 2015). The attractive features of FRP are high strength to weight ratio, maintenance free, corrosion resistant and ease of installation.

Externally bonded FRP is one of the retrofitting techniques that has been adopted for strengthening masonry structures. Hamilton III and Dolan (2001) presented the results of unreinforced concrete masonry walls strengthened with glass FRP composite oriented perpendicular to the masonry bed joints. The simply supported walls were subjected to out-of- plane uniform distributed load result from air-bag system. The GFRP composite increased load-carrying capacity approximately equivalent to the capacity provided by 1

#5 reinforcing bar spaced at 610 mm (24-in.) placed in the center of the wall. GFRP fracture and delamination corresponding to a drift ratio of approximately 1.6% were identified as modes of failure during this test. Tan and Patoary (2004) investigated the out-of-plane capacity of unreinforced masonry walls strengthened using EB and subjected to static laboratory load. The flexural capacity increased when the thickness of FRP was increased and different modes of failure were observed including premature debonding, punching shear, crushing of brick in compression or FRP rupture. The feasibility of using GFRP for masonry walls subjected to reverse cyclic loading was conducted (Ehsani, Saadatmanesh, & Velazquez-Dimas, 1999). Different densities of glass fabric were investigated. As a result of this study, tensile failure is controlled mode of failure and the strengthened walls capacity increased up to 32 times the weight of the wall corresponding to deflection 2% of the wall height. Mosallam [5] studied the out-of-plane behavior of unreinforced masonry walls strengthened with FRP composite. The results of this study confirmed that the FRP is an effective technique for strengthening. The mode of failure was due to the combination of compression failure followed by cohesive failure. The cyclic behavior of unreinforced masonry walls strengthened using glass fiber reinforced polymers (GFRPs) was investigated (Kalali & Kabir, 2012). These experimental tests demonstrate the ability of GFRPs to significantly improve strength, deformation capacity, and energy absorption in addition to keep the bricks together and maintain wall unit integrity. Although epoxy adhesive was approved as an effective bonding agent in many structural applications for strengthening, it may not be an optimal choice for other applications due to some disadvantages. These include hazardous poor behavior of epoxy at the glass transition temperature, incompatible with the masonry

surface, prohibited to be applied on damp surface, toxic fumes emission, moisture impermeability and flammability (Al-Abdwais & Al-Mahaidi, 2016; Al-Jabari et al., 2015; Hashemi & Al-Mahaidi, 2008). In order to overcome these drawbacks of FRP and epoxy system, FRCM has emerged as an alternative technique.

FRCM is a relatively new strengthening system has almost the same advantages of FRP system such as high strength to weight ratio, corrosion resistant and ease of installation in addition to overcome some of the drawbacks specially the fire resistance issue. Since cementitious material is more cost effective and preserves better the appearance of the original wall comparing with epoxy, it is more attractive and promising for strengthening of masonry structures (Turco, Secondin, Morbin, Valluzzi, & Modena, 2006). Many attempts have been carried out to use cementitious material as a bonding agent for strengthening unreinforced masonry (URM) walls for both NSM and externally-bonded (EB) systems. A new strengthening technique has recently been developed that uses fabric-reinforced cementitious matrix (FRCM), also known as textile-reinforced mortar (TRM) and textile-reinforced concrete (TRC). Retrofitting of URM concrete or clay brick walls with FRCM under uniformly distributed lateral load was investigated (Babaeidarabad & Nanni, 2015). An enhancement in flexural capacity of range 2.7-7.8 compared to unstrengthened specimens was reported. Based on fiber reinforcement ratio, two modes of failure were identified including flexure and shear failure. Unreinforced masonry walls strengthened with TRM and subjected to cyclic out-of-plane loading have also been investigated (Papanicolaou, Triantafillou, Papathanasiou, & Karlos, 2008). The effectiveness of TRM overlays was evaluated in comparison to that provided by FRP in the form of overlays or near-surface mounted (NSM) reinforcement.

It was concluded that TRM overlays provide substantial increase in strength and ductility. Compared with FRP, TRM may result in generally higher effectiveness in terms of strength and ductility. NSM strips offer lower strength but higher ductility due to controlled debonding. From the results obtained the authors concluded that TRMs comprise an extremely promising solution for the structural upgrading of masonry structures under out-of-plane loading.

In the current study, the behavior of reinforced masonry walls strengthened externally with FRP or FRCM system was investigated with emphasis on the load-deflection response, pre-yield stiffness, crack pattern and mode of failure mechanism. The motivation of this investigation is associated with the important of FRCM as an effective strengthening system and as an alternative technique for strengthening masonry structural elements. To achieve this goal, a total of twelve reinforced masonry walls, two as reference specimens and two sets of five specimens strengthened with EB FRP or FRCM system using different types and amount of fiber were constructed and tested. This paper presents the response and discussion of the behavior of these walls based on cyclic load-displacement curves.

2. RESEARCH SIGNIFICANCE

This paper focused on comparing the effectiveness and performance of reinforced masonry (RM) walls strengthened in flexure using externally bonded fiber reinforced polymer (EB FRP) and fiber reinforced cementitious matrix (FRCM) systems examining several variables. The effectiveness and contribution of fiber reinforced composite on improving the flexure strength, stiffness of reinforced masonry walls in addition to identify potential failure modes of the strengthened system is investigated through

experimental investigation. The study also aims to develop a database of experimental test results to help in validation of the design model presented in the next version of the ACI 440.7R document. The study attempts to fill some of the gaps in knowledge that have not been considered in current literature.

3. EXPERIMENTAL INVESTIGATION

This work represents a portion of a large research program conducted on the strengthening reinforced masonry walls using different strengthening techniques. Table 1 provides an overview of the strengthened walls, materials and systems, masonry bond pattern, and width of fabric sheet. This study considered 12 reinforced masonry walls specimens divided in three groups. In the first group, two specimens were designed as control and it's constructed in running and stack bond pattern. In the second group, five specimens were strengthened with EB composite (unidirectional E-glass fabric with an epoxy matrix and a CFRP laminate). In the third group, a total of five specimens were prepared and strengthened with FRCM composite, two specimens were strengthened by a carbon FRCM system and three walls are strengthened using a PBO FRCM system. Figure 1 illustrates control and strengthening systems. The main parameters considered in this study were:

• The overall effects of FRP and FRCM flexural strengthening of the reinforced masonry walls.

• The type and reinforcement ratio of fiber in different strengthening systems, carbon vs. glass in EB FRP and PBO vs. carbon in FRCM.

• The type of masonry wall bond pattern, running vs. stack.

3.1. DESCRIPTION AND CONSTRUCTION OF THE SPECIMENS

Reinforced masonry specimens were constructed with the same overall dimensions and longitudinal main reinforcement. Each specimen was constructed using 152.5 mm (6-in.) standard masonry blocks in running and stack bond pattern and type S mortar. The nominal dimensions of the walls were 1220 mm (48-in.) height by 610 mm (24-in.) length. The steel reinforcement was constant for all specimens (2#4) bars and the walls were fully grouted, which occurred four days after construction to preclude damage to the mortar joints during the vibration process.

3.2. STRENGTHENED SPECIMEN DESIGNATION

The specimen ID consisted of two parts as shown in Table 1. The first part represented fiber information (type and width). The first character identified the fabric types, namely C for carbon fiber, G for glass fiber, and PBO for Polypara-phenylene-benzo-bisthiazole fiber. The second character referenced the layer width. The second part of the ID identifies the number of layers and the wall bond pattern, S for stack and R for running bond.

3.3. MATERIAL CHARACTERIZATION

All the components of the reinforced masonry walls were tested to determine each material's mechanical properties. The properties of the materials that were used to construct the specimens are summarized in Table 2. The manufacturing properties of fiber and its bonding adhesive for both systems are presented in Table 3.

3.4. LOADING RATE AND TEST SETUP

The strengthened reinforced masonry specimens were tested under four-point bending, with simply supported boundaries as shown in Figure 2. An MTS double-acting hydraulic jack with a push-pull capacity of 620 kN (140 kips) was used to apply a vertical load on the specimen. The load was transferred to the masonry specimen by means of continuous steel plates and bars along the full width of specimens providing two equal line loads. A piece of thick rubber sheet was placed at all interfaces between the steel plate and specimen. The rubber distributed the load evenly and minimized any stress concentration due to unevenness of the wall surface. The distance between these two lines was 200 mm (8-in.). The load was applied in cycles of loading and unloading, as a displacement control, at a rate of 1.27 mm/min (0.05-in./min). The displacement amplitude increment was 6.35 mm (0.25-in.); double half loading cycle was applied for each amplitude level as illustrated in Figure 3. Displacements at the mid and third spans were measured using three Linear Variable Displacement Transducers (LVDTs) at each side. In addition, strain gauges were installed on the steel reinforcing and fiber to measure their strains during loading. It may be noted that in previous testing of FRP strengthened URM walls, an airbag was used to apply uniform load to the test walls adjacent to a vertical strong wall as the boundary element. However, because this testing program focused on FRP strengthened RM walls; airbag loading was not an option due to the wall capacity with the added internally fully grouted steel reinforcing.

4. STRENGTHENING PROCEDURE

The first step in the strengthening procedure is surface preparation, which includes cleaning the masonry surface manually with a wire brush to remove all

excessive mortar from the walls joints that were left from the construction process. The prepared surfaces were vacuumed after brushing to remove the residual dust. For EB FRP, Tyfo S epoxy resin mixed with silica fume to provide a putty filler layer that smoothed and leveled the prepared surface before composite material was installed. The purpose of using a putty layer is to fill in any irregularities on the surface and to prevent suction of the epoxy resin (Carney & Myers, 2003). The SEH51 fabric was saturated with Tyfo S epoxy resin before it was applied to the wall. The saturation process ensured good bonding with the substrate. The Tyfo S epoxy resin was mixed at a volume ratio of 100 parts A to 42 parts B. The epoxy was applied at room temperature [21°C (70°F)] between the minimum [4°C (40°F)] and maximum [38°C (100°F)] installation limits. The curing period for Tyfo S epoxy resin is three days at 60°C (140°F). SikaDur 30 adhesive used to bond the Aslan 400 CFRP strip. SikaDur30 mixed with a volume proportion of one part of component B to three parts of component A. The FRP sheet or laminate bonded to the tension face of the wall so that the fiber was perpendicular to the bed joints.

The procedure of FRCM strengthening was consisted of applying first layer of cementitious matrix with a nominal thickness of approximately 5 mm (0.2-in.) on the bottom surface of the specimen. 1- Ply of precut fabric was laid on the cementitious matrix, and then second layer of cementitious matrix with a nominal thickness of 5 mm (0.2-in.) was applied on the fabric. The procedure was repeated in case of multi-ply strengthening. It must be noted that mortar type x750 used with specimen strengthened with PBO, while mortar type x25 used with carbon strengthening system. All the strengthening procedures are shown in Figure 4.

5. EXPERIMENTAL TEST RESULTS AND DISCUSSION

The summary of the ultimate load, deflection, and stiffness for the three groups of twelve reinforced masonry walls are illustrated in Table 4. The cyclic load versus deflection curves for EB FRP and FRCM strengthened reinforced masonry walls are shown in Figure 5. The control specimens failed in crushing of concrete masonry unit in a compression zone as expected. The ultimate load for running and stack specimens were 41.8 kN (9.4 kips) and 38.18 kN (8.5 kips) respectively. The ductile behavior was observed and no sudden drop in the load due to existence of steel reinforcement bars.

The strengthened masonry walls achieved a higher load capacity due to high tensile strength of the fiber attached to the masonry substrate. The maximum ultimate loads were equal to 125.6 kN (28.2 kips) and 82.73 kN (18.6 kips) for masonry wall strengthened with 2 layers of GFRP and 2 layers CFRCM sheets respectively. The enhancement of flexural capacity is the ratio between the flexural capacity of strengthened wall and control specimen. The maximum enhancement was found to be 200 and 98% for masonry walls strengthened with 2 layers of GFRP sheets and 2ply of CFRCM respectively.

5.1. LOAD-DEFLECTION BEHAVIOR

Based on load-deflection curves under cyclic loading the behavior of strengthened walls can be divided into approximately three segments and that consistence with typical tri-linear idealized stress-strain behavior proposed by Jesse et al. 2008 (Jesse, Will, Curbach, & Hegger, 2008). The first segment is uncracked portion which controlled by the bed joints mortar properties and independent of strengthening system or main steel reinforcement. The load-deflection varies linearly up to the first mortar crack. Little

effect on cracking load was observed due to insignificant contribution of strengthening systems to the moment of inertia of the uncracked section in this stage.

The second portion is pre-yielding or (post crack) portion; it corresponds to the formation of cracks in bed joint mortar or concrete masonry unit in the critical bending moment region. This stage ends with yielding of steel reinforcement and the behavior of strengthened specimen is linear-elastic recognized through the change of stiffness. The stiffness of this part of the envelope depends on the volume proportion of the fibers and quality of the bond at fiber-bonding agent interface (Butler, Mechtcherine, & Hempel, 2010). The yield load increased for the strengthened wall comparing with control specimen.

The third phase is the post-yielding stage, where the existing fine cracks propagate and become wider up to failure caused either by rupture, debonding or slippage of the fabric from the matrix. Regardless of the type of failure, the effect of strengthening system can be noticed as the ultimate load capacity is expected to be higher than the unstrengthened specimen. Comparing with the second stage, the load and deflection increased due to high strength of fabric (responsible about increased capacity) and steel yielding (responsible about increased deflection). This phase is affected by a number of factors including presence of anchorage system, masonry bond pattern, fiber volume fraction and type of fabric. The general behavior of walls strengthened with FRCM system is a ductile behavior because of gradual loss of composite action due to slippage or debonding failure. The debonding mechanism is governed by the matrix/fiber interface. Sudden loss of composite was observed for specimen strengthened with EB FRP. The debonding mechanism generally happened in masonry substrate.

5.2. STIFFNESS AT PRE-YIELD STAGE

There is an insignificant effect of strengthening systems on initial stiffness of strengthened walls; however, the stiffness changes considerably at the pre-yield stage. At the pre-yield stage stiffness of strengthened specimen is greater than its corresponding control specimen. This higher stiffness is attributed to high modulus of fibers attached to the strengthened masonry wall and engagement at that stage. For comparison purpose, pre-yield stiffness, Kc, was normalized by dividing the fiber equivalent axial stiffness ($E_f * \rho_f$) where $\rho_f = Nb\ A_f/bd_f$ (see Table 4).

In these expressions: E_f =elastic modulus of fiber, ρ_f = fabric reinforcement ratio, N = number of fiber layer, b = width of the fiber layer, A_f = equivalent area of fabric per unit width, and d_f = effective depth of the fabric. Based on equivalent axial stiffness, the normalized pre-yield stiffness is presented in Table 4. From the results, it's clear that the type of fiber is not the only factor that affects the stiffness of the strengthened masonry wall. In one test wall case, a specimen strengthened with one ply of PBO was intentionally anchored by extended the PBO fiber sheet beyond the two supports (to fully anchor the sheet under the support and simulate a highly effective anchoring scenario) to study the effect of anchorage regardless of the specific type of anchorage system. This specimen presented a high pre-yield stiffness approximately the same pre-yield stiffness of specimen strengthened with two layers of PBO fiber without anchorage. The other factor that affects the pre-yield stiffness is fabric bond agent. Although the fiber axial stiffness of specimen strengthened externally with two layers of GFRP is approximately 36% of the corresponding axial stiffness of the specimen strengthened with PBO, the pre-yield stiffness for this specimen is more than double

compared to the corresponding specimen strengthened with PBO fiber. The reason behind this performance is the excellent bond characteristics of the epoxy compared to the cementitious material used in the FRCM system. The same reason is also valid when one compares the specimen strengthened with GFRP and specimen strengthened with CFRP laminate. The increase in stiffness is a function of fiber axial stiffness; however, the relation is not one to one. Doubling the fiber reinforcement ratio for carbon in FRCM system led to an increase in the pre-yield stiffness by 58%. For the EB FRP system, the pre-yield stiffness is increased by 61% when doubling the fiber reinforcement ratio of carbon fiber rather close when comparing to the FRCM system.

5.3. EXPERIMENTAL OBSERVATIONS AND MODES OF FAILURE

Reinforced concrete masonry walls generally behave in a flexural ductile mode due to steel reinforcement. The first observation is the formation of a flexural tensile crack initiated in the maximum moment region at the mortar bed joint with propagation upward in the grout. As the load increased beyond the cracking load, further flexural tensile cracks extend stepwise within the concrete masonry unit CMU. The control specimen failed as a large opening in the mortar bed joint occurred at a constant moment area associated with a crushing of masonry unit in compression zone. This occurred after yielding of steel reinforcing bar. It was also observed that the strengthening system affected the propagation of cracks within CMU.

The crack pattern for the specimen strengthened with one layer of PBO or carbon fiber in FRCM system as well as the control specimen was nearly identical. For these specimens cracks developed through the matrix and were also observed on the external surface of the matrix, which result in a fiber slippage failure. The specimen strengthened

with one ply of PBO with anchorage the PBO fiber sheet beyond the two supports [PBO(380)-1R] exhibited a fiber/matrix slippage initiated within the constant moment area and extends to the end of composite in gradual nature of failure. The normal and shear stresses increased as the number of FRCM layers increased and that resulting in debonding of the external matrix layer and fibers. It should be mentioned that in all specimens strengthened with FRCM system there was no part of masonry substrate attached to the composite after failure and post-test inspection. For all specimens strengthened with a single layer of PBO fabric, the failure was due to the slippage at the interface fiber/cementitious matrix. The failure was gradual with large slip values recorded at the fiber/matrix interface while negligible slips values were recorded at the cementitious matrix/concrete interface (Ombres, 2015).

For the specimens strengthened with EB FRP system, flexural cracks in the maximum moment region as well as shear cracks outside this region developed by increasing the applied load beyond the cracking load. The flexural cracks developed in masonry units strengthened with EB FRP were relatively wider than the cracks developed in masonry units strengthened with FRCM. The masonry cracks were oriented parallel to the bed joints. Cracks also extended along the FRP length due to high stress in this region. The mode of failure of specimen strengthened with one layer of GFRP was FRP rupture. The mode of failure was changed from debonding to shear failure in case of strengthening using 2 layers of GFRP. FRP debonding was the mode of failure of the specimens strengthened with CFRP laminate. The debonding failure in all its forms, whether intermediate crack (IC) or plate end-debonding failure generally happened in the masonry substrate. A strong adhesive between the GFRP and masonry would prevent the

debonding failure between the adhesive and concrete masonry or between the adhesive and FRP. Images reflecting the typical modes of failure for both systems are shown in Figure 6.

6. EVALUATION THE EFFICINCY OF STRENGTHENING SYSTEMS

The strengthening systems (EB FRP and FRCM) were evaluated for the application of reinforced masonry walls based on the effect of different parameters. Type and amount of fiber reinforcement ratio in addition to the effect of masonry bond pattern were considered in this evaluation. In order to ensure an equivalent comparison, the fiber axial stiffness was normalized to the lowest value.

6.1. EFFECT OF TYPE AND AMOUNT OF FIBER

Normalized axial stiffness was used to compare different strengthening systems as shown in Table 4. Normalization to a single layer GFRP ($k^f = 1880$ kN) yielded the following proportions for different fibers in different strengthening systems: for the EB FRP system, the specimen strengthened with CFRP is equivalent approximately to $5k^f$, while in the FRCM system, the specimen strengthened with one layer PBO or carbon are equivalent to $2.7k^f$or $3.9k^f$ respectively. Although the axial stiffness for the specimen strengthened with GFRP is less than other specimens, the flexural capacity of this specimen presented comparatively higher gains in load capacity than the other strengthened specimens. The reason behind that is the excellent bond of Tyfo S epoxy resin that used with GFRP compared with Sika Dur30 used with CFRP or cementitious material used in FRCM system. Material The load carrying capacity for strengthened specimen is affected by fiber axial stiffness and perfect bond of bonding agent. Increasing

the amount of fiber reinforcement ratio led to increase the gain in load capacity for the strengthened specimen using same bonding agent. The backbone load-displacement curves of walls strengthened with different types of fibers and different numbers of layers are compared in Figure 7. The effect of type of fiber for EB FRP and FRCM systems are shown in Figure 7a and 7b respectively. The load carrying capacity increased by double for specimen strengthened with two layers of GFRP while it increased by 85 % for the specimen strengthened with 2 strips of CFRP laminate. Using silica fume mixed with Tyfo S epoxy resin in specimens with GFRP reduced the porosity of the concrete unit and increased its compressive strength. The specimens with GFRP and epoxy resin showed a better behavior and higher gains in load capacity than the specimens with CFRP and SikaDur30 due to the epoxy's high debonding strain compared with SikaDur30.

The normalized fiber axial stiffness of the PBO fiber ($2.7k^f$) is approximately 71% of the carbon fibers ($3.9k^f$). The specimen strengthened with one ply of PBO was intentionally anchored; this specimen exhibited a high percent of gain in load capacity comparing with specimen strengthened with one ply carbon. Also, in terms of the maximum moment capacity, the specimen's strengthened with 2 layers of PBO or carbon fiber presented approximately the same moment capacity as shown in Figure 7b. This is due to improved bond performance for PBO compared to the carbon in FRCM system which is consistent with the conclusions of many studies (D'Antino, Carloni, Sneed, & Pellegrino, 2014; Jabr, 2017).

The effect of amount of fiber reinforcement ratio for EB FRP and FRCM systems are illustrated in Figure 7c and 7d. As expected, the flexural capacity increases as the number of layers increases (increased fiber reinforcement ratio). Doubling the fiber

reinforcement ratio in the EB CFRP system led to gains in ultimate load from 31 to 98%. In the case of the carbon FRCM system, doubling the fiber reinforcement ratio led to gains in ultimate load from 38 to 85%. For the same strengthening system, the relationship between fiber reinforcement ratio and flexural capacity is a proportional relationship with an optimum limit, but not one to one.

6.2. EFFECT OF MASONRY BOND PATTERN

In masonry construction, a running bond pattern is the most common type compared to stack bond pattern because it provides better interlocking of the masonry structural elements. The flexural strength of stack bond walls can be increased significantly by the use of bond beams or joint reinforcement (Committee, 1999).

The behavior of stack bond walls can be improved significantly by strengthening the continuous head joint. From Figure 8a and 8b it can be seen that strengthened stack wall can be designed to the same flexural capacity as running bond construction. The flexural strength and ductility can be improved significantly by continuing the fiber sheet over the head joint in the stack bond walls. After debonding, the stack bond specimen strengthened with EB GFRP behaved as two elements: a small (half CMU) beam and a large (full CMU). This behavior of the wall is due to the small width of GFRP sheet [200 mm (8-in.)], which is not enough to maintain continuity of the two elements to resist the load as a one unit. The strength capacity for the stack specimen was improved by 115% and 98% after strengthening using EB GFRP and PBO FRCM systems respectively. It is noteworthy that the initial stiffness for both the running and stack specimens was the same, but reduced in value for the stack specimen due to a crack formation in the continuous head joint.

7. SUMMARY AND CONCLUSIONS

An experimental study was conducted to evaluate and compare the flexural behavior of reinforced masonry walls strengthened with EB FRP or FRCM system. Twelve specimens were constructed and tested through this experimental program. Based on this investigation, the following conclusions are presented:

- Test results indicated that EB FRP and FRCM systems remarkably increase the flexural capacity of reinforced masonry walls. Moreover, the strengthening systems were effective in enhancing the stiffness of the strengthened walls.

- The load carrying capacity increased by double for the specimen strengthened with two layers of GFRP [G(200)-2R] while it increased by 85 % for specimen strengthened with 2 strips of CFRP laminate [C(50)-2R] due to the high debonding strain of epoxy used with GFRP. The specimen's strengthened with 2 layers of PBO [PBO(380)-2R and PBO(380)-2S] or carbon fiber [C(610)-2R] presented approximately the same moment capacity due to better bond performance for PBO compare to bond of the carbon in FRCM system.

- The strength capacity for the wall of stack bond pattern was improved by 115% in case of strengthening using EB FRP [G(200)-1S], while it improved by 98% in the case of strengthening using FRCM system [PBO(380)-2S]. For the FRCM system, the wall strengthened in a stack bond pattern can be designed to be as ductile as running bond construction.

- The pre-yielding stiffness for strengthened specimen is affected by fiber axial stiffness and fabric bond agent. For the same bonding agent, the increase in

stiffness of a strengthened specimen is a function of the fiber axial stiffness, but the relationship does not appear to be one to one.

- The failure mode was identified from the test results as a FRP rupture for specimens strengthened with one layer of GFRP or FRP debonding for specimens strengthened with CFRP laminate. The mode of failure changed from a debonding mode to a shear failure mode in the case of strengthening using 2 layers of GFRP so in a design strengthening application, the shear capacity would need to be considered and enhanced as warranted to prevent a primary brittle failure mode in shear. For the FRCM system, a slippage failure was identified for the specimen strengthened with one layer, while a debonding failure was reported for specimens strengthened with multiple layers.

ACKNOWLEDGEMENTS

This research was conducted at Missouri University of Science and Technology in the Structural Engineering Research Laboratory (SERL) in Rolla, Missouri. The authors gratefully wish to acknowledge the support of Midwest Block & Brick in Jefferson City, Missouri, Hughes Brothers in Seward, Nebraska, Sika USA Corporation, Ruredil S.p.A., San Donato Milanese, Italy and HCED (The Higher Committee for Education Development in Iraq). The authors also wish to thank the technical support staff at Missouri University S&T for their efforts in this research study.

TABLES AND FIGURES

LIST OF TABLES

LIST OF FIGURES

Table 1-Experimental test matrix for both strengthening systems

Wall	Strengthening system	Specimen ID	Type of FRP	Thickness of layer (mm)	Number of layers	Bond Pattern
1		Control-R	-	-	-	running
2		Control-S	-	-	-	stack
3	**EB FRP**	G(200)-1R	Glass	1.3	1	running
4		G(200)-1S	Glass	1.3	1	stack
5		G(200)-2R	Glass	1.3	2	running
6		C(50)-1R	Carbon	1.4	1	running
7		C(50)-2R	Carbon	1.4	2	running
8	**FRCM**	PBO(380)-1R	PBO	10	1	running
9		PBO(380)-2R	PBO	10	2	running
10		PBO(380)-2S	PBO	10	2	stack
11		C(610)-1R	Carbon	10	1	running
12		C(610)-2R	Carbon	10	2	running

Note: 1.0 mm=0.039-in.

Table 2-Results of the material properties

Material	Properties	Values (MPa)	Method
Concrete block	Prism compressive strength	21	ASTM C1314-12
Mortar type S	Compressive strength	17.5	ASTM C109-13
Grout	Compressive strength	35	ASTM C1019-13
Mortar x750	Compressive strength	35	ASTM C109-13
Mortar x25	Compressive strength	15	ASTM C109-13
Steel bar	Yield strength Modulus of Elasticity	471 203,000	ASTM A370-13

Note: 1.0 MPa = 145 psi.

Table 3-Mechanical properties of fiber and epoxy bonding adhesive

Material	Thickness (mm)	Ultimate tensile strength (MPa)	Elongation at break % (mm/mm)	Tensile Modulus (MPa)	Method
SHE-51 composite (E-glass)	1.3	575	2.2	26,100	ASTM D3039-14
Aslan 400 CFRP Strip	1.4	2400	1.87	131,000	ASTM D3039-14
PBO fiber	0.05	5800	2.15	270,000	ASTM D3039-14
Carbon fiber	0.05	4800	1.8	240,000	ASTM D3039-14
SikaDur 30	-	24.8	1	4482	ASTM D638-14
Tyfo S epoxy	-	72.4	5	3180	ASTM D638-14

Note : 1.0 GPa = 145.03 ksi; 1.0 MPa = 0.145 ksi; 1.0 mm/mm = 1.0-in./in.; 1.0 mm = 0.039-in.

Table 4-Summary of test results

Specimen ID	Ultimate load (kN)	Maximum deflection (mm)	Post-crack stiffness= K_c (kN/mm)	Normalized stiffness = $K_c/(E_f * \rho_f)$ (kN/mm)	Fiber axial Stiffness $k^f = E_f * A_f$ (kN)	Normalized fiber axial stiffness k^f	Gain in ultimate load* (%)	Mode of failure [a]
Control-R	41.8	61.72	4.812	-	-	-	-	C
Control-S	38.18	41.65	4.48	-	-	-	-	C
G(200)-1R	88.8	17.50	20.89	1.25	1880	k^f	112	R
G(200)-1S	82.2	13.46	14.07	0.84	1880	k^f	115	D
G(200)-2R	125.6	23.87	23.51	0.703	3758	$2k^f$	200	Sh
C(50)-1R	57.85	50.8	12.70	0.038	9170	$4.9k^f$	38	D
C(50)-2R	77.25	7.11	20.45	0.031	18,340	$9.8k^f$	85	D
PBO(380) -1R	75	83	11.12	0.463	5143	$2.7k^f$	79	S
PBO (380) -2R	79.22	11.94	10.72	0.22	10,287	$5.4k^f$	89.5	D
PBO (380) -2S	75.44	8.05	10.07	0.21	10,287	$5.4k^f$	97.5	D
C(610) - 1R	54.71	8.63	8.58	0.40	7320	$3.9k^f$	31	S
C(610) - 2R	82.73	61.72	13.62	0.32	14,640	$7.8k^f$	98	D

Notes: *Gain in ultimate load ratio= (failure load of the strengthened wall _ failure load of the control wall)/failure load of the control wall.

[a] Mode of failure designated by C = crushing of masonry, R = rupture of fiber, D = debonding, Sh = shear failure, S = slippage of fiber within cementitious matrix.

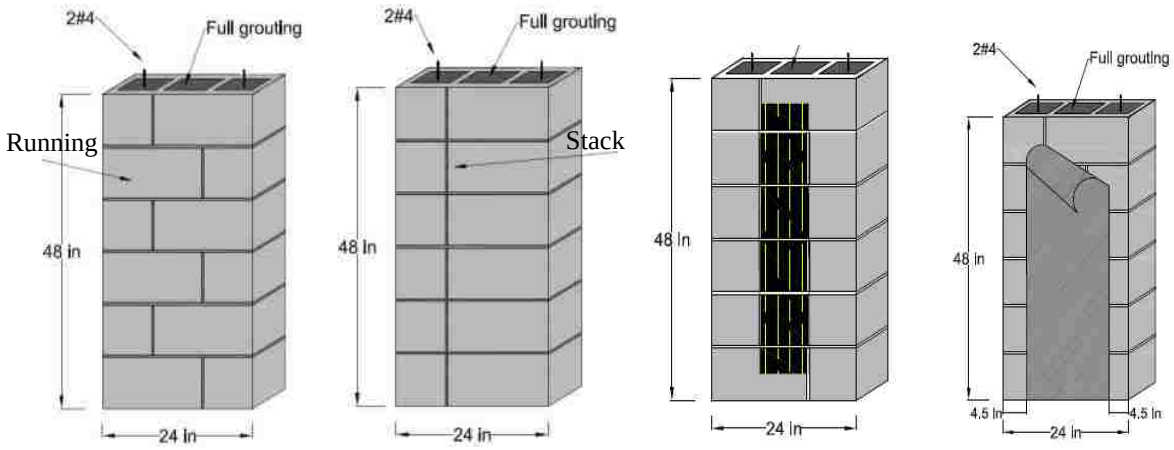

(a) Running bond (b) Stack bond (c) EB GFRP (d) PBO FRCM

Figure 1. Wall configuration and strengthening technique

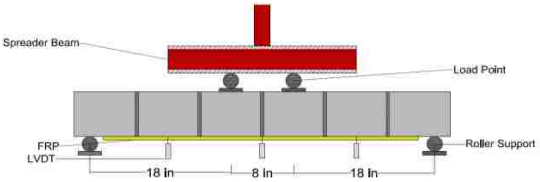

Figure 2. Four point load test set-up

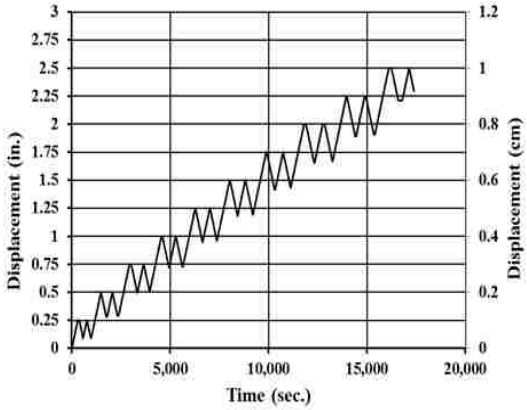

Figure 3. Loading protocol

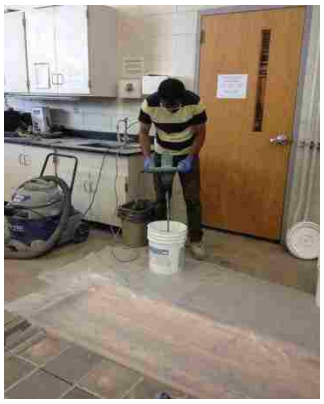

Mixing two part of epoxy

Saturate fiber in epoxy

Apply saturated sheet on wall

Preparing cementitious matrix

Apply matrix on wall

Apply fiber on matrix

Figure 4. Strengthening procedure for EB FRP and FRCM systems

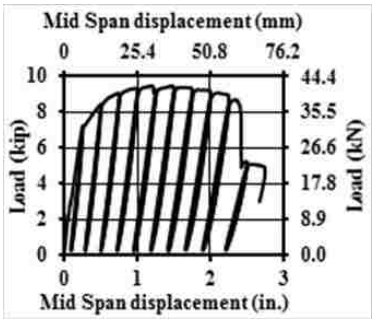

Control-R

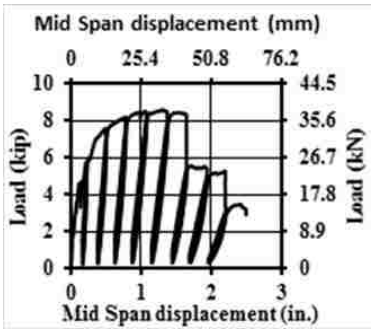

Control-S

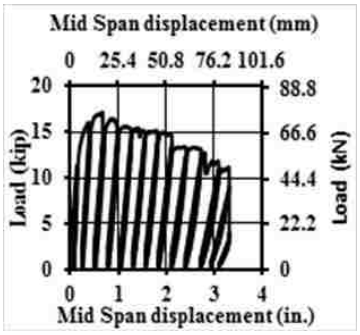

PBO(380)-1R

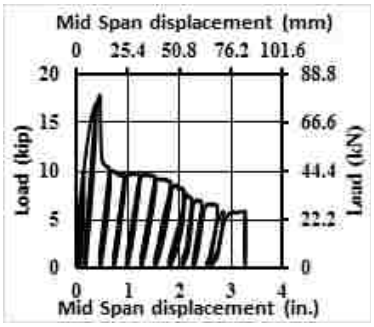

PBO(380)-2R

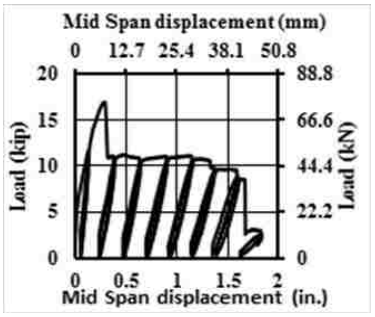

PBO(380)-2S

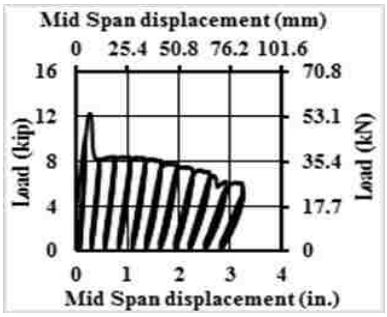

C(610)-1R

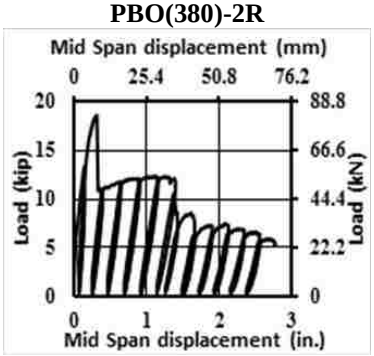

C(610)-2R

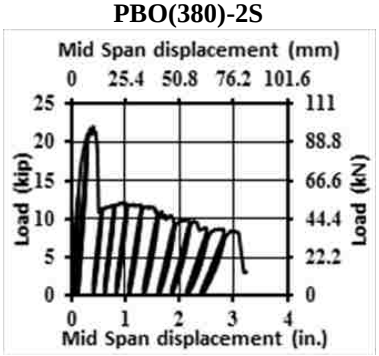

G(200)-1R

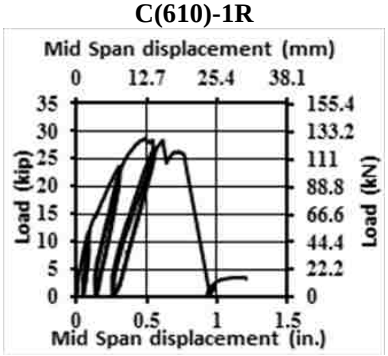

G(200)-2R

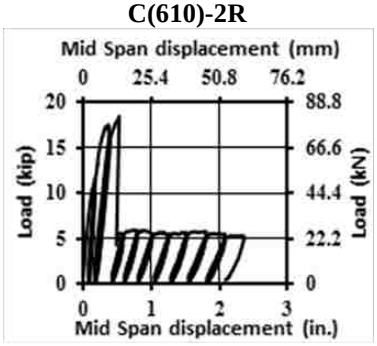

G(200)-1S

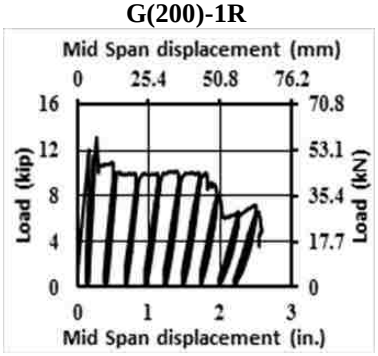

C(50)-1R

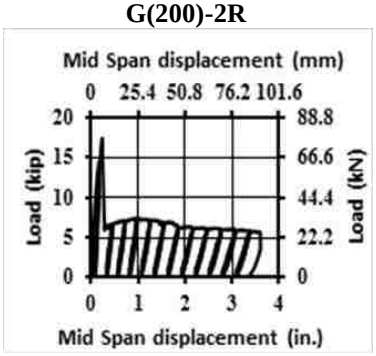

C(50)-2R

Figure 5. Load-deflection curves

Figure 6. Typical mode of failures

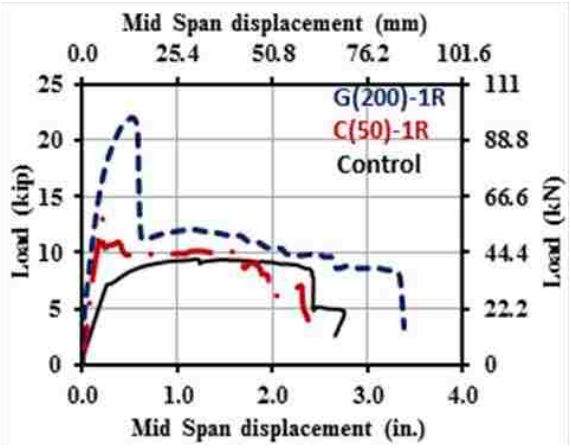

(a) Effect of type of fiber (EB FRP)

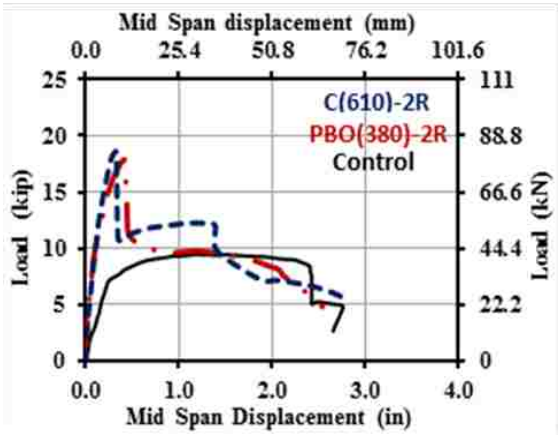

(b) Effect of type of fiber (FRCM)

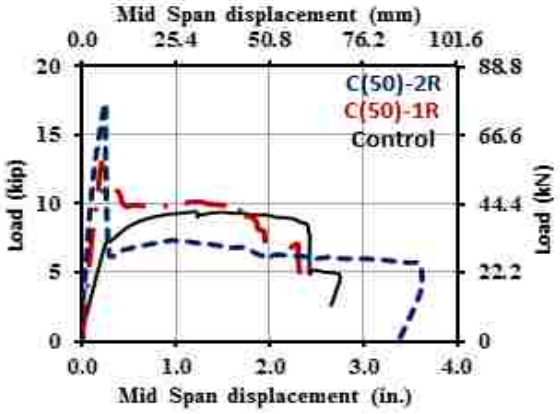

(c) Effect of amount of fiber (EB FRP)

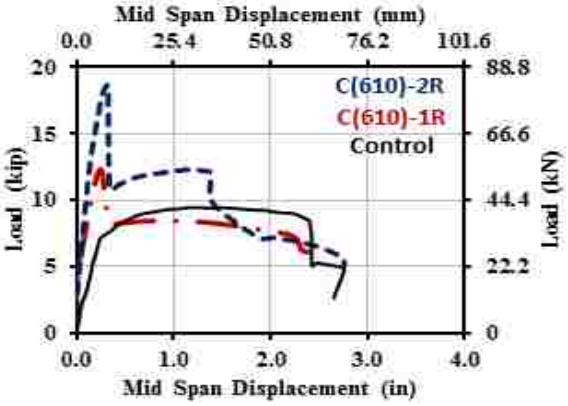

(d) Effect of amount of fiber (FRCM)

Figure7. Effect of type and amount of fiber on flexural capacity

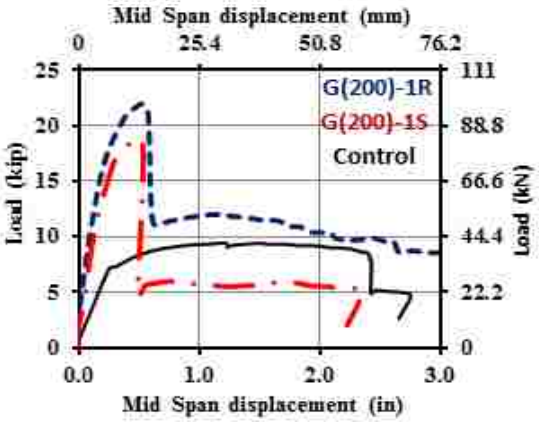

(a) Effect of masonry bond pattern (EB FRP)

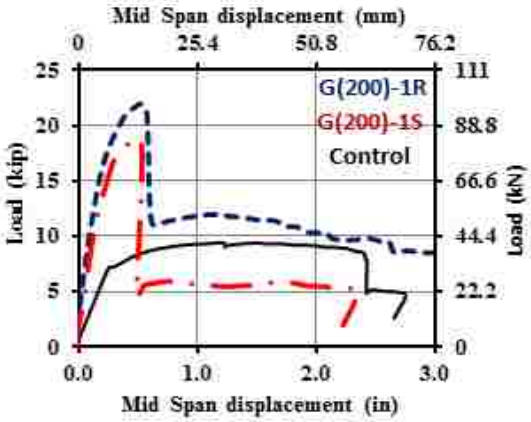

(b) Effect of masonry bond pattern (FRCM)

Figure 8. Effect of masonry bond pattern on flexural capacity

APPENDIX

The following symbols are used in the paper:

A_f = equivalent area of fabric per unit width, in.2 (mm2)

b = width of the fiber layer, in. (mm)

d_f = effective depth of the fabric, in. (mm)

E_f =elastic modulus of fiber, ksi (MPa)

N = number of fiber layer

ρ_f = fabric reinforcement ratio

REFERENCES

Al-Abdwais, A., & Al-Mahaidi, R. (2016). Modified cement-based adhesive for near-surface mounted CFRP strengthening system. Construction and Building Materials, 124, 794-800.

Al-Jabari, Z., Myers, J. J., & ElGawady, M. (2015). Out-of-Plane Strengthening of Reinforced Masonry Walls using Near-Surface Mounted (NSM) FRP Bars with Epoxy and Cementitious Materials. Advanced Composites in Construction, ACIC, 195-200.

Al-Jaberi, Z., Myers, J. J., & ElGawady, M. (2015). Influence of Near-Surface Mounted (NSM) FRP on the Out-of-Plane Behavior of Reinforced Masonry Walls. Paper presented at the 12th North American Masonry Conference.

Babaeidarabad, S., & Nanni, A. (2015). Out-of-Plane Strengthening of URM Walls with Fabric-Reinforced-Cementitious-Matrix (FRCM). Special Publication, 299, 1-12.

Butler, M., Mechtcherine, V., & Hempel, S. (2010). Durability of textile reinforced concrete made with AR glass fibre: effect of the matrix composition. Materials and Structures, 43(10), 1351-1368.

Carney, P., & Myers, J. (2003). Out-of-plane static and blast resistance of unreinforced masonry wall connections strengthened with FRP, Report 03-46. Center for Infrastructure Engineering Studies.

Committee, M. S. J. (1999). Building code requirements for masonry structures. American Concrete Institute, Detroit, MI., ISBN, 1929081022.

D'Antino, T., Carloni, C., Sneed, L., & Pellegrino, C. (2014). Matrix–fiber bond behavior in PBO FRCM composites: A fracture mechanics approach. Engineering Fracture Mechanics, 117, 94-111.

Ehsani, M., Saadatmanesh, H., & Velazquez-Dimas, J. (1999). Behavior of retrofitted URM walls under simulated earthquake loading. Journal of Composites for Construction, 3(3), 134-142.

Hashemi, S., & Al-Mahaidi, R. (2008). Cement based bonding material for FRP. Paper presented at the Proceedings of the.

Jabr, A. (2017). Flexural Strengthening of RC beams using Fiber Reinforced Cementitious Matrix, FRCM. University of Windsor (Canada).

Jesse, F., Will, N., Curbach, M., & Hegger, J. (2008). Load-bearing behavior of textile-reinforced concrete. Special Publication, 250, 59-68.

Kalali, A., & Kabir, M. (2012). Cyclic behavior of perforated masonry walls strengthened with glass fiber reinforced polymers. Scientia Iranica, 19(2), 151-165.

Mosallam, A. S. (2007). Out-of-plane flexural behavior of unreinforced red brick walls strengthened with FRP composites. Composites Part B: Engineering, 38(5), 559-574.

Ombres, L. (2015). Analysis of the bond between fabric reinforced cementitious mortar (FRCM) strengthening systems and concrete. Composites Part B: Engineering, 69, 418-426.

Papanicolaou, C. G., Triantafillou, T. C., Papathanasiou, M., & Karlos, K. (2008). Textile reinforced mortar (TRM) versus FRP as strengthening material of URM walls: out-of-plane cyclic loading. Materials and Structures, 41(1), 143-157.

Tan, K. H., & Patoary, M. (2004). Strengthening of masonry walls against out-of-plane loads using fiber-reinforced polymer reinforcement. Journal of Composites for Construction, 8(1), 79-87.

Turco, V., Secondin, S., Morbin, A., Valluzzi, M., & Modena, C. (2006). Flexural and shear strengthening of un-reinforced masonry with FRP bars. Composites Science and Technology, 66(2), 289-296.

III. PSEUDO-STATIC CYCLIC LOADING COMPARISON OF REINFORCED MASONRY WALLS STRENGTHENED WITH FRCM OR NSM FRP

Zuhair Al-Jaberia, John J. Myers, Mohamed A. ElGawady

ABSTRACT

Fiber reinforced polymer (FRP) composites show poor performance in high temperature and that justified the need to examine alternative strengthening techniques such as near surface mounted (NSM) reinforcement with cementitious adhesive or fabric-reinforced cementitious matrix (FRCM) systems. Evaluation of seismic performance of these strengthening systems is of high interest. In this study, twelve reinforced masonry walls were strengthened in out-of-plane direction using FRCM composite or NSM with cementitious adhesive that were built as a part of this study. FRCM strengthening composite materials consisted of one or two plies of carbon or PBO (polyparaphenylene benzobisoxazole) fabric embedded in cementitious mortar. The NSM technique consisted of carbon or glass bar(s) installed in slots that had been grooved into the masonry tension surface. For all these specimens, a constant mild steel reinforcement ratio (ρ) was used in fully grouted walls. These simply supported walls were tested under out-of-plane constant-amplitude displacement cycles. The key parameters for this investigation were bond pattern (stack and running) and the type and amount of fabric/NSM product. The behavior of the specimens is discussed with emphasis on the load deflection response, flexural capacity, energy dissipation, stiffness degradation, and ductility index. The test results indicated that the behavior of the slender (i.e. non-arching) reinforced masonry walls was significantly dependent on the type of fiber used. The maximum flexural enhancement was found to be 97% and 75%, and the dissipated energy of the specimen

with stack bond pattern was increased by 38% and 62% for masonry walls strengthened with FRCM and NSM system, respectively, compared to the control specimen. Different modes of failure occurred in the strengthened reinforced walls, including crushing of concrete block, as well as a debonding of NSM bar or fabric sheet from the masonry substrate and slippage of fabric within the cementitious matrix.

Highlights

- Reinforced masonry walls were strengthened with FRCM and NSM FRP bar and subjected to cyclic loading.
- Variables included type of strengthening technique, type of strengthening material, reinforcement ratio of repair material, and masonry bond pattern.
- Behavior was investigated in terms of ultimate capacity, deflection, ductility/energy dissipation, cyclic stiffness degradation, and mode of failure.
- Experimental results were compared to control reinforced masonry walls and the effects of the type and amount of fiber and masonry bond pattern is reported.

1. INTRODUCTION

The majority of existing masonry buildings has been constructed as unreinforced masonry (URM) structures in the absence of mandatory seismic design requirements. These structures possess very limited ductility so that its seismic performance has been considered to be sensitive to strong earthquakes or ground accelerations (Bruneau, 1994). Evaluation of out-of-plane stability of unreinforced masonry walls subjected to seismic excitation was conducted by Griffith, et al(Griffith, Magenes, Melis, & Picchi, 2003). A simplified procedure was assessed to evaluate this behavior by considering tri-linear curve as an idealization for nonlinear force displacement response. As a conclusion of

this study, initial stiffness is not crucial in determining the occurrence of collapse. The stiffness of the second and third branches of idealized force displacement curve (i.e., maximum strength and ultimate displacement capacity) is an important parameter for determining seismic design action. Reinforced masonry is obtained by placing and grouting vertical steel reinforcement in the open cells of masonry units to increase seismic capacity by resisting the load generated from earthquake. There are a large number of reinforced masonry buildings around the world in need of strengthening to meet the current seismic standards (Tobriner, 1984). Seismic strengthening of masonry structures reduces not only casualties and damage to buildings during earthquakes, but also the cost of first-aid activities, rescue, rubble removal, and permanent residential reconstruction (Yoshimura & Meguro, 2004). Extensive studies of masonry structures in the past two decades have been focused on strengthening masonry structures with emphasis on FRP and epoxy adhesive as a strengthening technique (Al-Jaberi, Myers, & ElGawady, 2016; Tumialan, Galati, & Nanni, 2003; Velazquez-Dimas, Ehsani, & Saadatmanesh, 2000). These studies reported that the strengthening of masonry structures using FRP composite was very effective to increase out-of-plane capacity for non-arching walls. FRP was preferred in the field of strengthening due to its high strength-to-weight ratio, corrosion resistance, and ease of installation (Tumialan et al., 2003). The NSM system has been proven as a viable option for strengthening in terms of applicability, practicality, and low impact on aesthetic. The behavior of near surface mounted (NSM) and carbon fiber reinforced polymer (CFRP) strengthened masonry walls in flexure was reported (Griffith, Kashyap, & Ali, 2013). The experimental results of this study indicated that the spacing of FRP strips played an important role in upgrading the out-of-

plane flexural capacity and increasing the displacement of specimens. Increased fiber reinforcement ratio resulted in higher strength capacity and a reduction in the displacement. For a constant fiber reinforcement ratio, close spacing resulted in improved wall strength and displacement response. The influence of NSM FRP on the out-of-plane behavior of reinforced masonry walls was investigated (Al-Jaberi, Myers, & ElGawady, 2015). As a result of this study, the capacity of strengthened walls was increased by 231% compared to the control specimen, and two basic types of failure modes were identified: FRP debonding and shear failure within concrete block unit. Although epoxy adhesive was approved as an effective bonding agent in many structural applications for strengthening, it may not be an optimal choice for other applications due to some limitations. These include hazardous poor behavior of epoxy at and above the glass transition temperature, incompatibility with the masonry surface, inability to be applied on damp surface, emission of toxic fumes, moisture impermeability, and flammability (Al-Abdwais & Al-Mahaidi, 2016; Al-Jabari, Myers, & ElGawady, 2015). When an FRP system is subjected to high temperature, the guidelines for the design of FRP-strengthened structures state that the contribution of FRP is neglected unless a fire protection system or insulation is used (Soudki & Alkhrdaji, 2005). In order to overcome these drawbacks of FRP and an epoxy system, NSM with cementitious material adhesive, or FRCM, has emerged as an alternative technique. Cementitious material is less expensive and preferable as a bonding agent due to its compatibility with masonry substrate (Turco, Secondin, Morbin, Valluzzi, & Modena, 2006). A few studies have considered cementitious material as an adhesive material. The flexural behavior of unreinforced masonry walls strengthened using NSM FRP with epoxy and cementitious

material was compared (Galati, Tumialan, & Nanni, 2006; Turco et al., 2006). In terms of capacity, almost similar results were achieved by using epoxy or cementitious paste as a bonding adhesive, but the specimens with cementitious material had gradual stiffness degradation and debonding failure. As a recommendation of these studies, improved performance for this system was observed when the size of the groove was approximately 2.25 times the diameter of FRP bar and the bond-dependent factor was recommended as 0.55 in the case of using circular FRP bars. Out-of-plane performance of URM walls using the NSM technique subjected to reverse cyclic load was investigated (Ismail & Ingham, 2012). Using twisted stainless steel bars in this study helped to provide a bi-linear behavior of the strengthened walls. The flexural capacity of strengthened walls increased by 434% compared to the control wall.

FRCM, also known as textile-reinforced mortar is an alternative strengthening technique and complementary to FRP systems. An FRCM system has almost the same advantages of an FRP system, such as high strength to weight ratio, corrosion resistance and ease of installation, but also overcomes some FRP drawbacks, especially the elevated temperature issue and application on damp surfaces. The flexural capacity of the structural element strengthened with FRCM is affected by several factors. Increasing the number of FRCM layers increased the flexural capacity, but the relation was not one to one (non-proportional relation). Also, the type of fiber affected the flexural capacity due to mode of failure and bond strength associated with each type. Moreover, the anchoring of FRCM could help to improve the capacity and ductility by delaying the mode of failure (Awani, El-Maaddawy, & Ismail, 2017). Previous studies have investigated strengthening URM walls using an FRCM system focusing on ultimate strength without

considering the seismic resistance. Retrofitting of URM concrete or clay brick walls with FRCM under uniformly distributed lateral load was conducted (Babaeidarabad & Nanni, 2015), and an enhancement in flexural capacity ranging from 2.7 to 7.8 compared to unstrengthened specimens was reported. The potential modes of failure for these strengthened specimens were identified, including flexure and shear failure, depending on fiber reinforcement ratio. The out-of-plane behavior of URM walls strengthened with FRCM under cyclic load was investigated by Ismail and Ingham (Ismail & Ingham, 2016). Based on the result of this study, the behavior of the strengthened specimen was ductile until the failure, and the capacity increased by the range 575%-786% compared to the control specimen with remarkable increment in displacement ductility.

Clay brick walls strengthened with carbon-FRCM and subjected to out-of-plane cyclic loading was tested (Papanicolaou, Triantafillou, Papathanasiou, & Karlos, 2008). The effectiveness of FRCM overlays was evaluated in comparison to that provided by FRP in the form of overlays or NSM reinforcement. It was concluded that FRCM overlays provide substantial increase in strength and ductility and comprise an extremely promising solution for the structural upgrading of masonry structures under out-of-plane loading. Compared with FRCM, NSM strips offer lower strength, but higher ductility due to a more controlled debonding. The inorganic matrix-grid composite was very effective in enhancing in-plane capacity and ductility ratio of masonry walls (Gattesco & Boem, 2015; Parisi, Iovinella, Balsamo, Augenti, & Prota, 2013). Diagonal compression tests on masonry specimens before and after the application of composite strengthening system were used to evaluate this system. Strengthening specimens from both sides produced further improvement in shear response, eliminating out-of-plane bending in the post-peak

softening phase. The experimental results evidenced that the maximum resistance increment is about 350% compared with the control specimen.

Most strengthening design guides are limited to unreinforced masonry structures due to a lack of experimental studies related to RM structures. This work reports the outcomes of an experimental study on the strengthening of RM walls using FRCM or NSM with a cementitious material as the bonding agent. For the NSM phase of work, two types of fibers were used, either GFRP bars, or CFRP bars and strips. Fabric composed of either PBO or carbon was used in the FRCM system. The comparison of the specimens is discussed with emphasis on the load-deflection response, crack pattern, energy dissipation, stiffness degradation, and ductility index. The main objective of this investigation is to study experimentally the behavior of RM walls strengthened with FRCM composite or NSM with cementitious adhesive. This work also studies the contribution of fiber reinforced composite on improving the flexure strength and pseudo-static cyclic characterizations of reinforced masonry walls, in addition to identify potential failure modes of strengthened specimens. This study will develop and provide a data base of experimental test results to validate the design model presented in the next version of the ACI 549.4R-13 document (ACI 549.4R-13, 2013).

2. EXPERIMENTAL PROGRAM SUMMARY

The experimental work presented in this paper is part of a large research program conducted on strengthening RM walls using different strengthening techniques. Table 1 provides an overview of the strengthened walls, materials and systems, wall bond pattern, and size of bars for NSM or width of fabric sheet for the FRCM system. This study considers tests and comparisons of twelve RM wall specimens, ten of which were

strengthened in out-of-plane with either FRP NSM bars (glass or carbon) or with FRCM (PBO or carbon). The reinforced walls were tested under cyclic load up to failure considering the overall effects of flexural strengthening systems, the effect of type and fiber axial stiffness, and the effect of type of masonry wall bond pattern.

2.1. MATERIAL CHARACTERIZATION

2.1.1. Masonry Wall Components and Steel. Concrete masonry units with nominal dimensions of 152 x 203 x 406 mm (6 x 8 x 16 in.) and type S mortar were used in the walls construction. A series of experimental tests was performed to determine mechanical properties of each component. Masonry prisms were constructed with two masonry concrete units and cured under the same lab conditions as the walls. A compressive strength test was conducted according to ASTM C1314-12, and the average compressive strength of the prisms was 22.4 MPa (3,250 psi) based on three prisms with a coefficient of variation (COV) of 3.54%. Standard mortar specimens were tested according to ASTM C109-13 to determine the average compressive strength of type S mortar. An average 28-day value of 16.7 MPa (2,420 psi) was obtained with a COV of 7.24%. Figure 1 illustrates the constitutive relationship curves for masonry prism and mortar. The 28-day average compressive strength of the grout according to ASTM C1019-13 was 28.95 MPa (4,200 psi) with a COV of 6.63%. An experimental tensile test for mild steel rebar according to ASTM A370-13 was conducted on three replicate specimens. Uniaxial load was applied gradually until failure, and then the average yield stress of the steel reinforcement bar at 0.5% offset was obtained 463.63 MPa (67.25 ksi) with a COV of 3.9% along with the average modulus of elasticity was 200.3 GPa (29,051 ksi) with a COV of 3.07%.

2.1.2. Fibers and Adhesive Agents. The properties of composite materials are dependent on the individual component properties, the manufacturing technique, and the quality control of the production process (Al-Salloum, Siddiqui, Elsanadedy, Abadel, & Aqel, 2011). The open mesh fabric of PBO consists of fiber toes disposed along orthogonal directions, with the main direction tensile strength greater than tensile strength of the secondary direction, while symmetric open mesh for carbon fabric. The FRP bars used in this study were made of fibers embedded in to vinylester matrix under the pultrusion process. Based on AC434 protocol (AC 434, 2011) the FRCM coupon test results are presented in Table 2, while the FRP bars mechanical properties with results are summarized in Table 2 and 3, respectively. Compressive strength tests according to ASTM C109-13 were performed on the cementitious-based embedding materials used with NSM and the adhesive agents (mortar x750 and x25) used with an FRCM system. The average compressive strength for the cementitious paste material was found to be 59.1 MPa (8,570 psi) with a COV of 4.7% at an age of 28 days. The average compressive strength for a matrix x750 used with PBO fabric was found to be 35 MPa (5 ksi) at an age of 28 days while it was 15 MPa (2,175 psi) with a COV of 5.13% for a matrix x25 used with carbon fabric.

2.2. CONSTRUCTION OF THE MASONRY WALLS

Twelve RM walls with dimensions of 1220 x 610 x 152 mm (48 x 24 x 6 in.) were constructed by a professional mason. Each specimen was constructed using 152.5 mm (6 in.) standard masonry concrete blocks in running and stack bond patterns. The steel reinforcement was constant for all specimens (2#4 bars) and the walls were fully grouted four days after construction to preclude damage to the mortar joints during the vibration

process. The steel reinforcement levels comply with specifications in design code. These reinforcements satisfied the reinforcement size limitation and were between the minimum and maximum reinforcement specified by MSJC-13. Two reinforced walls were used as control specimens in running and stack wall bond patterns. For both systems, the specimens were strengthened so that the fiber reinforcement ratio was less that the balance ratio and also to ensure there was no shear failure. Five walls were strengthened with NSM system and the remaining five walls were strengthened using FRCM system. The specimens strengthened with carbon FRCM completely covered the tension face of the wall, while PBO fiber covered only 380 mm (15 in.) of the wall width. Figure 2 illustrates the dimensions of control and strengthened specimens.

2.3. SPECIMENS DETAILS

The specimens' designation consisted of two parts. The first part consisted of two characters representing strengthening system information (fiber, thickness, or diameter). The first character identified the fiber type: "C" for carbon, "G" for glass, and "PBO" for polyparaphenylene benzobisoxazole. The second character represented the FRP diameter for NSM, or fiber thickness for FRCM system. The second part of the designation identified the amount of fiber in the tension face and the wall bond pattern. The first character represented the number of FRP bars for NSM, or number of layers for FRCM. The second character referred to the wall bond pattern applied: "R" for running and "S" for stack.

2.4. TEST SETUP AND INSTRUMENTATION

The strengthened reinforced masonry specimens were tested under four-point bending with simply supported boundaries, as shown in Figure 3. An MTS double-acting

hydraulic jack with a push-pull capacity of 620 kN (140 kips) was used to apply a vertical load on the specimen. The load was transferred to the specimen by means of continuous steel plates and bars along the full width of the external face of the reinforced walls to provide two equal line loads. A piece of thick rubber sheet was placed at all interfaces between the steel plate and specimen. The rubber sheet distributed the load evenly and minimized any stress concentration due to unevenness of the wall surface. The distance between these two lines was 200 mm (8 in.). The load was applied in cycles of loading and unloading as a displacement control at a rate of 1.25 mm/min (0.05 in./min) through an MTS computer control station up to the load peak value. The displacement amplitude increment was 6.35 mm (0.25 in.); double half loading cycle was applied for each amplitude level, as illustrated in Figure 4. Deflections at the mid and third spans were measured using three linear variable displacement transducers (LVDTs) at each side. In addition, strain gauges were installed on the steel and fiber to measure their strains during loading.

3. STRENGTHENING PROCEDURE

3.1. FRCM STRENGTHENING SYSTEM

The fabric with dimensions 1067 x 380 mm (42 x15 in.) for PBO and 1067 x 610 mm (42 x 24 in.) for carbon were prepared. The matrix was mixed as per the manufacturer specifications. The procedure of strengthening consisted of applying a first layer of cementitious matrix with a nominal thickness of approximately 5 mm (0.2 in.) on the tension surface of the specimen. A single ply of precut fabric was laid on the cementitious matrix and pressed gently into the first matrix layer. The second layer of cementitious matrix with a nominal thickness of 5 mm (0.2 in.) was then applied and

covered the fabric mesh. The procedure was repeated in the case of multi-ply strengthening.

3.2. NSM STRENGTHENING SYSTEM

No surface preparation was needed for the NSM system, and the strengthening procedure involved inserting FRP bar into a groove cut at the tension surface of the specimen. A special concrete saw was used to cut the grooves with dimensions double the diameter of the bar to avoid splitting failure of the epoxy cover (De Lorenzis & Nanni, 2002). Deformed FRP bars with a sand coating were used to improve the bond between the FRP bars and cementitious material. The cementitious material was placed into the grooves to cover 2/3 of the groove depth. The FRP bar was installed to mid-groove depth as it was pressed into the bonding agent which flowed around the bar to ensure a complete bond between the bar and the sides of the groove. The groove was then filled with more cementitious material, and the surface was leveled.

4. EXPERIMENTAL RESULTS AND DISCUSSION

The summary of the load (at yield and ultimate stage) and deflection (at yield and failure stage) for all specimens is reported in Table 4. The cyclic load versus deflection curves for specimens strengthened with FRCM or NSM is shown in Figure 5. The running and stack control specimens failed due to crushing of the concrete masonry unit in the compression zone with an ultimate load of 42 kN (9.4 kips) and 38 kN (8.5 kips), respectively. The general behavior of control specimens was ductile without sudden drop in the capacity due to the existence of steel reinforcement bars.

For both strengthening systems, the strengthened specimens achieved a higher load capacity due to the high tensile strength of the fiber attached to the tension face of

masonry substrate. The maximum ultimate loads were equal to 82.73 kN (18.6 kips) and 73.57 kN (16.5 kips) for specimens strengthened with two carbon layers in FRCM and one CFRP bar in NSM, respectively. The maximum flexural enhancement was found to be 97% and 75% for masonry walls strengthened with FRCM and NSM system, respectively. The behavior of the walls strengthened with NSM system was more ductile than the specimens strengthened with FRCM system. The ductile behavior was due to steel reinforcement and gradual loss of composite action resulting from debonding failure.

4.1. CRACK PATTERNS AND FAILURE MODES

The unstrengthened RM walls (control specimen) failed in a typical flexural ductile mode after developing bed joint mortar cracks in the maximum moment region. For strengthened specimens, the first observation was the flexural tensile crack initiated in the maximum moment region at the bed joint mortar, which then moved upward in the grout. A redistribution of the stresses, however, allowed for further flexural tensile cracks in the adjacent bed joint mortar and within the concrete masonry unit (CMU) to develop beyond the cracking load due to the existence of fiber. For the specimens strengthened with FRCM system, the level of CMU damage after ultimate load was less compared to the specimen strengthened with NSM system. The reason behind that is the large contact area between the substrate and FRCM strengthening system compared to NSM system, which led to a better distribution of load and eliminated stress concentration. The cracks developed during the loading are shown in Figure 6. Different modes of failure were observed during the experimental test; all these modes are shown in Figure 7. The control specimens showed ductile mode of failure with a large opening in the bed joint mortar at

the mid-span due to steel yielding. Crushing failure mode was reported at the final stage of loading. For the strengthened specimens, the modes of failure include the following:

- Debonding of FRCM at fiber/matrix interface: This type of failure occurred in specimens with a high fiber reinforcement ratio. The debonding started in the maximum moment region and propagated to the support direction. The surface of failure was at the fiber/matrix interface without detachment of the cementitious matrix from the masonry substrate.

- Extensive slippage of FRCM fiber mesh within the cementitious matrix: The fiber slippage is typically caused by the gradual loss of bond between the fibers and the matrix as exhibited by anchorage specimens strengthened with one ply of PBO. The PBO fiber of this specimen was extended beyond the two supports to study and simulate the effect of a highly anchored fabric regardless of a specific type of anchorage system. This specimen failed due to fabric slippage at the fiber/cementitious matrix interface.

- Debonding of FRP reinforcement bar: FRP bar was debonded from the masonry substrate, which is a general failure mode for walls strengthened with NSM and cementitious adhesive. The debonding failure surface occurred at the FRP bar/cementitious adhesive interface, and the failure was intermediate crack (IC) debonding due to localized splitting of the embedding material.

4.2. LOAD-DISPLACEMENT RESPONSE

The envelope load vs. deflection curves for all specimens is illustrated in Figure 8. The moment capacity and stiffness of the reinforced walls strengthened with fiber

increased as compared to the control specimens. Interestingly, for both systems, the wall's capacity dropped to approximately the same capacity of the control specimen after the failure of the composite system. As an important point in NSM system, the specimen strengthened using carbon strip with cementitious adhesive showed evidence of sliding inside the groove. This sliding developed more flexural capacity after debonding than the capacity of the control specimen because of the friction force that developed, which provided more ductility. The flexural capacity increased significantly as the number of layers increased (increased fiber reinforcement ratio) in the case of FRCM system. Doubling the fiber reinforcement ratio increased the flexural capacity by 234% and 30% for specimens strengthened with FRCM and NSM systems, respectively, as shown in Figure 8 (a and b). The behavior of the stack specimen improved when the continuous head joint was reinforced with an FRP bar or the tension face strengthened with PBO fabric sheet, as shown in Figure 8(c and d). The masonry walls constructed in stack or running bond patterns behaved almost the same in terms of capacity and mode of failure.

4.3. ANALYTICAL APPROACH AND COMPARISON WITH EXPERIMENTS

The out-of-plane flexural capacity of strengthened reinforced masonry walls is the sum of the three components' contribution, such as masonry, steel reinforcement, and strengthening system. The theoretical formulations are based on ACI 549.4R-13 (ACI549.4R-13, 2013). Trial and error procedure has been used in these codes. The depth to the neutral axis was assumed, then the strain level in each material was calculated. For the NSM with cementitious paste, based on experimental data, the maximum usable strain in the FRP is 55% of the ultimate fiber strain (Galati et al., 2006). For the FRCM system, the code recommended maximum usable strain in fabric as follow:

$$\varepsilon_{fe} = \min(\varepsilon_{fd}, 0.012) \quad (1)$$

where $\varepsilon_{fe}$is maximum usable strain in fabric in mm/mm (in./in.), ε_{fd} is the design fabric strain in mm/mm (in./in.). If the fiber strain greater or equal to the ultimate fiber strain, concrete crushing controls flexural failure of the section. If the fibers strain less than the ultimate fiber strain, FRP failure controls flexural failure of the section.

The validity of using ACI 549.4R-13 (ACI549.4R-13, 2013) procedure was tested by comparing the prediction ultimate capacity with experimental capacity for different specimens, as shown in Table 4. Good agreement was achieved for theoretical out-of-plane capacity compared with experimental results. For all specimens, the theoretical results were underestimated by a reasonable percent. The theoretical capacity of the specimen with anchored fabric was 35% less than the experimental due to limited strain considered in the analysis process.

4.4. ENERGY DISSIPATION

For structures subjected to seismic events, energy dissipation is an important property because it reduces the amplitude of the seismic response and thereby reduces the strength demands on the structure. Although it is difficult to estimate such an energy input during a seismic event, a proper design should ensure a larger energy dissipation capability of the structure than the demand (Said & Nehdi, 2004). Physically it is used as a ductility indicator since it represents the energy consumed by the structural system before failure. Mathematically, it represents the area enclosed by loops of loading and unloading for specimens subjected to cyclic loading. In the current study, the dynamic

energy dissipation has not been investigated; only static energy dissipation was considered. The energy dissipated by the masonry wall has been attributed to (1) friction along joints and existing cracks, (2) formation of new cracks, (3) crushing of units, and (4) yielding of main reinforcement (ElGawady, Lestuzzi, & Badoux, 2006). Fiber deformation or progressive rupture, in addition to the cracks in the cementitious material, would dissipate energy.

4.4.1. Cumulative Cyclic Energy Dissipation. The cumulative energy dissipation is an essential factor for evaluating the cyclic behavior of strengthened masonry walls. During seismic events, the accumulation of small deflections led to structural failure rather than a single large deflection (Shao & Mirmiran, 2005). The accumulation of dissipated energy versus the number of displacement cycles is shown in Figure 9 (a and b) for specimens strengthened with FRCM and FRP NSM, respectively. It is obvious that the cumulative dissipated energy is affected and dependent on the amplitudes of the displacement cycles. As expected, for low drift levels and for both strengthening systems, the friction along joints was small and there was no significant damage in any component of strengthened wall. For this level, the energy dissipation was low, which characterized the condition before significant inelastic deformation in the masonry and yielding of the main steel reinforcement. Beyond that, the energy dissipation was increased significantly as the applied drift increased due to many possible reasons, such as formation of longitudinal and diagonal cracking, yielding of main reinforcement, and the cracks in the cementitious matrix. The dissipation continued until the specimen experienced degradation of its resistance to the applied load.

The trend of energy dissipated was influenced by the mode of failure of strengthening system. For the FRCM system, the specimen strengthened with one ply of PBO FRCM exhibited excellent behavior in terms of energy dissipation. In this specimen, the fiber was intentionally anchored by extending it beyond the two supports to determine an upper bound capacity. The energy dissipation for this specimen was improved by 38% compared to the two-ply PBO without anchorage and 80% compared to the control specimen. For the first 25 cycles, the energy dissipation for specimens strengthened with carbon sheet was less than that of the control specimen for the same cycles. This behavior was attributed to the mode of failure that did not present full slippage of fiber in the cementitious material in addition to formation of less cracks and damage to the units compared to the control specimen. At the end of the test, the strengthened specimen was able to go through more cycles and presented higher energy dissipation than that of the control specimen.

For the NSM system, the specimen strengthened with one bar of GFRP presented higher dissipated energy compared to other specimens. The reason behind this was the gradual debonding of the bar which is not the case when fiber reinforcement ratio or fiber axial stiffness increased. For both systems, the behavior of stack specimen improved when the continuous head joint was reinforced by FRP bar or fabric sheet. The dissipated energy increased by 38% and 62% in case of strengthening using FRCM and NSM, respectively.

4.4.2. Normalized Cyclic Energy Dissipation. The energy dissipation for individual specimens was normalized with respect to the first virgin cycle in the cyclic response of reinforced wall under constant amplitude loading as shown in Figure 10 (a

and b). It can be observed that the curves of all specimens in both systems ran in a fairly narrow band, and the average of these curves can be represented by a single trendline.

The slope of the curves represents the rate of dissipated energy, which increased significantly after the first five cycles. The normalized accumulative dissipated energy curve is a function of the cycle's number; the trend of this function is almost a linear relation. Based on equivalent axial stiffness, the normalized accumulative energy dissipation is compared for specimens strengthened with different types of fibers and different types of strengthening systems, as shown in Table 5. From the results, it is clear that the strengthening system is an important factor that affects the amount of energy dissipation. The specimens strengthening using NSM with cementitious material presented better behavior of dissipated energy compared with specimen's strengthened using FRCM system. The specimen strengthened using NSM with an axial stiffness k^f has the same accumulative dissipated energy of specimens strengthened using FRCM system with axial stiffness $10k^f$. For both systems, higher levels of energy dissipation were observed in walls in running bond pattern in comparison to stack bond pattern walls. Also, the specimens with larger amounts (high fiber axial stiffness) of fiber reinforcement did not display higher levels of energy dissipation because the failure mechanism of the walls was changed.

4.5. STIFFNESS DEGRADATION

The stiffness degradation may be attributed to several factors, including the nonlinear deformations of the concrete block units, mortar cracking, flexural and shear cracking of masonry units, slippage or yielding of reinforcement, and debonding or slippage of fibers in FRCM or NSM systems. The stiffness was reduced due to the

loading unloading process, which causes initiation of micro-cracks in all concrete components (masonry unit, mortar, grout, cementitious matrix) and increases the deformability of the strengthened walls. The increase in deflection (deformation) increased the level of masonry damage, resulting in degradation in stiffness.

4.5.1. Theoretical and Experimental Out-of-plane Initial Stiffness. The initial stiffness was calculated as the slope of the load-displacement curve. This was determined to be equal to 125 kN/mm (716 kip/in.) for the control specimen. For specimens subjected to four-point load, the theoretical uncracked stiffness can be compared to the experimental initial stiffness using the following equation:

$$K_{th} = \frac{1}{\frac{a}{24E_m I_g}(3l^2 - 4a^2) + \frac{a}{\alpha A_n G_m}} \quad (2)$$

where E_m = modulus of elasticity; G_m = modulus of rigidity; l = wall height (span of the wall); a = distance from support to concentrated load; I = gross moment of inertia; A_n = cross-sectional shear area; and α = shape factor, which accounts for the distribution of shear stresses across the section and is equal to 0.83 for rectangular sections. This equation is considered the flexural and shear deformation of the cross section. Based on this equation, the theoretical initial stiffness depends only on the location of the concentrated load, material property f_m, and the geometry of the specimens which are the same for strengthened and control specimens. According to MSJC-2013 (MSJC, 2013), the modulus of rigidity of clay and concrete masonry shall be taken as $G_m = 0.4E_m$, and for concrete masonry, the modulus of elasticity shall be taken as $E_m = 900f_m$. Based on

these values, the theoretical stiffness was determined to be equal to 39 kN/mm (223 kip/in.) for all walls. The experimental initial stiffness was much lower than the theoretical uncracked stiffness for the control specimen and is approximately 31% of the theoretical value. This result is consistent with the theoretical initial stiffness for the walls subjected to in-plane load. For the masonry walls subjected to in-plane concentrated load, the theoretical uncracked stiffness can be determined as follows:

$$K_{th} = \frac{1}{\frac{h^3}{3E_m I} + \frac{h}{\alpha A_n G_m}} \tag{3}$$

Hart, Englekirk, and Hong (1988) reported that the ratio of the experimentally determined stiffness to that determined analytically based on elastic theory and the effective properties of wall sections ranges from 0.26 to 0.3. Accordingly, the theoretical initial stiffness equation suggested scaling down by a factor of 0.3 as follows:

$$K_{th} = \frac{0.3}{\frac{h^3}{3E_m I} + \frac{h}{\alpha A_n G_m}} \tag{4}$$

Hassanli, ElGawady, and Mills (2015) proved that the measured initial stiffness was lower than the theoretical uncracked stiffness, ranging from 42% to 64% of the theoretical value. It may be noted that all the strengthened specimens have almost the same uncracked stiffness due to the fact that the strengthening systems were not effectively engaged in this stage.

4.5.2. Determination and Evaluation of Stiffness Degradation. The secant stiffness was considered in determination the degradation of stiffness. The secant stiffness is the slope of the line drawn between minimum and maximum loads (point 1 and 2) of first cycle for each displacement interval, as shown in Figure 11. The secant stiffness was used to develop a qualitative estimation of the stiffness degradation in all specimens (Shannag, Abu-Dyya, & Abu-Farsakh, 2005). The secant stiffness degradation versus the corresponding cycle number was plotted for control and strengthened masonry walls as shown in Figure 12. The strengthened specimen had higher secant stiffness than its corresponding control specimen. This higher stiffness at the early stage (post cracked) can be attributed to the contribution of the high modulus of elasticity of the fibers attached to the tension face of strengthened wall beyond cracking of specimen. The stiffness degradation of the strengthened specimens is linear until failure. The sudden jump down in stiffness is expected at the stage of FRCM or NSM debonding. The control specimen behaved as a ductile member due to the steel reinforcement, but a sudden loss in stiffness of 30% within the first few cycles was observed. The secant stiffness for the strengthened wall dropped down to the level of the control wall stiffness when the mid-span deflection was about 25.4 mm (1 in.).

4.5.3. Normalized Stiffness Degradation. The stiffness degradation was normalized with respect to the secant stiffness of the control specimen for each displacement interval. Figure 13 presents the trend of degradation in stiffness for both strengthening systems. For the FRCM strengthening system, the stiffness degradation of the specimen strengthened with a single ply of PBO and anchored underneath the support was gradual compared to that of the corresponding control and that of the other

strengthened specimens. The normalized stiffness for this specimen started with 1.45 and ended with 1.4. This is a desirable behavior for structures subjected to seismic events. The other four specimens end with a normalized stiffness less than one due to block unit cracking and damage accumulating after strengthening system failure occurred. For the NSM system, the normalized stiffness of specimen strengthened with one carbon bar started with 1.27 and ended with 0.78. This specimen and others with high fiber reinforcement ratio ended with stiffness less than the control specimens. Beyond debonding failure, the specimen strengthened with one glass bar has approximately the same stiffness of the control specimen.

4.6. DUCTILITY INDEX AND EQUIVALENT VISCOUS DAMPING

Ductility is defined physically as the capacity of a material, cross section, structural element, or system to sustain large inelastic deformations prior to total collapse. Mathematically, the ductility is the ratio of ultimate/yielding parameters, elastic quantity (such as curvature, displacement, and strain energy). The structural element can resist load while sustaining large deflection due to the existence of steel reinforcement bars. The ability of a strengthened masonry wall to present large deformation after the yielding of steel reinforcement depends on many factors, such as mechanical properties of fiber, fiber to steel reinforcement ratio, and the effectiveness of the strengthening system. Since it is so hard to consider all these factors together for evaluating the ductility, the authors choose a method used in many references to define the ductility as follows (Kim & Shin, 2011; Priestley, Seible, & Calvi, 1996).

The ductility of strengthened wall is defined as the ratio of ultimate deflection to the deflection at yielding at mid-span of the longitudinal steel reinforcement. The

ultimate deflection was considered to be at the level of load 20% below the peak load value in the descending branch. The deflection at yield is evaluated based on the strain gauge reading of the steel bars, when the value of strain reaches 0.25%. Ductility index (DI) was obtained by dividing the ductility of the strengthened wall by corresponding ductility of the control specimen, as shown in Table 5. The DI definitely shows that strengthening in both techniques (EB-FRCM and NSM) results in significant losses in structural ductility of the strengthened reinforced masonry wall, especially for the FRCM system. The ductility ratio depends not only on the type and amount of the fiber reinforcement ratio, but also on other factors such as masonry bond pattern, cross section geometry of FRP bar, and the anchorage of the fiber.

For comparison, the amount of fiber reinforcement is expressed in terms of fiber axial stiffness k^f, which is given by $k^f = A_f \mathrm{E}_f$, where for FRCM system, A_f is the paddle area per unit width multiplied by the number of paddle of fabric within the width of fabric sheet, and for NSM system, A_f is the cross-sectional area of the FRP bar. For both systems, E_f is the fiber elastic modulus. The resulting number is normalized with respect to the lowest value of axial stiffness of both systems [axial stiffness of specimen G (2)-1R], as shown in Table 5.

For the specimens strengthened with the FRCM system, the strengthened walls showed relatively lower ductility as compared to the respective control specimen (except the specimen with consideration of end anchorage) due to bond slippage between the fabric sheet and masonry tension face. The ductility index of these strengthened walls is only about 33% to 54% of that of the original control reinforced wall. Ductility can be

enhanced if the end anchorages are used to overcome this loss and enable the strengthened masonry wall to restore more than double ductility of the control specimen.

The ductility of specimens strengthened with the NSM system is better than the ductility of specimens strengthened with the FRCM system. The strengthened walls show a delay in cracking, and debonding failure. The ductility index of specimens strengthened with carbon strip was improved by 88% compared to the control specimen due to sliding inside the groove. The other specimens presented ductility index approximately 60% to 97% of the control specimen. For the same amount of fiber reinforcement ratio, the ductility index of strengthened wall with running bond pattern is better than the corresponding wall with stack bond pattern. It loses approximately 16% of ductility due to this factor. The equivalent viscous damping ratio is a parameter that defines the damping behavior of the structural element. This parameter is a function of energy dissipation and the elastic strain energy and can be obtained as follows:

$$\xi_{eq} = E_d / 4\pi\, E_s \tag{5}$$

where E_s is stored strain energy, and E_d is dissipated energy calculated as the area of the first cycle for at each displacement amplitude level. The equivalent viscous damping is plotted against the number of cycles in Fig. 14. As shown in the figure, the equivalent viscous damping for both systems was relatively small, about 7% for NSM and 11% for FRCM, due to the nonlinear elastic response of the walls. For reinforced concrete structures, the equivalent viscous damping is typically considered to be 5% (Rodrigues, Furtado, & Arêde, 2017).

5. CONCLUSIONS

This paper presents experimental results in terms of cyclic response for strengthened RM walls using NSM with cementitious adhesive or FRCM systems. Twelve specimens were constructed and tested as part of the experimental program. According to this research, the following conclusions can be drawn:

1- Test results indicated that NSM and FRCM system remarkably increase the lateral load capacity of RM walls. The maximum flexural enhancement percent was found to be 97% and 75% for masonry walls strengthened with FRCM and NSM system, respectively. Moreover, the lateral capacity increase significantly as the fiber reinforcement ratio increased, especially for the specimens strengthened with FRCM system. The flexural capacity of stack pattern specimens improved when the continuous head joint was reinforced with an FRP bar or the tension face strengthened with PBO fabric sheet.

2- Small energy dissipation for low drift levels was observed due to insignificant damage in any component of strengthened wall at this level. The energy dissipation was increased as the applied drift increased. The energy dissipation for specimen strengthened with one anchorage ply was improved by 38% compared to the two-ply PBO without anchorage and 80% compared to the control specimen. This behavior was attributed to the mode of failure that present full slippage of fiber in the cementitious material in addition to the cracks developed in the masonry units compared to the control specimen. The specimen strengthened with one bar of GFRP presented a higher dissipated energy compared to other specimens, and 30% higher

than the control specimen. The reason behind this was the gradual debonding of the bar, which was not the case when fiber reinforcement ratio or fiber axial stiffness increased. The dissipated energy of the specimen with stack bond pattern was increased by 62% and 38% when strengthening using NSM and FRCM systems, respectively. The specimens strengthened using NSM with cementitious material presented better behavior of dissipated energy compared to specimens strengthened using the FRCM system.

3- The experimental initial stiffness was much lower than the theoretical uncracked stiffness for control specimen and is approximately 27% of the theoretical value. The stiffness of the control specimen had a sudden loss of 30% within the first few cycles, while the stiffness for the strengthened wall dropped down to the level of the control when the mid-span deflection was about 25.4 mm (1-in.). Beyond the failure of composite, the stiffness degradation of the specimen strengthened with one anchorage ply of PBO was gradual and 40% higher than the control specimen due to high tensile strength of the anchored fiber attached to the masonry substrate.. On the other hand, the specimen strengthened with one glass bar has approximately the same stiffness of the control specimen.

4- Strengthening in both systems (FRCM and NSM) results in significant losses in structural ductility of the strengthened specimens. Ductility can be enhanced if the end anchorages are used, or strip bar in the case of the NSM strengthening system. The anchorage or using rectangular cross section of FRP bar enables the strengthened specimen to upgrade the ductility by 122% or 88% of the control specimen for FRCM and NSM systems, respectively. The strengthened wall with CFRP strip demonstrated

a delay in cracking, and debonding failure due to sliding inside the groove. The loss of ductility for the specimen with stack bond pattern is 16% compared to the same specimen with running bond pattern.

5- The two types of failure modes identified from this study were associated with the strengthening systems were as follows: Debonding failure was observed for most specimens in both strengthening systems. The specimen with end anchorage in the FRCM system (PBO (380)-1R) presented slippage failure of fiber mesh within the cementitious matrix. The debonding failure surface for the FRCM system was fiber/matrix interface without detachment of the cementitious matrix from the masonry substrate, while for the NSM system, it occurred at FRP bar/cementitious adhesive interface.

ACKNOWLEDGEMENTS

The authors wish to acknowledge the support of Midwest Block & Brick in Jefferson City, Missouri and Hughes Brothers in Seward, Nebraska, Ruredil S.p.A., San Donato Milanese, Italy and HCED (The Higher Committee for Education Development in Iraq). The authors also wish to thank the technical support staff in not only the Department of Civil and Environmental Engineering but also the Center for Infrastructure Engineering Studies (CIES) at Missouri University of Science and Technology for their efforts in this research study. Any opinions, findings, conclusions, and recommendations presented in this paper are those of the authors and do not necessarily reflect the views of the sponsor or supporting agencies.

TABLES AND FIGURES

LIST OF TABLES:

LIST OF FIGURES:

Fig. 14. Comparison of equivalent viscous damping for masonry wall strengthened with
(a) FRCM
(b) NSM

Table 1 - Experimental test matrix

Wall	Strengthening system	Specimen ID	Type of FRP	Bar or strip size (#), or sheet width (mm)	Number of bars or layers	Bond pattern
1		Control-R				running
2		Control-S				stack
3	NSM	C(2)-1R*	Carbon	2	1	running
4		C(2)-1R	Carbon	2	1	running
5		G(2)-1R	Glass	2	1	running
6		G(2)-2R	Glass	2	2	running
7		G(2)-2S	Glass	2	2	stack
8	FRCM	PBO(380) -1R**	PBO	380	1	running
9		PBO (380) -2R	PBO	380	2	running
10		PBO (380) -2S	PBO	380	2	stack
11		C(610) -1R	Carbon	610	1	running
12		C(610) -2R	Carbon	610	2	running

Note: 1.0 mm=0.039 in. *specimen strengthened with carbon strip **anchored specimen

Table 2 - Mechanical Properties of FRCM coupon

Material	Thickness (mm)	Ultimate tensile strength (MPa)	Elongation at break %	Tensile modulus (GPa)	Method
PBO fiber	10	1880	1.47	127	AC434
Carbon fiber	10	970	1.33	75	AC434

Note : 1.0 GPa = 145.03 ksi; 1.0 MPa = 0.145 ksi; 1.0 mm/mm = 1.0 in./in.; 1.0 mm = 0.039 in.

Table 3 - Mechanical Properties of FRP bars and strip

Material	Dimension (mm)	Ultimate tensile strength (MPa)	Elongation at break %	Tensile modulus (GPa)	Method
Aslan 500 CFRP Strip	2x16	2241	1.81	124	ASTM D7205-11
Aslan 200 CFRP bar	6	2172	1.75	124	ASTM D7205-11
Aslan 100 GFRP bar	6	896	1.94	46	ASTM D7205-11

Note : 1.0 GPa = 145.03 ksi; 1.0 MPa = 0.145 ksi; 1.0 mm/mm = 1.0 in./in.; 1.0 mm = 0.039 in.

Table 4 - Summary of test results

Specimen ID	Load at yield P_y (kN)	Deflection at yield U_y (mm)	Deflection at failure U_u (mm)	Experimental Ultimate load $P_{u)exp}$ (kN)	Theoretical Ultimate load $P_{u)the}$ (kN)	$\frac{P_{u)exp}}{P_{u)the}}$	Gain in ultimate load ratio*	Mode of failure [a]
Control-R	35.58	11.20	61.00	42.00	37.9	1.10	-	C
Control-S	29.35	7.87	41.65	38.25	37.9	1.01	-	C
C(2)-1R*	39.14	3.00	31.24	62.63	62.2	1.00	49	D
C(2)-1R	49.82	4.57	24.13	73.57	62.2	1.18	75	D
G(2)-1R	38.25	3.55	17.52	60.00	47.6	1.25	43	D
G(2)-2R	9.60	5.33	21.60	65.60	57.3	1.14	56	D
G(2)-2S	42.70	8.12	25.40	60.00	57.3	1.04	57	D
PBO(380)-1R	55.60	4.32	53.85	76.10	56.0	1.35	81	S
PBO(380)-2R	54.70	4.57	8.64	79.40	73.6	1.08	89	D
PBO(380)-2S	63.20	4.32	8.64	75.44	73.6	1.02	97	D
C(610) - 1R	49.37	5.33	9.65	54.40	54.6	1.00	29	S
C(610) - 2R	71.20	5.33	9.90	82.70	71.0	1.16	97	D

Note: 1.0 mm=0.039 in. *specimen strengthened with carbon strip

Notes: *Gain in ultimate load ratio= (failure load of the strengthened wall _ failure load of the control wall)/failure load of the control wall.

[a] Mode of failure designated by C = crushing of masonry, D = debonding, S = slippage of fiber within cementitious matrix.

Table 5 - Accumulative energy dissipation and ductility index

Wall	Strengthening system	Specimen ID	Fiber axial stiffness $k^f = E_f * A_f$ (kN)	Normalized fiber axial stiffness k^f	Energy dissipation * (kN.m)	Normalized energy dissipation **	Ductility index μ_Δ
1		Control-R	-	-	2.32	43	1
2		Control-S	-	-	1.48	26	1
3	NSM	C(2)-1R*	4003	2.68 k^f	1.97	35	1.88
4		C(2)-1R	4003	2.68 k^f	1.62	24	0.97
5		G(2)-1R	1490	k^f	3.02	59	0.90
6		G(2)-2R	2980	$2k^f$	2.62	47	0.73
7		G(2)-2S	2980	$2k^f$	2.39	35	0.59
8	FRCM	PBO(380)-1R	5143	3.45 k^f	4.18	56	2.20
9		PBO(380)-2R	10287	6.9 k^f	3.03	43	0.54
10		PBO(380)-2S	10287	6.9 k^f	2.04	25	0.38
11		C(610)-1R	7320	4.9 k^f	2.45	30	0.33
12		C(610)-2R	14640	9.8 k^f	2.91	32	0.34

Note: 1.0 mm=0.039 in. *specimen strengthened with carbon strip

*Accumulative energy dissipation

**Normalized accumulative energy dissipation with respect to first cycle

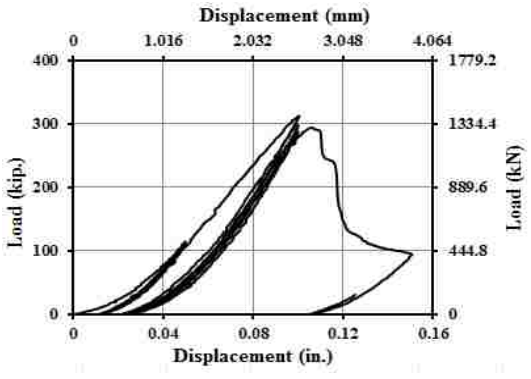

Load- displacement curve for masonry prism

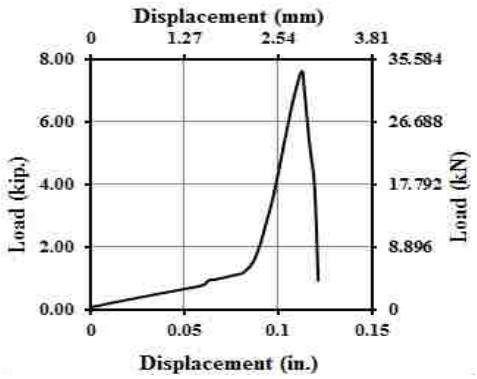

Load- displacement curve for mortar

Figure 1. Load- displacement curve for masonry prism and mortar

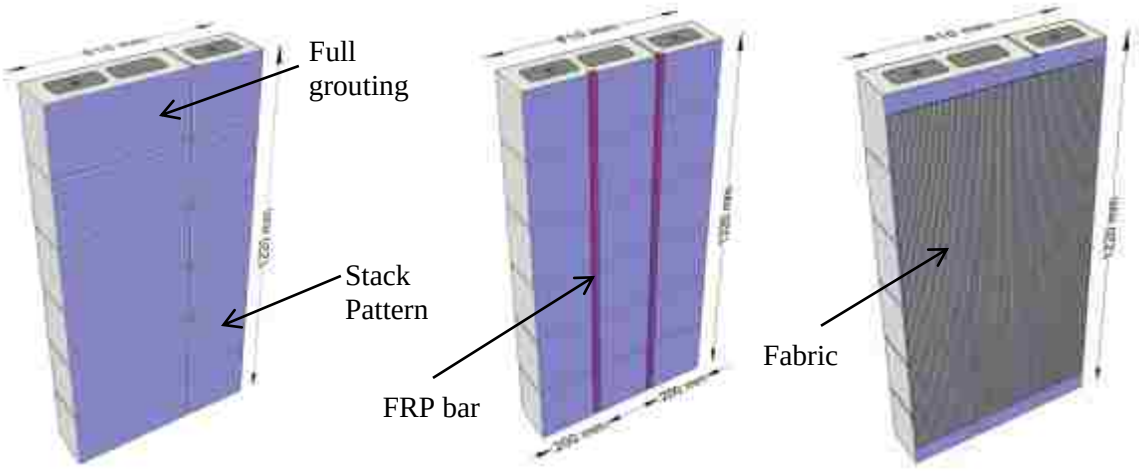

Figure 2. Test specimens: (a) stack pattern, (b) strengthened wall with NSM (c) strengthened wall with FRCM

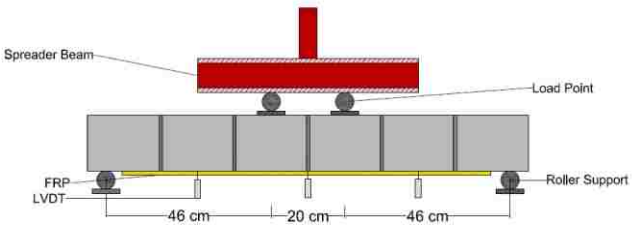

Figure 3. Test setup

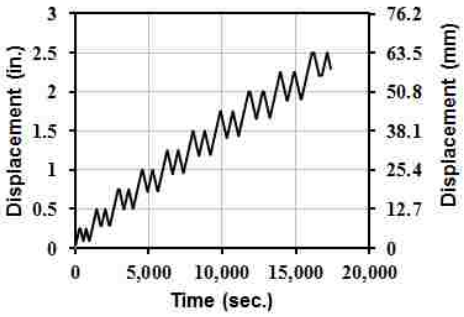

Figure 4. Cyclic loading protocol

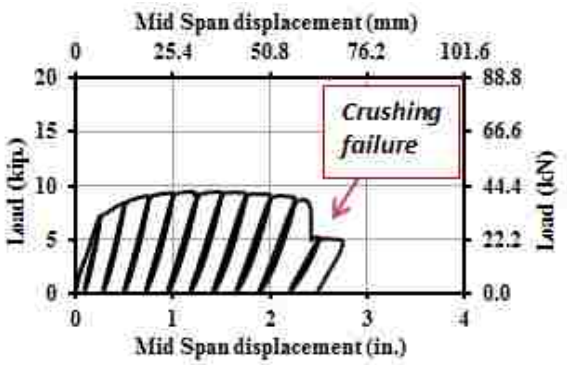

Control-R

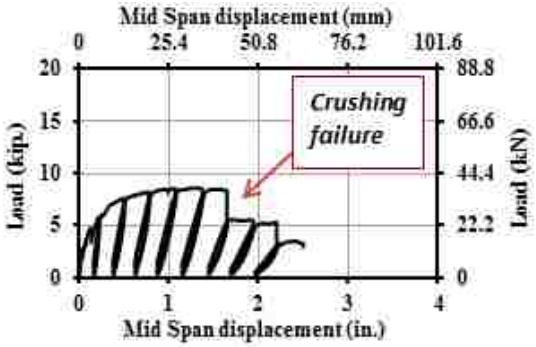

Control-S

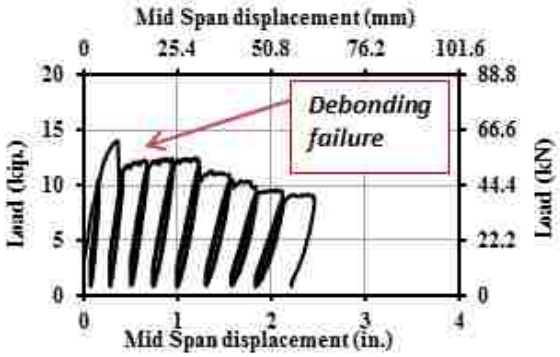

C(2)-1R*

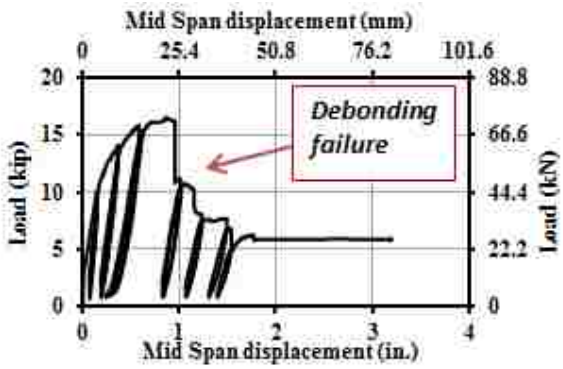

C(2)-1R

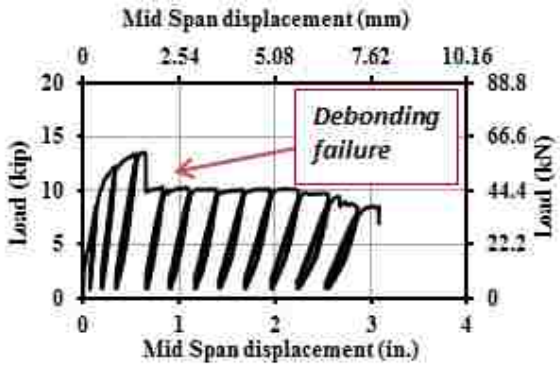

G(2)-1R

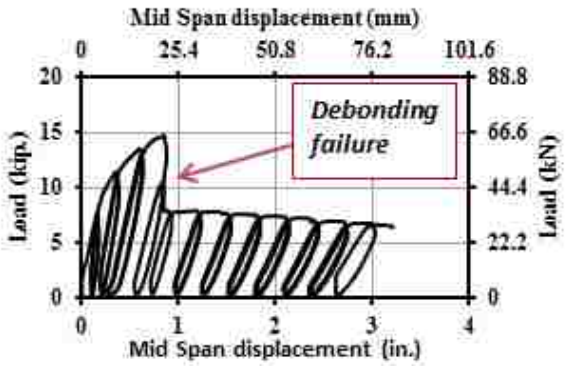

G(2)-2R

Figure 5. Load-displacement curves for test specimens

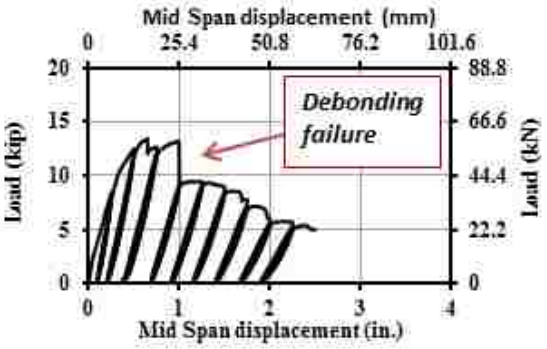

G(2)-2S

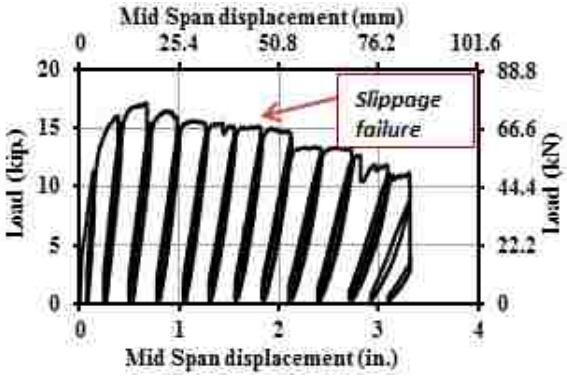

PBO(380) -1R

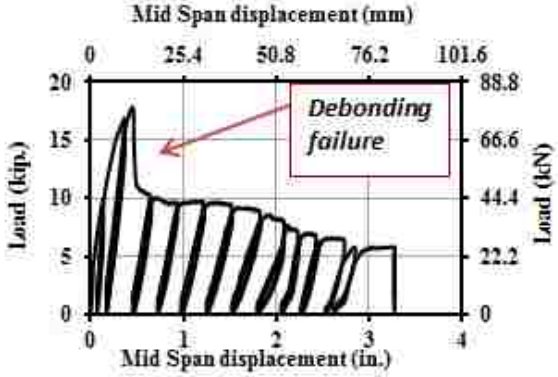

PBO(380) -2R

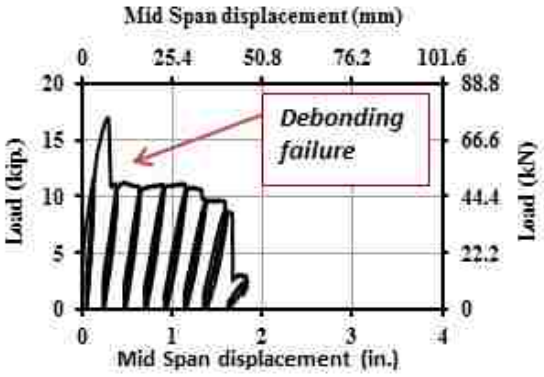

PBO(380) -2S

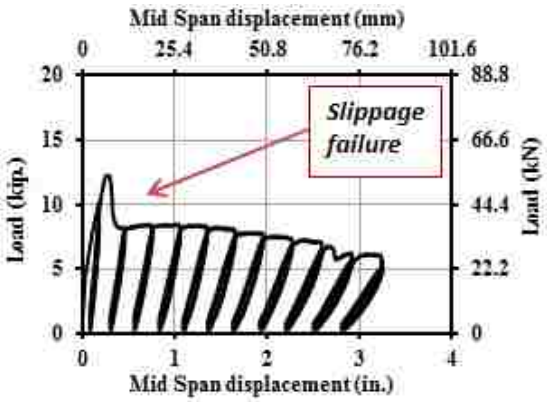

C(610) -1R

C(610) -2R

Figure 5. Load-displacement curves for test specimens (cont.)

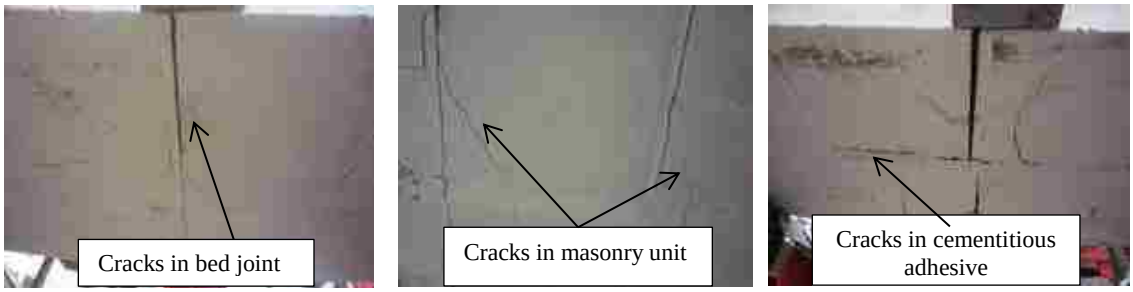

(a) Bed joint cracks (b) Masonry unit cracks (c) Cementitious adhesive cracks

Figure 6. Cracks developed during the loading

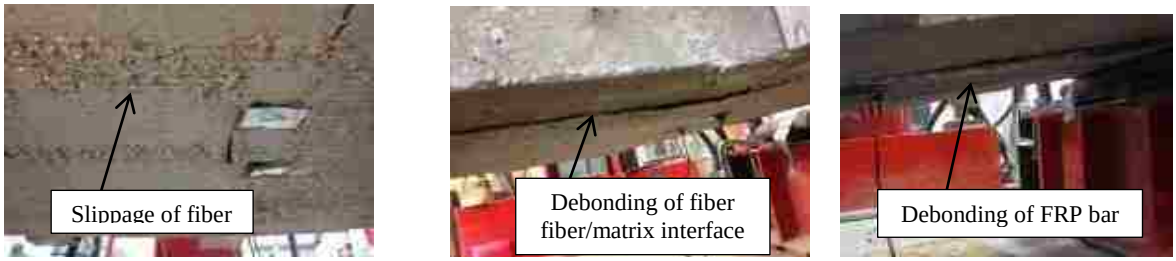

(a) FRCM-slippage (b) FRCM-debonding (c) NSM-debonding

Figure 7. Observed mode of failure

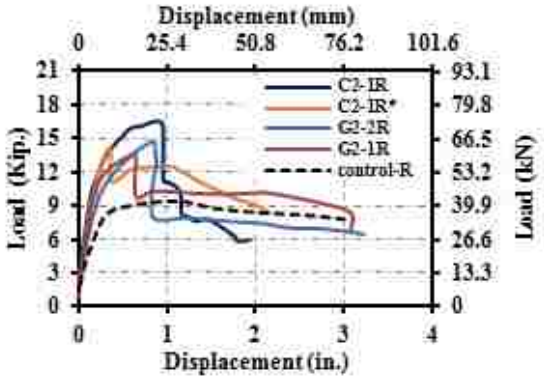

(a)

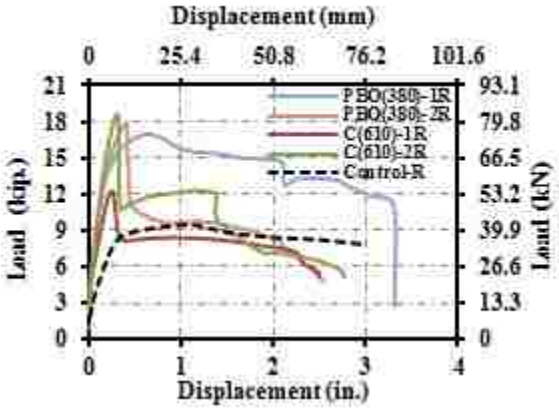

(b)

Effect of type and amount of fiber (a) NSM, (b) FRCM

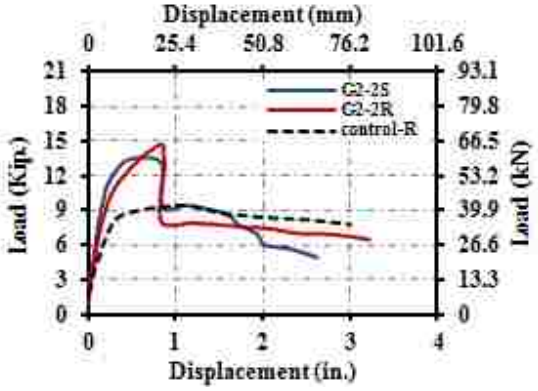

(c)

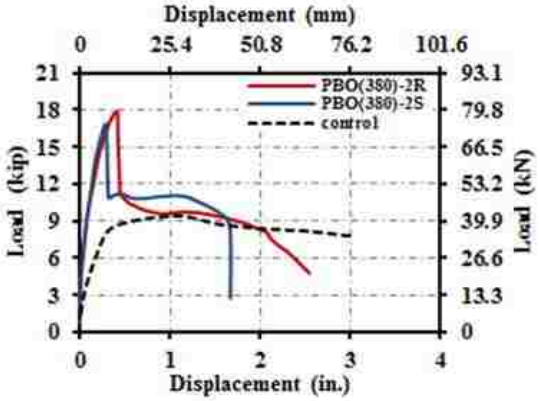

(d)

Effect of masonry bond pattern (c) NSM, (d) FRCM

Figure 8. Load-displacement curves for test specimens

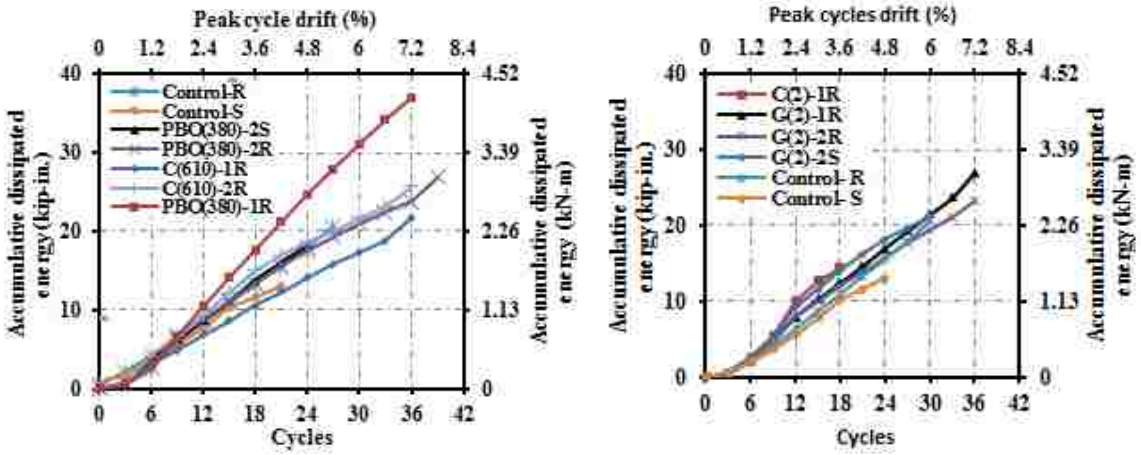

(a) (b)

Figure 9. Comparison of cumulative dissipated energy for masonry wall strengthened with (a) FRCM (b) NSM system

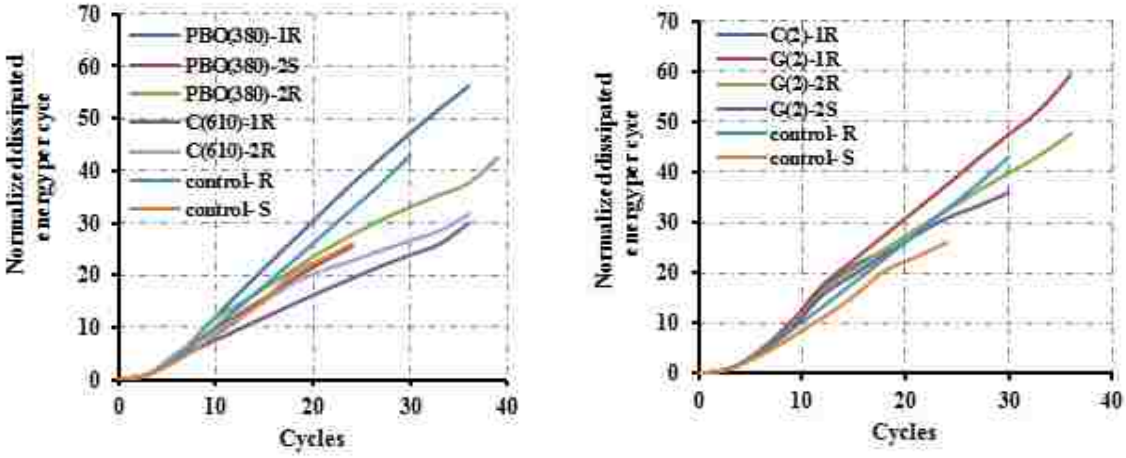

(a) (b)

Figure 10. Normalized dissipated energy variation with the cycle number for (a) FRCM, (b) NSM system

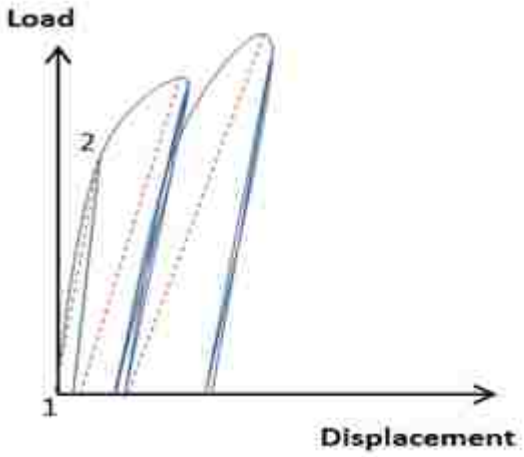

Figure 11. The procedure adopted for determining secant stiffness

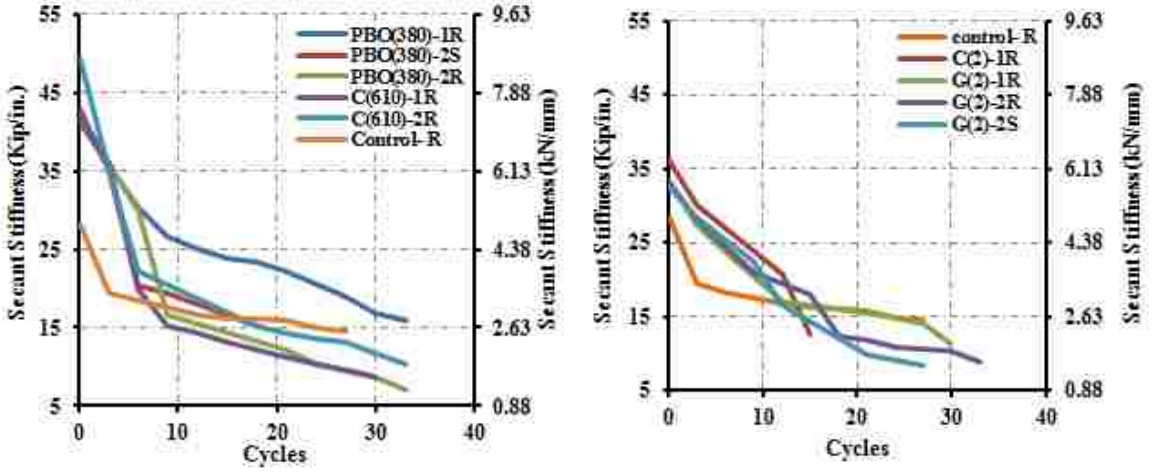

(a) (b)

Figure 12. Comparison of secant stiffness for masonry wall strengthened with (a) FRCM (b) NSM system

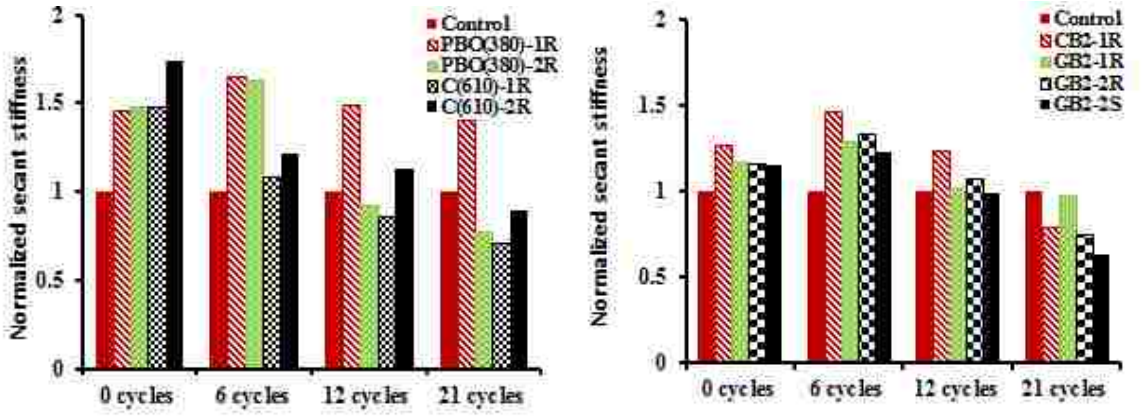

(a) (b)

Figure 13. Normalized secant stiffness for masonry wall strengthened with (a) FRCM (b) NSM system

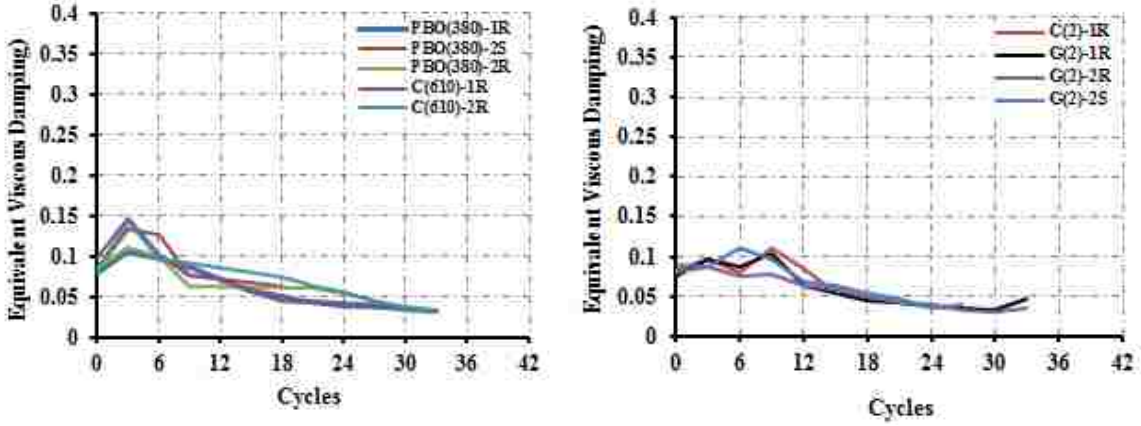

(a) (b)

Figure 14. Comparison of equivalent viscous damping for masonry wall strengthened with (a) FRCM (b) NSM system

REFERENCES

AC434. (2011). Proposed acceptance criteria for masonry and concrete strengthening using fiber-reinforced cementitious matrix (FRCM) composite system.

ACI549.4R-13. (2013). Guide to design and construction of externally bonded fabric-reinforced cementitious matrix (FRCM) systems for repair and strengthening concrete and masonry structures.

Al-Abdwais, A., & Al-Mahaidi, R. (2016). Modified cement-based adhesive for near-surface mounted CFRP strengthening system. Construction and Building Materials, 124, 794-800.

Al-Jabari, Z., Myers, J. J., & ElGawady, M. (2015). Out-of-Plane Strengthening of Reinforced Masonry Walls using Near-Surface Mounted (NSM) FRP Bars with Epoxy and Cementitious Materials. Advanced Composites in Construction, ACIC, 195-200.

Al-Jaberi, Z., Myers, J., & ElGawady, M. (2016). Flexural capacity of out-of-plane reinforced masonry walls strengthened with externally bonded(EB) FRP. Paper presented at the 7th International Conference on Advanced Composite Materials in Bridges and Structures Vancouver, British Columbia, Canada

Al-Jaberi, Z., Myers, J. J., & ElGawady, M. (2015). Influence of Near-Surface Mounted (NSM) FRP on the Out-of-Plane Behavior of Reinforced Masonry Walls. Paper presented at the 12th North American Masonry Conference.

Al-Salloum, Y. A., Siddiqui, N. A., Elsanadedy, H. M., Abadel, A. A., & Aqel, M. A. (2011). Textile-reinforced mortar versus FRP as strengthening material for seismically deficient RC beam-column joints. Journal of Composites for Construction, 15(6), 920-933.

Awani, O., El-Maaddawy, T., & Ismail, N. (2017). Fabric-reinforced cementitious matrix: A promising strengthening technique for concrete structures. Construction and Building Materials, 132, 94-111.

Babaeidarabad, S., & Nanni, A. (2015). Out-of-Plane Strengthening of URM Walls with Fabric-Reinforced-Cementitious-Matrix (FRCM). Special Publication, 299, 1-12.

Bruneau, M. (1994). State-of-the-art report on seismic performance of unreinforced masonry buildings. Journal of Structural Engineering, 120(1), 230-251.

De Lorenzis, L., & Nanni, A. (2002). Bond between near-surface mounted fiber-reinforced polymer rods and concrete in structural strengthening. ACI structural Journal, 99(2), 123-132.

ElGawady, M., Lestuzzi, P., & Badoux, M. (2006). Retrofitting of masonry walls using shotcrete. Paper presented at the Proceedings of NZSEE 2006 conference, New Zealand.

Galati, N., Tumialan, G., & Nanni, A. (2006). Strengthening with FRP bars of URM walls subject to out-of-plane loads. Construction and Building Materials, 20(1), 101-110.

Gattesco, N., & Boem, I. (2015). Experimental and analytical study to evaluate the effectiveness of an in-plane reinforcement for masonry walls using GFRP meshes. Construction and Building Materials, 88, 94-104.

Griffith, M. C., Kashyap, J., & Ali, M. M. (2013). Flexural displacement response of NSM FRP retrofitted masonry walls. Construction and Building Materials, 49, 1032-1040.

Griffith, M. C., Magenes, G., Melis, G., & Picchi, L. (2003). Evaluation of out-of-plane stability of unreinforced masonry walls subjected to seismic excitation. Journal of Earthquake Engineering, 7(spec01), 141-169.

Hart, G., Englekirk, R., & Hong, W. (1988). Structural Component Model of Flexural Walls. Paper presented at the Proceedings of the 4th Meeting of the Joint Technical Coordinating Committee on Mas-onry Research US-J apan Coordinated Earthquake Research Program, San Diego, Califor—knaafisenxn 13am airmen 1997sE.

Hassanli, R., ElGawady, M. A., & Mills, J. E. (2015). Experimental investigation of in-plane cyclic response of unbonded posttensioned masonry walls. Journal of Structural Engineering, 142(5), 04015171.

Ismail, N., & Ingham, J. M. (2012). In-situ and laboratory based out-of-plane testing of unreinforced clay brick masonry walls strengthened using near surface mounted twisted steel bars. Construction and Building Materials, 36, 119-128.

Ismail, N., & Ingham, J. M. (2016). In-plane and out-of-plane testing of unreinforced masonry walls strengthened using polymer textile reinforced mortar. Engineering Structures, 118, 167-177.

Kim, H. S., & Shin, Y. S. (2011). Flexural behavior of reinforced concrete (RC) beams retrofitted with hybrid fiber reinforced polymers (FRPs) under sustaining loads. Composite Structures, 93(2), 802-811.

MSJC. (2013). Building code requirements for masonry structures. ACI 530-13/ASCE 5-13, TMS 402-13.

Papanicolaou, C. G., Triantafillou, T. C., Papathanasiou, M., & Karlos, K. (2008). Textile reinforced mortar (TRM) versus FRP as strengthening material of URM walls: out-of-plane cyclic loading. Materials and Structures, 41(1), 143-157.

Parisi, F., Iovinella, I., Balsamo, A., Augenti, N., & Prota, A. (2013). In-plane behaviour of tuff masonry strengthened with inorganic matrix–grid composites. Composites Part B: Engineering, 45(1), 1657-1666.

Priestley, M. N., Seible, F., & Calvi, G. M. (1996). Seismic design and retrofit of bridges: John Wiley & Sons.

Rodrigues, H., Furtado, A., & Arêde, A. (2017). Experimental evaluation of energy dissipation and viscous damping of repaired and strengthened RC columns with CFRP jacketing under biaxial load. Engineering Structures, 145, 162-175.

Said, A., & Nehdi, M. (2004). Performance of structural concrete frames reinforced with GFRP grid. Paper presented at the Thirteenth world conference on earthquake engineering.

Shannag, M. J., Abu-Dyya, N., & Abu-Farsakh, G. (2005). Lateral load response of high performance fiber reinforced concrete beam–column joints. Construction and Building Materials, 19(7), 500-508.

Shao, Y., & Mirmiran, A. (2005). Experimental investigation of cyclic behavior of concrete-filled fiber reinforced polymer tubes. Journal of Composites for Construction, 9(3), 263-273.

Soudki, K., & Alkhrdaji, T. (2005). Guide for the design and construction of externally bonded FRP systems for strengthening concrete structures (ACI 440.2 R-02). Paper presented at the Structures Congress 2005: Metropolis and Beyond.

Tobriner, S. (1984). A history of reinforced masonry construction designed to resist earthquakes: 1755-1907. Earthquake Spectra, 1(1), 125-149.

Tumialan, J. G., Galati, N., & Nanni, A. (2003). FRP strengthening of URM walls subject to out-of-plane loads. ACI Structures Journal, 100(3), 312-329.

Turco, V., Secondin, S., Morbin, A., Valluzzi, M., & Modena, C. (2006). Flexural and shear strengthening of un-reinforced masonry with FRP bars. Composites Science and Technology, 66(2), 289-296.

Velazquez-Dimas, J. I., Ehsani, M. R., & Saadatmanesh, H. (2000). Out-of-plane behavior of brick masonry walls strengthened with fiber composites. ACI structural Journal, 97(3), 377-387.

Yoshimura, M., & Meguro, K. (2004). Proposal of retrofitting promotion system for low earthquake-resistant structures in earthquake prone countries. Paper presented at the Proc. on 13th World Conference on Earthquake Engineering, Vancouver, Canada.

IV. EXPERIMENTAL AND ANALYTICAL APPROACH FOR PREDECTION OUT-OF-PLANE CAPACITY OF REINFORCED MASONRY WALLS STRENGTHENED WITH EB-FRP

Zuhair Al-Jaberi, John J. Myers, Mohamed A. ElGawady

ABSTRACT

This extensive experimental study has shown the effectiveness of fiber reinforced polymer (FRP) external bonding (EB) in enhancing the flexural capacity of reinforced masonry (RM) walls subjected to out-of-plane cyclic load. Twelve reinforced masonry walls, 1220 mm (48 in.) long, 610 mm (24 in.) wide, 152 mm (6 in.) thick, were built using fully grouted concrete masonry units and type S mortar. The walls had three different steel reinforcement amounts, 2#3, 2#4, and 1#5, representing typical under-reinforced wall sections. The strengthened walls utilized two FRP types, glass fiber sheet (GFRP) and carbon fiber reinforced polymer laminate (CFRP). The walls were tested in four-point bending with an effective span of 1.12 m (44 in.) between the supports. They were subjected to cyclic load at a rate of 1.27 mm/min. (0.05in./min). The out-of-plane applied loads represented wind load, lateral earth pressure, and inertia force resulting from earthquakes. Four RM walls (stack and running) without strengthening were used as reference specimens. Six walls were externally strengthened using one and two sheets of GFRP. Two walls were strengthened with one and two CFRP laminate. The main parameters investigated in this study were the FRP composite (type and amount), the masonry bond pattern (stack and running), the steel reinforcement ratio (ρ), and the effect of surface preparation. This study investigated the impact of these parameters on the ductility, pre-yield stiffness, and an out-of-plane strength capacity of strengthened wall compared to an unstrengthened reinforced wall. The ultimate tensile strength of FRP

composite may not be fully utilized due to premature failure; however, through a simple model that was developed to predict the FRP debonding strain, the FRP effective strain can be achieved. The nonlinear analysis of reinforced masonry wall strengthened with FRP can be conducted using the moment–curvature relation. As a result of this study, the proposed model for predicting debonding strain and the moment-curvature relation present an excellent prediction compared to the experimental results. Different modes of failure, including compressive concrete crushing failure, FRP rupture, shear failure, and FRP debonding from the masonry substrate occurred in the strengthened reinforced walls.

1. INTRODUCTION

Many existing masonry structures around the world have been constructed to resist gravity and wind loads. Most of these structures were built with unreinforced masonry (URM) walls and perform poorly when subjected to out-of-plane load. The last few decades have seen the steel reinforced masonry walls as a typical type of wall systems. The out-of-plane flexural capacity was improved due to steel reinforcement in grouted cells of masonry walls. These structures may need to be strengthened for different reasons, among which are changes in use, construction or design defects, or to repair damage or deterioration. For these reasons, masonry walls that have insufficient out-of- plane strength to resist the forces generated by seismic events are in need of an upgrading capacity. Various strengthening techniques have been suggested to increase the flexural capacity of existing masonry walls. The following researchers (Al-Jaberi, Myers, & ElGawady, 2016; Churilov & Dumova-Jovanoska, 2012; Galati, Tumialan, & Nanni, 2006; Valluzzi, Da Porto, Garbin, & Panizza, 2014; Velazquez-Dimas, Ehsani, & Saadatmanesh, 2000) confirmed that the EB-FRP composite increases the out-of-plane

capacity of strengthened walls. Ehsani and Saadatmanesh (1996) studied the behavior of unreinforced masonry walls strengthened with FRP composite. The results of this study showed the effectiveness of EB-FRP for increasing flexure, shear strength, and ductility, for tested specimens. The mode of failure was governed by the amount of fiber reinforcement ratio. Tension failure occurred for specimens strengthened with low fiber reinforcement ratio, while a debonding failure happened for specimen strengthened with high fiber reinforcement ratio. The out-of-plane flexural behavior of masonry walls strengthened with different types of FRP was evaluated (Mosallam, 2007). Both types of fiber (E-glass and carbon) were confirmed in upgrading the flexural performance of strengthened walls. The mode of failure for strengthened specimens was due to a combination of compression failure of the masonry unit followed by a cohesive failure of FRP epoxy. The debonding failure is the major issue of concern in strengthening structural elements using FRP with epoxy. One of the reasons for this type of failure is the lack of good preparation of the substrate surface in contact with FRP composite system.

The effect of surface preparation was investigated for application of EB-FRP sheet and laminate in strengthening concrete structures (Mostofinejad & Mahmoudabadi, 2010). The results indicated that the effect of surface preparation prior to installing FRP sheets increased ultimate failure strength by 5-15% as compared to specimens strengthened without surface preparation. The influence of surface treatment was presented considering two types of treatment as a surface preparation (Toutanji & Ortiz, 2001). The results showed that surface preparation using water jet provides a better bonding strength comparing with specimen treated with sand blasting. URM wall

strengthened by GFRP and subjected to cyclic loading was studied by (Kuzik, Elwi, & Cheng, 2003). This study showed that the general behavior of the walls was very predictable. The strength and deformation characteristics of the strengthened wall were evaluated by presenting a simple model of the wall behavior. They concluded that increasing and decreasing the amount of bonded GFRP sheet reinforcement increased and decreased both the wall stiffness and the ultimate strength, respectively. Using an FRP composite dramatically increased the flexural capacity by more than twenty times that of unreinforced masonry wall. The vast majority of previous studies have focused on the behavior of unreinforced masonry walls. The first experimental database of reinforced masonry walls strengthened with EB-FRP was created (Shen, 2014). Three parameters were investigated in this study: type of FRP, FRP width, and number of FRP layers. It was proven that flexural capacity and post-crack stiffness of strengthened walls were related to the fiber reinforcement ratio. Also, the specimen strengthened with one GFRP layer failed by premature rupture of fiber, while the specimens strengthened with double layer of GFRP failed by IC debonding.

The research reported here extended the previous study by considering the behavior of fully grouted reinforced masonry walls strengthened with different types of FRP under half reversed cyclic loading. Twelve reinforced masonry walls were strengthened externally using GFRP sheets and CFRP laminate. The parameters considered were the FRP composite (type and amount), the masonry bond pattern (stack and running), steel reinforcement ratio, and the effect of surface preparation.

2. SCOPE OF THE RESEARCH

An experimental study was formulated to evaluate the performance of RM walls strengthened with EB-FRP. A series of twelve strengthened specimen tests were conducted, eight of which were strengthened in flexure with either unidirectional E-glass fiber (impregnated with an epoxy resin) or with CFRP/epoxy composite laminate system. The RM walls were tested under out-of-plane cyclic load to study the effect of different parameters such as the type of FRP composite, the fiber reinforcement ratio, the masonry bond pattern, the steel reinforcement ratio (ρ), and the effect of surface preparation. Table 1 provides details of the all masonry walls considered in this study. A simple and user-friendly model was developed to predict the FRP debonding strain. Also, the moment curvature relation was proposed to predict the full behavior of strengthened specimens. Supplementary material tests were conducted to determine the masonry components' properties (masonry unit, mortar, grout, and steel reinforcement) in addition to the EB-FRP system components (fiber and epoxy adhesive). This paper describes the experimental steps and presents the experimental and theoretical results in addition to conclusions from this research.

2.1. MATERIAL PROPERTIES

2.1.1. Masonry Wall Components and Steel. A series of tests was performed to determine each material's mechanical properties. Compressive strength test was conducted for masonry prisms constructed with two masonry concrete units and cured with the same lab condition of the walls. Also, the 28-day average compressive strength of the grout and type S mortar was evaluated. An experimental tensile test on three

specimens of mild steel was conducted. The results of all these tests based on ASTM standards associated with each test are summarized in Table 2.

2.1.2. Fibers and Bonding Materials. The mechanical properties of FRP are dependent on the fiber and resin properties, the manufacturing technique, and the quality control of the production process. The SEH fabrics are composed of glass fibers, while the Tyfo S epoxy matrix is an ambient cure adhesive composed of two components. According to the ASTM D3039-14, the minimum ultimate tensile strength and tensile modulus for the glass fiber composite in primary direction of Tyfo SHE-51 composite were 575 Mpa (83 ksi) and 26.1 GPa (3785 ksi) respectively. One layer of glass fiber composite with 1.3 mm (0.05 in.) thickness has an elongation at break of 2.1%. The pre-cured CFRP laminate used in this study was made of fibers embedded into epoxy resin under a pultrusion process with a typical 60% fiber content by volume. Based on ASTM D3039-14, the guaranteed tensile strength of CFRP is reported by the manufacturer to be 2400 MPa (350 ksi), with a tensile modulus of elasticity of 131 GPa (19000 ksi). The CFRP laminate with 1.4 mm (0.055 in.) thickness has an ultimate strain of 1.7% at failure.

Two types of structural bonding adhesive were selected for this study. Tyfo S epoxy matrix was used to bind SEH glass fiber. Components A and B of the matrix must be mixed at a volume ratio of 100:42 (A: B). SikaDur 30, an adhesive bonding material as a mixture of two parts, resin (A) and hardener (B), was used to bind CFRP laminate. The properties of the adhesive are as presented in Table 3. Bond strength between FRP and masonry substrate is critical to composite design systems. The bond strength was measured for GFRP and CFRP by pullout test based on ASTM D7913-14. Two

specimens for each type of fiber were used to validate test results since the mode of failure was bond failure in masonry substrate without rupture in tension, slip at anchoring section, or split at the concrete masonry unit as shown in Fig. 1. The bond strength of GFRP and CFRP systems were 5.2 MPa (765 psi) and 4 MPa (589 psi), respectively, which exceeds the minimum bond strength of $2.5\sqrt{f'_m}$. The adhesive strength generally exceeds the masonry strength in order to prevent the adhesive failure.

2.2. MASONRY WALL SPECIMENS AND IDENTIFICATION

The experimental program consists of twelve steel reinforced masonry walls with dimensions of 1220 x 610 x 152 mm (48 x 24 x 6 in.), as shown in Fig. 2. Each specimen was constructed using 152.5 mm (6 in.) standard masonry concrete blocks in running or stack masonry bond pattern. Four specimens served as an unstrengthened control to represent specimens in running or stack bond pattern with different steel reinforcement ratio, while the other specimens were strengthened with GFRP sheet or CFRP laminate for the EB-FRP system. Different steel reinforcement amounts of 2#3, 2#4, and 1#5 were used in fully grouted specimens of this study. These reinforcement levels comply with specification in MSJC-13 design code. These reinforcements satisfied the reinforcement size limitations, the minimum reinforcement ratio, and the maximum area of flexural tensile reinforcement.

The specimens are designated with two parts. The first part consisted of two characters represented the strengthening system information. The first character identified the number of FRP sheets or laminates: “S” for single sheet and “D” for double sheets. The second character represented the type of FRP, namely “C” for carbon and “G” for

glass. The second part identifies the internal steel reinforcement (number and size of steel rebar). For specimens with stack bond pattern, additional character “S” added between two parts.

2.3. TEST SETUP AND INSTRUMENTATION

All reinforced masonry walls were tested under four-point bending with simply supported boundaries, as shown in Fig. 3. An MTS double-acting hydraulic jack with a push-pull capacity of 620 kN (140 kips) was used to apply a vertical load on the specimen. The load was transferred to the masonry specimen by means of continuous steel plates and bars along the full width of specimens providing two equal line loads. A piece of thick rubber sheet was placed at all interfaces between the steel plate and specimen. The rubber distributed the load evenly and minimized any stress concentration due to unevenness of the wall surface. The distance between these two lines was 200 mm (8 in.). The FRP was 1118 mm (44 in.) long in order to ensure that the ends were not clamped by the supports. The load was applied in cycles of loading and unloading as a displacement control at a rate of 1.27 mm/min (0.05 in./min). The displacement amplitude increment was 6.35 mm (0.25 in.); double half loading cycle was applied for each amplitude level as illustrated in Fig. 4. Displacements at the mid and third spans were measured using three linear variable displacement transducers (LVDTs) at each side. In addition, strain gauges were installed on the steel reinforcement and fiber to measure their strains during loading. It may be noted that in previous testing of FRP strengthened URM walls, an airbag was used to apply uniform load to the test walls adjacent to a vertical strong wall as the boundary element. However, because this testing

program focused on FRP strengthened RM walls; airbag loading was not an option due to the wall capacity with the added internally fully grouted steel reinforcing.

3. SURFACE PREPARATION AND FRP INSTALLATION

The first step in the strengthening procedure is surface preparation, which includes manually removing all excessive joint mortar that was left from the construction process by using a wire brush. The residual dust resulting from the wire brushing process was vacuumed to ensure clean surface before FRP installation. The prepared surface should be even or levelled to prevent premature peeling of FRP under the loading process. Wet lay-up FRP is more sensitive to the unprepared surface because it follows the uneven surface. For specimens strengthened with GFRP, Tyfo S epoxy resin was mixed with silica fume to provide a viscous material served as a putty filler layer that smoothed and leveled the prepared surface before installation of the GFRP sheet. The pre-cut fabric was saturated with Tyfo S epoxy resin before it was applied to the tension surface of the specimen to provide good bonding with the substrate. The fabric was aligned, and the air bubbles were removed at the interface using a hand roller until the fabric was fully attached to the substrate. The Tyfo S epoxy resin was mixed at a volume ratio of 100 parts A to 42 parts B. The epoxy was applied at room temperature [21°C (70°F)] between the minimum [4°C (40°F)] and maximum [38°C (100°F)] installation limits. The curing period for Tyfo S epoxy resin is three days at 60°C (140°F). SikaDur 30 adhesive was used to bond the Aslan 400 CFRP strip. Before applying adhesive material, the sanded side of CFRP laminate was wiped with solvent for cleaning and bonding. SikaDur30 was mixed with a volume proportion of one part of component B to three parts of component A. The FRP sheet or laminate was bonded to the tension face of

the wall so that the direction of fiber was perpendicular to the bed joints. All the strengthened specimens were allowed to cure for at least two weeks prior to testing.

4. EXPERIMENTAL TEST RESULTS AND DISCUSSION

The cyclic load versus deflection curves for two control specimens (running and stack reinforced with 2#4) and all strengthened specimens are shown in Fig. 5. All control specimens failed in yielding of steel reinforcement followed by crushing of concrete masonry unit in a compression zone with a typical bilinear response. For the strengthened walls, the yield and ultimate load in addition to pre-yield stiffness were increased as compared to the control specimens. In terms of capacity, the post-failure behavior of strengthened wall was approximately the same as the control specimen.

The summary of the flexural behavior of all specimens in terms of experimental ultimate load and deflection, pre-yield stiffness, displacement ductility, strain for steel and fiber at ultimate, theatrical capacity, and the failure mode is illustrated in Table 4.

The maximum out-of-plane capacity for specimens strengthened with GFRP and CFRP improved significantly by 200% and 85% compared to the control specimen respectively. The pre-yield stiffness is defined as the slope of the load-displacement curve for tested specimens. The strengthened specimens exhibited a considerable improvement in pre-yield stiffness compared to the control specimen. The improvement in pre-yield stiffness of strengthened specimen depends on the fibers volume proportion and the quality of the bond at the fiber-bonding agent interface (Butler, Mechtcherine, & Hempel, 2010). The specimens with high fiber volume fraction and high debonding strain of epoxy exhibited maximum enhancement of pre-yield stiffness compared with other specimens. The ductility of the strengthened wall is determined from Eq. 1:

$$\mu = \frac{\Delta_u}{\Delta_y} \quad (1)$$

where μ is displacement ductility, Δ_u is ultimate displacement at mid-span (mm) and Δ_y is mid span-displacement at yielding of longitudinal steel reinforcement (mm). The ultimate displacement considered in this equation is at the level of capacity 20% below the peak load (Priestley, Seible, & Calvi, 1996). The displacement at yield is evaluated based on the strain gauge reading of the steel bars, when the value of strain reaches 0.23%. The displacement ductility of conventionally reinforced concrete masonry walls ranges from 4 to 12. However, the displacement ductility of reinforced masonry walls strengthened with EB-FRP generally ranges from 1.5 to 4.5. The same result was proven by many studies conducted on FRP-strengthened reinforced concrete beams (Chajes, Thomson, Januszka, & Finch, 1994; Ritchie, Thomas, Lu, & Connelly, 1990; Ross, Jerome, Tedesco, & Hughes, 1999).

The strain of internal steel reinforcement and FRP composite is presented in Table 4. For all strengthened specimens, the internal steel reinforcement yielded before FRP failure. The fiber effective strain may vary from 0.4-0.8 of ultimate fiber strain depending on many factors such as steel and fiber reinforcement ratio and maximum debonding strain of the adhesive agent.

4.1. EFFECT OF DIFFERENT PARAMETERS

The effect of the amount of fiber reinforcement ratio (ρ_f) is illustrated in Fig. 6 (a and b). It can be noticed that the flexural capacity increases when the FRP amount increases. Adding one sheet of GFRP ($\rho_f = 0.28\%$) or two GFRP sheets ($\rho_f = 0.56\%$) increased the flexure capacity by 134% to 200%, respectively. Doubling the carbon fiber

reinforcement ratio from ($\rho_f = 0.075\%$) to ($\rho_f = 0.15\%$) improved the enhancement of ultimate load from 38% to 85%, respectively. As a result, the relationship between fiber reinforcement ratio and flexural capacity is a proportional relationship with an optimum limit, but not one to one. Fig. 6 (c) represents the behavior of the same specimen with different types of FRP. In order to ensure an equivalent comparison, the fiber axial stiffness $(EA)_f$ was considered to evaluate the effect of FRP type. The fiber axial stiffness of the specimen strengthened with one strip of CFRP laminate $[(EA)_f = 9170\ \text{kN}\ (40788\ \text{kip.})]$ is 25% more than the fiber axial stiffness of the same specimen strengthened with one sheet of GFRP$[(EA)_f = 7308\ \text{kN}\ (32506\ \text{kip.})]$. Although the specimen strengthened with GFRP has less fiber axial stiffness, the flexural capacity of this specimen is higher than the specimens strengthened with CFRP. The load carrying capacity increased by double for the specimen strengthened with two sheets of GFRP, while it increased by 85% for the specimen strengthened with 2 strips of CFRP laminate. The reason behind that is the excellent bond of Tyfo S epoxy resin used with GFRP compared with Sika Dur30 used with CFRP. The specimen strengthened with GFRP sheet showed much greater mid-span deflection at FRP failure compared to the same specimen strengthened with CFRP laminate. Based on this result, the load carrying capacity for the strengthened specimen is affected by fiber axial stiffness and perfect bond of bonding agent. Increasing the amount of fiber reinforcement ratio increased the gain in load capacity for the strengthened specimen using the same bonding agent.

The effect of surface preparation on the capacity of the strengthened specimen can be seen in Fig. 6 (d). It can be noticed that the flexural capacity was improved by 10% by adding a putty filler layer as a base layer for GFRP sheet. The putty filler layer provides a

viscous material that reduced the porosity of the concrete unit and increased bond between the GFRP sheet and substrate. The mode of failure changed from FRP rupture (for the specimen with putty filler layer) to the debonding (for the specimen without surface preparation). The improvement in flexural capacity of masonry wall with stack bond pattern due to strengthening using GFRP is illustrated in Fig. 6 (e). The previous studies focused on improving the flexural capacity of walls with stack bond pattern by using bond beams or joint reinforcement because they provide better interlocking of the masonry structural elements (Committee, 1999).

The behavior of stack bond walls can be improved significantly by strengthening the specimen even though there is no reinforcement in continuous head joint. The strength capacity for the stack specimen was improved by 115% after strengthening with a single GFRP sheet compared to the control specimen. The strengthened stack wall can be designed close enough to the flexural capacity of running bond construction. After debonding, the stack bond specimen strengthened with EB GFRP behaved as two elements: a small width beam (half concrete masonry unit, CMU) and a large width beam (full CMU). This behavior of the wall is due to the small width of GFRP sheet, 200 mm (8 in.), which is not enough to maintain continuity of the two elements to resist the load as one unit. It is noteworthy that the initial stiffness for both the running and stack specimens was the same, but reduced in value for the stack specimen due to a crack formation in the continuous head joint.

Very limited experimental studies have considered the effect of varying longitudinal steel ratio on the behavior of strengthened structural elements. Fig. 6 (f) shows this effect, where the control flexural capacity and the initial stiffness are affected

by the longitudinal steel reinforcement ratio. The stiffness depends on external strengthening and the internal reinforcement ratio, so the stiffness of specimen reinforced with 2#4 bars was more than other specimens reinforced with 2#3 bars. The ultimate load and post peak behavior depend on the controlling mode of failure which is independent of the steel reinforcement ratio. The specimen reinforced with 2#4 bars failed by rupture of FRP (material fully used) followed by masonry crushing, while the specimen reinforced with 2#3 bars failed by FRP debonding from the substrate.

4.2. MODES OF FAILURE

All the control reinforced concrete masonry walls failed in a typical ductile tension mode. The compression zone at maximum moment region crushed after developing bed joint mortar cracks and significant flexural cracks in the maximum moment region. Vertical cracks were observed at the tension zone with a big opening at the mid span of control specimen. The strengthened specimens displayed two modes of failure, flexural and shear failure, in the block masonry unit. The flexural failure due to low fiber reinforcement ratio is represented by either rupture of the FRP composite or debonding from the specimen substrate. The SG-2#4 specimen was strengthened with single GFRP sheet, and the mode of failure was FRP rupture at the maximum moment region, as shown in Fig. 7 (a). Rupture of the FRP sheet was observed only in this specimen when the substrate was prepared using putty filler to increase the bond characteristics. In addition, even though FRP rupture is the preferred mode of failure, there is no guaranty that this mode of failure can be achieved all the time (Tumialan, Galati, & Nanni, 2003).

The specimen strengthened with the same reinforcement ratio of [SG-2#4*] but without surface preparation failed by debonding FRP composite. The FRP debonding is attributed to the loss of adhesive bond as a result of shear transfer at the fiber/masonry interface. The debonding started from a flexural tensile crack initiated in the bed joint of maximum moment region. Further flexural tensile cracks in the adjacent bed joint mortar and within the CMU developed due to redistribution of the stresses along the length of FRP composite, as shown in Fig. 7 (b). The specimen strengthened with high fiber reinforcement ratio [DG-2#4] failed by shear mode due to shear cracks developed within the CMU, as shown in Fig. 7 (c).

4.3. CONCRETE AND MASONRY CODE PROVISIONS FOR FRP STRAIN LIMIT

The prediction of FRP debonding strain is very critical in the design procedure to calculate the out-of-plane capacity of strengthened masonry walls. The bond capacity models of EB-FRP are either functions of maximum transferable load or maximum FRP strain. Most existing models are derived for reinforced concrete structural elements; on the other hand, a few models are based on measured FRP strain at debonding cracks of masonry samples. Table 5 shows a list of design models of existing codes and standards proposed for concrete and masonry structures. Based on experimental results, debonding failure is the control mode for most specimens of this study.

The five concrete/FRP debonding models adopted by common selected existing codes were evaluated in terms of applicability for strengthened masonry structures. The concrete compressive strength ($\grave{f_c}$) in these models was replaced by compressive strength of concrete masonry prism $\grave{f_m}$. Table 6 summarizes the ratio of prediction to experimental

debonding strain based on five concrete models. Among the five selected codes, the ACI 440.2R (2008) and the Chinese CECS-146 (2003) have good agreement with experimental data compared to other codes, but these codes are still very conservative in predicting debonding strain, as shown in Fig. 8. Also, TR55 (2004) and CNR DT-200 (2012) present a much lower predicted debonding strain compared to other codes. As a result, all the concrete models have a conservative prediction (all data are below the ideal line of Fig. 8) and much lower accuracy to predict debonding strain in terms of applicability in strengthened masonry structures.

The results of existing models for predicting debonding strain of strengthened masonry structures (ACI 440.7R (2010) and CNR DT-200 (2012)) are summarized in Table 6. ACI 440.7R (2010) sets limits for FRP strain at 45% of ultimate fiber strain ε_{fu} without any consideration to FRP or substrate properties. CNR DT-200 (2012) considers different parameters such as FRP properties, masonry properties, and optimal bond length, but this code considers the masonry ultimate compressive strain 0.35%, which is not applicable for concrete masonry units. CNR DT-200 (2012) has lower accuracy of average predicted/experimental debonding strain, which is 16%, comparing with 75% for ACI 440.7R (2010), as shown in Fig.9.

4.4. PROPOSED FRP DEBONDING STRAIN MODEL AND VALIDATION

It is important to develop a model for predicting the debonding strain of FRP-strengthened reinforced concrete masonry element based on experimental tests. In order to propose an appropriate bond reduction factor for RM walls, equivalent reinforcement ratio was considered. Equivalent reinforcement ratio is a factor combining the geometry, steel, and fiber properties together, as represented in Eq. 2.

$$\rho_{l,eq} = A_s/(b\, d_s) + (A_f E_f/E_s)/(b d_f) \quad (2)$$

The bond reduction factor $\frac{\varepsilon_{fd}}{\varepsilon_{fu}}$ as a function of equivalent reinforcement ratio ($\rho_{l,eq}$) was proposed for reinforced concrete beams and slabs strengthened with FRP as shown in Eq. 3 (Barros & Kotynia, 2008).

$$\frac{\varepsilon_{fd}}{\varepsilon_{fu}} = 0.9342 - 29.965\, \rho_{l,eq} \quad (3)$$

In the current study, the same parameter (equivalent reinforcement ratio) was considered to develop the bond reduction coefficient for reinforced masonry walls strengthened with EB-FRP and subjected to out-of-plane loading. The contrary relationship between $\frac{\varepsilon_{fd}}{\varepsilon_{fu}}$ and $\rho_{l,eq}$ was expressed in Eq. 4 and it is consistent with the previous study done for RC beams and slabs, as shown in Fig. 10.

$$\frac{\varepsilon_{fd}}{\varepsilon_{fu}} = 0.915 - 63\, \rho_{l,eq} \quad (4)$$

In order to validate the proposed debonding model, the model was compared with two selected masonry codes and then the model was implemented to predict the FRP debonding strain for existing database.

The performance of the proposed model was compared to the other two existing code models as shown in Fig.9. The proposed model was found to be an appropriate model in prediction of the FRP debonding strain for masonry members. For both codes, all the data

were below the ideal line except one data point of ACI 440.7R (2010) for specimen strengthened with CFRP laminate. In order to avoid this situation, the code provides another limitation for specimens strengthened with CFRP since the design approach was based on the glass and aramid fibers (Shen, 2014). This limitation represented by the total force per unit width transfers to the masonry substrate should not exceed 260 N/mm (1500 Ib/in.). This limitation was evaluated in current study, the ACI 440.7R very conservative since the average load transferred to the substrate is approximately five times the ACI value. This value was modified in draft version of ACI 440.7R to be not exceed 520 N/mm (3000 Ib/in.).

The only database for strengthened reinforced masonry walls was developed by Shen (2014). This database consisted of seven specimens strengthened with different glass and carbon reinforcement ratio. The accuracy of the proposed debonding model was further verified and assessed using the database of strengthened reinforced masonry walls tested by Shen (Shen, 2014). Table 7 shows the validation of the proposed FRP debonding model based on predicting the debonding strain for current walls and database specimens. The proposed model presents an excellent prediction with an average value of 85.66% for the current study and 97% for existing database.

4.5. MOMENT-CURVATURE FOR PREDICTING STRENGTHENED WALL BEHAVIOR

The nonlinear analysis of reinforced masonry wall strengthened with FRP can be conducted using the moment–curvature relation which is considers the change in strains associated with increase flexural capacity of cross section. The general moment-curvature relation is as expressed in Eq. 5.

$$\emptyset = \frac{\mathrm{M}_{ext}}{E_m I} \quad (5)$$

where $\emptyset$ is curvature in rad/in., E_m is masonry modulus of elasticity $= 900 f_m$, and I is cross section moment of inertia. The typical moment–curvature relation for a reinforced masonry section strengthened with FRP can be idealized to the trilinear stages as shown in Fig. 11. The first stage ends with initiation of cracks (uncracked), the second stage ends with steel reinforcement yielding (partially cracked), and the last stage ends with ultimate capacity due to failure at FRP or masonry unit (fully cracked).

4.5.1. Uncracked Stage. The model for this stage is linear elastic as long as the applied moment is less that the cracking moment. The cracking moment is the moment corresponding to first cracking and it shall be calculated based on modulus of rupture as shown in Eq. 6.

$$\mathrm{M}_{cr} = \frac{f_r \, I_g}{\mathrm{y}_t} \quad (6)$$

where f_r is modulus of rupture of masonry, I_g is gross moment of inertia including FRP for transformed uncracked section, and y_t is the distance from extreme tension face of cross section to the centroid. In the calculation of moment of inertia, the FRP composite is treated in the same way as the steel bars. The modulus of rupture value provided by MSJC (2013) took in consideration these parameters: the direction of flexural tensile stress, masonry and mortar type.

The mid-span deflection based on simple supported conditions for uncracked stage as presented by MSJC (2013) is:

$$\delta_u = \frac{5M_u\, h^2}{48\mathrm{E}_m\mathrm{I}_g} \qquad (7)$$

where δ_u is uncracked deflection , M_u is uncracked moment, and h is the height or span of masonry wall. The mid-span deflection for masonry wall subjected to four point load can be calculated also from Equation 8 for uncracked section, $I_e = I_g$.

$$\delta_u = \frac{(P_u/2)a}{24E_m I_e}(3l^2 - 4a^2) \qquad \text{for uncracked section, } I_e = I_g \qquad (8)$$

Where P_u is the uncracked load, E_m is modulus of elasticity; l is wall height (span of the wall); and a is the distance from support to concentrated load. Based on this equation, the theoretical initial stiffness depends only on the location of concentrated load, material property f_m and the geometry of the specimens which are the same for strengthened and control specimens. According to MSJC (2013), the modulus of elasticity of concrete masonry shall be taken as $E_m = 900f_m$. Based on many experimental studies, the experimental initial stiffness for in-plan and out-of-plan masonry walls was much lower than the theoretical uncracked stiffness and it's approximately 30 % of the theoretical value(Hart, Englekirk, & Hong, 1988; Hassanli, ElGawady, & Mills, 2015). Accordingly, the theoretical uncracked stiffness equation suggested scaling down by a factor 0.3. The curvature of the strengthened wall in this stage is:

$$\emptyset = \frac{\mathrm{M}_u}{E_m \mathrm{I}_g} \tag{9}$$

4.5.2. Partially Cracked Stage. If the applied moment is greater than the cracking moment, the cracks will initiate at the mid-span of the specimen and the pre-yield stiffness decrease compared to the uncracked stage. This stage ends with internal steel reinforcement yielding. Unlike the conventional unstrengthened reinforced masonry wall, the load can increased for strengthened specimen even after steel reinforcement yielding. The moment of inertia for cross section in the maximum moment (mid-span) region is calculated based on transformed cracked section. In the low moment region $(\mathrm{M} < \mathrm{M}_{cr})$, the gross moment of inertia is considered. The moment of inertia of any cross section along the length of the specimen is lies somewhere between gross and cracked moment of inertia. The effective moment of inertia is considered in this stage and it is a function of cracked and uncracked moment of inertia. The MSJC (2013) provide an equation for calculating the cracked moment of inertia considering cross section reinforced with steel bar only. In current study, the same equation is used with modification to include the FRP composite effect as shown in Eq. 10.

$$\mathrm{I}_{cr} = \frac{\mathrm{c}\, b^3}{12} + \frac{\mathrm{b}\, c^3}{4} + \mathrm{n}_s \mathrm{A}_s\, (\mathrm{d}_s - c)^2 + \mathrm{n}_f \mathrm{A}_f\, (\mathrm{d}_f - c)^2 \tag{10}$$

where c is distance from the fiber of maximum compressive strain to the neutral axis, b is width of section, n_s is steel to masonry modular ratio, n_f is fiber to masonry modular ratio, A_s is area of longitudinal steel reinforcement, A_f is area of FRP composite, d_s is

distance from the fiber of maximum compressive strain to the centroid of steel reinforcement, and d_f is distance from the fiber of maximum compressive strain to the centroid of FRP composite.

The Branson's model was adopted in current study to calculate the effective moment of inertia. This model was developed for reinforced concrete beams (Branson, 1977). This model represented by Eq. 11 has been considered by ACI code and MSJC (2013). The value of I_e depends on the level of applying load, for uncracked section, $I_e = I_g$, while for cracked section I_e is calculated from Eq. 11.

$$I_e = \left(\frac{M_{cr}}{M_{ext}}\right)^3 I_g + \left[1 - \left(\frac{M_{cr}}{M_{ext}}\right)^3\right] I_{cr} \; for \; (M_{ext} > M_{cr}). \quad (11)$$

Based on steel strain at yield and location of neutral axis, the curvature of this stage is calculated as shown in Eq. 12.

$$\emptyset_y = \frac{\varepsilon_y}{d_s - c} \quad (12)$$

The moment corresponding to the yield of the steel reinforcement is calculated from Eq.13.

$$M_y = \emptyset_y E_m I_e \quad (13)$$

4.5.3. Fully Cracked Stage. The strengthened specimens exhibited higher load capacity compared to the control specimen. The additional capacity depends on fiber reinforcement ratio, fiber tensile strength, and the bonding agent properties. Various models were proposed to represent the moment-curvature relation of the fully cracked stage. The simple model was proposed by (El-Mihilmy & Tedesco, 2000) which was straight line connecting yield and ultimate points in the moment-curvature relation, as shown in Fig.11. In the current study the trial and error procedure was proposed to achieve the ultimate strength of strengthened specimen. The proposed procedure based on many design assumptions such as:

- Strain compatibility between all masonry wall components.
- Based on MSJC (2013), the maximum usable strain for concrete masonry unit is 0.0025.
- Strain in steel reinforcement, FRP composite, and masonry are proportional to the distance from the neutral axis.
- The flexural tension stresses are resisted by steel and FRP reinforcement and there is no contribution from masonry unit in tension zone.
- The equilibrium condition is satisfied by balance the internal forces with external forces.
- Based on MSJC (2013), the masonry stress of $0.8\grave{f}_m$ is uniformly distributed over an equivalent compression stress block bounded by the top of compression zone and the distance 0.8c from the top of compression zone.

This procedure starts with assuming compression failure of concrete masonry at the extreme compression fiber. The neutral axis depth assumed and the strain level in steel and FRP is calculated based on its location from the neutral axis. If the FRP strain is greater or equal to the FRP debonding strain (calculated from proposed Eq.4), concrete masonry crushing controls flexural failure of the section, otherwise, the FRP failure controls flexural failure of the section. The effective stress in FRP and steel can be found from Eq. 14.

$$f_{fe} = \mathrm{E_f} * \varepsilon_{\mathrm{fe}}, \text{ and } f_s = \mathrm{E_s} * \varepsilon_{\mathrm{s}} \leq f_y \quad (14)$$

From the equilibrium equation, check the assumed depth of neutral axis c.

$$T_s + T_f = C \quad (15)$$

$$A_s f_s + A_f f_{fe} = 0.8\, \grave{f}_m * 0.8 * c * b \quad (16)$$

$$c = \frac{A_s f_s + A_f f_{fe}}{0.64\, \grave{f}_m * b} \quad (17)$$

The ultimate flexural strength ($\mathrm{M_{ult}}$)of the section strengthened with EB-FRP is computed from the Eq. 18.

$$M_{ult} = A_s f_s \left(d_s - \frac{\beta c}{2}\right) + A_f f_{fe} \left(d_f - \frac{\beta c}{2}\right) \quad 18$$

The flexural capacity should be compared to the theoretical shear capacity to verify the controlling mode of failure. The theoretical shear capacity V_n was calculated according to the MSJC (2013) as the smallest of:

$$3.8A_{nv}\sqrt{\grave{f}_m},\ 300\ A_{nv},\ 90A_{nv}+0.45N_u \tag{19}$$

where A_{nv} is net shear area, N_u is compressive force acting normal to the shear surface. Based on concrete masonry strain at ultimate and location of neutral axis, the curvature of this stage is calculated as shown in Eq. 20.

$$\emptyset_{ult} = \frac{\varepsilon_{c)ult}}{c_{ult}} \tag{20}$$

The effective moment of inertia of the cross section corresponding to e this stage is calculated from Eq. 21.

$$I_e = \frac{M_{ult}}{\emptyset_{ult} E_m} \tag{21}$$

Its assumed that the walls post-failure capacity dropped to approximately a load level equivalent to the measured yielding load.

4.6. COMPARISON ANALYTICAL APPROACH WITH EXPERIMENTS

The applicability of the presented analytical approach was tested by comparing the prediction behavior with experimental behavior for different specimens, as shown in Fig. 12. The theoretical ultimate capacity of reinforced walls has been calculated and compared with experimental results, as shown in Table 4. The proposed method succeeded for predicting full behavior of strengthened wall as close as possible to the experimental behavior, especially for the uncracked and partially cracked stage. For the fully cracked stage, it is very hard to predict the effective moment of inertia with high accuracy. The approximation of predicting the effective moment of inertia missed the value of ultimate deflection. As a result, the proposed approach predicts the strengthened wall behavior with reasonably good accuracy.

5. CONCLUSIONS

Based on the test results of reinforced masonry walls strengthened with externally bonded FRP, the main conclusions are as follows:

1- The out-of-plane flexural capacity and pre-yield stiffness remarkably increased with a reduction in displacement ductility for strengthened wall compared to unstrengthened reinforced masonry wall. The flexural capacity increased by three and two times for specimens strengthened with GFRP and CFRP compared to control capacity, respectively. The pre-yield stiffness depends not only on fiber reinforcement ratio, but also on the internal steel reinforcement ratio, maximum debonding strain for adhesive material, and the masonry bond pattern. As expected, the specimen strengthened with two GFRP sheets presented higher pre-yield stiffness, approximately four times compared with the control specimen. The displacement

ductility of conventionally reinforced concrete masonry walls ranges from 4 to 12. However, the displacement ductility of reinforced masonry walls strengthened with EB-FRP generally ranges from 1.5 to 4.5.

2- The surface preparation by adding a putty filler layer as a base layer for GFRP sheet improved the flexural capacity by 10%. The putty filler layer provides a viscous material that reduced the porosity of the concrete unit and increased bond between GFRP sheet and substrate. Also, the mode of failure changed from FRP rupture (for the specimen with putty filler layer) to FRP debonding (for the specimen without surface preparation).

3- The flexural capacity of stack specimens improved even though there was no reinforcement for continuous head joint. The strength capacity for the stack specimen was improved by 115% after strengthening compared to the control specimen. The initial stiffness for both the running and stack specimens was the same, but reduced in value for the stack specimen due to a crack formation in the continuous head joint.

4- The strengthened specimens displayed two modes of failure: flexural and shear failure. The flexural failure is represented by either rupture of the FRP composite or debonding from the specimen substrate. Most strengthened specimens exhibited a debonding failure due to loss of adhesive bond as a result of shear transfer at the fiber/masonry interface. Rupture of the FRP composite was observed only in the specimen strengthened with a single GFRP sheet when the substrate was prepared using putty filler to increase the bond characteristics. The specimen strengthened with high fiber reinforcement ratio (two GFRP sheets) failed by shear mode due to shear cracks developed within the CMU.

5- Among many codes, the FRP debonding strain of ACI 440.2R (2008) and the Chinese CECS-146 (2003) have good agreement with experimental data compared to other codes, but these codes are still very conservative and have much lower accuracy to predict FRP debonding strain. In regards to accuracy of masonry codes, CNR DT-200 (2012) has lower accuracy of average predicted/experimental debonding strain, which is 16%, comparing with 75% for ACI 440.7R (2010). The proposed model for predicting debonding strain presents an excellent prediction with an average value of 85.66% for the current study and 97% for existing database.

6- Using moment–curvature relation was very useful for predicting strengthened wall behavior, especially for uncracked and pre-yield stages, in addition to predicting the ultimate flexural capacity for the fully cracked stage.

ACKNOWLEDGEMENTS

This research was conducted at Missouri University of Science and Technology in the Structural Engineering Research Laboratory (SERL) in Rolla, Missouri. The authors gratefully wish to acknowledge the support of Midwest Block & Brick in Jefferson City, Missouri, and HCED (The Higher Committee for Education Development in Iraq). The authors also wish to thank the technical support staff at Missouri University S&T for their efforts in this research study.

TABLES AND FIGURES

LIST OF TABLES:

LIST OF FIGURES:

Table 1- Experimental test matrix

Wall	Specimen ID	Type of FRP	Sheet or laminate width (mm)	Number of sheets or laminates	Bond adhesive type	Bond pattern
1	Control -2#4	-	-	-	-	running
2	Control-S-2#4	-	-	-	-	stack
3	Control -2#3	-	-	-	-	running
4	Control -1#5	-	-	-	-	running
5	SG-2#4	Glass	200	1	Tyfo S epoxy	running
6	SG-S-2#4	Glass	200	1	Tyfo S epoxy	stack
7	DG-2#4	Glass	200	2	Tyfo S epoxy	running
8	SG-2#3	Glass	200	1	Tyfo S epoxy	running
9	SG-1#5	Glass	200	1	Tyfo S epoxy	running
10	SG-2#4*	Glass	200	1	Tyfo S epoxy	running
11	SC-2#4	Carbon	50	1	SikaDur30	running
12	DC-2#4	Carbon	50	2	SikaDur30	running

Note : 1.0 mm = 0.039 in. *Specimen without surface preparation.

Table 2: Mechanical Properties of masonry wall components and steel bars

Material	Properties	Values	Method
Concrete block	Prism compressive strength	21	ASTM C1314-12
Type S mortar	Compressive strength	17.5	ASTM C109-13
Grout	Compressive strength	35	ASTM C109-13
Steel bar	Yield strength	471	ASTM A370-13
	Modulus of Elasticity	20300	

Note : 1.0 MPa = 0.145 ksi

Table 3: Mechanical Properties of Adhesive Materials

Material	Ultimate tensile strength (MPa)	Elongation at break %	Tensile modulus (GPa)	Method
Tyfo S epoxy	72.4	5	3180	ASTM D638-14
SikaDur 30	24.8	1	4482	ASTM D638-14

Note : 1.0 GPa = 145.03 ksi; 1.0 MPa = 0.145 ksi; 1.0 mm/mm = 1.0 in./in.; 1.0 mm = 0.039 in.

Table 4-Summary of test results

Specimen ID	Ultimate load P^{exp} (kN)	Maximum deflection (mm)	Post-crack stiffness K_c (kN/mm)	Displacement ductility	Steel strain	GFRP strain	P^{the} (kN) **	$\frac{P^{exp}}{P^{the}}$	Mode of failure [a]
Control - 2#4	41.8	61.72	4.812	4.76	13772	-	37.9	1.10	C
Control-S-2#4	38.18	41.65	4.48	4.93	9927	-	37.9	1.01	C
Control - 2#3	27.85	57.4	4.3	11.88	14644	-	21.6	1.28	C
Control - 1#5	32.66	28	3.5	4.3	9250	-	29.9	1.09	C
SG-2#4	98	12.83	20.89	3.3	12614	17000	89.36	1.09	R
SG-S-2#4	82.2	13.46	14.07	2.8	10307	11958	89.36	0.92	D
DG-2#4	125.6	23.87	23.51	2.2	2570	12500	115.3	1.09	Sh
SG-2#3	83.3	16.51	17.4	4.33	11636	15800	82.3	1.01	D
SG-1#5	82.28	10.16	14.2	2.66	5267	15000	84.37	0.97	D
SG-2#4*	88.8	13.2	20.89	2.81	11350	16000	89.36	0.99	D
SC-2#4	57.85	9.4	12.70	2.6	12743	9800	59.33	0.97	D
DC-2#4	77.25	5.85	20.45	1.35	3038	6500	76.15	1.01	D

Notes: [a] Mode of failure designated by C = crushing of masonry, R = rupture of fiber, D = debonding, Sh = shear failure.

*Specimen without surface preparation.

**Theoretical load

Table 5: Debonding Models Provided by Different Codes for Concrete and Masonry

Concrete	
Code	FRP strain limit
ACI 440.2R (2008)	$\varepsilon_{fd} = 0.41\sqrt{\acute{f}_c/nE_f t_f} \leq 0.9\varepsilon_{fu}$
JSCE (2001)	$\varepsilon_{fd} = \sqrt{2G_f/nE_f t_f}$ where $G_f = 0.644(\acute{f}_c)^{0.19}$
Chinese Code CECS-146 (2003)	$\varepsilon_{fd} = k_b f_{ct}[(1/\sqrt{nE_f t_f}) - (0.2/L_d)]$ $where\ k_b = \sqrt{(2.25 - b_f/b)/(1.25 + b_f/b)}$
Concrete society TR55 (2004)	$\varepsilon_{fd} = 0.5k_b\sqrt{f_{ct}/nE_f t_f}$ $where\ k_b = 1.06\sqrt{(2 - b_f/b)/(1 + b_f/400)} \geq 1\ with\ b_f/b \geq 0.33$
CNR DT-200 (NRC 2012)	$\varepsilon_{fd} = 0.373\sqrt{k_b\sqrt{f_{ct}\acute{f}_c}/nE_f t_f}$ $where\ k_b = \sqrt{(2 - b_f/b)/(1 + b_f/b)} \geq 1.0\ with\ b_f/b \geq 0.25$
Masonry	
Code	FRP strain limit
ACI 440.7R (2008)	$\varepsilon_{fd} = k_m \varepsilon^*_{fu} \leq 0.9\ C_E \varepsilon^*_{fu}\ where\ k_m = 0.45$
CNR DT-200 (2004)	$f_{fdd} = \frac{1}{\gamma_{fd}\sqrt{\gamma_M}}\sqrt{\frac{2E_f \Gamma_{Fk}}{t_f}}\ where\quad \Gamma_{Fk} = C_1\sqrt{f_{mk} f_{mtm}}$ and C_1=0.015, $f_{mtm} = 0.1 f_{mk}$

Notes: b = width of cross section; b_f=width of FRP sheet; E_f= FRP modulus of elasticity; $\acute{f}_c$=compressive strength of concrete; f_{ct}= tensile strength of concrete; L_d= FRP distance from its end to the section where it is fully utilized; n= number of FRP plies; t_f= FRP ply thickness. ε_{fd}= debonding strain; k_m= reduction factor for debonding strain; f_{mk} = masonry compressive strength; f_{mtm}= masonry tensile strength

Table 6: Summary of predicted to experimental debonding strain

Specimen ID	$\varepsilon_{predicted}/\varepsilon_{experimental}$						
	Models for concrete structures					Models for Masonry structures	
	ACI 440.2R (2008)	JSCE (2001)	Chinese Code CECS-146 (2003)	Concrete Society TR55 (2004)	CNR DT-200 NRC (2012)	ACI 440.7R (2010)	CNR DT-200 NRC (2012)
SG-2#4	0.600	0.484	0.680	0.258	0.325	0.556	0.143
SG-S-2#4	0.853	0.688	0.967	0.368	0.462	0.790	0.203
DG-2#4	0.816	0.658	0.767	0.314	0.417	0.756	0.193
SG-2#3	0.645	0.521	0.732	0.278	0.349	0.598	0.153
SG-1#5	0.680	0.548	0.771	0.293	0.368	0.63	0.162
SG-2#4*	0.638	0.514	0.723	0.275	0.345	0.591	0.151
SC-2#4	0.448	0.361	0.518	0.223	0.249	0.781	0.106
DC-2#4	0.675	0.544	0.744	0.319	0.375	1.176	0.160
AVG. (%)	66.934	54	73.803	29.125	36.167	73.48	15.90
S.D. (%)	12.58	10.15	12.317	4.366	6.31	20.127	2.61

Table 7: Validation of proposed model

Specimen	FRP type	$\rho_f(\%)$	$\rho_s(\%)$	$\varepsilon_{experimental}$ $(\mu\varepsilon)$	$\varepsilon_{predicted}$ $(\mu\varepsilon)$	$\varepsilon_{predicted}/\varepsilon_{experimental}$
SG-2#4	GFRP	0.279	0.592	17000	10808	0.64
SG-S-2#4	GFRP	0.279	0.592	11958	10808	0.90
DG-2#4	GFRP	0.559	0.592	12500	10291	0.82
SG-2#3	GFRP	0.279	0.328	15800	14358	0.91
SG-1#5	GFRP	0.279	0.462	15000	12583	0.84
SG-2#4*	GFRP	0.279	0.592	16000	10808	0.68
SC-2#4	CFRP	0.0753	0.592	9800	8602	0.88
DC-2#4	CFRP	0.150	0.592	6500	8036	1.23
Shen (2014)	CFRP	0.077	0.323	8313	8078	0.97
Shen (2014)	CFRP	0.154	0.323	6751	7760	1.15
Shen (2014)	CFRP	0.204	0.323	5984	7561	1.26
Shen (2014)	CFRP	0.154	0.323	7751	7760	1.00
Shen (2014)	GFRP	0.066	0.323	13479	12035	0.89
Shen (2014)	GFRP	0.066	0.323	14172	12035	0.85
Shen (2014)	GFRP	0.133	0.323	11782	11966	1.02
Shen (2014)	GFRP	0.133	0.323	14936	11966	0.80

*Specimen without surface preparation.

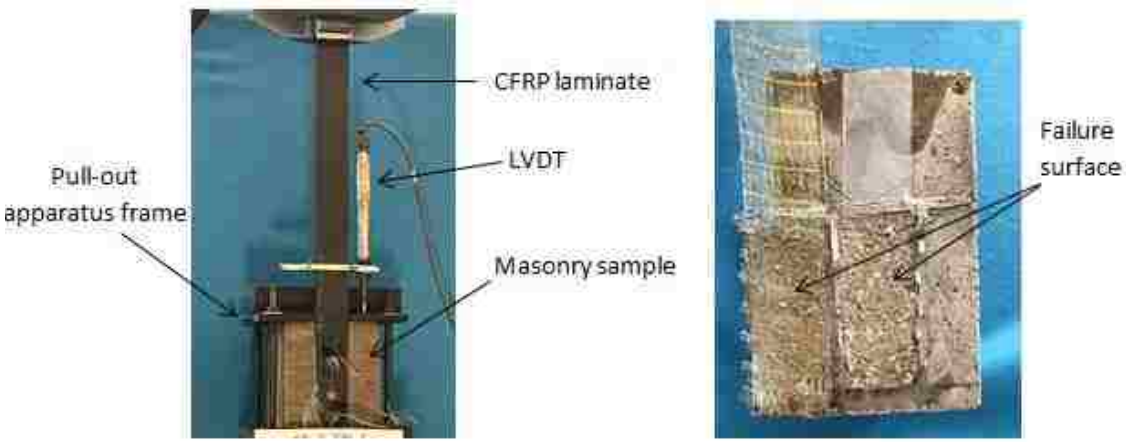

(a) (b)

Figure 1. Pull-out test: (a) test setup, (b) GFRP bond failure

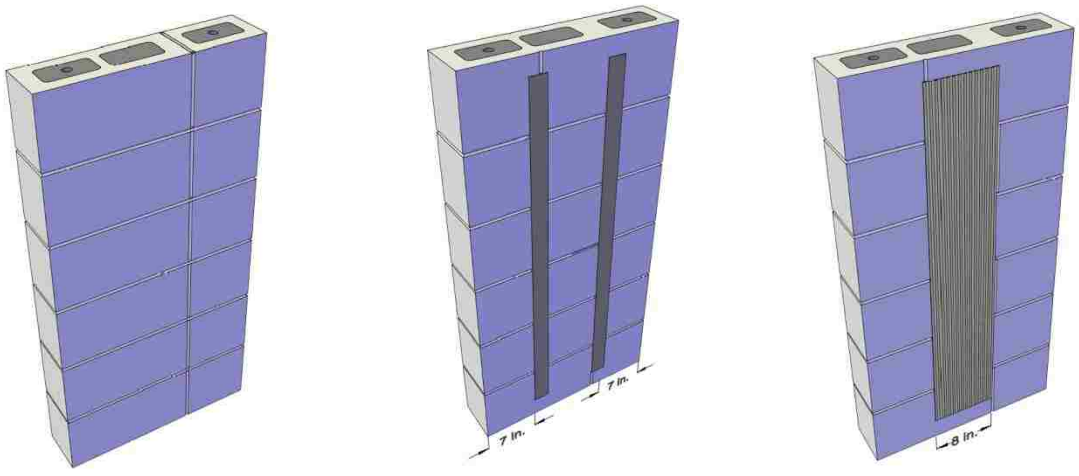

(a) (b) (c)

Figure 2. Test specimens: (a) stack pattern, (b) strengthened wall with CFRP (c) strengthened wall with GFRP

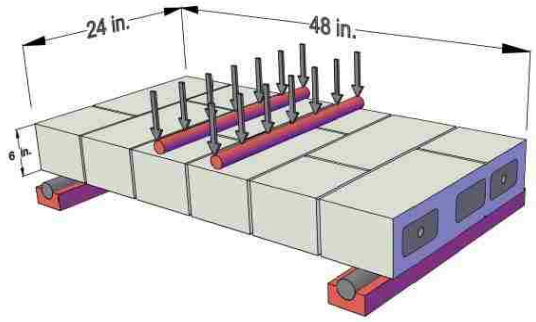

Figure 3. Test setup

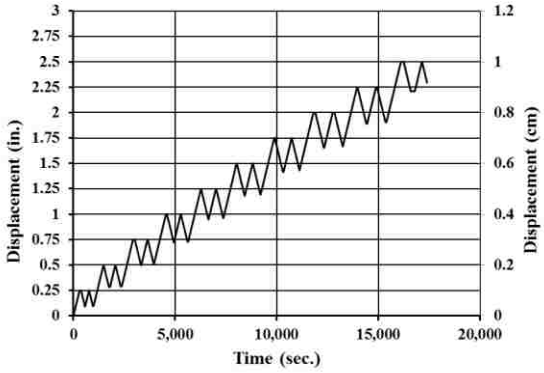

Figure 4. Cyclic loading protocol

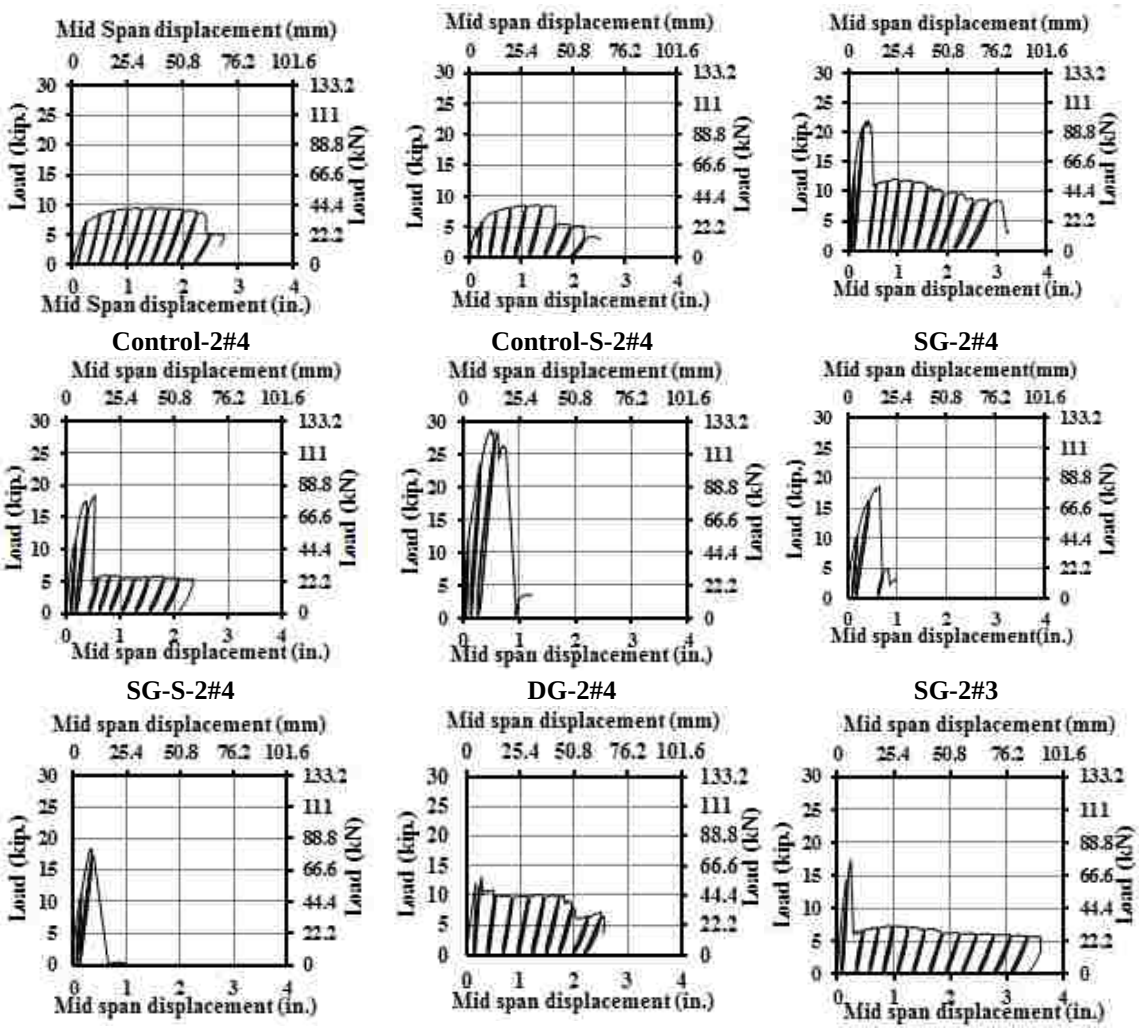

Figure 5. Load Deflection Curves

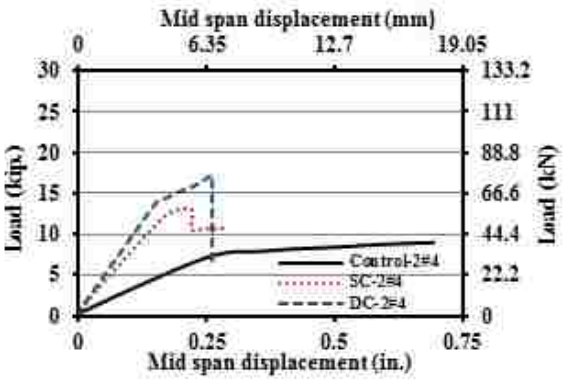

(a) Effect of CFRP amount

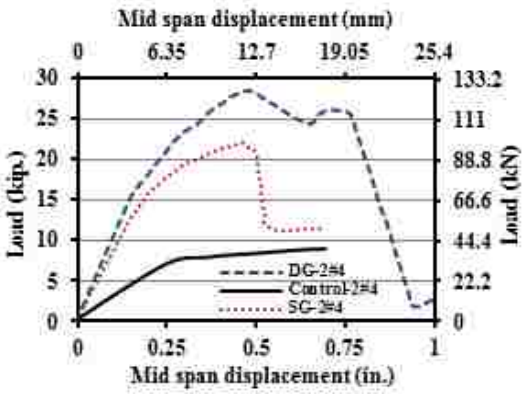

(b) Effect of GFRP amount

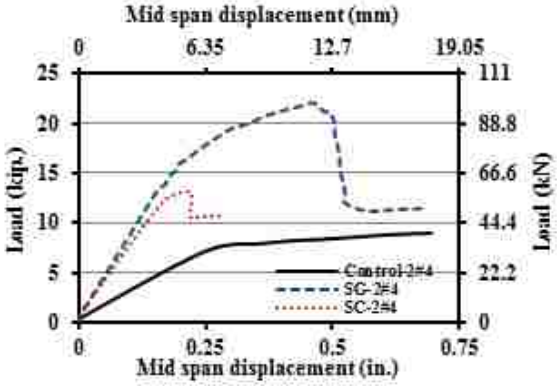

(c) Effect of FRP type

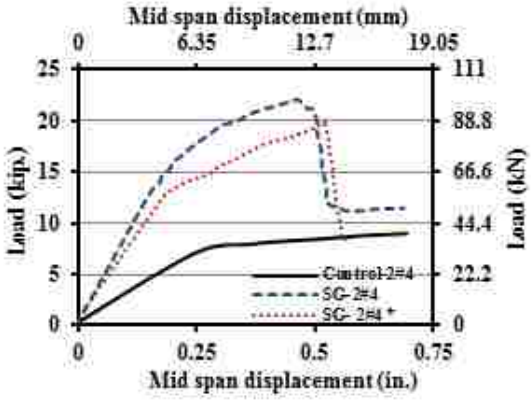

(d) Effect of surface preparation

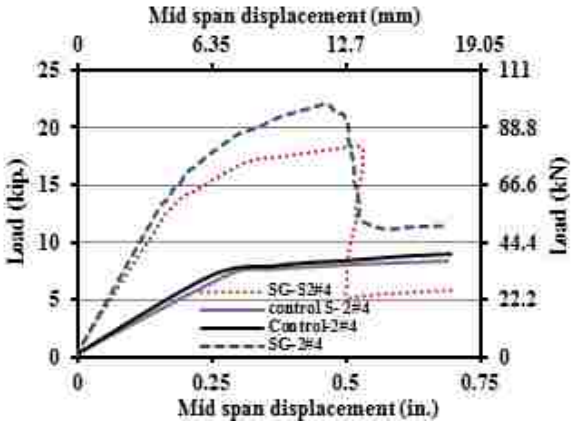

(e) Effect of masonry bond pattern

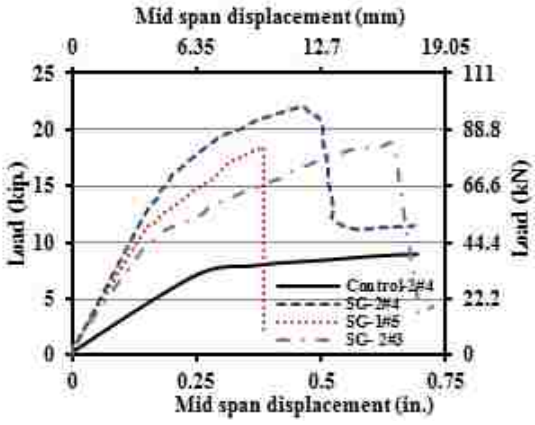

(f) Effect of steel reinforcement ratio

Figure 6. Effect of different parameters

(a) GFRP-rupture (b) FRP-debonding (c) Shear failure

Figure 7. Observed modes of failure

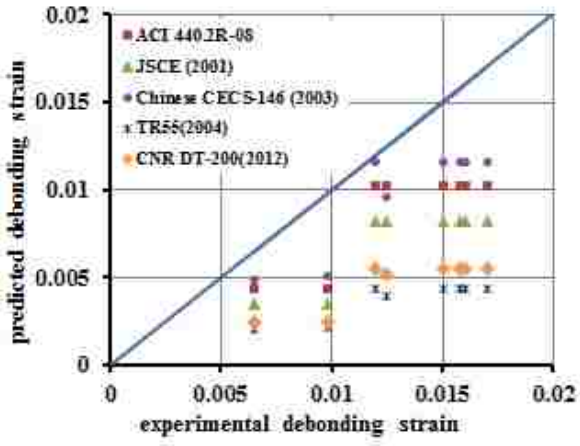

Figure 8. Experimental vs. predicted debonding strain for different concrete codes

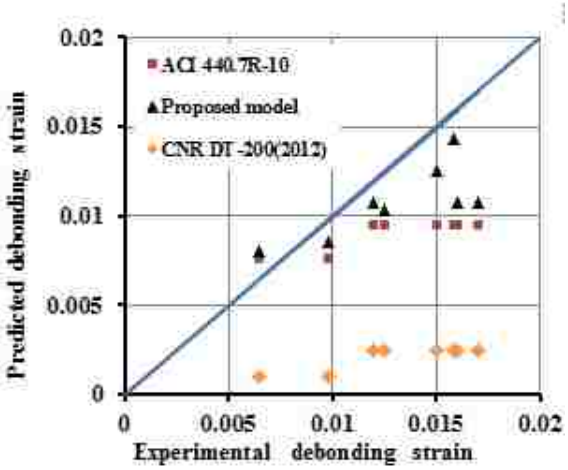

Figure 9. Experimental vs. predicted debonding strain for proposed and different masonry codes

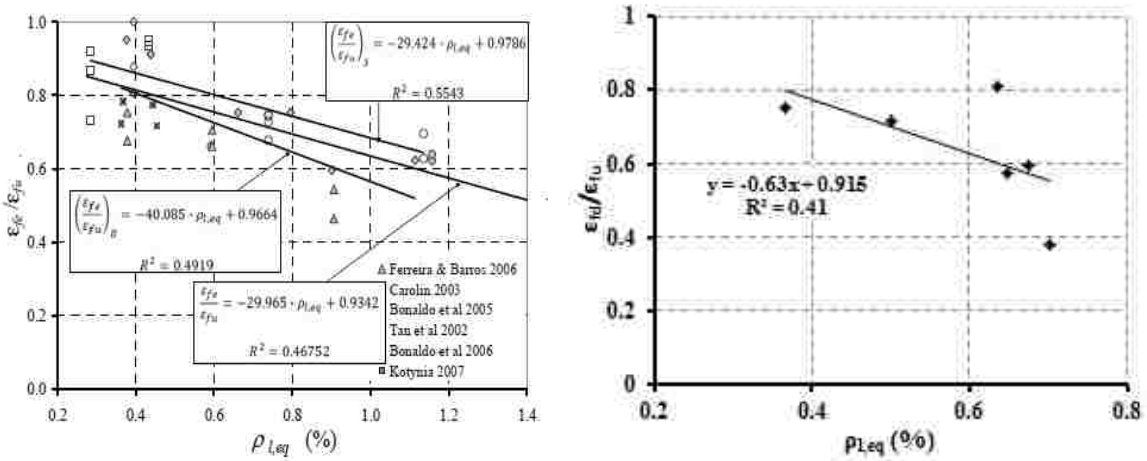

(a) (b)

Figure 10. Debonding dependent factor vs. equivalent reinforcement ratio:(a) RC beams and slabs (Barros & Kotynia, 2008) (b) reinforced masonry walls

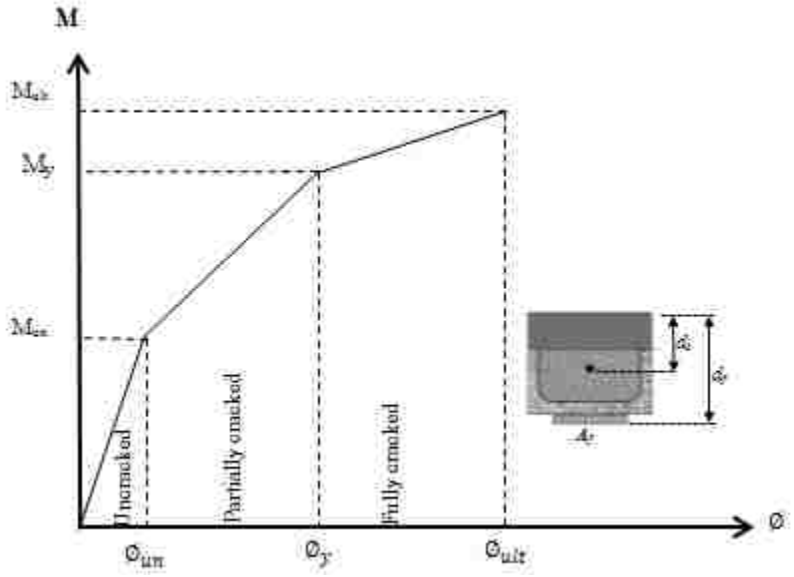

Figure11. Idealized moment-curvature relation of reinforced masonry section

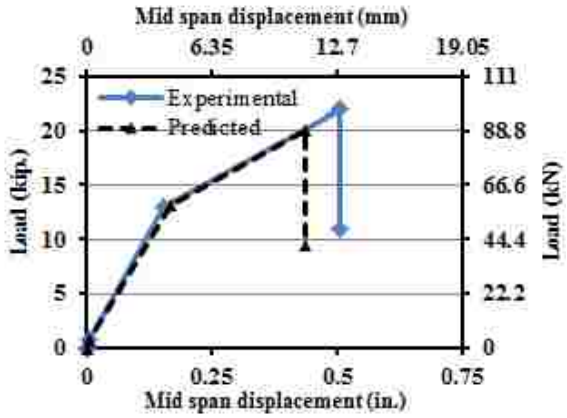

SG-2#4

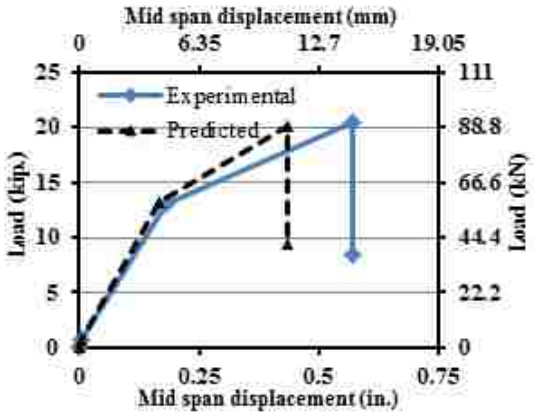

SG-2#4*

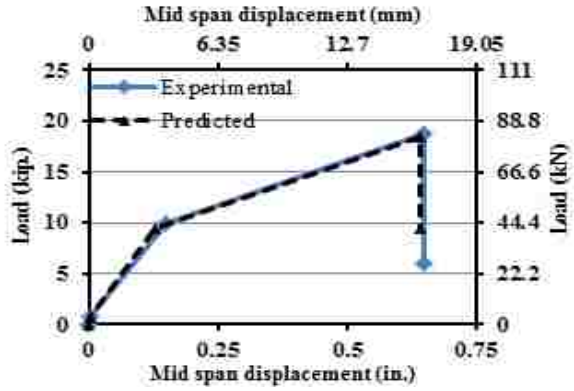

SG-2#3

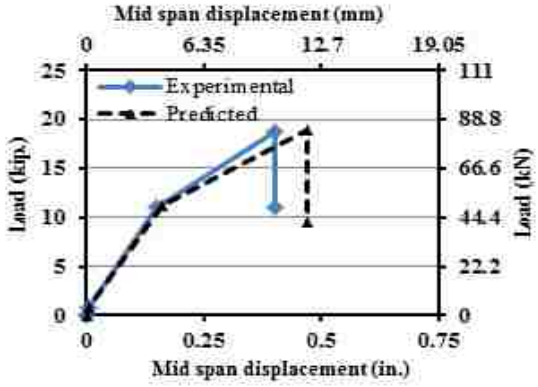

SG-1#5

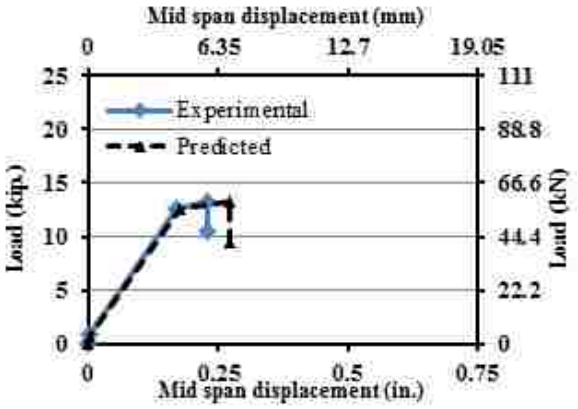

SC-2#4

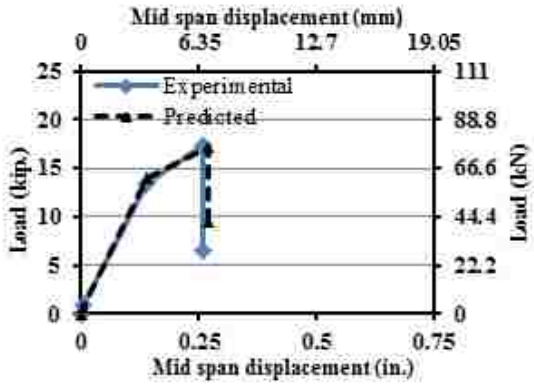

DC-2#4

Figure 12. Load-displacement curves for test specimens

REFERENCES

Al-Jaberi, Z., Myers, J., & ElGawady, M. (2016). Flexural capacity of out-of-plane reinforced masonry walls strengthened with externally bonded(EB) FRP. Paper presented at the 7th International Conference on Advanced Composite Materials in Bridges and Structures Vancouver, British Columbia, Canada

Barros, J. A., & Kotynia, R. (2008). Possibilities and challenges of NSM for the flexural strengthening of RC structures.

Branson, D. E. (1977). Deformation of concrete structures: McGraw-Hill Companies.

Butler, M., Mechtcherine, V., & Hempel, S. (2010). Durability of textile reinforced concrete made with AR glass fibre: effect of the matrix composition. Materials and Structures, 43(10), 1351-1368.

Chajes, M. J., Thomson, T. A., Januszka, T. F., & Finch, W. W. (1994). Flexural strengthening of concrete beams using externally bonded composite materials. Construction and Building Materials, 8(3), 191-201.

Churilov, S., & Dumova-Jovanoska, E. (2012). Experimental and analytical research of strengthening techniques for masonry. PhD thesis, University" Ss. Cyril and Methodius", Faculty of Civil Engineering, Skopje, Macedonia.

Committee, M. S. J. (1999). Building code requirements for masonry structures. American Concrete Institute, Detroit, MI., ISBN, 1929081022.

Ehsani, M., & Saadatmanesh, H. (1996). Seismic retrofit of URM walls with fiber composites. The Masonry Society Journal, 14(2), 63-72.

El-Mihilmy, M. T., & Tedesco, J. W. (2000). Deflection of reinforced concrete beams strengthened with fiber-reinforced polymer (FRP) plates. Structural Journal, 97(5), 679-688.

Galati, N., Tumialan, G., & Nanni, A. (2006). Strengthening with FRP bars of URM walls subject to out-of-plane loads. Construction and Building Materials, 20(1), 101-110.

Hart, G., Englekirk, R., & Hong, W. (1988). Structural Component Model of Flexural Walls. Paper presented at the Proceedings of the 4th Meeting of the Joint Technical Coordinating Committee on Mas-onry Research US-J apan Coordinated Earthquake Research Program, San Diego, Califor—knaafisenxn 13am airmen 1997sE.

Hassanli, R., ElGawady, M. A., & Mills, J. E. (2015). Experimental investigation of in-plane cyclic response of unbonded posttensioned masonry walls. Journal of Structural Engineering, 142(5), 04015171.

Kuzik, M. D., Elwi, A. E., & Cheng, J. R. (2003). Cyclic flexure tests of masonry walls reinforced with glass fiber reinforced polymer sheets. Journal of Composites for Construction, 7(1), 20-30.

Mosallam, A. S. (2007). Out-of-plane flexural behavior of unreinforced red brick walls strengthened with FRP composites. Composites Part B: Engineering, 38(5), 559-574.

Mostofinejad, D., & Mahmoudabadi, E. (2010). Grooving as alternative method of surface preparation to postpone debonding of FRP laminates in concrete beams. Journal of Composites for Construction, 14(6), 804-811.

Priestley, M. N., Seible, F., & Calvi, G. M. (1996). Seismic design and retrofit of bridges: John Wiley & Sons.

Ritchie, P. A., Thomas, D. A., Lu, L.-W., & Connelly, G. M. (1990). External reinforcement of concrete beams using fiber-reinforced plastics.

Ross, C. A., Jerome, D. M., Tedesco, J. W., & Hughes, M. L. (1999). Strengthening of reinforced concrete beams with externally bonded composite laminates. Structural Journal, 96(2), 212-220.

Shen, B. (2014). Fiber-Reinforced Polymer Strengthened Steel Reinforced Masonry Wallettes in Out-of-Plane Bending.

Toutanji, H., & Ortiz, G. (2001). The effect of surface preparation on the bond interface between FRP sheets and concrete members. Composite Structures, 53(4), 457-462.

Tumialan, J. G., Galati, N., & Nanni, A. (2003). FRP strengthening of URM walls subject to out-of-plane loads. ACI Structures Journal, 100(3), 312-329.

Valluzzi, M. R., Da Porto, F., Garbin, E., & Panizza, M. (2014). Out-of-plane behaviour of infill masonry panels strengthened with composite materials. Materials and Structures, 47(12), 2131-2145.

Velazquez-Dimas, J. I., Ehsani, M. R., & Saadatmanesh, H. (2000). Out-of-plane behavior of brick masonry walls strengthened with fiber composites. ACI structural Journal, 97(3), 377-387.

V. OUT-OF-PLANE BEHAVIOR OF REINFORCED MASONRY WALLS STRENGTHENED WITH FIBER COMPOSITE EXPOSED TO COMBINED ENVIRONMENTAL CONDITIONS

Zuhair Al-Jaberi, John J. Myers, Mohamed A. ElGawady

ABSTRACT

Fiber reinforced polymer (FRP) composite have been used effectively to strengthen reinforced masonry and concrete structures. However, the performance of FRP composite strengthening systems is still of great concern especially when it's exposed to harsh environmental conditions. In this study, an effort was made to investigate the flexural behavior of strengthened reinforced masonry walls under exposure to different weathering actions. The masonry walls were strengthened with different strengthening systems such as: near surface mounted (NSM) FRP bars, externally bonded (EB) FRP sheets or laminates, and fiber reinforced cementitious matrix (FRCM) system. The performance of twenty-two strengthened masonry walls was investigated by exposing ten of the specimens to 350 different environmental cycles through a computer-controlled environmental chamber. Thirty-two masonry units represented sixteen case were strengthened with the same systems to study the effect of the same regime on bond behavior. These cycles are proposed to simulate 20 years of the typical in-situ weather conditions of the Central US. Two sets of ten walls and sixteen masonry unit specimens strengthened using different types of fiber such as glass and carbon in NSM and EB, in addition to polyparaphenylene benzobisoxazole (PBO) and carbon in FRCM system were considered. The first set was tested after at least 28 days as a curing period of laboratory conditions, while the other set was tested after 72 days of exposure to combined environmental conditions. The walls tested in four-point bending under cyclic load, while

the strengthened masonry unit tested under single-lap direct shear. In terms of flexural capacity, the specimen strengthened with CFRP bar was affected by weathering condition more than the specimens strengthened with CFRP strip or GFRP bar. Also, the result showed that overall the three strengthening systems exhibited excellent performance when subjected to cycles of heating and cooling prior to test. Different modes of failure occurred in the strengthened reinforced walls, including a punching shear failure through the concrete block, as well as debonding of fiber reinforcement from the masonry substrate.

Highlights

- Reinforced masonry walls were strengthened with FRP (bars, laminate, and sheets) and FRCM system subjected to cyclic loading.
- Effect of environmental conditions on flexural and bond behavior were investigated in terms of ultimate capacity, ultimate strain, and mode of failure.
- Variables included type of strengthening technique, type of fibers and adhesive material, and masonry bond pattern.
- Experimental results for specimens under laboratory conditions were compared to the results of the same specimens subjected to cycles of environmental conditions.

1. INTRODUCTION

Strengthening of masonry structures is often required after a certain period of time due to code modifications, construction errors, overloading, destructive environmental conditions or mechanical damage. Fiber reinforced polymer (FRP) techniques have become popular for strengthening in the last decade due to their light weight and non-corrosive makeup. The NSM and EB repair technique has been proposed and applied in

the field to increase the flexural capacity for both unreinforced and reinforced masonry walls (Al-Jaberi, Myers, & ElGawady, 2015; De Lorenzis, Tinazzi, & Nanni, 2000; Galati, Tumialan, & Nanni, 2006; Valluzzi, Da Porto, Garbin, & Panizza, 2014). Typically, epoxy adhesives are used to fill the pre-cut grooves in case of NSM or cover prepared surface to bond the FRP bar or sheet to the structural element. Epoxy has proven to provide excellent bond and durability behavior. In high temperature applications, the guidelines for design of FRP strengthened structures recommend use of fire protection system or insulation to prevent epoxy approaching transition temperature (Soudki & Alkhrdaji, 2005). In terms of durability, the existing researches on strengthening using FRP were focuses on environmental degradations factors individually. The temperature action is one of these environmental factors. Silva et al. (Silva, Fernandes, Sena-Cruz, Azenha, & Barros, 2014) investigated the behavior of concrete specimens strengthened with NSM-CFRP strips under thermal cycles. These specimens were submitted to thermal cycles and tested up to failure using four point bending and pullout direct test for slab and cubic specimens respectively. The results indicate that the slabs capacity and damage mechanism were not affected by thermal cycle's range of -15°C to 60°C. Nevertheless, the bond strength increased with the number of thermal cycles. Effects of elevated temperature on NSM-FRP strengthening systems were conducted (Paul J Burke, Bisby, & Green, 2013). Under sustained service loads, the strengthened system was capable of withstanding over 40 min at 100 °C but less than 10 min at 200 °C. NSM technique fails at elevated temperature by debonding at the adhesive-concrete interface. Significant losses in bond resistance at elevated temperature, since the experimental tests occurred at temperatures exceeding the glass transition temperature (T_g) of the epoxy adhesive.

The effect of elevated service temperature on EB FRP and concrete surface was reported (Leone, Matthys, & Aiello, 2009). Relevant influence of the temperature on bond strength and mode of failure was proven as results of this study. At 80 ^{o}C (176 ^{o}F), the bond strength of FRP sheet, GFRP sheet, and CFRP laminate was reduced by 54%, 72%, and 25%, respectively. Changing the temperature from 50 to 80 ^{o}C (122-176 ^{o}F) resulted in changing the mode of failure from cohesion to adhesion failure. Bond failure at interface occurred at temperature higher than T_g due to loss the bonding strength of adhesive material at interface.

Using a cementitious material as an alternative adhesive agent in the NSM technique or in FRCM system is very attractive especially at high temperature applications. Cementitious material was able to support sustained load for more than four hours when the temperature was 100 °C (212 °F) and approximately one hour at 200 °C (392 °F) (Paul J Burke et al., 2013). The mode of failure was debonding at the FRP-cementitious interface. The performance of NSM and cementitious material was evaluated by Burke (Paul Jonathan Burke, 2008). For high temperature exposure 100 °C (212 °F), cementitious adhesive presented excellent behavior, allowing the strengthening system to remain structurally effective for more than five hours under sustained load. The effect of high temperature ranging from 20 to 120 ^{o}C (68 to 248 ^{o}F) on mechanical behavior of FRCM system was conducted by Donnini et al. (Donnini, y Basalo, Corinaldesi, Lancioni, & Nanni, 2017). The tensile strength of FRCM reinforced with carbon was reduced by 11% when subjected to the elevated temperature up to 120 ^{o}C (248 ^{o}F) which is insignificant in terms of resistance applied load and bond to the substrate. Developed research on strengthening using advanced composite has focused on

the short-term durability performance of strengthened structural elements and has rarely considered the full structure's lifetime. In addition, durability research has been mostly dedicated to examining environmental degradation factors individually rather than all together in a synergistic manner.

Cold environments and freeze-thaw cycling of NSM FRP is the second factor that was investigated individually. Flexural performance of NSM carbon/vinylester FRP tape strengthened concrete slabs at low temperatures was investigated (P. Burke, Bisby, & Green, 2008). The effects of adhesive type (cementitious or epoxy) and groove width were discussed at both room (21°C) and low (-26°C) temperature. The results showed no discernable negative impacts on the performance of any of the strengthened members using epoxy or cementitious grout adhesives at low temperature. The experimental results for the flexural and bond performance of NSM FRP to evaluate the freeze-thaw durability were presented (Mitchell, 2010). No negative impacts on the performance of NSM with grout adhesive material after exposed to freeze-thaw cycles. Minor changes in ultimate capacity of NSM with epoxy system after exposure to freeze-thaw cycles. The Pull-out test of NSM with epoxy adhesive experienced a 27% average drop in ultimate load after 150 freeze-thaw cycles. Al-Mahmoud et al. (Al-Mahmoud, Mechling, & Shaban, 2014) investigated the effect of environmental exposure (freeze-thaw cycles and salt water immersion) on NSM CFRP rod strengthened specimens and embedded in cementitious material. The specimens were exposed to up to 300 freeze–thaw cycles; no change in bond strength for NSM FRP rod resulted after this exposure. Soliman et al. (Soliman, El-Salakawy, & Benmokrane, 2010) conducted a small scale pull-out test to study the bond performance of NSM FRP under 200 freeze/thaw cycles. The main mode of failure for

exposed specimens with cement adhesive was splitting of adhesive material with a failure load about 40-56% of that of their counterparts with epoxy adhesive. The effects of freezing and thawing conditions on EB FRP was reported by Cromwell et al. (Cromwell, Harries, & Shahrooz, 2011). This factor can degrade FRP material and the bond at fiber/matrix interfaces due to micro-cracking that results from expanded the frozen absorbed moisture led to more brittle FRP behavior.

Moisture has been observed to be another important deteriorating agent for specimens strengthened with advanced composites. Pull-off tests were used to evaluate the effect of moisture on FRP-masonry bond (Ghiassi, Silva, Marcari, Oliveira, & Lourenço, 2012). Constant relative humidity (RH) of 100% at 23°C (73.4°F) was applied on strengthened specimens for eight weeks. The degradation was investigated on the conditioned specimens for two periods (four and eight weeks) of exposure to evaluate the bond performance. The results indicate 15% and 23% reductions in bond strength for conditioned specimens after four and eight weeks of exposure, respectively. Based on this result, moisture exposure can reduce the bond strength of the FRP-masonry elements significantly within a two month period of exposure. The bond failure mode was affected by exposure to accelerated wet/dry cycling. The failure after this exposure occurred at the adhesive-substrate interface. In contrast, for the specimens not exposed to wet/dry cycling, bond failure always occurred in a very thin mortar layer of the concrete (Dai, Yokota, Iwanami, & Kato, 2010).

There is a lack of long-term data on the performance of strengthened masonry walls under combined environmental exposure. The evaluation of the long-term performance of a strengthened structure requires the assessment of the durability of both

the strengthening components and the involved materials under combined environmental action to simulate the natural weathering conditions. The assessment of long-term durability required evaluation for flexural and bond behavior of the masonry strengthened with advanced composite material. This research focused on the effect of combined environmental cycles on flexural and bond behavior of reinforced masonry walls and masonry specimens strengthened with the NSM, EB, and FRCM systems. This study was motivated by the need to increase the knowledge on the long-term expected durability of the three strengthening techniques using epoxy or cementitious material as an alternative choice to epoxy agent as adhesive material. This paper presents an experimental program in which out-of-plane four point load tests were carried out for evaluating the flexure behavior and pull-out tests were considered to evaluate the bond behavior of specimens before and after environmental exposure. The behavior was evaluated in terms of ultimate capacity, ultimate strain, and mode of failure.

2. SCOPE AND GOAL OF THIS STUDY

The purpose of this study is to present the results of flexural performance of reinforced masonry walls and bond behavior of strengthened specimens with different strengthening techniques such as NSM, EB, and FRCM system with epoxy and cementitious adhesive when exposed to combined environmental conditions. An additional purpose is to study the possibility of change in design flexural capacity or expected failure mechanism due to combined environmental actions. This study investigated how the combination of different environmental cycles can affect the long-term behavior of the strengthened walls which is more representative of structural elements in the field. Twenty-two strengthened masonry walls were investigated by

exposing ten of the specimens to 350 different environmental cycles through a computer-controlled environmental chamber. Thirty-two masonry units strengthened with the three strengthening systems were used to study the effect of the same regime on bond behavior. These cycles are proposed to simulate 20 years of the typical in-situ weather conditions of the Central US.

3. EXPERIMENTAL PROGRAM

This experimental program investigates the out-of-plane and bond resistance of advanced composite to different weathering action. The experimental program can be divided in two parts. Twenty-two reinforced masonry walls were tested in the first part. These specimens divided in two sets, the first set consisted of control specimens and ten strengthened masonry walls while the second set includes ten strengthened specimen subjected to environmental cycles before test. In the second part of experimental program, Thirty-two hollow concrete masonry units with nominal dimensions 200 x 200 x 152 mm (8 x 8 x 6 in.) were used. Two identical specimens were considered for each case. The specimens of this part were divided in two phases. The first phase focused on bond behavior when the advance composite was subjected to tension force at laboratory temperature, while the other phase investigated the performance of specimens exposed to the same environmental cycles that the masonry walls exposed to.

3.1. TESTING SPECIMENS

The reinforced masonry walls for all specimens have the same overall dimensions and longitudinal main steel reinforcement. Each wall constructed using standard masonry blocks 152.5 mm (6 in.) in running and stack pattern and type S mortar. The nominal dimensions of these walls were 1220 mm (48 in.) length by 610 mm (24 in.) width. They

were grouted four days after construction to ensure stability during the vibration process. The reinforcement ratio (ρ) for mild steel was constant for all specimens (2#4) steel bars. These strengthened wall configurations, in addition to cross section of block unit are shown Figure 1.

3.2. TEST MATRIX AND WALL SPECIMENS' DESIGNATION

For the walls tested under out-of-plane flexural load, the specimen designated with four parts as shown in Table 1: The first part represents the strengthening system, "N" for NSM, "E" for EB and "F for FRCM. The second part consisted of two characters (type and amount of fiber). The first character represents type of fiber: namely "C" for carbon, "G" for glass and "PBO" for polyparaphenylene benzobisoxazole, while the second character represents the number of bars or sheets. The third part referenced the masonry bond pattern and the adhesive material; a character ''R'' represented running bond pattern, and ''S'' represented a stack bond pattern, while a character "E" and "C" represented epoxy and cementitious material, respectively. The fourth part identified the exposure condition: namely "L" for laboratory conditions and "EN" for environmental chamber exposure. For the specimens tested pull-out load, the specimens designated with the same designation of the walls in the first part in one exception, there is no bond pattern in the specimen name. The test matrix of second part is shown in Table 2.

3.3. MATERIAL CHARACTERIZATION

A series of tests were performed to determine each material's mechanical properties. A compressive strength test was conducted on two blocks masonry prisms according to ASTM C1314-12 (ASTM.(2012), 2012), and the average compressive strength of three prisms was 22.4 MPa (3,250 psi). The average compressive strength of

type S mortar and grout was conducted according to ASTM C109-13 (ASTM.(2013), 2013), the average 28-day value of 16.7 MPa (2,420 psi) and 28.95 MPa (4,200 psi) was obtained for type S mortar and grout, respectively. An experimental tensile test for mild steel rebar according to the ASTM A370-13 was conducted on three replicate specimens. Uniaxial load was applied gradually until failure, and then the average yield stress of the steel reinforcement bar at 0.5% offset was obtained 463.63 MPa (67.245 ksi) along with the average modulus of elasticity was 200.3 GPa (29,051 ksi).

The tensile tests of NSM-FRP bars with fiber content more than 70% by weight were conducted according to ASTM D7205 (ASTM.(2011), 2011). The average guaranteed tensile strength, tensile modulus of elasticity, and ultimate strain are presented in Table 3. The adhesive material used in NSM system was BASF ADH 1420 epoxy resin. Based on ASTM D 638 (ASTM.(2014), 2014), the manufacture ultimate tensile strength and elongation at break were 27.6 MPa (4000 psi) and 1%, respectively.

For the EB, a composite of SEH glass fabrics are saturated in Tyfo S epoxy matrix to produce a composite used in wet-layup process. Based on ASTM D7205-11 (ASTM.(2011), 2011), the 1.3 mm (0.05 in.) thickness of the glass fiber composite has an ultimate tensile strength and tensile modulus of 575 MPa (83 ksi) and 26.1 GPa (3785 ksi) respectively, in addition to an elongation at break of 2.1%. Typical 60% fiber content by volume used to produce the pre-cured CFRP laminate. Based on ASTM D7205 (ASTM.(2011), 2011), the mechanical properties of CFRP laminate are presented in Table 3. Two types of structural bonding adhesive were selected for this study. Tyfo S epoxy matrix was used to bind SEH glass fiber. Components A and B of the epoxy were mixed at a volume ratio of 100:42. SikaDur 30, an adhesive bonding material used to

bind CFRP laminate. The properties of the EB adhesive materials are as presented in Table 4. For the FRCM system, based on AC434 (AC434, 2011), the mechanical properties of FRCM coupons with different types of fibers are summarized in Table 5. Compressive strength tests according to ASTM C109-13 (ASTM.(2013), 2013) were performed on the cementitious-adhesive agents. Matrices (matrix x750 used to bond PBO fabric and matrix x25 used to bond carbon fabric) are inorganic cementitious matrices mixed with water to work like a mortar for the binding process. The average compressive strength for a matrix x750 was found to be 35 MPa (5 ksi) at an age of 28 days, while it was 15 MPa (2.175 ksi) for a matrix x25.

4. PROCEDURE AND SPECIMEN PREPARATION

The NSM strengthening procedure involved inserting FRP bar into a groove cut at the tension surface of the specimen without surface preparation. The groove dimension was double the diameter of the bar to avoid splitting failure of the adhesive cover (De Lorenzis & Nanni, 2002). Compressed air was used to clean and vacuum the grooves prior FRP installation process. The groove filled with epoxy by 2/3 of the groove depth, and then the FRP bar was pressed into the bonding agent to mid-groove depth to allow epoxy resin flowed around the bar which ensures a complete bond between the bar and the sides of the groove. The groove was then filled with more epoxy resin or leveled by removing excessive adhesive. Surface preparation and levelling is very important step in the EB system. Wire brush was used for cleaning the surface and then the surface was vacuumed to remove the residual dust. In order to prevent premature peeling of FRP, the surface should be even and leveled before installation advanced composite. For specimens strengthened with GFRP, Tyfo S epoxy resin with little amount of silica fume

was applied to serve as putty layer that help to prepare surface before installation of the GFRP sheet. To ensure good bonding between the fabric and substrate, the pre-cut glass fabric was saturated in epoxy before applying on prepared surface of the specimen. The fabric was aligned in the direction of the load path, and the air bubbles were removed at the interface using a hand roller until the fabric was fully attached to the substrate. The epoxy was applied at room temperature 21°C (70 °F) which is satisfying the temperature installation limits. The second type of fiber used in EB system was Aslan 400 CFRP laminate. SikaDur 30 adhesive was used to bond the CFRP laminate with masonry substrate after cleaning the roughened face of laminate with solvent to improve the bonding.

The same procedure of EB system for surface preparation was used in FRCM system. The prepared surface was cleaned using low pressure water before applying cementitious matrix to ensure wet surface which is prevent absorption of cementitious matrix water. The matrix was mixed as per the manufacturer specifications and the strengthening procedure as follow: first layer of cementitious matrix with a nominal thickness of approximately 5 mm (0.2 in.) was applied. A single ply of precut fabric was laid on the cementitious matrix and pressed gently into the first matrix layer. The second layer of cementitious matrix with a nominal thickness of 5 mm (0.2 in.) was then applied and covered the fabric mesh. All the strengthened specimens were allowed to cure by placing wet clothes on their surface then the specimens tested after 28 day.

For the specimens used in bond behavior evaluation, the advanced composite located in a plane of symmetry of the concrete masonry unit and the same procedure of strengthening systems was followed. The total length of FRP bar or fiber sheet was 840

mm (33 in.) and the bonded length was 100 mm (4 in.). To monitor the fiber slip failure, 12 mm (0.5 in.) was left for the bottom of the specimen. A duct tape was used as a bond breaker for a length of 90 mm (3.5 in.) form the top of the specimen in order to ensure specific bonded length. The diameter of FRP bar was 10 mm (0.375 in.), while the sheet or laminate width was 50 mm (2 in.). The free end of fiber was attached to the aluminum pipe (in case of NSM) or steel plates bolted together with four bolts (in case of EB-Epoxy or FRCM) to enable uniform load application without damage or slippage of gripped fiber. The description of strengthened specimens was illustrated in Fig. 2.

5. TEST SETUP AND INSTRUMENTATION

5.1. FOUR-POINT LOAD TEST

An MTS double-acting hydraulic jack with a push-pull capacity of 965 MPa (140 kips) was used to apply a vertical load on the simply supported specimen, as shown in Fig. 3. The load was transferred to the masonry specimen by means of continuous steel plates and bars along the full width of specimens providing two equal line loads. A piece of thick rubber sheet was placed at all interfaces between the steel plate and specimen. The rubber distributed the load evenly and minimized any stress concentration due to unevenness of the wall surface. The distance between these two lines was 200 mm (8 in.). The FRP was 1118 mm (44 in.) long to prevent the ends clamping by the supports. The load was applied in cycles of loading and unloading as a displacement control at a rate of 1.27 mm/min (0.05 in./min). The displacement amplitude increment was 6.35 mm (0.25 in.); double half loading cycle was applied for each amplitude level as illustrated in Fig. 4. Displacements at the mid and third spans were measured using three linear variable displacement transducers (LVDTs) at each side. In addition, strain gauges were installed

on the steel reinforcement and fiber to measure their strains during loading. It may be noted that in previous testing of FRP strengthened URM walls, an airbag was used to apply uniform load to the test walls adjacent to a vertical strong wall as the boundary element. However, because this testing program focused on FRP strengthened RM walls; airbag loading was not an option due to the wall capacity with the added internally fully grouted steel reinforcing.

5.2. PULL-OUT TEST

A single-lap shear test was considered to study shear debonding between advanced composite and masonry substrate. The masonry specimen was restrained against vertical movement during the test by a steel frame bolted to the testing machine base. A thick steel plate was inserted between the frame and the top of the specimen to ensure uniform distributed pressure over the restrained specimen. The steel frame was positioned inside MTS universal testing machine 250 kN (56.2 kip.) capacity. The load was applied as a displacement control at a rate of 0.25 mm/min (0.01in./min) through an MTS computer control station up to the load peak value. The global slip measured between the fiber and the top of the specimen using LVDT. In addition, strain gauges were installed on three location of bonded length at 25 mm (1 in.), 50 mm (2 in.), and 75 mm (3 in.) from the bottom of the bonded length. The pull-out test setup is shown in Fig.5.

6. ENVIRONMENTAL EXPOSURE

The exposure cycle consisted of a combination of severe freeze-thaw cycles, extreme temperature cycles, high relative humidity cycles, and indirect ultra-violet radiation exposure. The exposure regime was selected to simulate the seasonal changes in

an environment such as the Midwest in the United States in an accelerated manner. A computer-controlled environmental chamber is used to simulate 350 different environmental cycles. This regime consisted of the following:

Freeze-thaw cycles: 100 cycles that simulated the effects of the winter season. Each freeze-thaw cycle consisted of freezing at -17.8°C (0°F) for 50 minutes and thawing at 4.4°C (40 °F) for 50 minutes. The transition period between freezing and thawing was 30 minutes.

Extreme temperature cycles: to simulate the summer season effects, 150 alternating cycles of extreme temperature from 27 to 50°C (80 to 120°F) was used. Extreme temperature cycles consisted of temperature variation between 27°C (80°F) for 25 minutes and 50°C (120°F) for 25 minutes. The transition period between high and low temperature was 20 minutes.

Relative humidity cycles: the relative humidity were carried out between 60% and 100% and maintained for 20 minutes each, transition period between 100% and 60% humidity was 30 minutes. Relative humidity cycles were carried out at constant temperatures of 15.5°C (60°F) and 26.7°C (80°F).

The order of cycling was 50 freeze-thaw cycles, 20 RH cycles at constant temperature of 15.5°C (60°F), first set of 40 extreme temperature cycles, 20 RH cycles at constant temperature of 26.7°C (80°F), second set of 40 extreme temperature cycles, 20 RH cycles at constant temperature of 15.5°C (60°F) and third set of 40 extreme temperature cycles. The exposure regime is shown in Fig. 6. The strengthened walls and masonry units were subjected to the exposure regime inside the environmental chamber as shown in Fig. 7.

7. TEST RESULTS AND DISCUSSION

In order to study the effect of sever environmental conditions on strengthened reinforced masonry walls; the individual components (masonry unit and adhesive), and strengthened masonry walls in addition to bond between different strengthening systems and masonry substrate should be evaluated before and after exposure.

7.1. INDIVIDUAL COMPONENTS

The use of cementitious adhesive in place of epoxy as a groove filler in NSM or adhesive matrix in EB system has recently been explored in an attempt to lower the material cost and to eliminate the drawbacks of using epoxy. The mode of failure for laboratory set of the walls strengthened with cementitious adhesive was controlled by the bonding agent property. The debonding failure surface was either in the masonry-adhesive interface or in adhesive layer itself. As a result, the effect of environmental cycles on cementitious adhesive should consider since the structural behavior or mode of failure of the strengthened specimens was affected by this component. The mechanical properties of the cementitious adhesive subjected to thermal cycles and freeze and thawing cycles were determined by using uniaxial compression test. The result showed that the compressive strength of conditioned cementitious adhesive was reduced by 9%. This reduction in strength was due to hair cracks developed in the adhesive materials as a result of temperature change during freeze-thaw cycling and water expands during freezing process. For this reason, the mode of failure was expected to govern by cementitious adhesive.

Three individual concrete masonry units were sampled and tested to evaluate compressive strength according to ASTM C140/C140M-16 (ASTM.(2016), 2016) under

laboratory and environmental conditions. The masonry units are capped in accordance with ASTM C1552 (ASTM.(2015), 2015). A fibrous composite laminated cap was used to provide a smooth bearing surface and to distribute the load over the top and bottom of masonry unit. A rigid 610 x 305 x 51 mm (24 x 12 x 2-in.) steel loading plate was used to apply the loads. The maximum stress was averaged of three samples for each set. The result showed that the compressive strength of conditioned masonry unit was reduced by 10 %. This reduction in strength attributed to microcracks due to increasing internal voids pressure that generated after freezing the absorbed water.

Tensile tests, according to provisions of ACI 440 (ACI 440, 2001) were conducted by (Micelli & Nanni, 2004) to study the change in longitudinal mechanical properties of FRP. The tensile strength of GFRP bars subjected to the environmental cycles showed a good durability resistance comparing with control bar. Carbon bars showed degradation in tensile strength by approximately 5%. The mechanical behavior of FRCM system under temperature was conducted by Donnini et al. The tensile strength of FRCM system was reduced by 11% when subjected to the elevated temperature up to 120 ^{o}C (248 ^{o}F) (Donnini, y Basalo, Corinaldesi, Lancioni, & Nanni, 2017). The results of the effect of environmental cycles on individual components are illustrated in Fig. 8.

7.2. BOND BETWEEN ADVANCED COMPOSITE AND MASONRY UNIT

The results of the ultimate force, strain at failure, reduction in ultimate force and mode of failure for laboratory and conditioned specimens are presented in Table 6. Each row in the table represents the average test results of two identical specimens. It was observed that the ultimate load significantly decreased by an average 18.32% and 12.9% for specimens strengthened with GFRP-epoxy and PBO-cement, respectively. Based on

normalized axial stiffness which gives an indication about the amount of fibers used in each specimen, the amount of fiber is not the factor that affected the bond ultimate force. Since all strengthened specimens failed by debonding, the reduction in the ultimate force of exposed specimens was due to degradation of the adhesive material and masonry unit. Specimens strengthened with epoxy adhesive exhibited excellent bond capacity after exposure compared with specimens strengthened with cementitious adhesive. However, the GFRP-epoxy specimen exhibited high reduction percent due to large contact area compared with NSM system and due to low resistance to the cycles of temperature compared to the procured CFRP laminate. The relationships between pull-out force and global slip of representative specimens of different strengthening systems are shown in Fig. 9. The specimens were grouped based on the strengthening system so that each figure represents the comparison between laboratory and environmental exposure. For the NSM and EB system, the pull-out force vs global slip curves were characterized by a linear relation up to the ultimate load, and then the capacity dropped suddenly due to complete debonding as a result of concrete or adhesive cover splitting as shown in Fig. 9 (a-f). The FRCM strengthened specimens' curves were characterized by bilinear response. The response consisted of linear uncracked with high axial stiffness and nonlinear post-cracked up to the ultimate load. The response ended with gradual drop of capacity as shown in Fig. 9 (g and h). The nonlinear behavior was attributed to the micro-damage of the fiber-matrix interface and the gradual post-peak response caused by gradual loss of fiber-matrix bond.

The mode of failure depends of the load transfer mechanism between strengthening system and the substrate. The load transfer mechanism is different between

NSM or EB form a side and FRCM from other side. The debonding surface for NSM or EB specimens was either fiber-adhesive surface or adhesive-substrate surface. The effect of environmental conditions exposure on NSM and EB strengthening system was represented by changing the mode of failure from debonding due to concrete splitting to debonding due to adhesive material splitting. The same behavior for specimens strengthened with NSM GFRP and NSM CFRP was observed due to the similarity of FRP bar surface and the adhesive used in this system. In the FRCM strengthening system, it was observed that the debonding failure always occurred at the fiber-matrix interface. The debonding failure was initiated as a result of microcracks in the matrix that led to 13% reduction in bond capacity. It is worth mentioning that at the failure, the fiber attached with second layer of matrix separated from the first layer of FRCM system. The modes of failure are illustrated in Fig. 10.

7.3. FLEXURAL BEHAVIOR OF STRENGTHENED WALL

The load versus deflection curves were grouped based on the strengthening system is shown in Fig. 11. From the results of individual components and bond behavior, the results for strengthened masonry walls were expected to be affected by the all these components together since the debonding failure surface is in the masonry-adhesive interface or in adhesive layer itself. Same overall behavior of strengthened walls for both sets (laboratory and environmental conditions) was observed. The behavior can be divided into three phases, the pre-crack, cracked, and post-yield phase. The pre-cracked phase was characterized by linear behavior with insignificant effect of fiber on stiffness. The cracked phase was recognized through the descending of slope as a result of cracks generated in the mortar of masonry walls. The type and amount of fibers of

strengthening system affected the cracked stiffness of strengthened specimen. The post-yield phase was characterized by yielding of steel reinforcement and ends with strengthening system failure.

For the specimens strengthened using NSM system, the ultimate flexural capacity of the wall strengthened by glass fiber had insignificant change comparing with the wall strengthened with carbon bar. The reduction of ultimate capacity of specimen strengthened with one carbon bar was 34%. The reason behind that could be attributed to the reduction of tensile strength of all components (CFRP bar, cementitious adhesive and masonry unit). The effect of combined environmental cycles led to make the mode of failure more gradual debonding failure comparing with mode of failure for specimen under lab conditions. The stiffness for each specimen was reduced due to loading-unloading process which is cause initiation of micro-cracks in all concrete components (masonry unit, mortar, grout, cementitious material) and increase the deformability of the strengthened walls. The secant stiffness was considered in determination the degradation of stiffness. The secant stiffness is the slope of the line drawn between minimum and maximum loads of first cycle. The specimens strengthened with cementitious adhesive presented an excellent response by allowing the strengthening technique structurally effective but the stiffness of these specimens reduced higher than the specimens strengthened with epoxy. Based on the results presented in Fig. 11, the stiffness of exposed specimens strengthened with GFRP was reduced by 5 and 15% when epoxy or cementitious adhesive used, respectively. High percent of reduction in stiffness of exposed specimens strengthened with CFRP was observed. The stiffness degradation

changed from 17 to 37% as a result of changing the adhesive material from epoxy to cementitious agent, respectively.

The behavior of walls with stack bond pattern was improved by reinforcing the continuous head joint with FRP bars. Insignificant influence of the environmental conditions on the behavior of stack strengthened wall. The reduction in flexural capacity was 9%, while the reduction in secant stiffness was only 5%.

Same cracks generated during the test of both sets of specimens. The first flexural tensile crack was hair crack initiated at the block mortar in the maximum moment region, then the cracks developed at other bed joints. Further flexural tensile cracks developed in masonry unit or adhesive material when the specimen loaded at level beyond the cracking load. The masonry cracks were oriented at 45^{o}. In term of cracks pattern, the difference between epoxy and cementitious material as an adhesive agent is the extending of cracks along the groove sides as a result of the epoxy's high tensile strength. The cementitious material itself, however, cracked during loading. As a result, the embedding material deteriorated gradually. Flexural shear and shear cracks outside the constant moment region, in addition to concrete unit crushing, were generated during later stages of loading. The cracks were less for the specimens strengthened with FRCM system. In this system large contact area was covered by the fiber which was keep the cracks developed on adhesive matrix then move to the masonry unit as a result of losing bond. The cracks patterns are shown in Figure 12.

The most common mode of failure that controls the behavior of reinforced masonry walls strengthened with FRP is a debonding failure of the NSM FRP bar rather than FRP bar rupture. The mode of failure for the specimens strengthened with CFRP

strip or GFRP bar in this study both before and after environmental cycles was a debonding failure. The specimen under laboratory condition and strengthened with CFRP-epoxy was failed by shear, while it's failed by debonding when it's subjected to environmental action as a result of bond degradation. On the other hand, Debonding of FRCM at fiber/matrix interfaces started in the maximum moment region and propagated to the support direction. The surface of failure was at the fiber/matrix interface without detachment of the cementitious matrix from the masonry substrate. All the modes of failure of strengthened walls were consistence with the modes of failure of masonry units under pull-out force. The observed modes of failure are illustrated in Figure 13.

8. CONCLUSIONS

An experimental program was implemented to study the effect of combined environmental cycles on flexural behavior of reinforced masonry walls strengthened with different strengthening systems. The bond behavior under pull-out test before and after exposure was investigated. According to this research, the following conclusions can be drawn:

1- For the individual components, the mechanical properties of the cementitious adhesive, masonry unit, FRP bars, and FRCM subjected to thermal different environmental conditions were reduced by not more than 11%. This reduction in strength was due to hair cracks developed in the different components as a result of temperature change during freeze-thaw cycling and water expands during freezing process.

2- The ultimate load significantly decreased by an average 18.32% and 12.9% for specimens strengthened with GFRP-epoxy and PBO-cement, respectively. The

GFRP-epoxy specimen exhibited high reduction percent due to large contact area compared with NSM system and due to low resistance to the cycles of temperature compared to the procured CFRP laminate. The same reason can be presented for the high reduction value for the capacity of specimens' strengthened FRCM system. The effect of environmental conditions exposure on the bond of NSM and EB strengthening system was represented by changing the mode of failure from debonding due to concrete splitting to debonding due to adhesive material splitting. In the FRCM strengthening system, it was observed that the debonding failure always occurred at the fiber-matrix interface.

3- The stiffness of exposed specimens strengthened with GFRP was reduced by 5 and 15% when epoxy or cementitious adhesive used, respectively. High percent of reduction in stiffness of exposed specimens strengthened with CFRP was observed. The stiffness degradation changed from 17 to 37% as a result of changing the adhesive material from epoxy to cementitious agent, respectively. The reduction of flexural ultimate capacity of specimen strengthened with one carbon bar was 34%, while insignificant changed in capacity of the other specimens.

4- The behavior of walls with stack bond pattern was improved by reinforcing the continuous head joint with FRP bars. Insignificant influence of the environmental conditions on the behavior of stack strengthened wall. The reduction in flexural capacity was 9%, while the reduction in secant stiffness was only 5%.

5- The most common mode of failure that controls the behavior of reinforced masonry walls strengthened with FRP is a debonding failure rather than fiber rupture. The mode of failure for the specimens strengthened with CFRP strip or GFRP bar before

and after environmental cycles was a debonding failure. The specimen under laboratory condition and strengthened with CFRP-epoxy was failed by shear, while it's failed by debonding when it's subjected to environmental action as a result of bond degradation. The surface of failure of specimens strengthened with FRCM was at the fiber/matrix interface without detachment of the cementitious matrix from the masonry substrate. All the modes of failure of strengthened walls were consistence with the modes of failure of masonry units under pull-out force.

ACKNOWLEDGEMENTS

The authors wish to acknowledge the support of Midwest Block & Brick in Jefferson City, Missouri and Hughes Brothers in Seward, Nebraska, Ruredil S.p.A., San Donato Milanese, Italy and HCED (The Higher Committee for Education Development in Iraq). The authors also wish to thank the technical support staff in not only the Department of Civil and Environmental Engineering but also the Center for Infrastructure Engineering Studies (CIES) at Missouri University of Science and Technology for their efforts in this research study. Any opinions, findings, conclusions, and recommendations presented in this paper are those of the authors and do not necessarily reflect the views of the sponsor or supporting agencies.

TABLES AND FIGURES

LIST OF TABLES

LIST OF FIGURES

Table 1 – Experimental test matrix (Part 1)

Wall	Strengthening system	Specimen ID	Type of fiber	Number of bars or sheets	Groove dimension or sheet width (mm)	Adhesive material
1		Control-R	-	-	-	-
2		Control-S	-	-	-	-
3	NSM-Epoxy	N-C1-RE-L*	Carbon	1	17.8*25.5	E-ADH 1420
4		N-C1-RE-L	Carbon	1	19*19	E-ADH 1420
5		N-G1-RE-L	Glass	1	19*19	E-ADH 1420
6		N-C1-RE-En*	Carbon	1	17.8*25.5	E-ADH 1420
7		N-C1-RE-En	Carbon	1	19*19	E-ADH 1420
8		N-G1-RE-En	Glass	1	19*19	E-ADH 1420
9	NSM-Cementitious	N-C1-RC-L	Carbon	1	19*19	C-MasterFlow928
10		N-G1-RC-L	Glass	1	19*19	C-MasterFlow928
11		N-G2-SC-L	Glass	2	19*19	C-MasterFlow928
12		N-C1-RC-En	Carbon	1	19*19	C-MasterFlow928
13		N-G1-RC-En	Glass	1	19*19	C-MasterFlow928
14		N-G2-SC-En	Glass	2	19*19	C-MasterFlow928
15	EB-Epoxy	EB-G1-RE-L	Glass	1	200	E-Tyfo S
16		EB-C1-RE-L	Carbon	1	50	E-SikaDur 30
17		EB-G1-RE-En	Glass	1	200	E-Tyfo S
18		EB-C1-RE-En	Carbon	1	50	E-SikaDur 30
19	FRCM-Cementitious	F-C1-RC-L	Carbon	1	610	C-matrix x25
20		F-PBO1-RC-L	PBO	1	380	C-matrix x750
21		F-C1-RC-En	Carbon	1	610	C-matrix x25
22		F-PBO1-RC-En	PBO	1	380	C-matrix x750

Note: 1.0 mm = 0.039 in.

Table 2 – Experimental test matrix (Part 2)

Wall	Strengthening system	Specimen ID	Type of fiber	Number of bars or sheets	Groove dimension or sheet width (mm)	Adhesive material
1	NSM-Epoxy	N-C1-E-L	Carbon	1	19*19	E-ADH 1420
2		N-G1-E-L	Glass	1	19*19	E-ADH 1420
3		N-C1-E-En	Carbon	1	19*19	E-ADH 1420
4		N-G1-E-En	Glass	1	19*19	E-ADH 1420
5	NSM-Cementitious	N-C1-C-L	Carbon	1	19*19	C-MasterFlow928
6		N-G1-C-L	Glass	1	19*19	C-MasterFlow928
7		N-C1-C-En	Carbon	1	19*19	C-MasterFlow928
8		N-G1-C-En	Glass	1	19*19	C-MasterFlow928
9	EB-Epoxy	EB-G1-E-L	Glass	1	50	E-Tyfo S
10		EB-C1-E-L	Carbon	1	50	E-SikaDur 30
11		EB-G1-E-En	Glass	1	50	E-Tyfo S
12		EB-C1-E-En	Carbon	1	50	E-SikaDur 30
13	FRCM-Cementitious	F-C1-C-L	Carbon	1	50	C-matrix x25
14		F-PBO1-C-L	PBO	1	50	C-matrix x750
15		F-C1-C-En	Carbon	1	50	C-matrix x25
16		F-PBO1-C-En	PBO	1	50	C-matrix x750

Note: 1.0 mm=0.039 in.

Table 3 - Mechanical Properties of FRP

Material	Dimension (mm)	Ultimate tensile strength (MPa)	Elongation at break %	Tensile modulus (GPa)	Method
Aslan 100 GFRP bar	10	827	1.79	46	ASTM D7205-11
Aslan 200 CFRP bar	10	2172	1.75	124	ASTM D7205-11
Aslan 400 CFRP laminate	2x50	2400	1.87	131	ASTM D7205-11
Aslan 500 CFRP strip	4.5x16	1965	1.5	124	ASTM D7205-11

Note : 1.0 GPa = 145.03 ksi; 1.0 MPa = 0.145 ksi; 1.0 mm/mm = 1.0 in./in.; 1.0 mm = 0.039 in.

Table 4: Mechanical Properties of Adhesive Materials

Material	Ultimate tensile strength (MPa)	Elongation at break %	Tensile modulus (GPa)	Method
Tyfo S epoxy	72.4	5	3180	ASTM D638-14
SikaDur 30	24.8	1	4482	ASTM D638-14

Note : 1.0 GPa = 145.03 ksi; 1.0 MPa = 0.145 ksi; 1.0 mm/mm = 1.0 in./in.; 1.0 mm = 0.039 in.

Table 5 - Mechanical Properties of FRCM coupon

Material	Thickness (mm)	Ultimate tensile strength (MPa)	Elongation at break %	Tensile modulus (GPa)	Method
PBO fiber	10	1880	1.47	127	AC434
Carbon fiber	10	970	1.33	75	AC434

Note : 1.0 GPa = 145.03 ksi; 1.0 MPa = 0.145 ksi; 1.0 mm/mm = 1.0 in./in.; 1.0 mm = 0.039 in.

Table 6 - Summary of bond test results

Strengthening system	Specimen ID	Ultimate force P_u (kN)	Reduction in ultimate force* (%)	Fiber axial stiffness $k^f = E_f * A_f$ (kN)	Normalized fiber axial stiffness	Strain at failure mm/mm	Mode of failure **
NSM-Epoxy	N-G1-E-L	37.36	-	3278	6.87 k^f	0.00906	D-C/SP
	N-C1-E-L	37.10	-	8836	18.52 k^f	0.00852	D-C/SP
NSM-Cementitious	N-G1-C-L	33.55	-	3278	6.87 k^f	0.0081	D-C/SP
	N-C1-C-L	28.91	-	8836	18.52	0.0069	D-C/SP
EB-EBOXY	EB-G1-E-L	15.56	-	477	1.0 k^f	0.00790	D-F/E
	EB-C1-E-L	23.56	-	9170	19.22 k^f	0.00124	D-F/E
FRCM	F-PBO1-C-L	4.90	-	736	1.54 k^f	0.00220	D-F/M
	F-C1-C-L	3.58	-	1914	4.0 k^f	0.00150	D-F/M
NSM-Epoxy	N-G1-E-En	35.05	6.60	3278	6.87 k^f	0.00868	D-SP
	N-C1-E-En	33.50	10.75	8836	18.52 k^f	0.00746	D-SP
NSM-Cementitious	N-G1-C-En	30.5	10.00	3278	6.87 k^f	0.0076	D-SP
	N-C1-C-En	25.2	14.60	8836	18.52	0.0062	D-SP
EB-EBOXY	EB-G1-E-En	13.15	18.32	477	1.0 k^f	0.00750	D-F/E
	EB-C1-E-En	22.24	6.00	9170	19.22 k^f	0.00118	D-F/E
FRCM	F-PBO1-C-En	4.34	12.9	736	1.54 k^f	0.00340	D-F/M
	F-C1-C-En	3.2	11.87	1914	4.0 k^f	0.00130	D-F/M

Note : 1.0 kN = 0.224 kip; 1.0 mm/mm = 1.0 in./in.

*Reduction in ultimate force ratio= (failure load of the lab specimen- failure load of the exposed specimen)/ failure load of the exposed specimen

**D-C/SP: debonding due to concrete splitting, D-Sp: debonding due to splitting of the adhesive cover, D-SL: debonding due to shearing in laminate, D-F/M: debonding at fiber- matrix interface, D-F/E: debonding at fiber- epoxy interface, and S-F/E: slipping at fiber- epoxy interface.

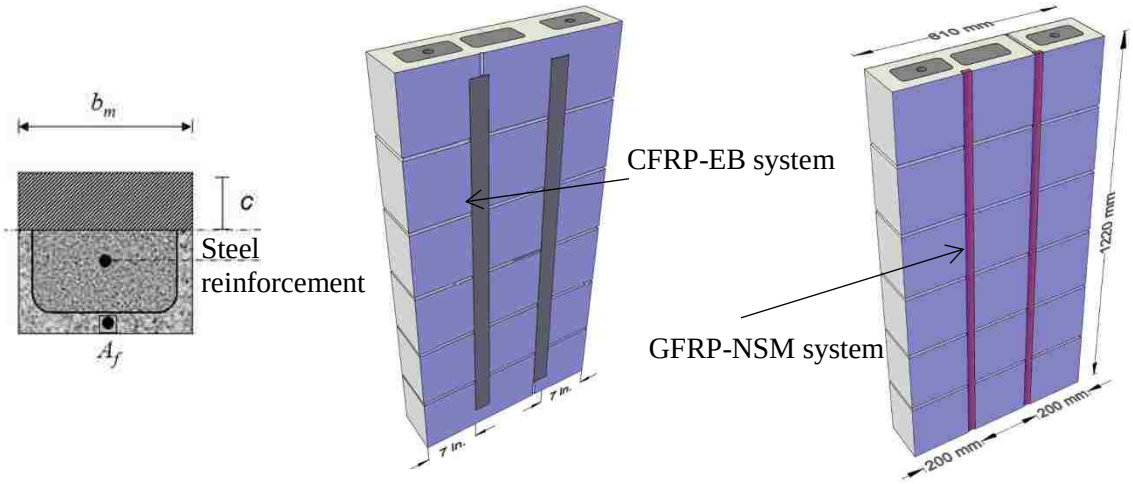

Figure 1. Cross section and strengthened masonry wall

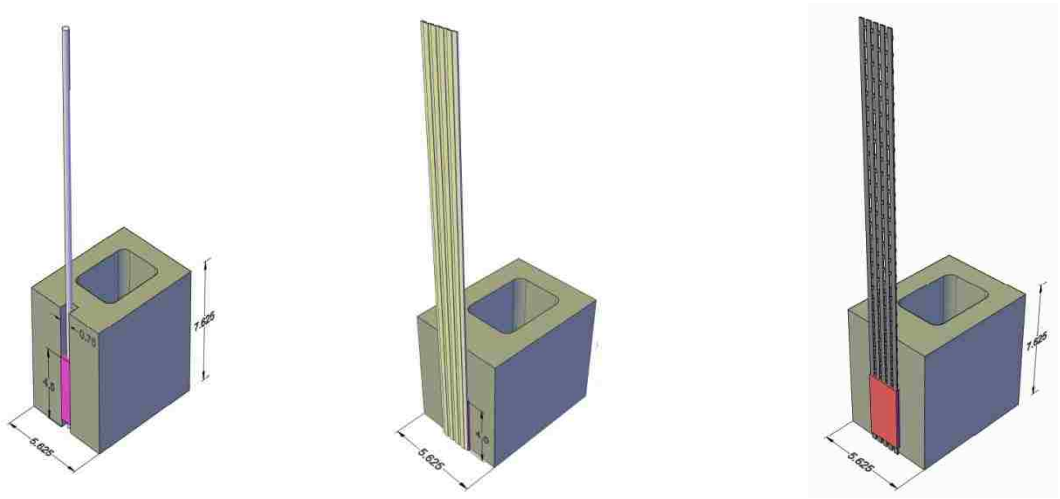

NSM-FRP EB-FRP FRCM

Figure 2. Typical specimen dimensions with different strengthening systems

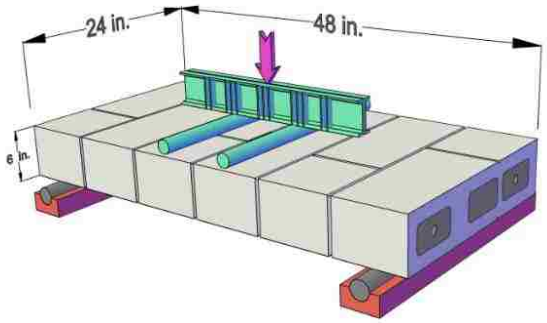

Figure 3. Four-point test setup

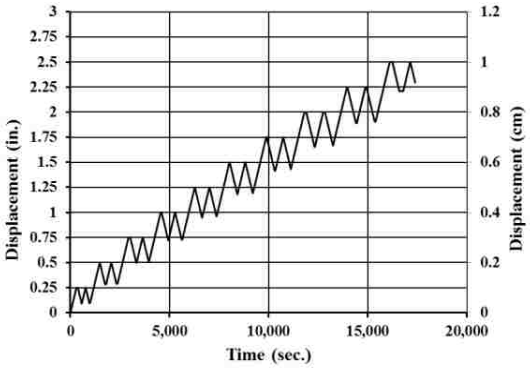

Figure 4. Cyclic loading protocol

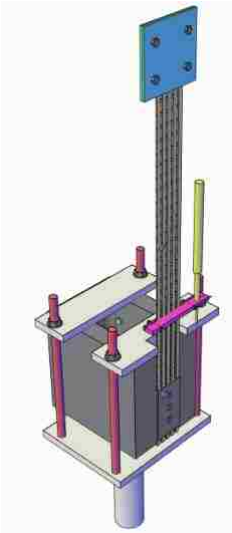

Figure 5. Pull-out test

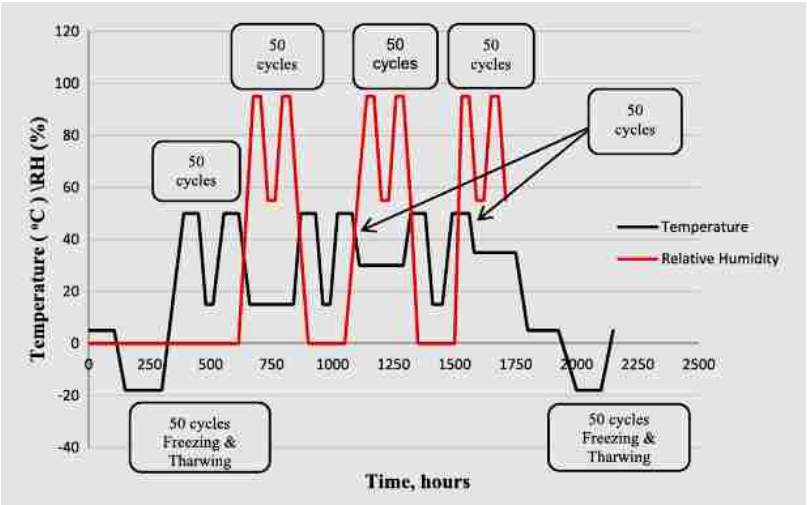

Figure 6. Exposure regime

(a) (b)

Figure 7. Specimens in environmental chamber (a) strengthened masonry units, (b) strengthened RM walls

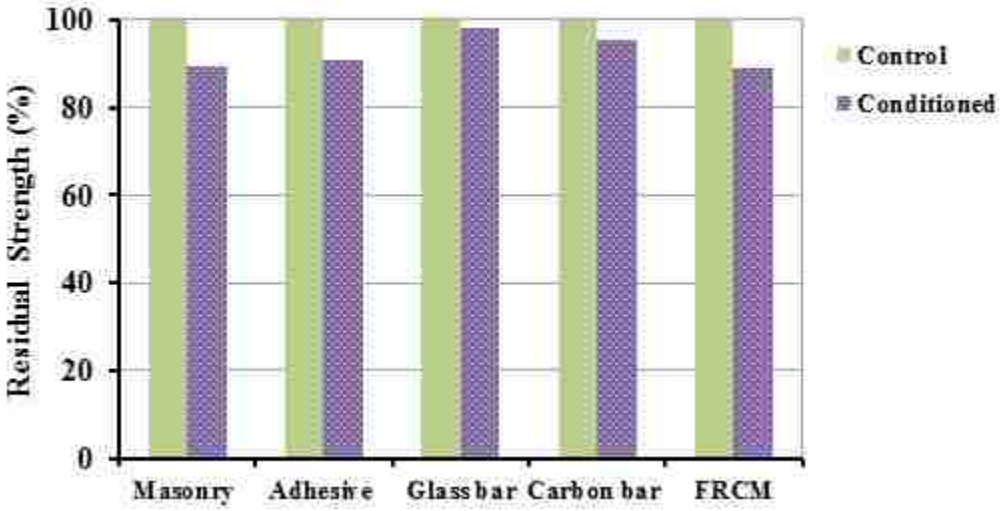

Figure 8. Effect of environmental cycles on individual components

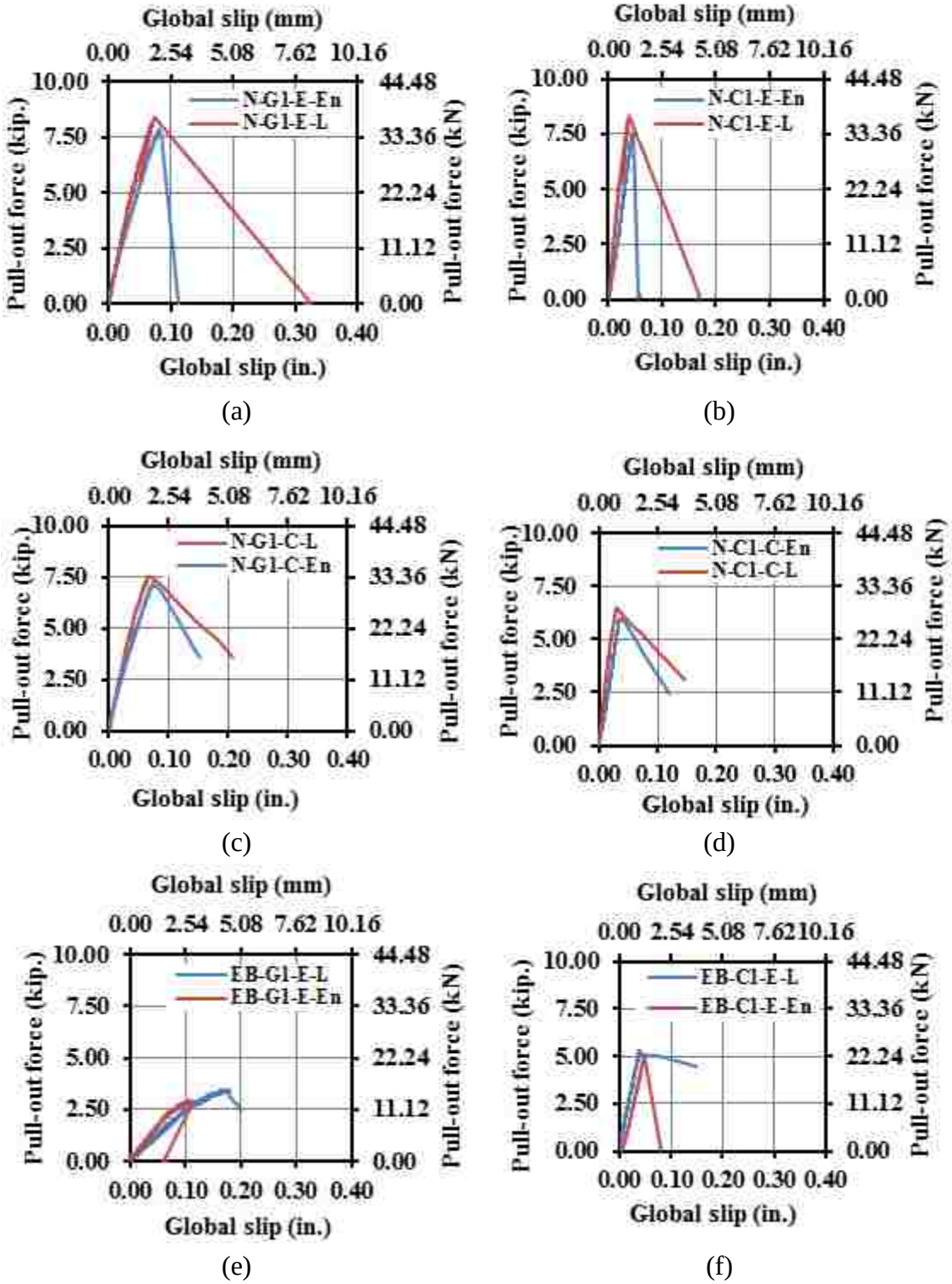

Figure 9. Effect of exposure condition on (a and b) NSM-epoxy, (c and d) NSM-cementitious, (e and f) EB- epoxy, and (g and h) FRCM-cementitious systems

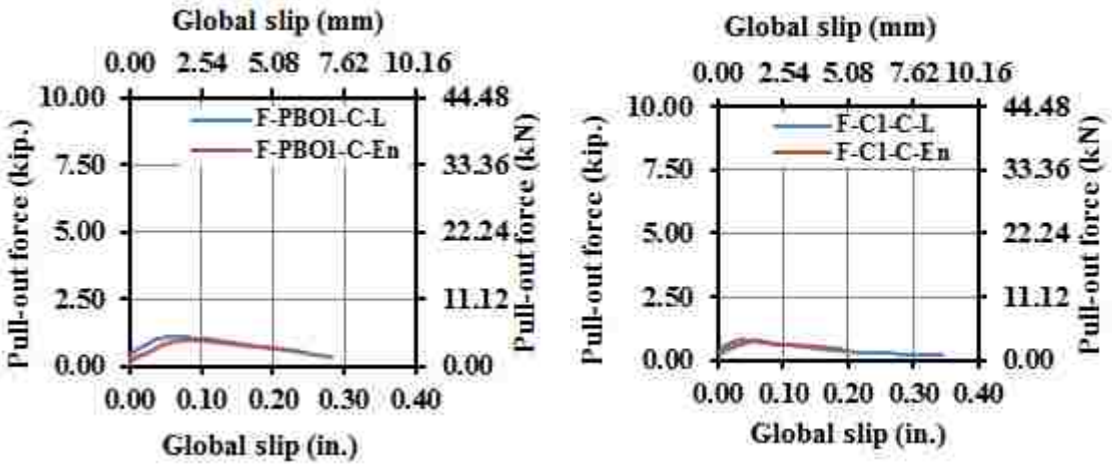

(g) (h)

Figure 9. Effect of exposure condition on (a and b) NSM-epoxy, (c and d) NSM-cementitious, (e and f) EB- epoxy, and (g and h) FRCM-cementitious systems (cont.)

N-G1-E-En

N-C1-E-En

EB-C1-E-En

EB-G1-E-En

F-PBO1-C-En

F-C1-C-En

N-G1-E-L

N-C1-E-L

EB-C1-E-L

EB-G1-E-L

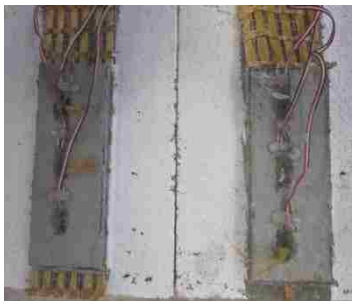

F-PBO1-C-L

F-C1-C-L

Figure10. Modes of failure for strengthening specimens under laboratory and environmental exposure

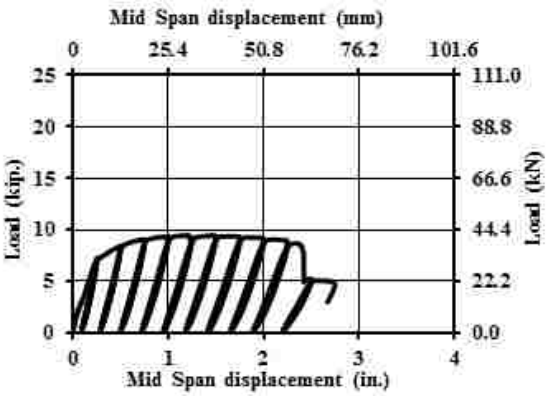

Control-R

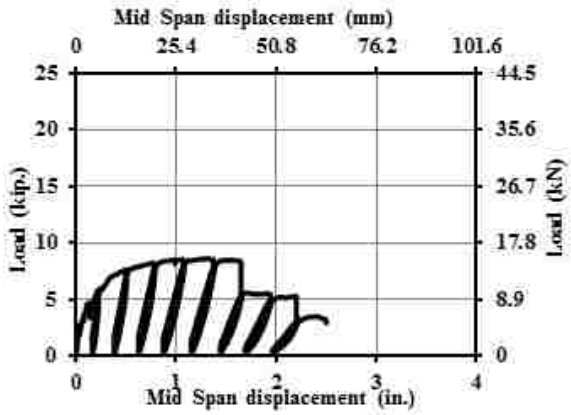

Control-S

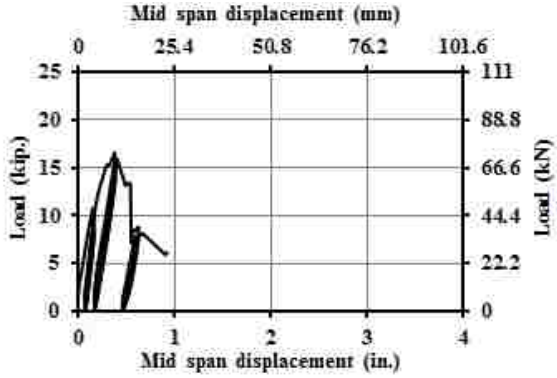

N-C1-RE-L*

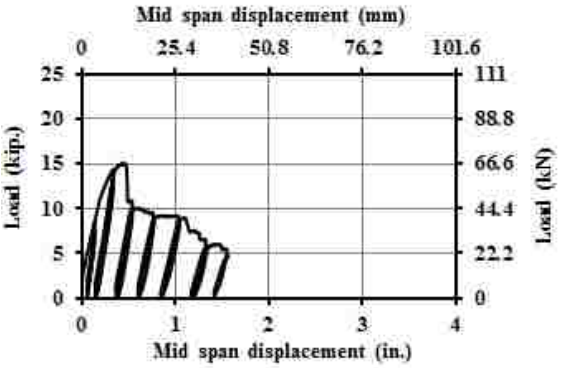

N-C1-RE-En*

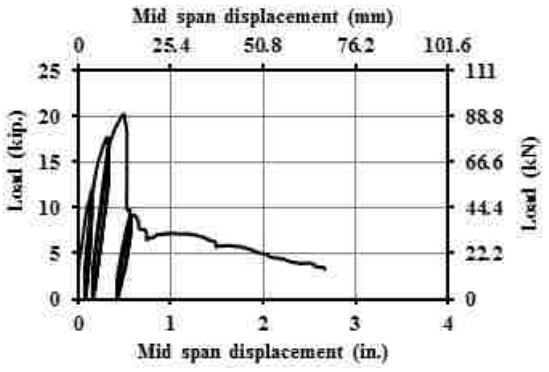

N-C1-RE-L

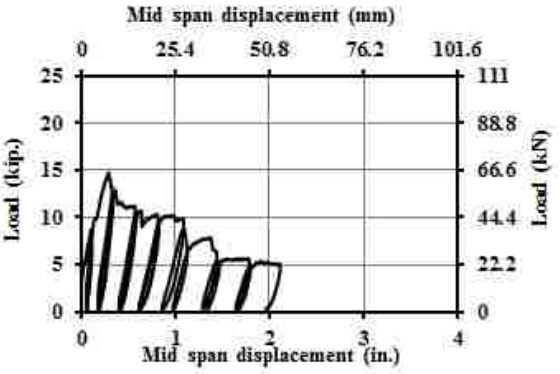

N-C1-RE-En

Figure11. Load-deflection response for strengthening specimens under laboratory and environmental exposure

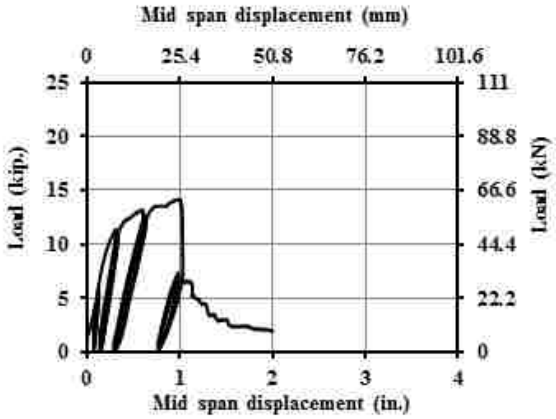

N-G1-RE-L

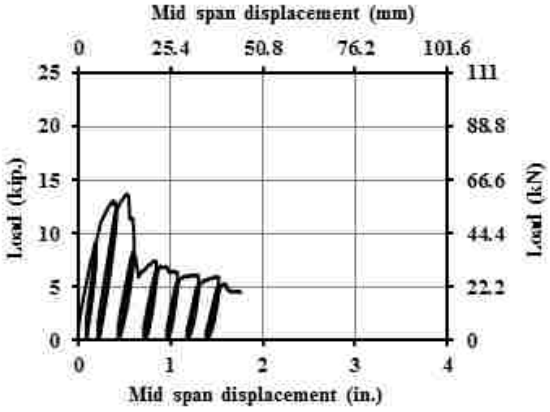

N-G1-RE-En

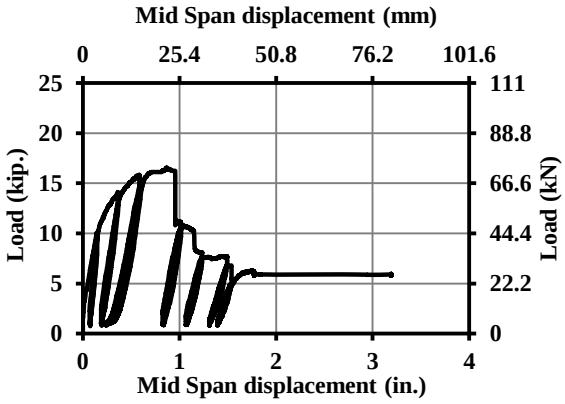

N-C1-RC-L

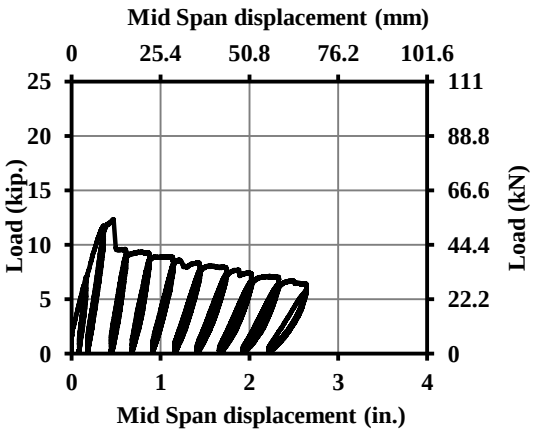

N-C1-RC-En

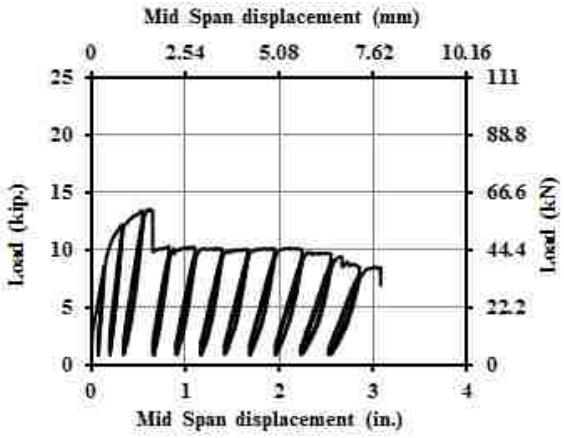

N-G1-RC-L

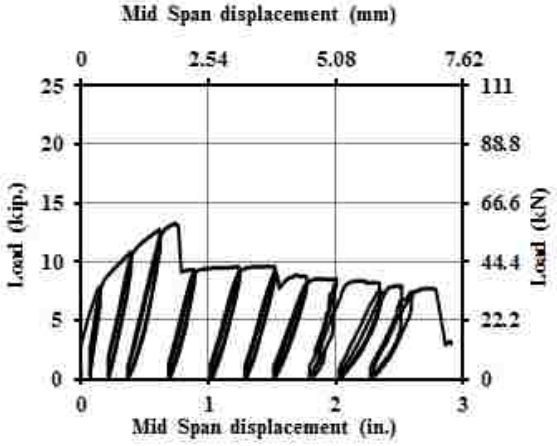

N-G1-RC-En

Figure11. Load-deflection response for strengthening specimens under laboratory and environmental exposure (cont.)

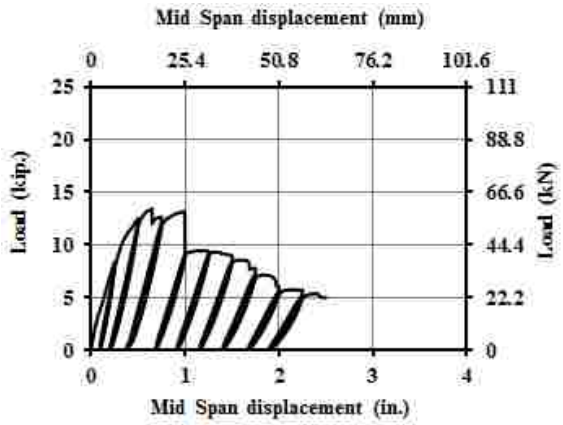

N-G2-SC-L

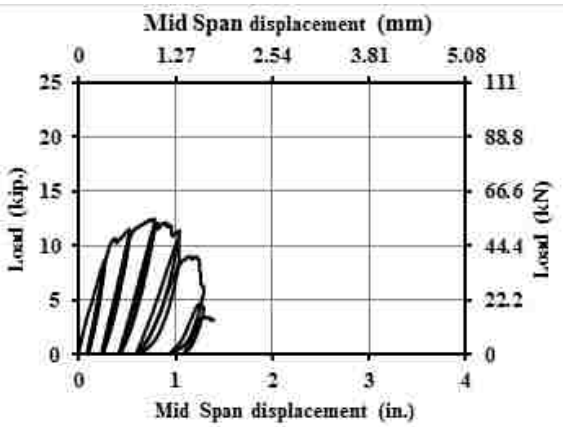

N-G2-SC-En

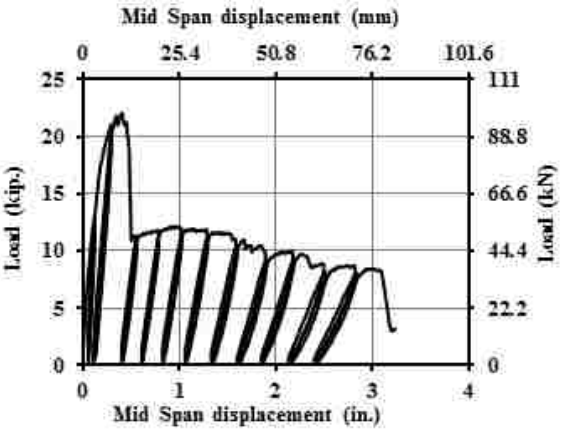

EB-G1-RE-L

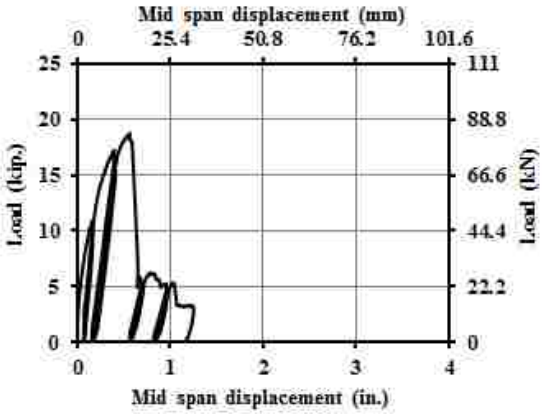

EB-G1-RE-En

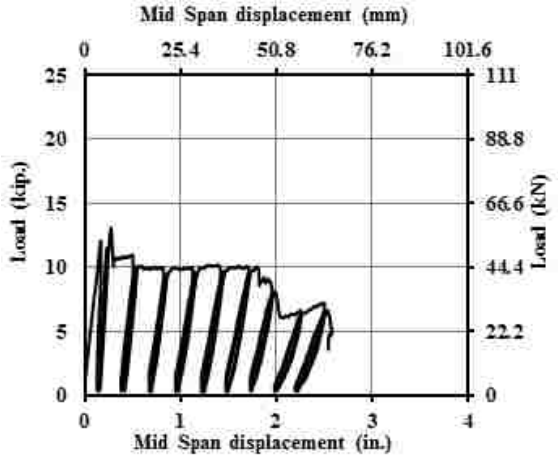

EB-C1-RE-L

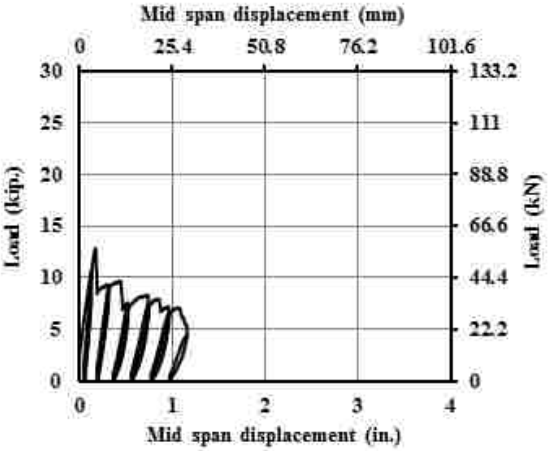

EB-C1-RE-En

Figure11. Load-deflection response for strengthening specimens under laboratory and environmental exposure (cont.)

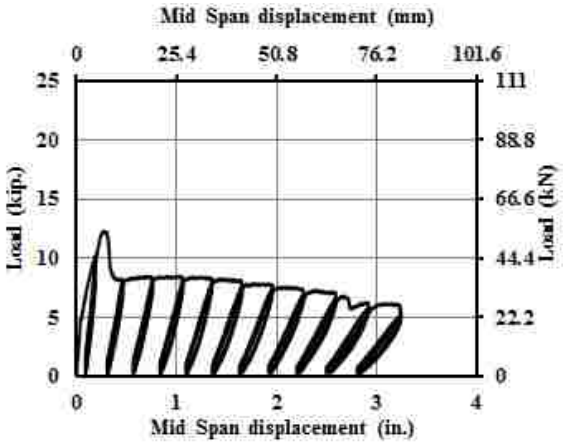

F-C1-RC-L

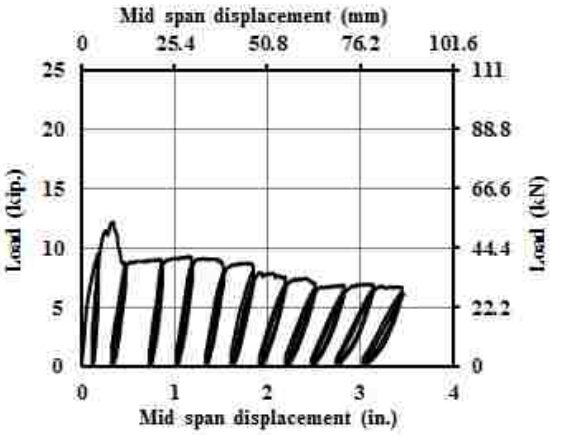

F-C1-RC-En

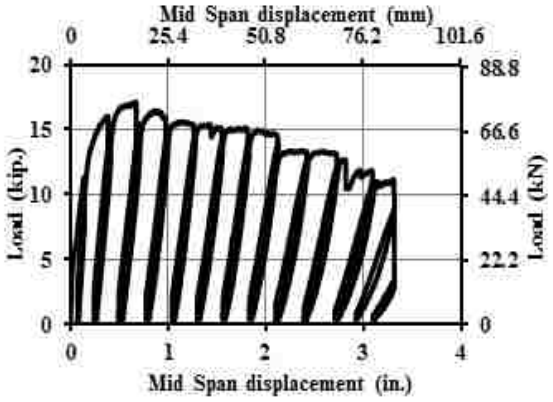

F-PBO1-RC-L

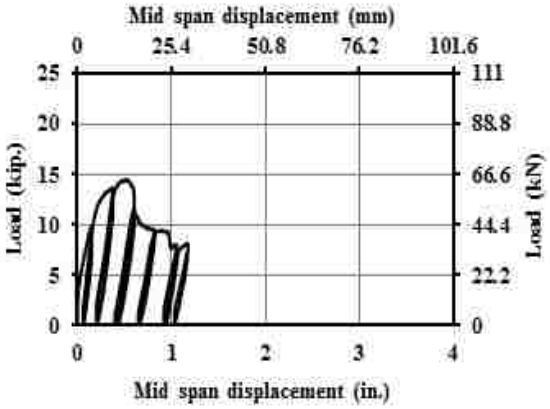

F-PBO1-RC-En

Figure11. Load-deflection response for strengthening specimens under laboratory and environmental exposure (cont.)

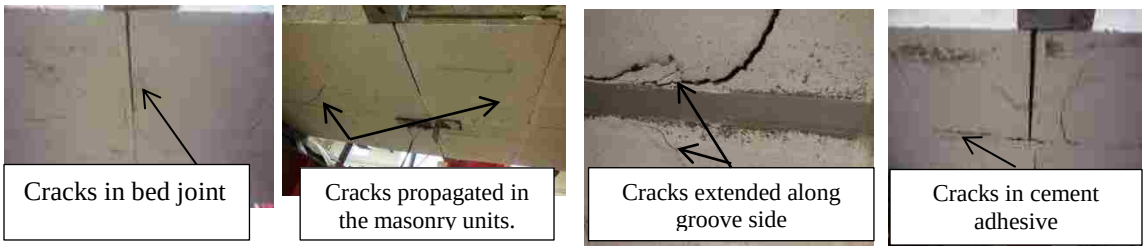

Figure12. Cracks developed during loading

Figure 13. Observed modes of failure

REFERENCES

ACI 440. (2001). Guide for the design and construction of concrete reinforced with FRP bars.

AC434. (2011). Proposed acceptance criteria for masonry and concrete strengthening using fiber-reinforced cementitious matrix (FRCM) composite system.

Al-Jaberi, Z., Myers, J. J., & ElGawady, M. (2015). Influence of Near-Surface Mounted (NSM) FRP on the Out-of-Plane Behavior of Reinforced Masonry Walls. Paper presented at the 12th North American Masonry Conference.

Al-Mahmoud, F., Mechling, J.-M., & Shaban, M. (2014). Bond strength of different strengthening systems–Concrete elements under freeze–thaw cycles and salt water immersion exposure. Construction and Building Materials, 70, 399-409.

ASTM.(2011). (2011). Standard test method for tensile properties of fiber reinforced polymer matrix composite bars. ASTM D7205/D7205M-06.

ASTM.(2012). (2012). Standard Test Method for Compressive Strength of Masonry Prisms, ASTM C1314 - 12.

ASTM.(2013). (2013). Standard Test Method for Compressive Strength of Hydraulic Cement Mortars (Using 2-in. or [50-mm] Cube Specimens), ASTM C109/C109M - 13.

ASTM.(2014). (2014). Standard Test Method for Tensile Properties of Plastics1 ASTM D638-14.

ASTM.(2015). (2015). Standard practice for capping concrete masonry units, related units and masonry prisms for compression testing. ASTM C1552-15.

ASTM.(2016). (2016). Standard test method for sampling and testing concrete masonry units. ASTM C140/C140M-16.

Burke, P., Bisby, L., & Green, M. (2008). Performance of NSM FRP strengthened concrete slabs at low temperatures. Paper presented at the Fourth Int. Conf. on FRP Composites in Civil Engineering (CICE 2008), International Institute for FRP in Construction (IIFC), Winnipeg, Manitoba, Canada.

Burke, P. J. (2008). Low and high temperature performance of near surface mounted FRP strengthened concrete slabs.

Burke, P. J., Bisby, L. A., & Green, M. F. (2013). Effects of elevated temperature on near surface mounted and externally bonded FRP strengthening systems for concrete. Cement and Concrete Composites, 35(1), 190-199.

Cromwell, J., Harries, K., & Shahrooz, B. (2011). Environmental durability of externally bonded FRP materials intended for repair of concrete structures. Construction and Building Materials, 25(5), 2528-2539.

Dai, J.-G., Yokota, H., Iwanami, M., & Kato, E. (2010). Experimental investigation of the influence of moisture on the bond behavior of FRP to concrete interfaces. Journal of Composites for Construction, 14(6), 834-844.

De Lorenzis, L., & Nanni, A. (2002). Bond between near-surface mounted fiber-reinforced polymer rods and concrete in structural strengthening. ACI structural Journal, 99(2), 123-132.

De Lorenzis, L., Tinazzi, D., & Nanni, A. (2000). Near surface mounted FRP rods for masonry strengthening: bond and flexural testing. Paper presented at the Proceedings of the international conference on composite engineering.

Donnini, J., y Basalo, F. D. C., Corinaldesi, V., Lancioni, G., & Nanni, A. (2017). Fabric-reinforced cementitious matrix behavior at high-temperature: Experimental and numerical results. Composites Part B: Engineering, 108, 108-121.

Galati, N., Tumialan, G., & Nanni, A. (2006). Strengthening with FRP bars of URM walls subject to out-of-plane loads. Construction and Building Materials, 20(1), 101-110.

Ghiassi, B., Silva, M. M., Marcari, G., Oliveira, D. V., & Lourenço, P. B. (2012). Moisture effects on the bond strength of FRP-masonry elements. Paper presented at the 6th International Conference on FRP Composites in Civil Engineering.

Leone, M., Matthys, S., & Aiello, M. A. (2009). Effect of elevated service temperature on bond between FRP EBR systems and concrete. Composites Part B: Engineering, 40(1), 85-93.

Micelli, F., & Nanni, A. (2004). Durability of FRP rods for concrete structures. Construction and Building Materials, 18(7), 491-503.

Mitchell, P. (2010). Freeze-thaw and sustained load durability of near surface mounted FRP strengthened concrete.

Silva, P., Fernandes, P. M. G., Sena-Cruz, J., Azenha, M., & Barros, J. A. (2014). Behaviour of concrete elements strengthened with near surface mounted CFRP strips under thermal cycles. Paper presented at the 7th International Conference on Fiber Reinforced Polymer (FRP) Composites in Civil Engineering (CICE 2014).

Soliman, S. M., El-Salakawy, E., & Benmokrane, B. (2010). Bond performance of near-surface-mounted FRP bars. Journal of Composites for Construction, 15(1), 103-111.

Soudki, K., & Alkhrdaji, T. (2005). Guide for the design and construction of externally bonded FRP systems for strengthening concrete structures (ACI 440.2 R-02). Paper presented at the Structures Congress 2005: Metropolis and Beyond.

Valluzzi, M. R., Da Porto, F., Garbin, E., & Panizza, M. (2014). Out-of-plane behaviour of infill masonry panels strengthened with composite materials. Materials and Structures, 47(12), 2131-2145.

VI. EFFECT OF DIRECT EXPOSURE TO THE SERVICE TEMPERATURES ON BOND BETWEEN ADVANCED COMPOSITE AND CONCRETE MASONRY UNIT FOR NSM AND EB TECHNIQUES

Zuhair Al-Jaberi, John J. Myers, Chandrashekhara, K.

ABSTRACT

The durability of fiber reinforced polymer (FRP) and fiber reinforced cementitious matrix (FRCM) for strengthening structural elements has been rather extensively studied in the literature. The influence of directly applying temperature on bond behavior represents an open topic that needs to be considered in more detail. This study is one of the initial studies to investigate the advanced composite bond behavior when subjected to tension force simultaneously with applying temperature. The temperatures considered in this study were at freezing -18 ^{o}C (0 ^{o}F), ambient 21 ^{o}C (70 ^{o}F), and high service temperature 49 ^{o}C (120 ^{o}F), which covers much of the spectrum of structural element service temperatures in the field. The key parameters investigated include different strengthening system under different level of temperature. A total of 36 specimens were subjected to single-lap direct shear simultaneously with applying temperature, and 12 specimens were tested after exposure to the cycles of heating and cooling temperature. The results showed a high reduction of FRP-epoxy bond properties up to 59% when exposed to high service temperatures, while there was insignificant reduction for FRCM bond when subjected to the same temperature.

1. INTRODUCTION

The interest in advanced composites in repairing and strengthening infrastructure elements has considerably increased, especially as the application of fiber reinforced

polymer (FRP) using near surface mounted (NSM) or externally bonded (EB) techniques have become more well established. The main advantage of FRP strengthening systems is the high strength-to-weight ratio alongside its corrosion resistance. The epoxy resin used to adhere the FRP bars or sheets to concrete masonry units (CMUs) may be influenced by the service temperature with respect to the glass transition temperature (Tg). The Tg is the temperature that separates the solid phase (brittle or glassy state) and liquid phase (rubbery state) of the material, and it is one of the most important properties for epoxy resin because the polymer loses the bond performance at this temperature (Hollaway, 2010). In fact, the effectiveness of the strengthening systems is influenced significantly by the bond properties of the adhesive between the advanced composite and substrate interface.

Masia et al. (2015) used a pull-out test was used to characterize the bond behavior of the NSM FRP to masonry unit. This test was conducted to evaluate temperatures at which the FRP bond becomes ineffective and to investigate whether the bond deterioration due to elevated temperatures is reversible or not. It was found that under sustained load, relative movement between FRP bar and the masonry unit was initiated at temperatures close to the Tg of epoxy adhesive. For specimens that were subjected to a heating and cooling process prior to loading, the original bond strength was restored after cooling and the specimen failed with the same mode as the control specimens. Palmieri et al. (2011) reported that the mode of failure was affected when the temperature is greater than Tg. For specimens under normal laboratory temperature, the failure was characterized by debonding with splitting of the resin. As a result of increasing the temperature, the FRP bar was pulled out due to loss of bond at the FRP-resin interface

and the mechanical properties of resin changed. The bond-slip behavior of NSM FRP bars under low and high temperature was investigated by several authors (Alvarez et al., 2007, Soliman et al., 2010, Fernandes et al., 2018, Novidis et al., 2007, Yu and Kodur, 2014). The results of specimens reinforced with GFRP subjected to 40 and 60 ^{o}C (104 and 140 ^{o}F) and also specimens reinforced with glass fiber reinforced polymer (GFRP) and carbon fiber reinforced polymer (CFRP) subjected to 200 freeze/thaw cycles were presented. Based on the experimental results, a reduction in bond strength by 26% occurred for specimens subjected to 60 ^{o}C (140 ^{o}F), and there was no significant deterioration in the bond after 200 freeze/thaw cycles. The mode of failure for specimens' strengthened using epoxy adhesive was concrete tension with or without splitting of adhesive material, while there was splitting at the concrete adhesive interface when using cementitious material.

The results of an experimental test to investigate the effect of elevated service temperature on EB FRP bonding was reported (Leone et al., 2009, Burke et al., 2013). At 80 ^{o}C (176 ^{o}F), the bond strength was reduced by 54%, 72%, and 25% for CFRP sheet, GFRP sheet, and CFRP laminate, respectively. With increasing temperature from 50 to 80 ^{o}C (122-176 ^{o}F), the mode of failure changed from cohesion to adhesion failure. If the temperature was higher than Tg, the bonding strength of adhesive material reduced more than that of concrete and led to bond failure at the interface. The EB system lost bond strength at 60 ^{o}C (140 ^{o}F), which is close to the epoxy Tg due to phase change and exhibited different material properties as reported by (Cromwell et al., 2011). The durability and long-term performance of EB FRP-brick masonry bond under harsh environment was investigated by (Maljaee et al., 2016). The specimens were exposed to

temperature cycles (between 10 ^{o}C and 50 ^{o}C) and constant relative humidity 90%. As a result of this study, the linear elastic behavior of primer and epoxy adhesive changed to nonlinear behavior, this change was associated by reduction in both strength and stiffness.

FRP with epoxy has some drawbacks: poor behavior of the resin at temperatures above the glass transition temperature, emission of toxic fumes, and moisture impermeability (Hashemi and Al-Mahaidi, 2008, Al-Jabari et al., 2015, Al-Abdwais and Al-Mahaidi, 2016). Using a cementitious material as an alternative adhesive agent is very appealing and eliminates these drawbacks in addition to the capability to control cracks propagation to ensure an excellent utilization of the fiber (Sui et al., 2018). The FRCM system was introduced within the last decade for strengthening existing structures. The effectiveness of externally bonded systems depends on the bond at the composite-masonry interface.

Donnini et al. (2017) evaluated the mechanical behavior of the FRCM system at high temperature. This evaluation includes bond testing for specimens strengthened with dry carbon fabrics and subjected to temperature ranging from 20 to 120 ^{o}C (68 to 248 ^{o}F). Although the result of FRCM reinforced with carbon experienced a reduction by 11% in tensile strength when subjected to elevated temperature up to 120 ^{o}C (248 ^{o}F), the FRCM system still maintained adequate resistance and bond to the substrate. Bisby et al. (2011) examined both FRCM and FRP bond performance at ambient and high temperature. The results showed that the FRCM system exhibited superior performance at elevated temperature up to 80 °C (176 ºF). The capacity of specimens strengthened with FRCM experienced reductions of only 6% at 50 °C (122 ºF) and 28% at 80 °C (176 ºF), while

the capacity of specimens strengthened with FRP reduced by 52% at 50 °C (122 ºF) and 74% at 80 °C (176 ºF).

Previous durability research on bond behavior has primarily focused on exposure to harsh environmental conditions and testing the specimens after exposure to said conditions, which enables the adhesive material to reset before performing the bond test. However, this research focused on studying the bond behavior under direct application of different temperature (freeze, ambient, high temperature), which is more representative of structural elements in the field. This study will help to investigate for the first time the bond behavior when the advanced composite (FRP or FRCM) is subjected to tension force simultaneously with applying temperature.

The key parameters investigated include (1) different types of strengthening system such as NSM-FRP, EB-FRP, and FRCM system, (2) different types of matrix used for bonding fibers such as epoxy resin in NSM and EB or cementitious-based material in FRCM system, (3) different levels of temperature applied to the specimen such as at freezing temperature -18 ^{o}C (0 ^{o}F), at ambient temperature 21 ^{o}C (70 ^{o}F), and at hot temperature 49 ^{o}C (120 ^{o}F). A total of forty-eight (48) specimens were strengthened and tested under single-lap direct shear. Thirty-six (36) of these specimens were subjected to tension force simultaneously with applying temperature, and the remaining twelve (12) specimens were tested following exposure to the cycles of heating and cooling.

2. OBJECTIVE AND PROPOSED RESEARCH PLAN

The aim of this research is to investigate and gather knowledge on bond behavior of different strengthening systems such as NSM-FRP, EB-FRP, and FRCM system under

different levels of temperature and tensile load simultaneously. This will be done by interpreting the experimental test results in terms of pull-out force, advanced composite strain, effectivity index, and failure mechanisms. In terms of bonding agent, the suitability of using a cement-based material at different temperatures as an alternative bonding agent instead of epoxy for strengthening existing structures was investigated. The other objective was to compare the performance of specimens exposed to temperature and load concurrently with the performance of specimens subjected to cycles of the same temperature before loading.

3. EXPERIMENTAL PROCEDURE

Forty-eight (48) hollow concrete masonry units with nominal dimensions 200 x 200 x 152 mm (8 x 8 x 6 in.) were used in this study. The typical specimen dimensions with strengthening systems are illustrated in Fig. 1. The experimental work presented in this paper consisted of two phases. The first phase focused on bond behavior when the composite (FRP or FRCM) was subjected to tension force simultaneously with applying temperature, while the second phase investigated the performance of specimens exposed to the 150 cycles of heating 50 ^{o}C (122 ^{o}F) and cooling -18 ^{o}C (0 ^{o}F) and tested later after exposure, which represents the conventional procedure.

Tables 1 and 2 provide an overview of the strengthening technique, types of fibers, adhesive material, and temperature when applying load for phase one and two, respectively.

3.1. STRENGTHENING MATERIALS AND EXPERIMENTAL PARAMETERS

The specimens were prepared in three groups. The first group represents specimens strengthened using NSM, while the other groups consider specimens

strengthened using EB with epoxy or using the FRCM technique. For the NSM technique, two types of FRP bars were used, namely GFRP and CFRP, with a 9.5 mm (3/8 in.) diameter. These bars are sand-coated and have spiral fiber twisted around the bar in order to improve the mechanical friction and interlock with the masonry substrate. Tensile tests were conducted on FRP bars with fiber content greater than 70% by weight to determine their mechanical properties. The average guaranteed tensile strength, tensile modulus of elasticity, and ultimate strain were obtained based on ASTM D7205-11 (ASTM, 2011) and are presented in Table 3. The average transverse and longitudinal coefficients of thermal expansion (CTE) for GFRP as referred to by the manufacturer are 30×10^{-6} C^{-1} and 8.3×10^{-6} C^{-1} per transverse and longitudinal direction, respectively. For the CFRP bars, the average transverse and longitudinal CTE are 89×10^{-6} C^{-1} and -4.5×10^{-6} C^{-1} per transverse and longitudinal direction, respectively. The resin matrix of the NSM technique was BASF ADH 1420 epoxy resin. Based on ASTM D638-14 (ASTM, 2014), the tensile strength and elongation at break provided by the manufacturer were 27.6 MPa (4000 psi) and 1%, respectively. The epoxy heat deflection temperature was 50 ^{o}C (122 ^{o}F).

The EB technique consisted of SHE fabric and Tyfo S epoxy. The SHE fibers are composed of glass fibers, while the Tyfo S epoxy matrix is an ambient cure adhesive composed of two components. Tyfo SHE-51 composite is unidirectional glass fabric oriented at 0^{o} with a secondary cross fiber at 90^{o} to hold the primary fabric together.

The pre-cured CFRP laminate used in this study was made of fibers embedded into epoxy resin under a pultrusion process with an average fiber content of 60% by volume. The mechanical properties for the glass fiber composite in primary direction of

Tyfo SHE-51 composite and CFRP laminate are illustrated in Table 3. Two types of epoxy resins were selected for this strengthening technique, Tyfo S manufactured by FYFE and SikaDur 30 epoxy matrix manufactured by Sika. Tyfo S epoxy matrix was used to bond SEH-51 glass fiber. Components A and B of the matrix represents a resin and hardener components were mixed at a volume ratio of 100:42 (A:B) to offer wide range of mechanical and thermal properties. The manufacturer properties for ultimate tensile strength and maximum strain were 72.4 MPa (10490 psi) and 5%, respectively. SikaDur 30, an adhesive bonding material that is a mixture of two parts, resin (A) and hardener (B), was mixed at a volume ratio of 100:30 to bind CFRP laminate. Based on ASTM D638-14 (ASTM, 2014), the tensile strength and elongation at break provided by the manufacturer were 24.8 MPa (3600 psi) and 1%, respectively.

For the FRCM technique, the open mesh fabric consists of fiber toes disposed along orthogonal directions with $0^o/90^o$ orientation and spaced 10 mm (0.4 in.), with main direction tensile strength greater than secondary direction tensile strength. Based on AC434 (2011), the mechanical properties of fibers used in FRCM system are summarized in Table 4. Compressive strength tests according to ASTM C109-13 (ASTM, 2013) were performed on the cementitious-adhesive agents (mortar x750 and x25) used with an FRCM system. Matrix x750 used to bond PBO fabric, and matrix x25 used to bond carbon fabric are inorganic cementitious matrices mixed with water to work like a mortar for the binding process. The average compressive strength for a matrix x750 was found to be 35 MPa (5 ksi) at an age of 28 days, while it was 15 MPa (2.175 ksi) for a matrix x25. According to ASTM C1314-12 (ASTM, 2012), the average compressive strength of a masonry unit was found 21 MPa (3,000 psi).

3.2. SPECIMENS' IDENTIFICATION

The specimens were designated with three parts. The first part represents the strengthening system, NSM, EB, or FRCM. The second part identifies the type of fiber: namely "C" for carbon, "G" for glass and "PBO" for polyparaphenylene benzobisoxazole. The third part refers to the temperature at the test. For specimens of phase 2, which are subjected to cycles of different temperature, "Cy" notation is added as a fourth part to represent this factor. As an example, the code NSM-G-A-Cy refers to a specimen strengthened by NSM using GFRP bar and tested in ambient temperature after applying cycles of different temperature.

4. STRENGTHENING PROCEDURE

For all strengthening techniques, the advanced composite is located at the plane of symmetry of the concrete masonry unit. The total length of FRP bar (in NSM technique) or fiber sheet (in EB- Epoxy or FRCM) was 840 mm (33 in.), and the bonded length was 100 mm (4 in.), where 12 mm (0.5 in.) was left for the bottom of the specimen to monitor the fiber slip failure. The sheet and laminate width was 50 mm (2 in.). The free end of the fiber was attached to the aluminum pipe (in case of NSM) or steel plates bolted together with four bolts (in case of EB-Epoxy or FRCM) to enable uniform load application without damage or slippage of gripped fiber. To ensure specific bonded length, duct tape was used as a bond breaker for a length of 90 mm (3.5 in.) from the top of the specimen. The description of the strengthened specimens is illustrated in Fig. 1.

4.1. NSM STRENGTHENING SYSTEM

No surface preparation was needed for the NSM system, and the strengthening procedure involved inserting FRP bar into a groove cut at the tension surface of the specimen. A grinder with a diamond concrete blade was used to cut the groove with a dimension double the diameter of the bar to avoid splitting failure of the adhesive cover (De Lorenzis and Nanni, 2002). Before placing epoxy resin, the grooves were vacuumed and cleaned using compressed air. The epoxy resin was injected to cover 2/3 of the groove depth. The FRP bar was installed to mid-groove depth by being pressed into the bonding agent, which flowed around the bar to ensure a complete bond between the bar and the sides of the groove. The groove was then filled with more epoxy resin, and the surface was leveled by removing excessive adhesive.

4.2. EB-EPOXY SYSTEM

The first step in the strengthening procedure is surface preparation and levelling, which includes manually cleaning the surface using a wire brush and vacuuming to remove the residual dust. The levelled and dried surface should be adopted to prevent premature peeling of FRP resulting from an uneven surface under applied load. For specimens strengthened with GFRP, Tyfo S epoxy resin was applied to serve as a prime filler layer to prepare the surface before installation of the GFRP sheet. The pre-cut SEH51 fabric was saturated with Tyfo S epoxy resin before it was applied to the prepared surface of the specimen to provide good bonding with the substrate. The fabric was aligned, and the air bubbles were removed at the interface using a hand roller until the fabric was fully attached to the substrate. The epoxy was applied at room temperature 21 °C (70 °F), which satisfies the temperature installation limits. The curing period for Tyfo

S epoxy resin is three days at 60 °C (140 °F). SikaDur 30 adhesive was used to bond the Aslan 400 CFRP laminate. Before applying SikaDur 30, the roughened face of CFRP laminate was wiped with solvent for cleaning to improve the bonding. The FRP sheet or laminate was bonded to the masonry specimen so that the fiber was in the direction of the load path. All the strengthened specimens were cured for one week prior to testing.

4.3. FRCM STRENGTHENING TECHNIQUE

The surface was prepared by removing any substance that may affect the bonding between the matrix and substrate. The surface was prepared using a surface grinder to remove weak parts at the surface and then was vacuumed and cleaned using low-pressure water before applying cement matrix to ensure a clean and wet surface, which prevents absorption of the water of cementitious matrix. The matrix was mixed as per the manufacturer specifications. After surface preparation, a first layer of cementitious matrix with a nominal thickness of approximately 5 mm (0.2 in.) was applied. A single ply of precut fabric was laid on the cementitious matrix and pressed gently into the first matrix layer. The second layer of cementitious matrix with a nominal thickness of 5 mm (0.2 in.) was then applied to cover the fabric mesh. All the strengthened specimens were cured by placing wet clothes on their surface for 72 hours and stored under laboratory conditions until pre-conditioning/testing. The specimens were tested after 28 days. The test specimens for different strengthening systems are shown in Fig. 2.

5. TEST SETUP AND INSTRUMENTATION

A single-lap shear test was considered to study shear debonding between the advanced composites and masonry substrate. The masonry specimen was restrained against vertical movement during the test by a steel frame bolted to the testing machine

base. A thick steel plate was inserted between the frame and the top of the specimen to ensure uniform distributed pressure over the restrained specimen. The steel frame was positioned inside a chamber with dimensions 300 mm x 600 mm x 800 mm (12 in. x 24 in. x 32 in.), as shown in Fig. 3. The maximum temperature capacity is 100 ^{o}C (212 ^{o}F), while the minimum temperature is -70 ^{o}C (-94 ^{o}F). To minimize the time of the test the specimens were pre-conditioned using an oven and refrigerator. The specimens were heated in the oven or cooled in the refrigerator and then moved to the chamber. The chamber was installed around the MTS universal testing machine with a 250 kN (56.2 kip.) capacity.

The load was applied in displacement control at a rate of 0.25 mm/min (0.01 in./min) through an MTS computer control station up to the load peak value. The global slip was measured between the fiber and the top of the specimen using high temperature linear variable displacement transducers (LVDTs). In addition, strain gauges were installed on three locations of bonded length at 25 mm (1 in.), 50 mm (2 in.), and 75 mm (3 in.) from the bottom of the bonded length. Four type-K thermocouples with diameter of 1.2 mm (0.047 in.) were fixed at different locations.

6. HEATING AND FREEZING PROCEDURE

Specimens in phase 1 of the study were heated up to 49 oC (120 oF) in a furnace or cooled down to -18 oC (0 oF) in a refrigerator, and then the specimens were brought to the chamber that was attached to the MTS universal testing machine to ensure that the specimens were at temporal with desired temperature. The specimens were loaded when the readings of four thermocouples were close enough as shown in Fig. 4. Temperature on tested specimens was measured from four thermocouples placed 1) inside the core of

the concrete block unit, 2) outside the surface of the concrete block unit, 3) at the adhesive layer, and 4) at the fiber of different strengthening systems. The locations of thermocouples are illustrated in Fig. 5. All the wires were connected to the data acquisition system outside the environmental chamber. For specimens in phase 2 of the study, the specimens were subjected to the conventional heating and freezing cycles in the environmental chamber as follows:

1- Freeze-thaw cycles: 100 freeze and thaw cycles were applied on strengthened specimens. Each freeze-thaw cycle consisted of freezing at -17.8 °C (0 °F) for 50 minutes and thawing at 4.4 °C (40 °F) for 50 minutes. The transition period between freezing and thawing was 30 minutes.
2- High temperature cycles: 150 alternating cycles of extreme temperature from 27 to 50 °C (80 to 120 °F) were used. An extreme temperature cycle consisted of temperature variation between 27 °C (80 °F) for 25 minutes and 50 °C (120 °F) for 25 minutes. The transition period between high and low temperature was 20 minutes.

The exposure regime of heating and cooling for specimens in the environmental chamber is shown in Fig. 6. All the specimens were subjected to an identical heating and cooling rate to ensure the consistency of the temperature during the loading process.

7. EXPERIMENTAL TEST RESULTS AND DISCUSSION

The summary of the ultimate pull-out force (Pu), normalized pull-out force with respect to the fiber axial stiffness, mid-bonded length strain at maximum force (εu), the effectivity index representing the ratio between the ultimate pull-out force at different temperatures to the ambient ultimate pull-out force (Pu/Pu,A), and the mode of failure for

all specimens is reported in Table 5. This table represents the average test results obtained from two identical specimens for each case. It was observed that the ultimate load significantly decreased at 48 oC (120 oF) by an average 50% for specimens strengthened with epoxy as adhesive material. On the other hand, there is no discernible negative effect of -18 oC (0 oF) on the performance of advanced composite in all strengthening systems when compared to the performance at ambient temperature. The reduction in the ultimate pull-out force for high temperature specimens was due to degradation of the epoxy adhesive. Based on normalized ultimate pull-out force, the specimens strengthened with EB-GFRP exhibited excellent bond capacity at ambient temperature due to large contact area compared with NSM system and due to high debonding strain for the epoxy used in this system compared with other types of epoxy.

7.1. PULL-OUT FORCE-GLOBAL SLIP RELATIONSHIP AND FAILURE MODES

Both phases included three strengthening systems (NSM, EB, and FRCM); two samples were considered per each case. For the NSM, the average maximum pull-out force was 37.36 kN (8.4 kip.), while it was 23.56 kN (5.3 kip.) and 4.9 kN (1.1 kip.) for EB and FRCM systems, respectively. The relationships between pull-out force and global slip of representative specimens of different strengthening systems are shown in Figs. 7, 8, and 9. The specimens were grouped based on the strengthening system. For the NSM and EB system, the pull-out force vs global slip curves were characterized by a linear relation up to the ultimate load, and then the capacity dropped suddenly due to complete debonding as a result of concrete or epoxy cover splitting. The heated specimens exhibited a gradual failure due to softening of the (concrete- resin) interface up to failure, as shown in Fig. 7 (a and b) and Fig. 8 (a and b).

On the other hand, the FRCM strengthened specimens' curves were characterized by bilinear response. The first stage was linear uncracked with high axial stiffness, while the second stage was nonlinear post-cracked up to the ultimate load, followed by gradual drop of capacity as shown in Fig. 9 (a and b). The nonlinear behavior was attributed to the micro-damage of the fiber-matrix interface and the gradual post-peak response caused by gradual loss of fiber-matrix bond. The load transfer mechanism for strengthening systems with epoxy is different from the load transfer mechanism of FRCM system. The key factor for this mechanism is the bond between the strengthening system and the substrate. The debonding surface for NSM or EB specimens subjected to ambient or low temperature was either fiber-epoxy surface or epoxy-substrate surface. For the same specimens subjected to high temperature, the bond was totally lost due to adhesive softening. The debonding failure occurred due to concrete splitting, epoxy cover splitting, shearing in laminate, or FRP slipping at the fiber-epoxy interface.

In the FRCM strengthening system, there are two interfaces: fiber-matrix interface and matrix-substrate interface. For all temperatures examined in this study, it was observed that the matrix-substrate bond is perfect during the loading process and the debonding failure always occurred at the fiber-matrix interface. The debonding failure was initiated as a result of microcracks in the matrix. In the post-crack stage, the load was increased due to friction (fiber-matrix slip) between the fiber and the matrix along the bonding length. The failure occurred at low load levels compared to the epoxy adhesive. It is worth mentioning that the first layer of FRCM system was still bonded to the masonry substrate even after the specimen's failure. All the modes of failure are illustrated in Fig. 10. The main mode of failure was adhesive splitting at the concrete-

cement interface. The failure occurred at low load levels compared to the epoxy adhesive, as given in Table 3.

7.2. ADHESIVE MATERIALS (EPOXY VS. CEMENTITIOUS MATRIX)

The effectiveness of a strengthening system depends highly upon the bond performance of the fiber with the substrate. In the current study, two adhesive materials were used, epoxy and cementitious matrix. The bond performance was evaluated based on normalized pull-out force with respect to the fiber axial stiffness and by visually examining the debonding surface. For ambient and low temperature, the normalized pull-out force for EB-G specimens was greater than other specimens in other strengthening systems, as shown in Table 5 due to a large contact area and high debonding strain for the epoxy used in this system compared with other systems. The other indication about the bond strength is the debonding surface at failure. For the specimens strengthened with EB-G the debonding surface included part of the concrete substrate, which is not the case for the FRCM system.

Most previous studies have focused on the bond characterization between FRP and substrate rather than on the behavior of the adhesive material itself. The current experimental results presented a significant reduction in the FRP-epoxy bond behavior when exposed to elevated temperatures compared to FRCM bond behavior. The reduction of FRP bond was due to a rapid deterioration of the epoxy-substrate adhesion when the temperature exceeded the heat distortion temperature (HDT) of the epoxy. The HDT is an important property of the epoxy resin and gives an indication about the temperature at which the material starts to soften. The HDT is defined by ASTM D 648 (ASTM, 2016) as the temperature that causes 0.25 mm (0.01 in.) deflection under a

centered standard stress of 455 kPa (66 psi). The HDT for all epoxies used in this study was 50 ^{o}C (120 ^{o}F), which is slightly lower than the glass transition temperature (Tg) and is the reason behind a slippage failure for the specimen strengthened using epoxy and subjected to 50 ^{o}C (120 ^{o}F). Similar findings were obtained by Bascom and Cottington (1976), who reported a reduction of epoxy tensile strength by 35% at 50 ^{o}C, which is lower than Tg (68 ^{o}C).

At high temperatures, the FRCM system exhibited excellent bond performance with substrate compared with the same system at ambient and low temperature. There was no change in FRCM bond performance (capacity and mode of failure) for all three levels of temperature (low, ambient, high) investigated.

7.3. TEMPERATURE

The effects of temperature on different strengthening systems are more evident by looking at the column charts in Fig. 11. For NSM and EB systems, the decrease of the ultimate pull-out force can be observed for temperatures close to the HDT. In particular, ultimate pull-out force was decreased compared to ultimate pull-out force of the same specimens at ambient temperature. The ultimate capacity was decreased by 48% for specimens strengthened with NSM, 59% in the case of specimens strengthened with EB-GFRP sheets, and 42% for specimens strengthened with CFRP-EB laminate. The reduction in pull-out force capacity is due to dramatic reduction of FRP bond to the substrate. The temperature affected the mode of failure by changing from mixed cohesive-adhesive with concrete detached at ambient and low temperature to perfect adhesive at elevated temperature. In the NSM system, the effectivity index was almost the same for specimens strengthened with GFRP and CFRP since the same type of epoxy

was used for both types of fiber. In EB system, the pull-out force for specimens strengthened with GFRP were less than the capacity of specimens strengthened with CFRP due to high temperature resistance for pre-cured CFRP laminate compared to wet-layup GFRP sheets.

For the specimens strengthened with FRCM system, the effectiveness of resisting applied load was not significantly affected by the change of temperature. It was observed that the capacity and mode of failure of specimens strengthened with PBO or carbon almost remained the same for all three temperatures.

7.4. EXPOSURE CONDITION

The average maximum pull-out force was 33.56 kN (7.5 kip) for NSM, while it was 22.24 kN (5.0 kip) and 4.34 kN (0.97 kip) for EB and FRCM systems, respectively. The pull-out force vs. global slip curves for specimens strengthened with different strengthening systems are shown in Fig. 12. For the epoxy strengthening systems exposed to cycles of heating followed by cooling, microcracks that generated in adhesive material changed the mode of failure from debonding due to concrete splitting to debonding due to epoxy splitting. The same behavior for specimens strengthened with NSM GFRP and NSM CFRP was due to the similarity of FRP bar surface and the epoxy adhesive used in this system. The compressive strength of the cementitious matrix was slightly deteriorated when exposed to cyclic temperature due to microcracks occurring as a result of the freezing and thawing process. The cementitious adhesive used in FRCM strengthening system experienced strength reductions of 9% when subjected to cyclic change in temperatures. In order to compare all strengthening systems in the second phase (subjected to cyclic temperature), the effectivity index was considered as shown in

Fig. 13. The effectivity index for specimen strengthened with EB GFRP was 85%, which is less than the effectivity index of EB CFRP. This performance was attributed to the excellent quality control of the manufactured CFRP laminate compared to GFRP wet-layup. The reduction of pull-out capacity due to the cyclic exposure to the temperatures close to the HDT of the epoxy adhesive was insignificant due to the reset process of epoxy prior to the bond test.

8. CONCLUSIONS

This paper presents comparison study on bond behavior under direct load and service temperature of different strengthening systems. This comparison has provided an understanding about the bond behavior under low, ambient and high temperature. Forty-eight specimens were fabricated and tested as part of the experimental program. According to this research, the following conclusions can be drawn:

1- For the epoxy strengthening systems, the relation of pull-out force and global slip was linear up to the ultimate and then the capacity dropped either suddenly due to complete debonding (in case of low and ambient temperature) or gradually due to softening of the concrete-resin interface (in case of high temperature)

2- For all three temperatures, the behavior of specimens strengthened with FRCM system was characterized by bilinear response. The first stage was linear uncracked with high axial stiffness, while the system was cracked in the second stage followed by gradual drop of capacity due to micro-damage of the fiber-matrix interface and the gradual loss of the fiber-matrix bond.

3- Debonding mode of failure was identified from this study as follows: debonding due to concrete or epoxy cover splitting, debonding due to shearing in laminate,

debonding at the fiber- matrix interface, debonding at the fiber-epoxy interface, and slipping at the fiber-epoxy interface.

4- Reduction of FRP-epoxy bond properties was up to 59% when exposed to high service temperatures, while there was insignificant reduction for the FRCM bond when subjected to the same temperature. This reduction was attributed to the rapid deterioration of the epoxy-substrate adhesion when the temperature is close to or exceeds the heat distortion temperature (HDT) of the epoxy. The high service temperature, 49 oC (120 oF), affected mode of failure by changing from mixed cohesive-adhesive with concrete detached to perfect adhesive.

5- In EB system, the pull-out force for specimens strengthened with GFRP was less than the capacity of specimens strengthened with CFRP due to high temperature resistance for pre-cured CFRP laminate compared to wet-layup GFRP sheets. On the other hand, the performance of CFRP and GFRP in NSM system was the same due to identical surface of bars and epoxy used in this system. The effectiveness of PBO and carbon in FRCM system to resist applied load was not significantly affected by the change of temperature.

6- For the epoxy strengthening systems exposed to cycles of heating and cooling, microcracks generated in adhesive material that changed the mode of failure from debonding due to concrete splitting to the debonding due to epoxy splitting associated with pull-out force reduction by 10%.

ACKNOWLEDGEMENTS

The authors wish to acknowledge the support of Midwest Block & Brick in Jefferson City, Missouri and Hughes Brothers in Seward, Nebraska, Ruredil S.p.A., San

Donato Milanese, Italy and HCED (The Higher Committee for Education Development in Iraq). The authors also wish to thank the technical support staff in not only the Department of Civil and Environmental Engineering but also the Center for Infrastructure Engineering Studies (CIES) at Missouri University of Science and Technology for their efforts in this research study. Any opinions, findings, conclusions, and recommendations presented in this paper are those of the authors and do not necessarily reflect the views of the sponsor or supporting agencies.

TABLES AND FIGURES

LIST OF TABLES

LIST OF FIGURES

Table 1 – Experimental test matrix (Phase 1)

Wall	Strengthening system	Specimen ID	Type of fiber	Bar diameter or sheet width (in.)	Temperature at test (^{o}F)	Adhesive material
1	**NSM**	NSM-G-A	Glass	3/8	70	ADH 1420
2		NSM-G-120	Glass	3/8	120	ADH 1420
3		NSM-G-0	Glass	3/8	0	ADH 1420
4		NSM-C-A	Carbon	3/8	70	ADH 1420
5		NSM-C-120	Carbon	3/8	120	ADH 1420
6		NSM-C-0	Carbon	3/8	0	ADH 1420
7	**EB-EBOXY**	EB-G-A	Glass	2	70	Tyfo S
8		EB-G-120	Glass	2	120	Tyfo S
9		EB-G-0	Glass	2	0	Tyfo S
10		EB-C-A	Carbon	2	70	SikaDur 30
11		EB-C-120	Carbon	2	120	SikaDur 30
12		EB-C-0	Carbon	2	0	SikaDur 30
13	**FRCM**	FRCM-PBO-A	PBO	2	70	matrix x750
14		FRCM-PBO-120	PBO	2	120	matrix x750
15		FRCM-PBO-0	PBO	2	0	matrix x750
16		FRCM-C-A	Carbon	2	70	matrix x25
17		FRCM-C-120	Carbon	2	120	matrix x25
18		FRCM-C-0	Carbon	2	0	matrix x25

Note: 1.0 mm=0.039 in., $T(°C) = [T(°F) – 32] \times 5/9$

Table 2 – Experimental test matrix (Phase 2)

Wall	Strengthening system	Specimen ID	Type of fiber	Bar diameter or sheet width (in.)	Temperature at test (^{o}F)	Adhesive material
1	NSM	NSM-G-A-Cy	Glass	3/8	70	ADH 1420
2		NSM-C-A-Cy	Carbon	3/8	70	ADH 1420
3	EB-EPOXY	EB-G-A- Cy	Glass	2	70	Tyfo S
4		EB-C-A- Cy	Carbon	2	70	SikaDur 30
5	FRCM	FRCM-PBO-A- Cy	PBO	2	70	matrix x750
6		FRCM-C-A- Cy	Carbon	2	70	matrix x25

Note: 1.0 mm=0.039 in., $T(°C) = [T(°F) – 32] \times 5/9$

Table 3 - Mechanical Properties of FRP

Material	Dimension (mm)	Ultimate tensile strength (MPa)	Elongation at break %	Tensile modulus (GPa)	Method
Aslan 100 GFRP bar	10	827	1.79	46	ASTM D7205-11
Aslan 200 CFRP bar	10	2172	1.75	124	ASTM D7205-11
Aslan 400 CFRP Laminate	2x50	2400	1.87	131	ASTM D7205-11
Tyfo SHE-51	1.3	575	2.1	26.1	ASTM D7205-11

Note : 1.0 GPa = 145.03 ksi; 1.0 MPa = 0.145 ksi; 1.0 mm/mm = 1.0 in./in.; 1.0 mm = 0.039 in.

Table 4 - Mechanical Properties of FRCM coupon

Material	Thickness (mm)	Ultimate tensile strength (MPa)	Elongation at break %	Tensile modulus (GPa)	Method
PBO fiber	10	1880	1.47	127	AC434
Carbon fiber	10	970	1.33	75	AC434

Note : 1.0 GPa = 145.03 ksi; 1.0 MPa = 0.145 ksi; 1.0 mm/mm = 1.0 in./in.; 1.0 mm = 0.039 in.

Table 5 - Summary of test results

Wall	Phase	Strengthening system	Specimen ID	Ultimate force P_u (kN)	Effectivity index $P_u/P_{u,A}$	Normalized ultimate force (P_u/E_fA_f)	Strain at maximum force ε_u (mm/mm)	Mode of failure*
1	Phase 1	NSM	NSM-G-A	37.36	1.00	0.0114	0.00906	D-C/SP
2			NSM-G-120	19.60	0.52	0.0060	0.00312	S-F/E
3			NSM-G-0	37.05	0.99	0.0113	0.00830	D-SP
4			NSM-C-A	37.10	1.00	0.0042	0.00852	D-C/SP
5			NSM-C-120	20.56	0.55	0.0023	0.00340	S-F/E
6			NSM-C-0	36.94	0.99	0.0042	0.00808	D-SP
7		EB-EBOXY	EB-G-A	15.56	1.00	0.0326	0.00790	D-F/E
8			EB-G-120	6.45	0.41	0.0135	0.00324	S-F/E
9			EB-G-0	16.69	1.07	0.0350	0.00842	D-F/E
10			EB-C-A	23.56	1.00	0.0026	0.00124	D-F/E
11			EB-C-120	13.80	0.58	0.0015	0.00127	S-F/E
12			EB-C-0	23.51	0.99	0.0026	0.00120	D-SL
13		FRCM	FRCM-PBO-A	4.90	1.00	0.0071	0.00220	D-F/M
14			FRCM-PBO-120	4.83	0.98	0.0070	0.00200	D-F/M
15			FRCM-PBO-0	5.84	1.19	0.0085	0.00250	D-F/M
16			FRCM-C-A	3.58	1.00	0.0018	0.00150	D-F/M
17			FRCM-C-120	3.45	0.96	0.0018	0.00112	D-F/M
18			FRCM-C-0	3.72	1.03	0.0019	0.00140	D-F/M
19	Phase 2	NSM	NSM-G-A-Cy	35.05	0.94	0.0107	0.00868	D-SP
20			NSM-C-A-Cy	33.50	0.90	0.0038	0.00746	D-SP
21		EB-EBOXY	EB-G-A- Cy	13.15	0.85	0.0275	0.00750	D-F/E
22			EB-C-A- Cy	22.24	0.94	0.0024	0.00118	D-F/E
23		FRCM	FRCM-PBO-A- Cy	4.34	0.90	0.0059	0.00340	D-F/M
24			FRCM-C-A-Cy	3.46	0.96	0.0018	0.00130	D-F/M

Note : 1.0 kN = 0.224 kip; 1.0 mm/mm = 1.0 in./in.

*D-C/SP: debonding due to concrete splitting, D-Sp: debonding due to splitting of the epoxy cover, D-SL: debonding due to shearing in laminate, D-F/M: debonding at fiber- matrix interface, D-F/E: debonding at fiber- epoxy interface, and S-F/E: slipping at fiber- epoxy interface.

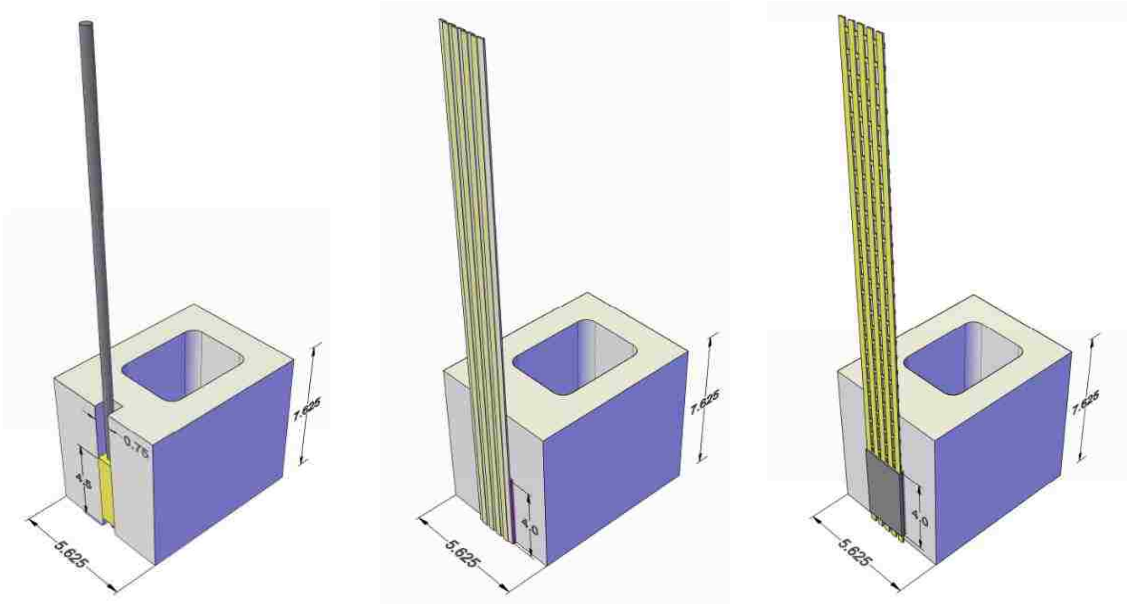

NSM-FRP EB-FRP FRCM

Figure1. Typical specimen dimensions with different strengthening systems

(a) (b) (c)

Figure 2. Test specimens: (a) EB-GFRP, (b) NSM-FRP (c) EB-CFRP

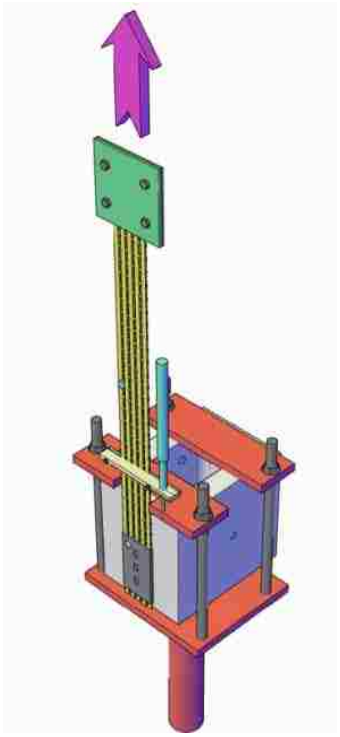

Steel frame

Heating and cooling chamber

Figure 3. Test setup

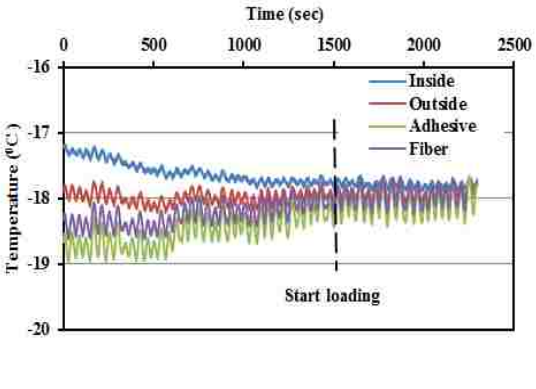

(a)

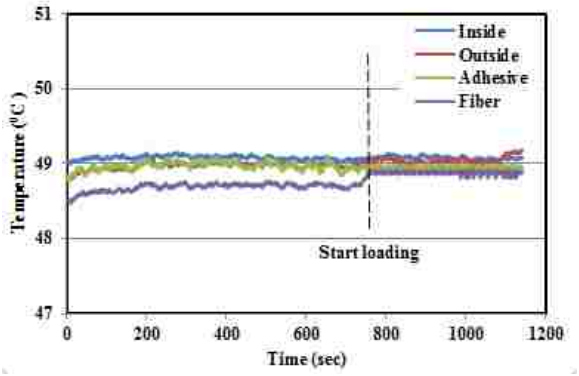

(b)

Figure 4. Time- temperature curve obtained from the four thermocouples for a specimen tested under (a) cooling down to (-18 ^{0}C.) and (b) heated up to (49 ^{0}C.)

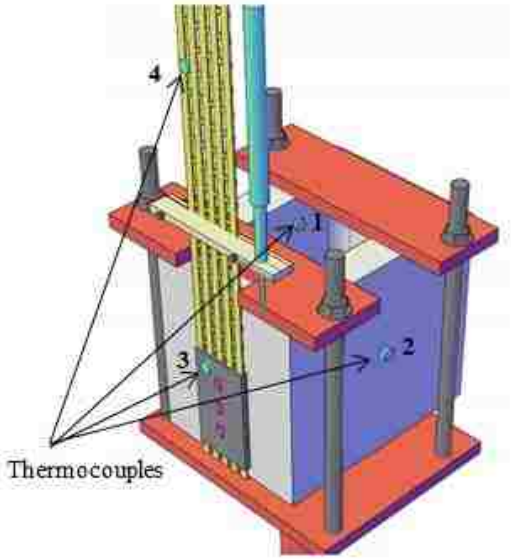

Figure 5. Locations of thermocouples

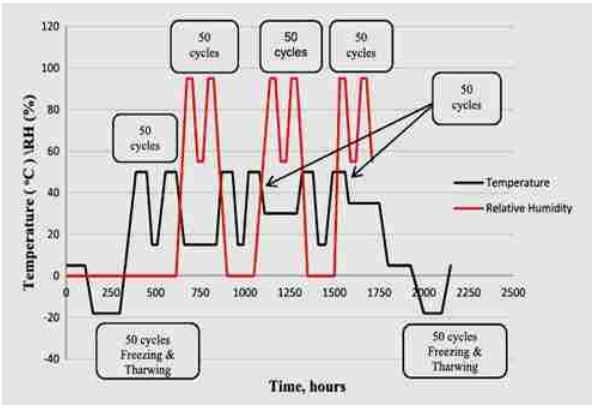

Figure 6. Exposure regime of heating and cooling

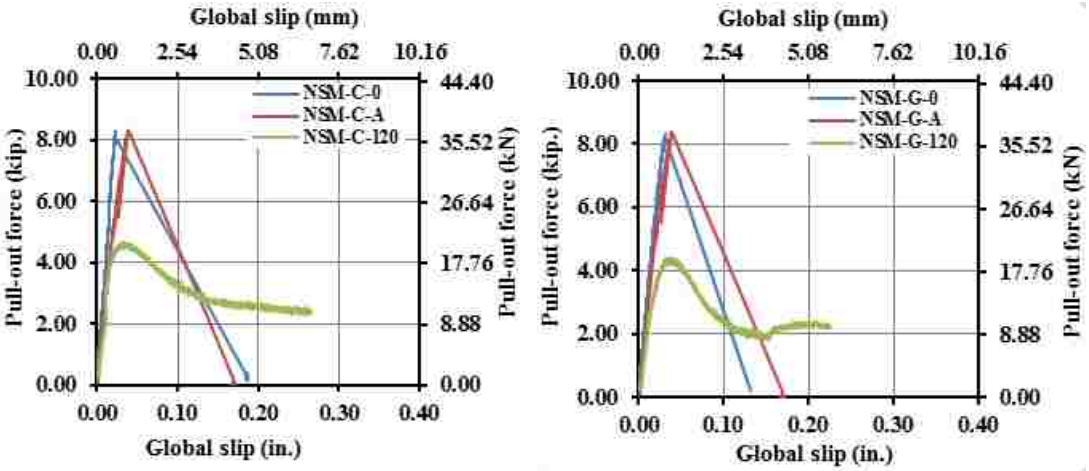

(a) (b)

Figure 7. Pull-out force vs. global slip relationship for (a) NSM-CFRP, (b) NSM-GFRP

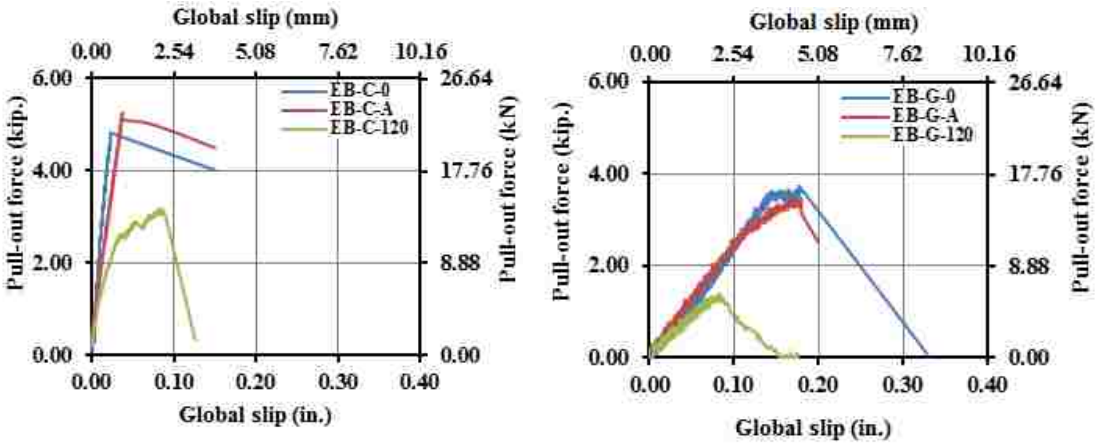

(a) (b)

Figure 8. Pull-out force vs. global slip relationship for (a) EB-CFRP, (b) EB-GFRP

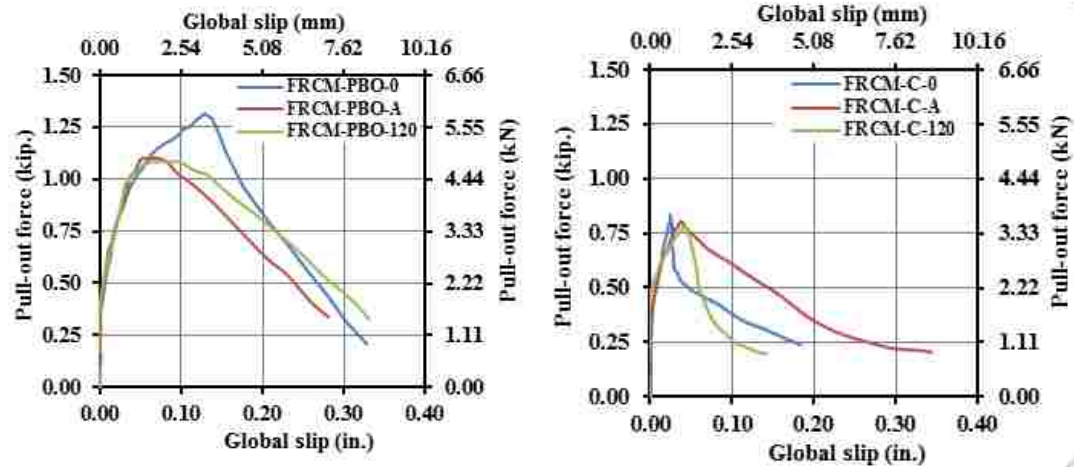

(a) (b)

Figure 9. pull-out force vs. global slip relationship for (a) FRCM-PBO, (b) FRCM-carbon


NSM-G-A-Cy


NSM-C-A-Cy


EB-C-A-Cy

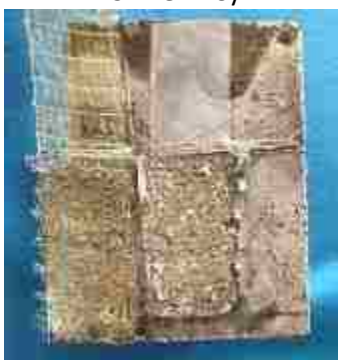
EB-G-A-Cy


FRCM-PBO-A-Cy


FRCM-C-A-Cy


NSM-G-0


NSM-C-0


EB-C-0


EB-G-0


FRCM-PBO-0


FRCM-C-0

Figure10. Modes of failure for all strengthening system in different temperatures

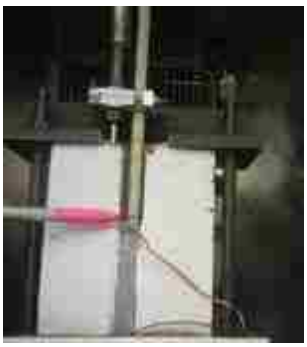
NSM-G-120

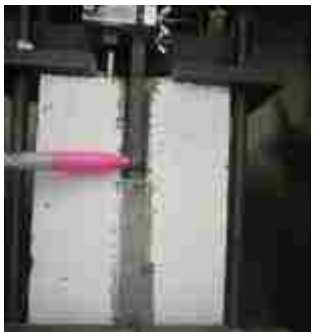
NSM-C-120


EB-C-120


EB-G-120


FRCM-PBO-120


FRCM-C-120


NSM-G-A


NSM-C-A


EB-C-A


EB-G-A


FRCM-PBO-A


FRCM-C-A

Figure10. Modes of failure for all strengthening system in different temperatures (cont.)

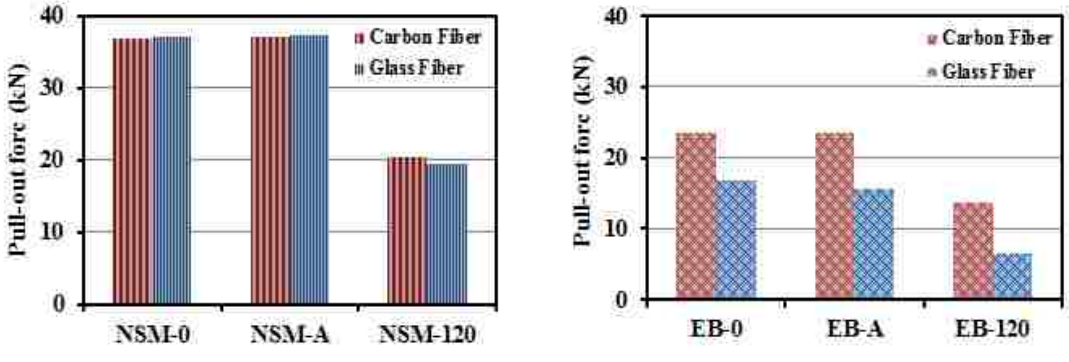

(a) (b)

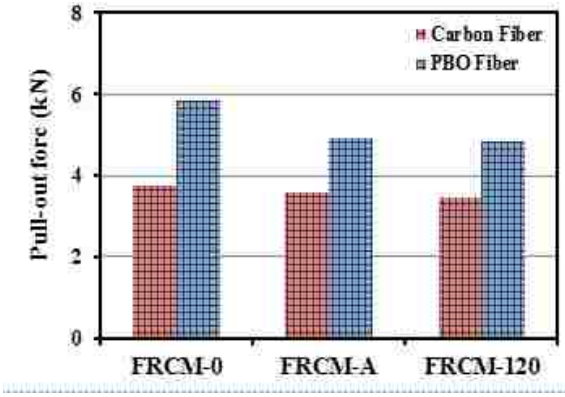

(c)

Figure 11. Effect of temperature on (a) NSM, (b) EB, and (c) FRCM systems

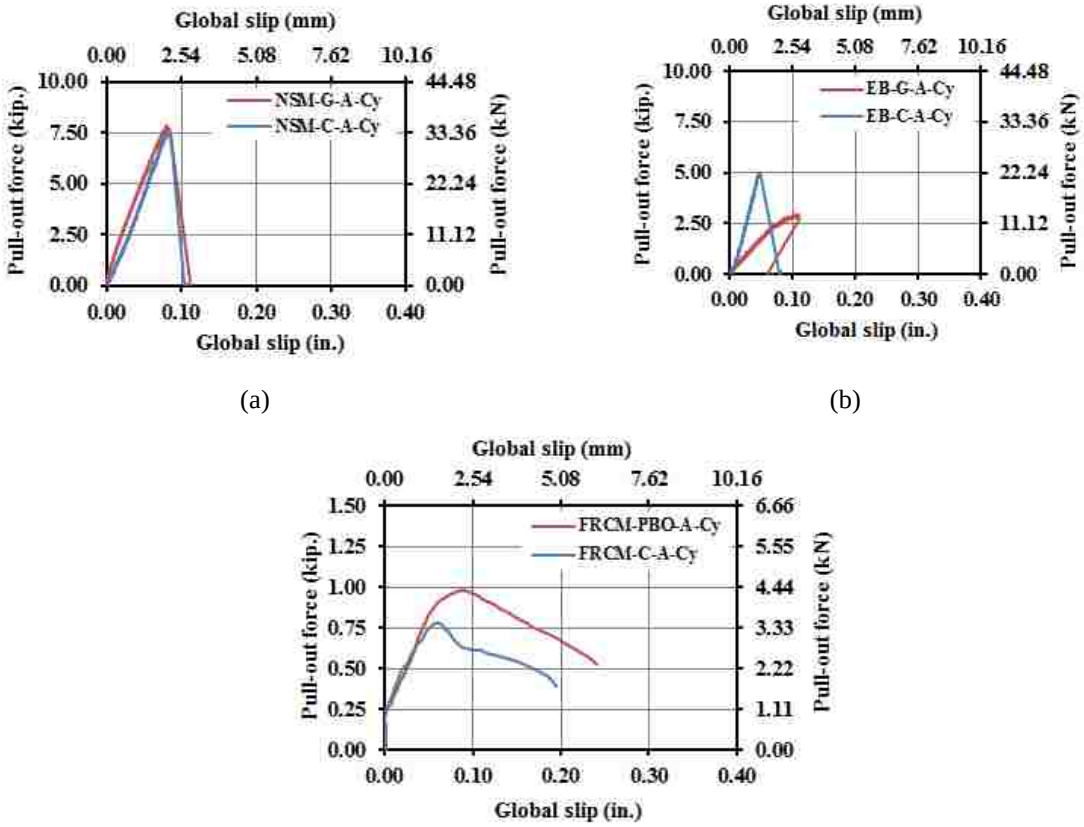

Figure 12. Effect of exposure condition on (a) NSM, (b) EB, and (c) FRCM systems

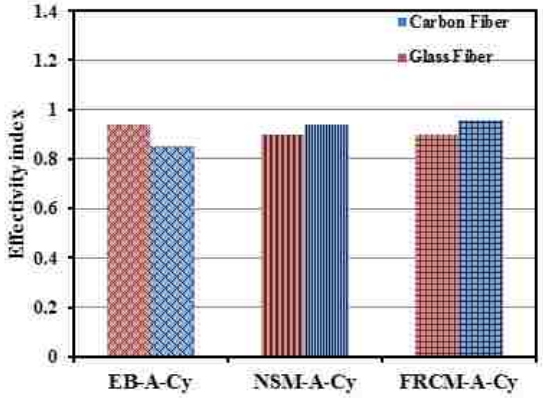

Figure 13. Effectivity index for different strengthening systems

REFERENCES

AC434. (2011). Proposed acceptance criteria for masonry and concrete strengthening using fiber-reinforced cementitious matrix (FRCM) composite system.

Al-Abdwais, A., & Al-Mahaidi, R. (2016). Bond behaviour between NSM CFRP laminate and concrete using modified cement-based adhesive. Construction and Building Materials, 127, 284-292.

Al-Jabari, Z., Myers, J. J., & ElGawady, M. (2015). Out-of-Plane Strengthening of Reinforced Masonry Walls using Near-Surface Mounted (NSM) FRP Bars with Epoxy and Cementitious Materials. Advanced Composites in Construction, ACIC, 195-200.

Alvarez, A., Zaidi, A., & Mamsoudi, R. (2007). Bond slip behaviour of FRP bars under low and high temperature—experimental and theoretical studies. CDCC-2007, 523-530.

ASTM.(2011). (2011). Standard test method for tensile properties of fiber reinforced polymer matrix composite bars. ASTM D7205/D7205M-06.

ASTM.(2012). (2012). Standard Test Method for Compressive Strength of Masonry Prisms, ASTM C1314 - 12.

ASTM.(2013). (2013). Standard Test Method for Compressive Strength of Hydraulic Cement Mortars (Using 2-in. or [50-mm] Cube Specimens), ASTM C109/C109M - 13.

ASTM.(2014). (2014). Standard Test Method for Tensile Properties of Plastics1 ASTM D638-14.

ASTM.(2016). (2016). Standard Test Method for Deflection Temperature of Plastics Under Flexural Load in the Edgewise Position, ASTM D648 - 16.

Bascom, W. D., & Cottington, R. L. (1976). Effect of temperature on the adhesive fracture behavior of an elastomer-epoxy resin. The Journal of Adhesion, 7(4), 333-346.

Bisby, L., Stratford, T., Smith, J., & Halpin, S. (2011). FRP versus fiber reinforced cementitious mortar systems at elevated temperature. Special Publication, 275, 1-20.

Burke, P. J., Bisby, L. A., & Green, M. F. (2013). Effects of elevated temperature on near surface mounted and externally bonded FRP strengthening systems for concrete. Cement and Concrete Composites, 35(1), 190-199.

Cromwell, J., Harries, K., & Shahrooz, B. (2011). Environmental durability of externally bonded FRP materials intended for repair of concrete structures. Construction and Building Materials, 25(5), 2528-2539.

De Lorenzis, L., & Nanni, A. (2002). Bond between near-surface mounted fiber-reinforced polymer rods and concrete in structural strengthening. ACI structural Journal, 99(2), 123-132.

Donnini, J., y Basalo, F. D. C., Corinaldesi, V., Lancioni, G., & Nanni, A. (2017). Fabric-reinforced cementitious matrix behavior at high-temperature: Experimental and numerical results. Composites Part B: Engineering, 108, 108-121.

Fernandes, P., Sena-Cruz, J., Xavier, J., Silva, P., Pereira, E., & Cruz, J. (2018). Durability of bond in NSM CFRP-concrete systems under different environmental conditions. Composites Part B: Engineering, 138, 19-34.

Hashemi, S., & Al-Mahaidi, R. (2008). Cement based bonding material for FRP. Paper presented at the Proceedings of the.

Hollaway, L. (2010). A review of the present and future utilisation of FRP composites in the civil infrastructure with reference to their important in-service properties. Construction and Building Materials, 24(12), 2419-2445.

Leone, M., Matthys, S., & Aiello, M. A. (2009). Effect of elevated service temperature on bond between FRP EBR systems and concrete. Composites Part B: Engineering, 40(1), 85-93.

Masia, M. J., Shen, J., Simundic, G., & Page, A. W. (2015). Behaviour of NSM FRP masonry bond under elevated temperatures. Proceedings of the Institution of Civil Engineers-Construction Materials, 169(1), 27-38.

Novidis, D., Pantazopoulou, S., & Tentolouris, E. (2007). Experimental study of bond of NSM-FRP reinforcement. Construction and Building Materials, 21(8), 1760-1770.

Palmieri, A., Matthys, S., & Taerwe, L. (2011). Bond behavior of NSM FRP bars at elevated temperatures. Paper presented at the first middle east conference on smart monitoring, Assessment and Rehabilitation Civil Structures.

Soliman, S. M., El-Salakawy, E., & Benmokrane, B. (2010). Bond performance of near-surface-mounted FRP bars. Journal of Composites for Construction, 15(1), 103-111.

SECTION

3. SUMMARY, CONCLUSIONS AND RECOMMENDATIONS

3.1. SUMMARY OF RESEARCH

The purpose of this research was to evaluate the behavior of reinforced masonry walls strengthened with advanced composite and subjected to out-of-plane pseudo-static cyclic load, in addition to evaluating the durability and bond behavior of different strengthening systems. The main parameters considered in this study were type and amount of fibers, masonry bond pattern, the adhesive material used for bonding, and steel reinforcement ratio. The total test matrix of this study included forty-two reinforced masonry walls to study the effectiveness of different strengthening systems in enhancing out-of-plane flexural capacity, ten strengthened reinforced masonry walls to evaluate the effect of long-term environmental exposure, and fifty-six specimens to investigate the bond behavior between the advanced composite and the concrete masonry unit at different temperatures.

This section contains the conclusions from the three experimental and analytical phases and recommendations for the future work.

3.2. CONCLUSIONS

The following section summarizes the conclusions from both the experimental and analytical studies of the reinforced masonry walls strengthened with different strengthening systems.

3.2.1. Flexural Behavior of Strengthened Masonry Walls.

- The strengthened reinforced masonry walls' (non-arching walls) behavior was significantly dependent on the type and amount of fiber. A wall strengthened with GFRP had higher displacement ductility than the same wall strengthened with CFRP due to high stiffness of CFRP. For the NSM system, the capacity increased by 150% for the specimen strengthened with one GFRP bar and 236% for the specimen strengthened with two carbon strips compared to the control wall. For the EB system, the load-carrying capacity increased by double for the specimen strengthened with two layers of GFRP, while it increased by 85% for the specimen strengthened with two strips of CFRP laminate due to the high debonding strain of epoxy used with GFRP. The specimens strengthened with two layers of PBO or carbon fiber in the FRCM system presented approximately the same moment capacity due to better bond performance for PBO compared to the bond of the carbon in FRCM system. Test results indicated that NSM with cement adhesive and FRCM system remarkably increase the lateral load capacity of RM walls by 75% and 97%, respectively.
- Two basic types of failure modes were identified from the test results. The first was related to fibers, which include rupture, slippage, or debonding. The second was related to the concrete block unit, which includes crushing of masonry unit or shear-type failure. FRP rupture was identified for specimens strengthened with one layer of GFRP, while FRP debonding was identified for specimens strengthened with one bar GFRP in NSM or CFRP laminate in EB system. The mode of failure changed from a debonding mode to a shear failure mode in the case of strengthening using two layers of GFRP sheets, two GFRP bars, and one CFRP bar, so in a design strengthening

application, the shear capacity would need to be considered and enhanced as warranted to prevent a primary brittle failure mode in shear. For the FRCM system, a slippage failure was identified for the specimen strengthened with one layer, while a debonding failure was reported for specimens strengthened with multiple layers. Finally, the gradual failure of the specimens strengthened with a cementitious bonding material was observed comparing with a more sudden failure for specimen strengthened using an epoxy material.

- The flexural capacity and ductility of stack pattern specimens improved when the continuous head joint was reinforced with an FRP bar or the tension face strengthened with PBO fabric sheet. The strength capacity for the stack specimens was improved by 115% after strengthening with one layer of GFRP compared to the control specimen. The initial stiffness for both the running and stack specimens was the same, but reduced in value for the stack specimens due to a crack formation in the continuous head joint.
- The compression fiber reinforcement has insignificant impact on the stiffness of the pre-yielding stage, but flexural capacity of specimens reinforced with two GFRP bars was increased by 11% compared with strengthened wall without compression fiber reinforcement. The maximum measured compressive strain in the NSM FRP reinforcing bars was 0. 2% which is 11% of the rupture strain of the FRP reinforcing bar.
- The change of reinforcement ratio affected the stiffness, but had little effect on the ultimate strength since the stiffness depended on the steel and FRP. The behavior of

the wall with 1#5 steel bar was brittle due to stress concentration that initiated cracks and led to sudden failure.

For the EB system, the surface preparation by adding a putty filler layer as a base layer for GFRP sheet improved the flexural capacity by 10%. The putty filler layer provided a viscous material that reduced the porosity of the concrete unit and increased bond between the GFRP sheet and substrate. Also, the mode of failure changed from FRP rupture (for the specimen with putty filler layer) to FRP debonding (for the specimen without surface preparation).

3.2.2. Analytical Study of Strengthened Masonry Walls.

- Among many codes, the FRP debonding strain of ACI 440.2R (2008) and the Chinese CECS-146 (2003) has good agreement with experimental data compared to other codes, but these codes are still very conservative and have much lower accuracy to predict FRP debonding strain. In regards to accuracy of masonry codes, CNR DT-200 (2012) has lower accuracy of average predicted/experimental debonding strain, which is 16%, compared with 75% for ACI 440.7R (2010). The proposed model for estimating debonding strain presents an excellent prediction with an average value of 85.66% for the current study and 97% for existing database.
- Using moment–curvature relation was very useful for predicting strengthened wall behavior, especially for uncracked and pre-yield stages, in addition to predicting the ultimate flexural capacity for the fully cracked stage.
- The experimental initial stiffness was much lower than the theoretical uncracked stiffness for the control specimen and was approximately 31% of the theoretical value. The stiffness of the control specimen had a sudden loss of 30% within the first

few cycles, while the stiffness for the strengthened wall dropped down to the level of the control when the mid-span deflection was about 25.4 mm (1-in.). Beyond the failure of the composite, the stiffness degradation of the specimen strengthened with one anchorage ply of PBO was gradual and 40% higher than the control specimen due to high tensile strength of the anchored fiber attached to the masonry substrate. The pre-yield stiffness depends not only on fiber reinforcement ratio, but also on the internal steel reinforcement ratio, maximum debonding strain for adhesive material, and the masonry bond pattern. For the same bonding agent, the increase in stiffness of a strengthened specimen is a function of the fiber axial stiffness, but the relationship does not appear to be one to one.

- Small energy dissipation for low drift levels was observed due to insignificant damage in the components of strengthened wall at this level. The energy dissipation was increased as the applied drift increased. The energy dissipation for specimen strengthened with one anchorage ply of PBO improved by 38% compared to the two-ply PBO without anchorage and 80% compared to the control specimen. This behavior was attributed to the mode of failure (i.e., full slippage of fiber in the cementitious material) in addition to the cracks developed in the masonry units compared to the control specimen. The specimen strengthened with one bar of GFRP and cement-based adhesive presented a higher dissipated energy compared to other specimens, and 30% higher than the control specimen. The reason behind this was the gradual debonding of the bar, which was not the case when fiber reinforcement ratio or fiber axial stiffness increased. The dissipated energy of the specimen with stack bond pattern increased by 62% and 38% when strengthened using NSM and FRCM

systems, respectively. The specimens strengthened using NSM with cementitious material presented better behavior of dissipated energy compared to specimens strengthened using the FRCM system.

- Strengthening in both systems (FRCM and NSM with cement-based adhesive) resulted in significant losses in structural ductility of the strengthened specimens. Ductility can be enhanced if the end anchorages are used, or strip bar in the case of the NSM strengthening system. Using anchorage or rectangular cross section of FRP bar enables the strengthened specimen to upgrade the ductility by 122% or 88% of the control specimen for FRCM and NSM systems, respectively. The strengthened wall with CFRP strip shows a delay in cracking and debonding failure due to sliding inside the groove. The loss of ductility for the specimen with stack bond pattern is 16% compared to the same specimen with running bond pattern. The displacement ductility of conventionally reinforced concrete masonry walls ranges from 4 to 12. However, the displacement ductility of reinforced masonry walls strengthened with EB-FRP generally ranges from 1.5 to 4.5.

3.2.3. Durability and Bond Behavior of Strengthening Systems.

- The ultimate load significantly decreased due to environmental exposure by an average 18.32% and 12.9% for specimens strengthened with GFRP-epoxy and PBO-cement, respectively. The GFRP-epoxy specimen exhibited high reduction percent due to large contact area compared with NSM system and due to low resistance to the cycles of temperature compared to the procured CFRP laminate. The same reason can be presented for the high reduction value for the capacity of specimens' strengthened FRCM system. The effect of environmental conditions exposure on the bond of NSM

and EB strengthening system was represented by changing the mode of failure from debonding due to concrete splitting to debonding due to adhesive material splitting. In the FRCM strengthening system, it was observed that the debonding failure always occurred at the fiber-matrix interface.

- The secant stiffness of specimens strengthened with GFRP and exposed to environmental conditions was reduced by 5 and 15% when epoxy or cementitious adhesive used, respectively. High percent of reduction in stiffness of exposed specimens strengthened with CFRP was observed. The stiffness degradation changed from 17 to 37% as a result of changing the adhesive material from epoxy to cementitious agent, respectively.
- The behavior of walls with stack bond pattern was improved by reinforcing the continuous head joint with FRP bars. Insignificant influence of the environmental conditions on the behavior of stack strengthened wall. The reduction in flexural capacity was 9%, while the reduction in secant stiffness was only 5%.
- For the epoxy strengthening systems, the relation of pull-out force and global slip was linear up to the ultimate and then the capacity dropped either suddenly due to complete debonding (in case of low and ambient temperature) or gradually due to softening of the concrete-resin interface (in case of high temperature)
- For all three temperatures, the behavior of specimens strengthened with FRCM system was characterized by bilinear response. The first stage was linear uncracked with high axial stiffness, while the system was cracked in the second stage followed by gradual drop of capacity due to micro-damage of the fiber-matrix interface and the gradual loss of the fiber-matrix bond.

- Debonding mode of failure was identified from this study as follows: debonding due to concrete or epoxy cover splitting, debonding due to shearing in laminate, debonding at the fiber- matrix interface, debonding at the fiber-epoxy interface, and slipping at the fiber-epoxy interface.
- High reduction of FRP-epoxy bond properties were up to 59% when exposed to high service temperatures, while there was insignificant reduction for the FRCM bond when subjected to the same temperature. This reduction was attributed to the rapid deterioration of the epoxy-substrate adhesion when the temperature is close to or exceeds the heat distortion temperature (HDT) of the epoxy. The high service temperature, 49 ^{o}C (120 ^{o}F), affected mode of failure by changing from mixed cohesive-adhesive with concrete detached to perfect adhesive.
- For the epoxy strengthening systems exposed to cycles of heating and cooling, microcracks generated in adhesive material that changed the mode of failure from debonding due to concrete splitting to the debonding due to epoxy splitting associated with pull-out force reduction by 10%.

3.3. RECOMMENDATIONS FOR FUTURE WORK

Extensive research was carried out during the course of this project, including experimental and analytical study for strengthening reinforced masonry walls. Future work is required to address the following issues:

- Different types of masonry units, such as clay bricks, should be strengthened and tested in order to generate a more robust database and validate the proposed design approach.

- Different boundary and load conditions should be considered, especially fully reversed cyclic loading, in order to observe the behavior and potential failure modes.
- Partially grouted masonry walls strengthened with different strengthening systems should be tested, in addition to consideration of applying the axial load combined with out-of-plane loading.
- The slenderness ratio should be increased by increasing the size of the test specimens to report the controlling failure mechanism with and without arching action.

REFERENCES

ACI 440.2R-08. (2008). Guide for the design and construction of externally bonded FRP systems for strengthening concrete structures.

ACI 440.7R-10. (2010). Guide for the design and construction of externally bonded FRP systems for strengthening unreinforced masonry structures.

Al-Abdwais, A., & Al-Mahaidi, R. (2016). Modified cement-based adhesive for near-surface mounted CFRP strengthening system. Construction and Building Materials, 124, 794-800.

Al-Jabari, Z., Myers, J. J., & ElGawady, M. (2015). Out-of-Plane Strengthening of Reinforced Masonry Walls using Near-Surface Mounted (NSM) FRP Bars with Epoxy and Cementitious Materials. Advanced Composites in Construction, ACIC, 195-200.

Al-Jaberi, Z., Myers, J., & ElGawady, M. (2016). Flexural capacity of out-of-plane reinforced masonry walls strengthened with externally bonded(EB) FRP. Paper presented at the 7th International Conference on Advanced Composite Materials in Bridges and Structures Vancouver, British Columbia, Canada

Al-Mahmoud, F., Mechling, J.-M., & Shaban, M. (2014). Bond strength of different strengthening systems–Concrete elements under freeze–thaw cycles and salt water immersion exposure. Construction and Building Materials, 70, 399-409.

Alvarez, A., Zaidi, A., & Mamsoudi, R. (2007). Bond slip behaviour of FRP bars under low and high temperature—experimental and theoretical studies. CDCC-2007, 523-530.

Babaeidarabad, S., & Nanni, A. (2015). Out-of-Plane Strengthening of URM Walls with Fabric-Reinforced-Cementitious-Matrix (FRCM). Special Publication, 299, 1-12.

Bisby, L., Stratford, T., Smith, J., & Halpin, S. (2011). FRP versus fiber reinforced cementitious mortar systems at elevated temperature. Special Publication, 275, 1-20.

Burke, P., Bisby, L., & Green, M. (2008). Performance of NSM FRP strengthened concrete slabs at low temperatures. Paper presented at the Fourth Int. Conf. on FRP Composites in Civil Engineering (CICE 2008), International Institute for FRP in Construction (IIFC), Winnipeg, Manitoba, Canada.

Burke, P. J. (2008). Low and high temperature performance of near surface mounted FRP strengthened concrete slabs.

Burke, P. J., Bisby, L. A., & Green, M. F. (2013). Effects of elevated temperature on near surface mounted and externally bonded FRP strengthening systems for concrete. Cement and Concrete Composites, 35(1), 190-199.

Carney, P., & Myers, J. (2003). Out-of-plane static and blast resistance of unreinforced masonry wall connections strengthened with FRP, Report 03-46. Center for Infrastructure Engineering Studies.

Churilov, S., & Dumova-Jovanoska, E. (2012). Experimental and analytical research of strengthening techniques for masonry. PhD thesis, University" Ss. Cyril and Methodius", Faculty of Civil Engineering, Skopje, Macedonia.

Cromwell, J., Harries, K., & Shahrooz, B. (2011). Environmental durability of externally bonded FRP materials intended for repair of concrete structures. Construction and Building Materials, 25(5), 2528-2539.

Dai, J.-G., Yokota, H., Iwanami, M., & Kato, E. (2010). Experimental investigation of the influence of moisture on the bond behavior of FRP to concrete interfaces. Journal of Composites for Construction, 14(6), 834-844.

De Lorenzis, L., Nanni, A., & La Tegola, A. (2000). Bond of Near Surface Mounted FRP Rods in Concrete Masonry Units. Paper presented at the Proceedings of the Seventh Annual International Conference on Composites Engineering (ICCE/7), Denver, Colorado, July.

De Lorenzis, L., & Teng, J. (2007). Near-surface mounted FRP reinforcement: An emerging technique for strengthening structures. Composites Part B: Engineering, 38(2), 119-143.

De Lorenzis, L., Tinazzi, D., & Nanni, A. (2000). Near surface mounted FRP rods for masonry strengthening: bond and flexural testing. Paper presented at the Proceedings of the international conference on composite engineering.

Dizhur, D., Griffith, M., & Ingham, J. (2014). Out-of-plane strengthening of unreinforced masonry walls using near surface mounted fibre reinforced polymer strips. Engineering Structures, 59, 330-343.

Donnini, J., y Basalo, F. D. C., Corinaldesi, V., Lancioni, G., & Nanni, A. (2017). Fabric-reinforced cementitious matrix behavior at high-temperature: Experimental and numerical results. Composites Part B: Engineering, 108, 108-121.

Ehsani, M., & Saadatmanesh, H. (1996). Seismic retrofit of URM walls with fiber composites. The Masonry Society Journal, 14(2), 63-72.

Fernandes, P., Sena-Cruz, J., Xavier, J., Silva, P., Pereira, E., & Cruz, J. (2018). Durability of bond in NSM CFRP-concrete systems under different environmental conditions. Composites Part B: Engineering, 138, 19-34.

Galati, N., Tumialan, G., & Nanni, A. (2006). Strengthening with FRP bars of URM walls subject to out-of-plane loads. Construction and Building Materials, 20(1), 101-110.

Ghiassi, B., Silva, M. M., Marcari, G., Oliveira, D. V., & Lourenço, P. B. (2012). Moisture effects on the bond strength of FRP-masonry elements. Paper presented at the 6th International Conference on FRP Composites in Civil Engineering.

Griffith, M. C., Kashyap, J., & Ali, M. M. (2013). Flexural displacement response of NSM FRP retrofitted masonry walls. Construction and Building Materials, 49, 1032-1040.

Grillo, V. E. (2003). FRP/Steel Strengthening of Unreinforced Concrete Masonry Piers. University of Florida.

Hamilton , H., & Dolan, C. (2001). Flexural capacity of glass FRP strengthened concrete masonry walls. Journal of Composites for Construction, 5(3), 170-178.

Hamoush, S., McGinley, M., Mlakar, P., & Terro, M. J. (2002). Out-of-plane behavior of surface-reinforced masonry walls. Construction and Building Materials, 16(6), 341-351.

Hashemi, S., & Al-Mahaidi, R. (2008). Cement based bonding material for FRP. Paper presented at the Proceedings of the.

Hashemi, S., & Al-Mahaidi, R. (2010). Investigation of bond strength and flexural behaviour of FRP-strengthened reinforced concrete beams using cement-based adhesives. Australian Journal of Structural Engineering, 11(2), 129-139.

Kuzik, M. D., Elwi, A. E., & Cheng, J. R. (2003). Cyclic flexure tests of masonry walls reinforced with glass fiber reinforced polymer sheets. Journal of Composites for Construction, 7(1), 20-30.

Leone, M., Matthys, S., & Aiello, M. A. (2009). Effect of elevated service temperature on bond between FRP EBR systems and concrete. Composites Part B: Engineering, 40(1), 85-93.

Masia, M. J., Shen, J., Simundic, G., & Page, A. W. (2015). Behaviour of NSM FRP masonry bond under elevated temperatures. Proceedings of the Institution of Civil Engineers-Construction Materials, 169(1), 27-38.

Mitchell, P. (2010). Freeze-thaw and sustained load durability of near surface mounted FRP strengthened concrete.

Mosallam, A. S. (2007). Out-of-plane flexural behavior of unreinforced red brick walls strengthened with FRP composites. Composites Part B: Engineering, 38(5), 559-574.

Mostofinejad, D., & Mahmoudabadi, E. (2010). Grooving as alternative method of surface preparation to postpone debonding of FRP laminates in concrete beams. Journal of Composites for Construction, 14(6), 804-811.

Nanni, A., & Tumialan, J. G. (2003). Fiber-reinforced composites for the strengthening of masonry structures. Structural engineering international, 13(4), 271-278.

Novidis, D., Pantazopoulou, S., & Tentolouris, E. (2007). Experimental study of bond of NSM-FRP reinforcement. Construction and Building Materials, 21(8), 1760-1770.

Palmieri, A., Matthys, S., & Taerwe, L. (2011). Bond behavior of NSM FRP bars at elevated temperatures. Paper presented at the first middle east conference on smart monitoring, Assessment and Rehabilitation Civil Structures.

Papanicolaou, C. G., Triantafillou, T. C., Papathanasiou, M., & Karlos, K. (2008). Textile reinforced mortar (TRM) versus FRP as strengthening material of URM walls: out-of-plane cyclic loading. Materials and Structures, 41(1), 143-157.

Petersen, R. B., Masia, M. J., & Seracino, R. (2009). Bond behavior of near-surface mounted FRP strips bonded to modern clay brick masonry prisms: influence of strip orientation and compression perpendicular to the strip. Journal of Composites for Construction.

Shen, B. (2014). Fiber-Reinforced Polymer Strengthened Steel Reinforced Masonry Wallettes in Out-of-Plane Bending.

Silva, P., Fernandes, P. M. G., Sena-Cruz, J., Azenha, M., & Barros, J. A. (2014). Behaviour of concrete elements strengthened with near surface mounted CFRP strips under thermal cycles. Paper presented at the 7th International Conference on Fiber Reinforced Polymer (FRP) Composites in Civil Engineering (CICE 2014).

Soliman, S. M., El-Salakawy, E., & Benmokrane, B. (2010). Bond performance of near-surface-mounted FRP bars. Journal of Composites for Construction, 15(1), 103-111.

Soudki, K., & Alkhrdaji, T. (2005). Guide for the design and construction of externally bonded FRP systems for strengthening concrete structures (ACI 440.2 R-02). Paper presented at the Structures Congress 2005: Metropolis and Beyond.

Stone, D., Tumialan, G., Nanni, A., & Parretti, R. (2002). Near-surface mounted FRP reinforcement: application of an emerging technology. Concrete, 36(5).

Tan, K. H., & Patoary, M. (2004). Strengthening of masonry walls against out-of-plane loads using fiber-reinforced polymer reinforcement. Journal of Composites for Construction, 8(1), 79-87.

Tobriner, S. (1984). A history of reinforced masonry construction designed to resist earthquakes: 1755-1907. Earthquake Spectra, 1(1), 125-149.

Toutanji, H., & Ortiz, G. (2001). The effect of surface preparation on the bond interface between FRP sheets and concrete members. Composite Structures, 53(4), 457-462.

Tumialan, G., Tinazzi, D., Myers, J., & Nanni, A. (2000). Field evaluation of unreinforced masonry walls strengthened with FRP composites subjected to out-of-plane loading. Paper presented at the 2000 Structures Congress, American Society of Civil Engineers, Philadelphia, Pennsylvania.

Tumialan, J. G., Galati, N., Namboorimadathil, S. M., & Nanni, A. (2002). Strengthening of masonry with FRP bars. Paper presented at the 3rd. Int. Conf. on Composites in Infrastructure (ICCI 2002).

Tumialan, J. G., Galati, N., & Nanni, A. (2003). FRP strengthening of URM walls subject to out-of-plane loads. ACI Structures Journal, 100(3), 312-329.

Tumialan, J. G., Micelli, F., & Nanni, A. (2001). Strengthening of masonry structures with FRP composites Structures 2001: A Structural Engineering Odyssey (pp. 1-8).

Turco, V., Secondin, S., Morbin, A., Valluzzi, M., & Modena, C. (2006). Flexural and shear strengthening of un-reinforced masonry with FRP bars. Composites Science and Technology, 66(2), 289-296.

Valluzzi, M. R., Da Porto, F., Garbin, E., & Panizza, M. (2014). Out-of-plane behaviour of infill masonry panels strengthened with composite materials. Materials and Structures, 47(12), 2131-2145.

Valluzzi, M. R., Valdemarca, M., & Modena, C. (2001). Behavior of brick masonry vaults strengthened by FRP laminates. Journal of Composites for Construction, 5(3), 163-169.

Velazquez-Dimas, J. I., Ehsani, M. R., & Saadatmanesh, H. (2000). Out-of-plane behavior of brick masonry walls strengthened with fiber composites. ACI structural Journal, 97(3), 377-387.

Willis, C., Kashyap, J., & Griffith, M. (2009). Flexural behaviour of NSM CFRP retrofitted masonry wallettes under static and cyclic loading. Paper presented at the International Symposium on FRP Reinforcement for Concrete Structures (9th: 2009: Sydney, Australia).

Willis, C., Seracino, R., & Griffith, M. (2010). Out-of-plane strength of brick masonry retrofitted with horizontal NSM CFRP strips. Engineering Structures, 32(2), 547-555.

VITA

Zuhair Al-Jaberi was born in Baghdad, Iraq. He received his Bachelor of Civil Engineering degree in 2002 and his Master of Science in Structural Engineering degree in 2006 from Baghdad University. During his Master research, he conducted a study on a dynamic analysis of concrete block machine foundation. He was granted a PhD scholarship by the Higher Committee for Education Development in Iraq (HCED) and began his PhD at Missouri University of Science and Technology in January 2013.

After graduation with Bachelor degree, he worked with the Engineering Consultative Bureau of Baghdad University from 2004-2006 and Al-Nahrain University for one year. Also, he worked as a Q.C engineer at many companies in different projects. Finally, he worked as a faculty member in Civil Engineering department of the University of Al-Nahrain, Baghdad, Iraq. He has been a member of many professional organizations such as; American Concrete Institute (ACI), American Society of Civil Engineering (ASCE), The Masonry Society (TMS), and Iraqi Engineers Union. His research interests include the sustainable use of composite materials for structural strengthening and repair of concrete and masonry systems. In May 2018, he received his Ph.D. in Civil Engineering from Missouri University of Science and Technology.